Alma Mater Studiorum – Università di Bologna

DOTTORATO DI RICERCA IN

CHIMICA

Ciclo XXVIII

Settore Concorsuale di afferenza: 03/C1

Settore Scientifico disciplinare: CHIM/06

Supramolecular Photoresponsive Systems

Presentata da: Maria Stefania Ferrito

Coordinatore Dottorato Prof. Aldo Roda

Relatore Prof. Stefano Masiero

Esame finale anno 2016

Abstract

This PhD research project deals with the synthesis and characterization of supramolecular photoresponsive systems based on the azobenzene unit. In particular, three different systems have been explored. In *Chapter II* project on Azobenzene-cyclodextrin inclusion complexes it will be introduced. The aim of this study was to obtain relatively simple, water-soluble derivatives, whose self-assembly could be reversibly controlled by light. On the basis of previous results, this opens the possibility of directly converting light into mechanical energy via osmosis. To this purpose, several new azobenzene functionalized cyclodextrins as well as several mixtures containing cyclodextrins and azobenzene derivatives have been synthesized, fully characterized and studied The inclusion complexes thus formed and their light-driven disassembly were studied by means of several complementary techniques including NMR, UV, CD, ICT, mass spectroscopy. The most suitable systems were used in experiments, still in progress, of light-to-mechanical energy conversion. In *Chapter III* project on Azobenzene-guanosine hybrids it will be reported. Several novel azobenzene-guanosine hybrids were synthesized for the purpose of investigating the effect of cis-trans photoisomerization on guanosine self-assembly. Lipophilic guanosines in organic solvents can form either ribbon-like supramolecular polymers or, in the presence of alkali metal ions, G-quartet based supramolecular complexes. These complexes were fully characterized for newly synthesized azobenzene-guanosine hybrids. In the absence of ions, the ribbon-like supramolecular polymer gives rise to a gel-like system, which on further investigation turned out to be a lyotropic liquid crystalline phase. Photoisomerization to the cis form induces the transition to an isotropic solution, in a reversible fashion. In addition, the G-quartet structure obtained in the presence of alkali metal ions can be disassembled by light. Finally in *Chapter IV* it will reported results obtained for Oligoazobenzenes's project. While several examples of electron-rich conjugated polymers are known and find application e.g. as electron donors in "plastic" photovoltaics, no examples are reported on the use of electron-poor conjugated polymers as acceptor counterpart. In particular, no polyazobenzenes having the (-C_6H_4-N=N-) repeat unit have ever been reported. Although no polymeric has been obtained yet, we succeeded in synthesizing several homologues up to a tetramer. The compounds were subjected to photophysical, photochemical and electrochemical characterization as well as to charge mobility studies thanks to a collaborative project.

Index

Chapter I

Supramolecular Chemistry

1 Supramolecular Chemistry

1.1 Introduction

"***Atoms are letters, molecules are the words, supramolecular entities are the sentences and the chapters"***

The innovative branch of chemistry that mainly deals with weak intermolecular interactions and self organization is called "Supramolecular Chemistry". Jean-Marie Lehn was one of the founding fathers of Supramolecular Chemistry, and Nobel Prize winner with Pedersen and Donald J. Cram, "*for their development and use of molecules with structure-specific interactions of high selectivity*". He described the supramolecular chemistry as "chemistry beyond the molecule", whereby a "supramolecule" is a specie that is held together by non covalent interactions between two or more covalent molecules or ions. The concept of "Supramolecule" spread so widely, that modern supramolecular chemistry has become interdisciplinary among chemistry, biology, physics and material science. Supramolecular chemistry's main principles can be resumed as follows:

- *Molcecular recognition*: supramolecular formation complex can be driven by specific interactions between host and guest and their geometric complementary.

- *Self-Assembly*: a large complex molecular system can be formed by weak interactions between small and simple building blocks.

1.2 Molecular recognition

Molecular recognition is the selective coordination of two different species with complementary structures: the host and the guest. One definition of hosts and guests was given by Donald Cram, which states: " *the host component is defined as an organic molecule or ion whose binding sites converge in the complex… The guest component is any molecule or ion whose binding sites diverge in the complex"*[1].

[1] Cram, *D.J., Angew. Chem., Int. Ed. Engl*. 25, **1986**, 1039-1134

The driving force for the recognition between host and guest could be steric and electronic interactions. The host must have two basic requirements to coordinate selectively a substrate:

- *Complementarity stereochemistry of coordination sites*: binding sites receptor must have a spatial arrangement corresponding to the binding sites of the substrate, in such a way as to achieve the largest number of non covalent interactions and ensure the stability of the supramolecular adduct ("lock and key systems").

- *Preorganization of the Ligand*: if a host has already, before the coordination, a structural conformation similar to the one that it will have in the adduct, the energy required to bring the receptor in the final form will be smaller, the adduct formation will be more rapid, and the species formed more stable. In general the receptor must have a size, a shape and a specific architecture. The more the receptor and substrate are pre-arranged, more selective will be the molecular recognition.

The first pioneering work on molecular recognition came from the industrial chemist Charles Pedersen, that discovered crown ethers in 1967 by serendipity, analyzing an unwanted byproduct of a failed reaction[2]. In 1960, while attempting to synthetize metal deactivators, in order to prevent the oxidative degradation of petroleum products and rubber caused by trace of metal ion impurities, he isolated some white crystals in a very low yield[3]. He was interested in the different solubility behavior in alcohol, in the presence and in the absence of sodium cations. Pedersen found that Sodium cations could be held in the cavity of the macrocycle, thanks to electrostatic ion-dipole interactions, and this was the explanation for different solubility properties. Later the templating effect exerted by metal ions was better explained by Green, who suggested that the formation of the macrocycle from open chained ligand could involve cations *via* cation-dipole interactions. The templating effect can be illustrated as in Figure 1.

[2] C.J.Pedersen, *JACS , 89 (26),* **1967**, 7017

[3] C.J.Pedersen, *Org. Synth.6*, **1988**, 395

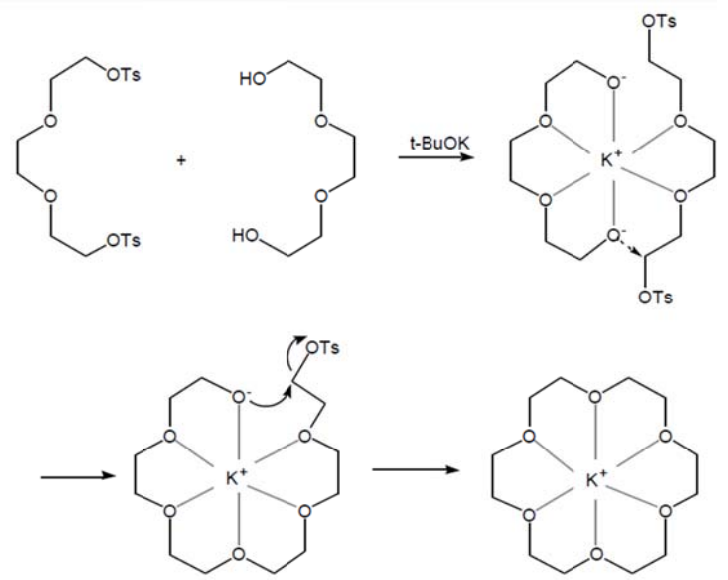

Figure 1: Templating effect illustration.

Since then, different kind of crown ethers were synthetized and the correlations between the cavity size, cationic radius and stability of the complexes were deep studied. In 1969 at Universite Louis Pasteur in Strasbourg, inspired by Pedersen's work, Lehn and his co-workers found that by replacing oxygen atoms with nitrogen atoms, the two-dimensional monocyclic structures could be developed into three-dimensional bi- and tricyclic structures. These three dimensional structures display much stronger complexation ability and higher selectivity toward metal ions[4,5].

Moreover, by changing the length and the number of oxygen atoms, Lehn could improve the selectivity of the cryptands for ions. In the same years Donald Cram, with the help of molecular models, designed a new class of receptors, characterized by a spherical cavity, called spherands.

Compared to cryptands, spherands showed more rigidity with binding sites fixed in an octahedral arrangement around the cavity. As a consequence of increased rigidity, the ability of the ligand to undergo conformational reorganization decreases and they result more "preorganized".

For a specific guest, less conformational changes and minimal energy for the association are required for a more highly preorganized ligand. The effect of topology, preorganization and other factors, such as solvation upon complexation and selectivity, has been generalized as "*preorganization principle*"[6] and *"complementarity principle"*. According to preorganization

[4] Dietrich, B.; Lehn, J. -M.; Sauvage, J.-P. *Tetrahedron Lett.* **1969**, *34*, 2885.

[5] Graf, E.; Lehn, J. -M. *J. Am. Chem. Soc.* **1975**, *97*, 5022.

[6] Cram, D. J. *J. Inclusion Phenom.* **1988**, *6*, 397, Cram, D. J.; DeGrandpre, M. P.; Knobler, C. B.; Trueblood, K. N.; *J. Am. Chem. Soc.* **1984**, *106*, 3286, Cram, D. J. in *From Design to Discovery* American Chemical Society, Washington DC, **1991**, p 9.

principle , *" the more highly hosts and guests are organized for binding and low solvation prior to their complexation, the more stable will be their complexes"*[7].

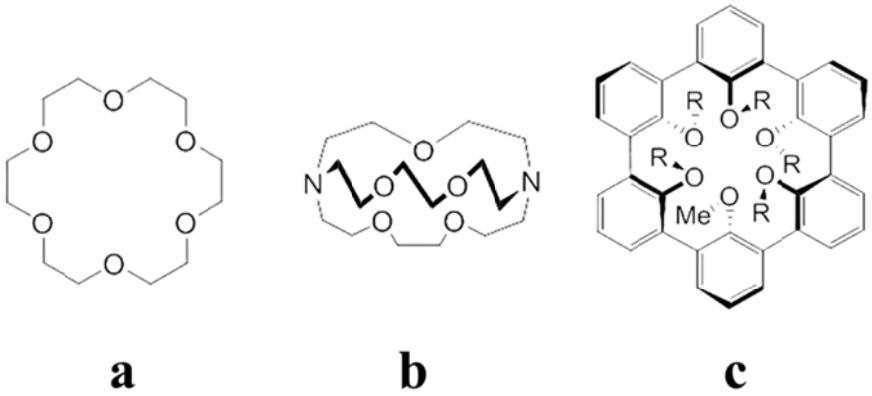

Figure 2: Chemical structure of crown ether (a), cryptand (b), and spherand (c).

To date, several progress have been made in the synthesis and design for a large number of inclusion complexes, and their use finds application in different technology fields. In particular cyclodextrins are the one of the most widely used receptors in host-guest chemistry, as it will be discussed in the next chapter.

1.3 Self-assembly

Molecular self-assembly usually takes advantage of weak supramolecular interactions (ionic, hydrophobic, van der Waals, hydrogen and coordination bonds), but can also make use of kinetically labile covalent bonds[8]. Non-covalent interactions are the dominant type of interaction between supermolecules in supermolecular chemistry,[3] and are critical in maintaining the three-dimensional structure of large molecules.

A non-covalent interaction differs from a covalent bond in that it does not involve the sharing of electrons, but rather involves more dispersed variations of electromagnetic

[7] D.J.Cram. *Pers. Comm*. **1988**

[8] Supramolecular Chemistry: From Molecules to Nanomaterials, eds. P. Gale and J. Steed, Wiley-VCH Verlag GmbH & Co.KGaA, Weinheim, **2012.**

interactions between molecules[9]. The chemical energy released in the formation of non-covalent interactions is typically in the order of 1-5 kcal/mol and they generally include:

- *Hydrogen Bonds:* attractive interaction between an electronegative atom and a hydrogen atom bonded to another electronegative atom.

- *Electrostatic Interaction:* the attraction of ions or molecules with full permanent charges of opposite signs.

- *Van der Waals's forces:* electrostatic interactions involving permanent or induced dipoles (or multipoles). These include the following:

  - *permanent dipole-dipole interactions*
  - *dipole-induced dipole interactions*
  - *induced dipole-induced dipole interactions*, commonly referred to as London dispersion forces

Weak interactions and self-organization enable the construction of relatively large and complex molecular systems. In biological systems, there are many kinds of biomolecules such as proteins, nucleic acids, polysaccharides, which interact each other via non covalent interactions, to form highly ordered structures as cells and tissues.

These structures form more highly ordered architectures such as bones, flesh, and organs in a hierarchical way, through non covalent interactions between the surface of them, and perform indispensable functions to maintain life and living organism, such as self-healing themselves from external damage, contraction-expansion to produce mechanical work, and transferring genetic codes to the subsequent generation. The core concept of formation of these structures is self-assembly via molecular recognition.

The most important and clarifier example of self-assembly is constituted by DNA. When the strands are mixed together under appropriate conditions and hydrogen bonds are formed between complementary base pairs, the formation of the DNA double helix, from two complementary deoxyribonucleic acids, is spontaneous and reversible.

[9] Anslyn, Eric, *Modern Physical Organic Chemistry*. University Science Book, **2004**.

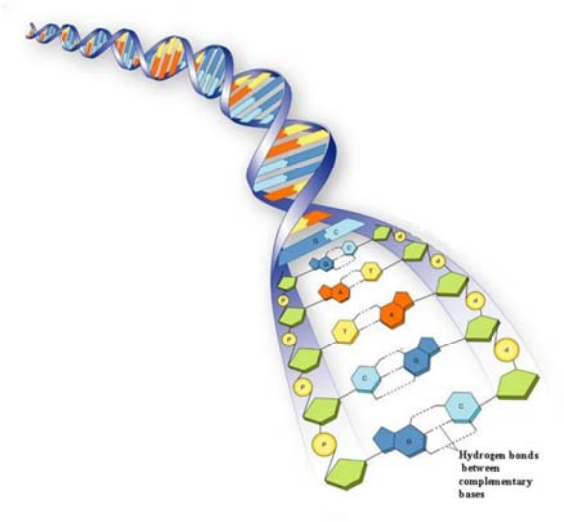

Figure 3: DNA double helix, illustration hydrogen bonds between complementary base pairs.

Understanding molecular recognition in biological systems leads to the construction of artificial, biomimetic systems, The construction of nanostructures based on supramolecular self-assembly has been subject of interest for the past forty years, and chemists have acquired a high control of objects at that scale by encoding their molecular constituents[10]. The preparation of well-defined architectures could afford new relevant materials with peculiar physicochemical properties. In addition, one of the most interesting aspect of self-assembled structures relies on the reversibility of the non-covalent interactions, that gives to these systems a dynamic nature.

2 Stimuli responsive systems

2.1 Introduction

Living organism are constantly detecting stimuli of various types from the environment in which they live, using the five senses : sight, hearing, smell , taste and touch. The sensitivity is due to the presence of specific receptors , particular cells capable of picking up the signals and react to different stimuli . Some cells are able to pick up sounds, others are sensitive to light, heat, cold and so on. The receptors convert the stimulus received into a pulse of electrical type, which represents the manner in which the cells of the nervous system transmit stimuli. Contraction-extension movement, exclusion of foreign materials by white blood cell and antibodies, and transportation of

[10] E. Busseron, Y.Ruff, E. Moulin and N. Giuseppone, *Nanoscale*, **2013**, 5, 7098

oxygen are the consequence of chemical reactions that occur after a stimulus. Inspired from biological macromolecules, several artificial stimuli-responsive supramolecular architectures have been designed. In the last decades external stimuli-responsive systems were subject of interest by the scientific community[11,12,13,14].

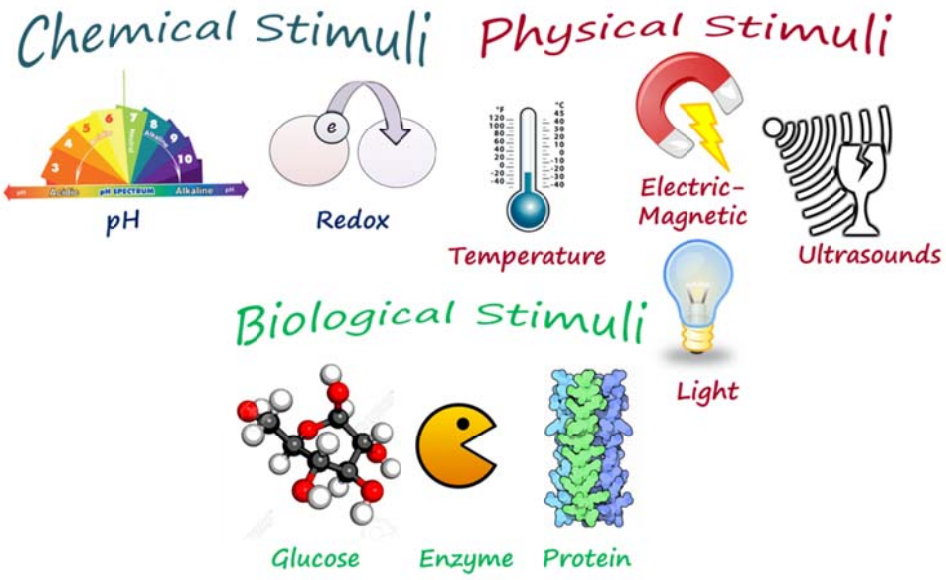

Figure 4: External stimuli involved in supramolecular chemistry.

Several kinds of stimuli can be used, as temperature, pH, magnetic fields or light. The incorporation into an assembly of a stimuli responsive unit (e.g. a switchable functionality) leads to the conversion from one state to another, giving rise to observable, and sometimes macroscopic, changes.

2.2 Stimuli

- **Temperature**

Temperature is one of the most common stimuli used in supramolecular chemistry. Compared to covalent bond, non covalent interactions are more temperature dependent. and its variations can

[11] Ghandi, M.V.; Thompson, B.S., *Smart Materials and Structures*, **1992**, Chapman & Hall, London

[12] Feringa, B.L.; Browne, W.R., *Molecular switches*, **2011,** Wiley-VCH, Germany

[13] Urban, M.W., *Handbook of stimuli responsive materials*, **2011**, Wiley-VCH, Germany

[14] Minko,S., *Responsive polymer materials: design and applications, 1st ed*, **2006**; Blackwell pub.: Ames Yowa

change the equilibrium between species. Altering temperature also can result as a change in structural arrangement, disaggregation phenomena, change in the degree of polymerization and so on.

- **pH**

Another common stimulus is represented by pH, but compared to other stimuli, pH results an internal stimulus, and thus requires alteration of the chemical environment. . The complexity of reversibility is drawback that arises with the use of pH-responsive materials, as the solution must be removed or extracted before reuse and this may also alter the physical environment[15]. pH's variation of a medium convert weak acid and bases from their acidic form to their basic form, changing their states from charged to uncharged and *vice versa*. Due to electrostatic interaction's change, a structural and conformational change occurs in the system. The design of materials modified with pH-sensitive moieties, with variable functions (adhesion, redox properties and so on), has been widely investigated. For instance, Figure 5 shows an example reported by Katz group of a bioelectronic device based on the switching of a pH-responsive polymer.[16].

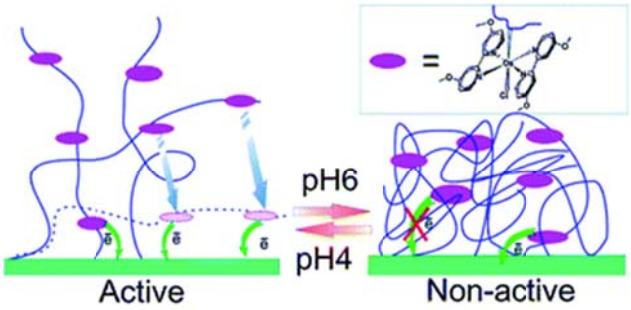

Figure 5: Electrochemically active and inactive states of a redox polymer on electrode surface, by pH-controlled variations.

- **Ultrasounds**

An effective stimulus that can be applied is represented by ultrasounds. It has been reported that many supramolecular architectures, generally gels, change their properties if exposed to ultrasonic stimulation. An example of these systems is represented by Miyazaki work, on an ethylene-vinyl

[15] Urban, M.W., *Handbook of stimuli responsive materials*, **2011**, Wiley-VCH, Germany

[16] Tam, T.K.; Ornatska, M.; Pita,M.;Minko, S.; Katz, E.; *J.Phys, Chem. C* **2008**, 112 (22), 8438-8445

alcohol copolymer system capable to release insulin in diabetic rats by external ultrasound irradiation[17].

- **Electric and magnetic field**

An alternative mechanism of stimulation is the application of electric and magnetic fields. Electro-magnetic external field as a stimulus represents an enormous advantage, because it can be applied or removed instantaneously with a specific direction, which can give rise to anisotropic deformation. Electro-magnetic fields represent the most convenient stimuli for signal control[18,19,20,21], and compared to systems that respond to changes in electrolyte concentration or pH or temperature they result faster[22]. To date, many examples of electro-responsive polymers and gels have been used to prepare materials that swell, shrink, or bend after an electric or magnetic field is imposed[23,24].

The conversion of electro-magnetic energy into mechanical energy has promising applications in biomechanics, artificial muscle actuation, sensing, energy transduction, sound dampening, chemical separations, and controlled drug delivery. Most of the examples of electric responsive systems, reported in literature, are based on polyelectrolyte hydrogels[25], where anisotropic swelling ore de-swelling is due to charged ions migrating towards the anode or cathode side of the gel.

---

[17] Miyazaki, S., Yokouchi, C., and Takada,M, „*J. Pharm. Pharmacol*, *40*, **1988,** 716–717.

[18] M. Zrinyi, Colloid Polym Sci, 278, **2000**, 98–103

[19] G. Filipcsei, I. Csetneki, A. Szilagyi, M. Zrinyi, *Adv Polym Sci, 206*, **2007,** 137–189

[20] Bar-Cohen, *Electroactive Polymer actuators as artificial muscles: reality, potential, and challanges,2nd ed.*; **2004,** SPIE Press: Bellingham, Wash.

[21] Mohsen,S; Kwang, J.K., **2004,** Smart Mater. Struct., 14 (1), 197

[22] M. Zrinyi, *Trends Polym Sci, 5* , **1997**, 280–285

[23] G. Filipcsei, J. Feher, M. Zrinyi, J, *Mol Struct*, 554, **2000**, 109–117

[24] T. Shiga, *Adv Polym Sci, 134,* **1997**, 131–163

[25] (a) Kim, S.J., Kim, H.I., Shin, S.R., *J. Appl. Polym. Sci.*, 92, **2004**, 915–919. (b) Kim, S.J., Park, S.J., Lee, S.M., Lee, Y.M., Kim, H.C., and Kim, S.I. *J. Appl.Polym. Sci.*, 89, **2003**, 890–894. (c) Kim, S.J., Park, S.J., Shin, M.-S., Kim, S.I. , *J. Appl.Polym. Sci.*, 86, **2002**, 2290–2295. (d) Kim, S.J., Yoon, S.G., Lee, S.M., Lee,S.H., and Kim, S.I. „*J. Appl. Polym.Sci.*, 91, **2004**, 3613–3617.

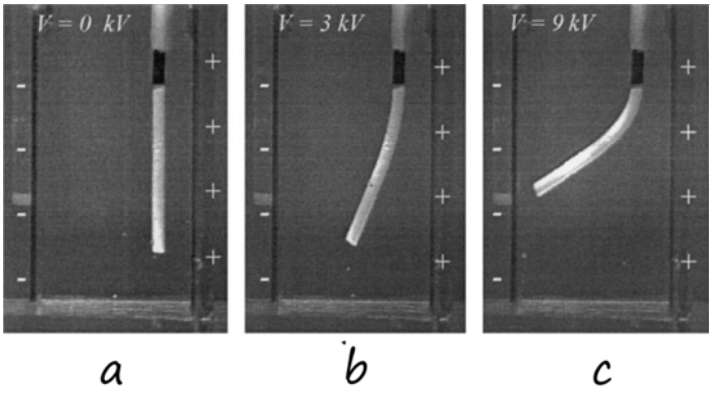

Figure 6: Bending of an electric field responsive PDMS gel in uniform electric field[26].

Magnetic responsive systems generally are composed of inorganic magnetic nanoparticles that are physically entrapped, and a distortion in shape and size occurs reversibly as a non-uniform magnetic field is imposed[27].

- **Molecule-responsive systems**

From the beginning of Supramolecular chemistry, the field that advantaged more was the analytical one[28]. Supramolecular complexes can boost the sensing of a wide range of molecules, such as gases, solvents, oxidizing/reducing agents, using a receptor with steric and electronic specific characteristics. A common approach to obtain molecule responsive systems is to use scaffolds modified with receptors for specific target molecule. Besides environmental field, , the sensing of ions can find wide application also for clinical purposes taking advantage from the high stability of host-guest complexes. Amendola[29] et al. investigated the affinity of azacryptands towards perrhenate anion. Host compounds being capable to encapsulate ReO_4^- are of great interest and they could lead to the development of new materials, useful for the preconcentration and extraction of

[26] G. Filipcsei et al., *Journal of Molecular Structure* 554, **2000**, 109–117

[27] (a) Barsi, L., Buki, A., Szabo, D., and Zrinyi, M. *Prog. Colloid. Polym. Sci.*, 102, **1996**, 57–63; (b) Szabo, D., Szeghy, G., and Zrinyi, M. *Macromolecules*, 31, **1998**, 6541–6548; (c) Zrinyi, M., Barsi, L., Szabo, D., and Kilian, H.G. , *J. Chem. Phys.*, 106, **1997**, 5685–5692.

[28] Hans-Jorg Schneider , *Supramolecular Systems in Biomedical*, **2013**, Royal Society of Chemistry

[29] Amendola, V., Alberti, G., Bergamaschi, G., Biesuz, R., Boiocchi, M., Ferrito, S. and Schmidtchen, *Eur. J. Inorg. Chem.,* **2012**.

^{188}Re from radionuclides generator for therapeutic application in oncology, nuclear medicine and interventional cardiology[30].

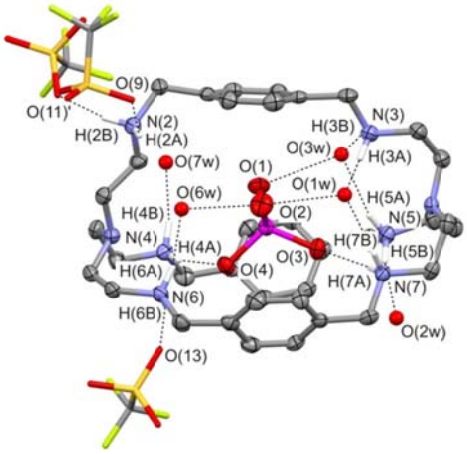

Figure 7: A simplified view of the molecular structure of the $[aH_6{\cdot}ReO_4](CF_3SO_3)_5{\cdot}8(H_2O)$ crystal, (a = two-bistren-azacryptand with p-xyxlil spacer).

To date, research and design of a great variety of novel systems to construct bio-molecules responsive sensors, actuators and drug delivery systems has been used so far because of their potential applications as smart biomaterials. Molecular imprinting represents one of the most attractive technique to design biomimetic polymers with molecular cavities devoted to recognition of substrates[31,32,33]. After polymerization of prearranged functionalized monomers around a print molecule, a cavity is formed. Removing the print molecule, the molecular cavity formed can thus recognize the print molecules by reversible binding and shape complementarity.
Despite synthetic receptors have been widely reported in the literature, cyclodextrin remains the most used receptor in host-guest inclusion chemistry.

- **Light**

Light, is another popular stimulus, which has been well documented. The energy of an electromagnetic wave varies over a wide range, depending on wavelength. Because far ultraviolet light (λ=10-200 nm) has an energy greater or equal to covalent bond, usually is not used. On the other hand, infrared light, (λ= 0.7-2000 μm) does not have sufficient energy to excite the electronic

[30] W.A.Volkert, T.J. Hoffmann**,** *Chem.Rev*., **1999**

[31] G.Wulff, *Angew. Chem. Int. Ed. Engl.,34*, **1995,** 1812-1832

[32] K. Shea, *Trends Polym. Sci. 2*, **1994,** 166-173

[33] T. Miyata et al, *Advanced Drug delivery Reviews*, 54, **2002,** 79-98

transitions, that are necessary to induce structural changes. Thus, near UV and visible light, (λ= 200-750 nm) are more often used as stimuli for photo-responsive systems, that will be deeply described in the next chapters.

3 Photochromic Molecular Switches.

Photo-responsive systems are constructed using moieties that absorb near UV and/or visible light, and this leads to structural changes:

- *photoisomerization*
- *photodimerization*
- *photoinduced decomposition* and other.

Controlling molecular self-assembly by an external light stimulus is advantageous, because photochemical reactions occur very rapidly and thereby a fast response can be obtained. Light is also advantageous in view of its ready availability as a mild energy source[34].

Various classes of compounds that undergo photo-isomerization were used as photochromic molecular switches, such as *azobenzenes, diarylethenes, spyropyrans* and other. Among the photo-switching molecules, the most widely used are azobenzene derivatives, because of their photo-stability, that allow to perform several cycles of photo-isomerization without loss of performance or chemical purity.

[34] R. Ballardini, V. Balzani, A. Credi, M. T. Gandolfi, M. Venturi, Acc. Chem. Res. **2001**, 34, 445–455

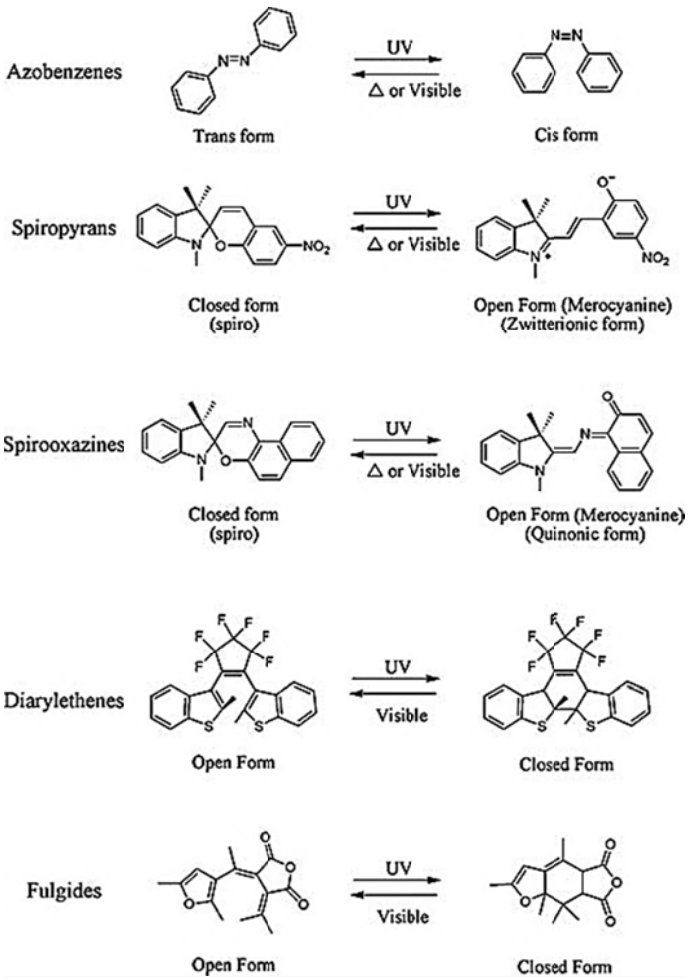

Figure 8: Photo-chromic molecular switches.

3.1 Spiropyrans

Using UV and/or visible light, *spiropyrans* undergo reversible photo-isomerization between a stable and a metastable state. The closed spirocyclic form can be reversibly converted to a highly polar hydrophilic zwitterionic merocyanine isomer, that has a much larger dipole moment as showed in Figure 9. The thermal conversion from the merocyanine isomer back to the closed spirocyclic form occurs typically slowly at room temperature in non-polar media, while the photochemical isomerization with visible light occurs on a much faster timescale[35,36,37].

[35] R. Rosario, D. Gust, M. Hayes, J. Springer, A. Garcia, Langmuir **2003**, 19, 8801–8806.

[36] R. Rosario, D. Gust, M. Hayes, F. Janke, J. Springer, A.A. Garcia, Langmuir **2002**, 18, 8062–8069.

[37] R. Rosario, D. Gust, A.A. Garcia, M. Hayes, J.L. Taraci, T. Clement, J.W. Dailey, S.T. Picraux, J. Phys. Chem. B **2004**, 108, 12640–12642.

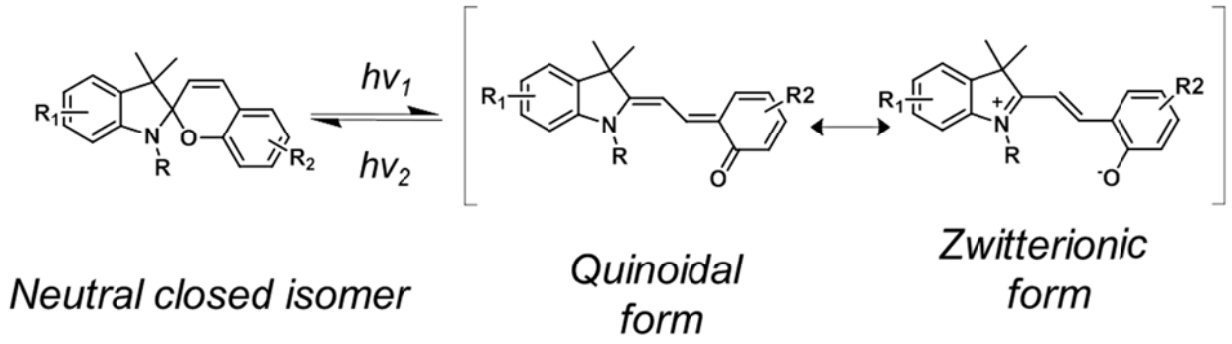

Figure 9: Schematic representation of the reversible photoisomerization of spiropyran moieties.

3.2 Dithienylethenes

1,2-Dithienylethenes consist of two isomers, a closed form and an open form of the molecule as showed in Figure 10. They are reversible molecular switches, consisting of conjugated parts connected by a switching element[38,39]. The closed form exhibits better electrical conductance properties than the open form, as a consequence of the π-conjugation. In the closed forms this extends over the entire molecule, while it is restricted to each half of the molecule in its open form. The transition from closed to open form takes place at wavelengths $500 < \lambda < 700$ nm; for the reverse, one requires $300 < \lambda < 400$ nmFurthermore, dithienylethenes usually exhibit excellent thermal stability.

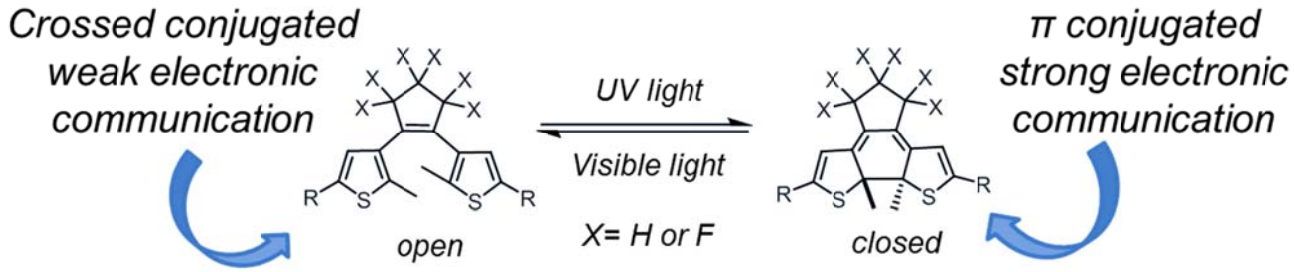

Figure 10: Reversible photocyclization of 1,2-dithienylethene moieties upon UV–Vis light irradiation.

[38] B.L. Feringa (Ed.), *Molecular Switches*, Wiley-VCH, Weinheim, **2001**. B.L. Feringa (Ed.), Wiley-VCH, Weinheim, **2001**, p. 001.

[39] M. Irie, *Chem. Rev.* **2000**, *100*, 1683–1684.

3.3 Alkenes

The photochemical isomerization process of alkenes have been widely studied[40,41]. Simple stilbenes result however unattractive as switches, because of undesired photochemical side reactions; on the other hand interesting switches have been prepared from olefins including overcrowded alkenes[42] and maleimides[43]. One of the most advantageous aspect of these systems is represented by their thermal and photochemical stability.

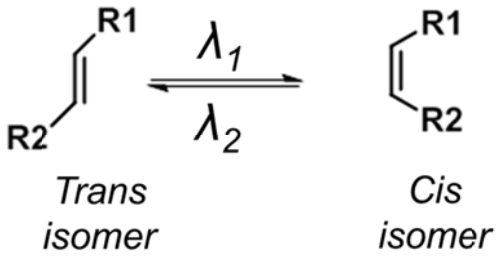

Figure 11: General scheme for the photochemical interconversion between the *cis* and *trans* configurations of an alkene.

These molecular switches have been largely investigated to obtain light-driven molecular rotary motors[44]. Molecular shuttles constructed from interlocked molecules, such as rotaxanes or catenanes[45], take advantage from the photo-isomerization of alkenes, which is able to modulate the strength of association between hydrogen-bonded systems[46], and to allow the motion of the mechanically interlocked subunits in response to an external trigger like light[47].

[40] C. Dugave and L. Demange, Chem. Rev., **2003**, 103, 2475–2532

[41] B.L. Feringa (Ed.), Molecular Switches, Wiley-VCH, Weinheim, **2001**. B.L. Feringa (Ed.), Wiley-VCH, Weinheim, **2001**, p. 001.

[42] B.L. Feringa, Acc. Chem. Res. **2001**, 34, 504–513.

[43] E.R. Kay, D.A. Leigh, Hydrogen bond-assembled synthetic molecular motors and machines, in: T.R. Kelly (Ed.), Molecular Machines, Topics Curr. Chem. **2005**, 262.

[44] N. Koumura, R.W.J. Zijlstra, R.A. van Delden, N. Harada, B.L. Feringa, Nature **1999**, 401, 152–155.

[45] E.R. Kay, D.A. Leigh, Synthetic molecular machines, in: T. Schrader, A.D. Hamilton (Eds.), Functional Artificial Receptors, Wiley-VCH, Weinheim, **2005**.

[46] V. Balzani, A. Credi, F.M. Raymo, J.F. Stoddart, Angew. Chem. Int. Ed. **2000**, 39, 3349–3391.

[47] J.F. Stoddart, Acc. Chem. Res. **2001**, 34, 410–411

3.4 Azobenzenes

Since the compound was isolated nearly eighty years ago by G.S. Hartley,[48] azobenzene's photoreactivity has been subject of a widespread interest. In particular, azobenzene derivatives have been used for the design of artificial molecular systems, such as polymers[49], protein probes[50], molecular machines[51], etc. Compared to other photochromic switches, azobenzene exhibits remarkable photo-stability even after prolonged irradiation cycles and functional activity under a wide range of experimental conditions. Azobenzene can exist in two geometric isomers, *trans* and *cis*.

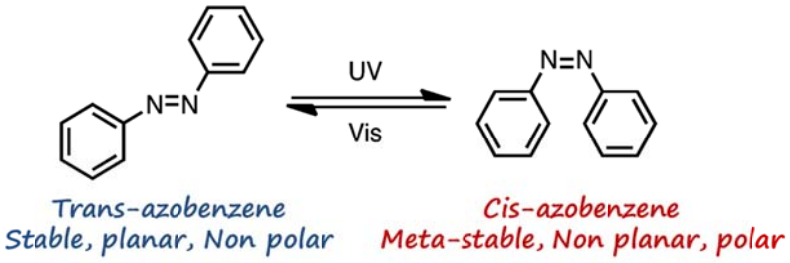

Figure 12: Reversible photoisomerization of azobenzene upon UV–Vis irradiation. **T**he *trans*-isomer is planar while the *cis*-isomer is bent and more compact.

The two isomers show a different arrangement of their aromatic moieties: consequently their differ in several physical properties[52], such as geometry, dipole moment and absorption spectra[53]. The conversion between these states can be driven by light or occur thermally in the dark. *Trans-to-cis*

[48] Hartley, G.S., Nature, **1937,** 140,3537,281

[49] (a) C.-U. Bang, A. Shishido and T. Ikeda, *Macromol. Rapid Commun.,* **2007,** 28, 1040–1044; (b) F. Puntoriero, P. Ceroni, V. Balzani, G. Bergamini and F. Voegtle, *J. Am. Chem. Soc*., **2007**, 129, 10714–10719; (c) R. M. Parker, J. C. Gates, H. L. Rogers, P. G. R. Smith and M. C. Grossel, *J. Mater. Chem*., **2010**, 20, 9118–9125.

[50] (a) M.R. Banghart, A. Mourot, D. L. Fortin, J. Z.Yao, R.H. Kramer and D. Trauner, *Angew. Chem., Int. Ed*., **2009,** 48, 9097–9101. (b) Y. Kim, J. A. Phillips, H. Liu, H. Kang and W. Tan, *Proc. Natl. Acad. Sci. U. S. A.*, **2009**, 106, 6489–6494. (c) J. Wang, H.-B. Liu and C.-S. Ha, *Tetrahedron,* **2009**, 65, 9686–9689. (d)M. Banghart, K. Borges, E. Isacoff, D. Trauner and R.H. Kramer, Nat. Neurosci., 2004, 7, 1381–1386.

[51] (a) Y. Norikane and N. Tamaoki, *Org. Lett*., **2004**, 6, 2595–2598; (b) H. Murakami, A. Kawabuchi, K. Kotoo, M. Kunitake and N. Nakashima, *J. Am. Chem. Soc*., **1997**, 119, 7605–7606; (c) T. Muraoka, K. Kinbara and T. Aida, *Nature*, **2006**, 440, 512–515.

[52] H. Rau, *Photochemistry and photophysics*, **1990,** CRC Press, Boca Raton

[53] Bandara, H.M.D.; Burdette, S.C.; *Chem. Soc. Rev.,* **2012,** 41,1809-1825

isomerization occurs by irradiation with UV light and the process is fast and reversible; in particular for unsubstituted azobenzene, photoisomerization results to be faster than thermal isomerization, and as consequence the two process are well-separated in time. The trans isomer is thermodynamically more stable than the cis isomer, (the energy barrier at room temperature is c.a. 50KJ/mol), thus *cis-to-trans* isomerization occurs spontaneously in the dark. Functionalization of azobenzene with different substituents results in a change in spectroscopic properties and isomerization mechanism.

3.4.1 Azobenzene isomerization mechanism

Structural analyses by X-ray and computational experiments have shown that the trans isomer adopts a planar structure with C_{2h} symmetry, while the two phenyl rings are twisted by 30° in the gas phase[54].

The low-energy absorption spectrum of trans isomer (Figure 13) displays two bands, a strong band in the near UV spectral region, (λ max ~ 320 nm, ε ~ 22000 L $mol^{-1}cm^{-1}$), associated with absorption of the dipole-allowed, π-π* transition, and a weak band in the visible region, (λ max ~ 450 nm, ε ~ 400 L $mol^{-1}cm^{-1}$), that refers to n- π* transitions, formally dipole-forbidden.. On the other hand cis isomer assumes a non-planar structure with C_2 symmetry, and its absorption spectrum is characterized by weaker bands in UV region, (λ max ~ 270 nm, ε ~ 5000 L $mol^{-1}cm^{-1}$; λ max ~ 250 nm, ε ~ 11000 L $mol^{-1}cm^{-1}$), and another band in the visible region, (λ max ~ 450 nm, ε ~ 1500 L $mol^{-1}cm^{-1}$), that absorb more strongly than for the trans isomer..

[54] (a) C. J. Brown, *Acta Crystallogr*., **1966**, 21, 146–152. (b) C. R. Crecca and A. E. Roitberg, *J. Phys. Chem. A*, **2006,** 110, 8188–8203. (c) M. Traetteberg, I. Hilmo and K. Hagen, J. *Mol. Struct*., **1977**, 39, 231–239.

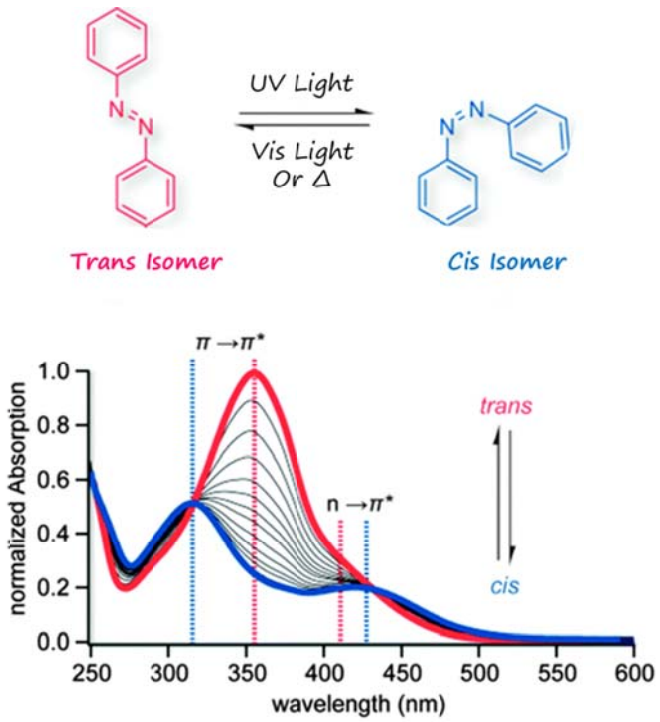

Figure 13: UV-Vis Spectra upon photisomerization.

While in stilbene, the isomerization occurs exclusively by rotation and the quantum yield equals unity[55], several photo-isomerization mechanism have been hypothesized, and the first consideration have been based on photo-isomerization yield, in different solvent, concerning excitation from the ground state to the first and the second excited state[56].

A simplified Jablonski diagram, in Figure 14, reports the S_0, (ground state, singlet state), and S_1 and S_2 state (first and second singlet excited state) of azobenzene. The S_1 state, corresponding to n-π* transition can be generated by direct excitation of the ground state, ($S_1 \leftarrow S_0$), or from intersystem crossing relaxation of S_2 state[57]. The excitation to the S_2 state instead corresponds to the π-π* transition.

[55] Rodier, J. M.; Myers, A. B. *J. Am. Chem. Soc.* **1993,** *115,* 10791–10795.

[56] (a) J. Ronayette, R. Arnaud, P. Lebourgeois and J. Lemaire, Can. *J. Chem*. 52, **1974,** 1848; (b) G. Zimmermann, L.-Y. Chow and U.-J. Paik, *J. Am. Chem. Soc*., **1958** 80, 3528; (c) D. Gegiou, K. A. Muszkat and E. Fischer, *J. Am. Chem. Soc*., **1968,** 90, 12.

[57] H. M. D. Bandara, S. C. Burdette, *Chem. Soc. Rev*., **2012**, 41, 1809–1825

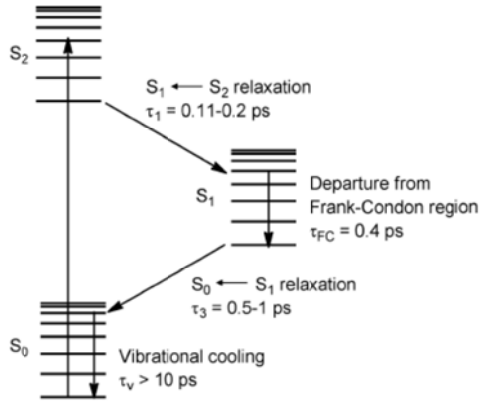

Figure 14: A simplified Jablonski diagram excitation from the ground state to the first and the second excited states of azobenzene.

The main mechanisms recognized for the photo-isomerization of azobenzene are reported in Figure 15:

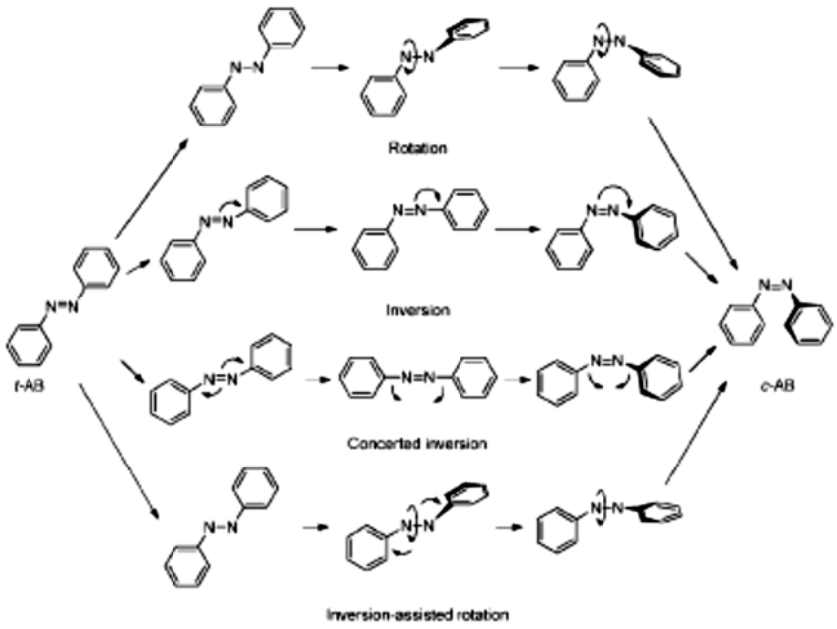

Figure 15: Schematic representation of main mechanisms recognized for the photo-isomerization.

Originally privileged hypothesis[58], was that in S_1 and S_2 photo-isomerization can occur according to two different mechanisms, defined respectively the *inversion of nitrogen atom*, and *torsion of double bond* ***N=N*.** Later on, this hypothesis has been supported by the observation that some

[58] H. Rau and E. Luddecke, J. *Am. Chem. Soc*. 104, **1982**, 1616.

azobenzene derivatives, where the rotation of the N=N double bond was not allowed, could isomerize, and their quantum yields for π-π* transition were greater than for unsubstituted azobenzene[59]. Isomerization by rotation implies the rupture of the N=N π bond and free rotation around N-N bond, as reported in figure 16, in which the N-N-C angle remains 120° while C-N-N-C angle changes.

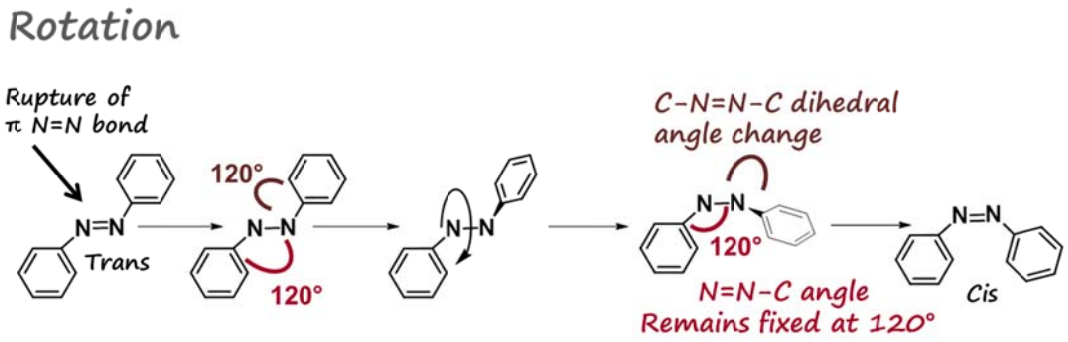

Figure 16: Rotation mechanism of azobenzene upon photo-isomerization.

The inversion mechanisms instead involves a transition state with one *sp* hybridized azo-nitrogen atom, as one angle increases to 180°, (N=N-C), while the C-N=N-C decrease at 0°.

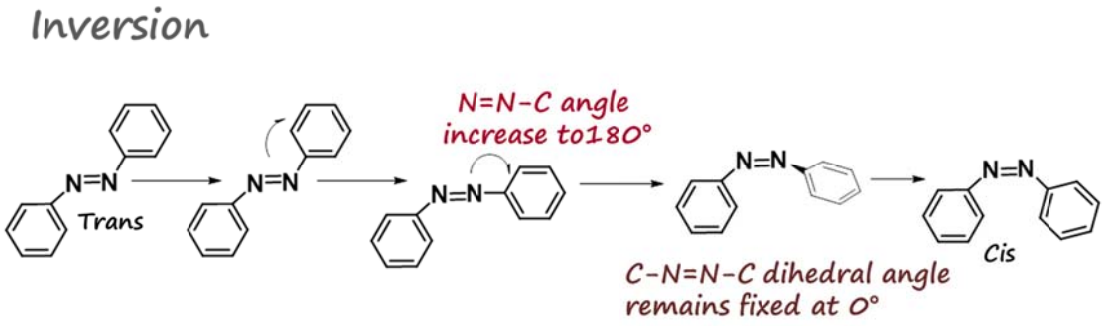

Figure 17: Inversion mechanism of azobenzene upon photo-isomerization.

[59] (a) H. Rau, *J. Photochem*. 26, **1984,** 221; (b) A. W. Adamson and R. Wachter, *J. Am. Chem. Soc*. 100, **1978,** 1298; (c) H. Rau and S. Yu-Quan, *J. Photochem. Photobiol. A 42*, **1988**, 321.

Inversion mechanism can be lead form n-π* transition, ($S_0 \leftarrow S_1$), of nonbonding electron pairs of nitrogen atoms, while on the other hand in the rotation mechanism a π-π* transition, ($S_0 \leftarrow S_2$) can be involved, as resumed in Figure 18[60].

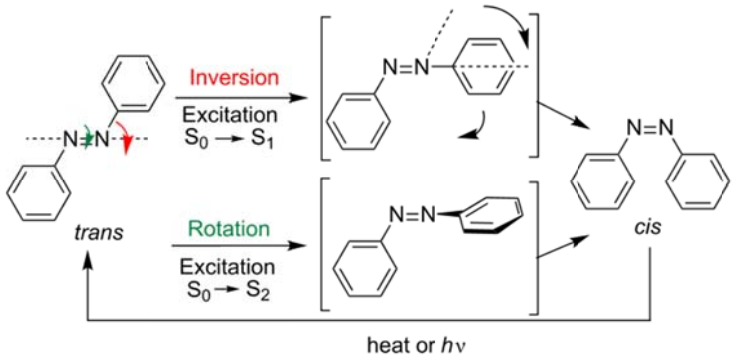

Figure 18: Comparison between rotation and inversion mechanism of azobenzene upon photo-isomerization.

Besides rotation and inversion, also *concerted inversion* and *inversion assisted rotation* have been proposed as possible pathways[61]. In the first one both N=N-C angles increase to 180°, and a linear transition occurs.

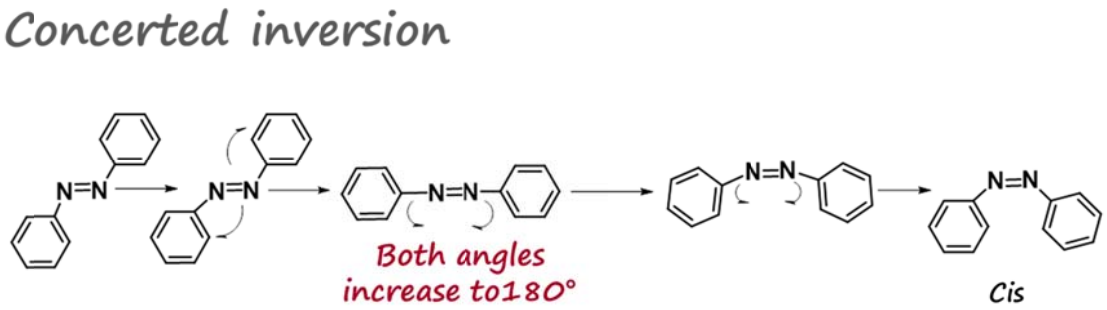

Figure 19: Concerted inversion mechanism of azobenzene upon photo-isomerization.

In the *inversion assisted rotation* mechanism, both angles change simultaneously, but the transition state has no net dipole moment.

---

[60] (a) Marcandalli, B.; Pellicciari-Di Liddo, L.; Di Fede, C.; Bellobono, I. R.*J. Chem. Soc., Perkin Trans. 2* **1984,** 589–593; (b) Nishimura, N.; Tanaka, T.; Asano, M.; Sueishi, Y.*J. Chem. Soc., Perkin Trans. 2* **1986,** 1839–1845.

[61] (a) J. L. Magee, W. Shand, Jr. and H. Eyring, *J. Am. Chem. Soc*.,**1941**, 63, 677–688; (b) D. Y. Curtin, E. J. Grubbs and C. G. McCarty, *J. Am. Chem. Soc*., **1966**, 88, 2775–2786.

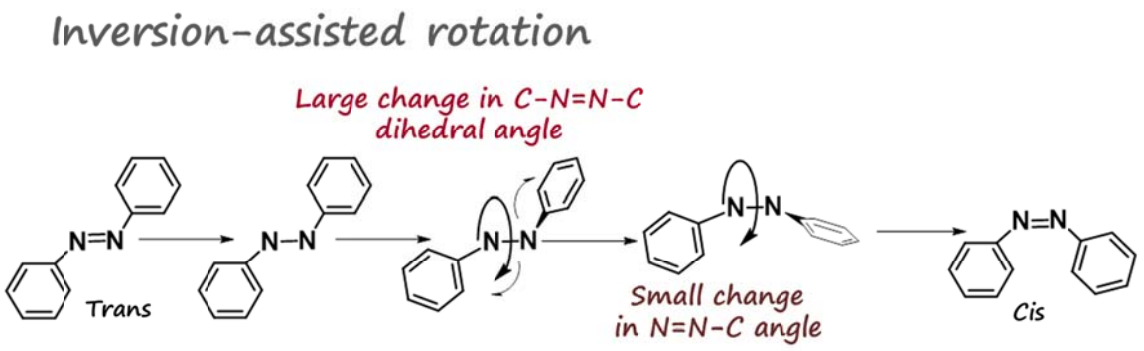

Figure 20: Inversion-assisted rotation mechanism of azobenzene upon photo-isomerization.

Trans and cis isomers can be obtained from relaxation phenomena from all four mechanisms; as consequence a photo-stationary state is reached, in which both isomers are present.

3.4.2 Quantum yield of isomerization

Different factors can affect the quantum yield of photo-isomerization; in particular irradiation wavelength, solvent, temperature and the activation energy barrier. The quantum yield of trans to cis isomerization, following n-π* transition, is affected by solvent polarity, and in particular, it increases with increasing polarity of the solvent. On the other hand, cis-to-trans isomerization, following π-π* transition is not affected by the polarity of the solvent. The viscosity of the solvent does not play an important role on isomerization quantum yield, except in the case of isomerization that proceeds with rotation mechanism, as in the case of stilbene. Summarizing, the viscosity and the polarity of the solvent has an effect on the mechanism of the photo-isomerization: polar and non-viscous solvents promote rotation, while non-polar and viscous solvents promote inversion mechanism[62].

3.4.3 Azobenzenes as molecular switches

The different chemical and physical properties of trans and cis azobenzene isomers, the fast interconversion between the two isomers through light and the easy synthetic step to obtain it, make azobenzene an ideal component in the design of photo-responsive systems. Azobenzene represents the most used component in the design of photoresponsive systems.

[62] Bandara, H.M.D.; Burdette, S.C.; *Chem. Soc. Rev.,* **2012,** 41,1809-1825

The first example of supramolecular self-assemblies modulated by light have been proposed by Shinkai et al. in 1987. An azobenzene functionalized by a crown ether on one end and an ω-ammoniumalkyl chain on the other, has been prepared. As reported in
Figure 21a, a self-assembled system consisting of cyclic oligomers forms in organic media when in trans state, while in the cis state the molecule exists as discrete monomer. Another example is represented by a mixed system composed of an azo-dicrown ether and an oligomethylene-α-ω-diammonium cation (
Figure 21b): as in the previous example, a polymeric assembly is formed by the trans isomer. In both examples, cis isomer can form only "closed" supramolecular structures, and its less aggregative behavior is due to a bent conformation, that turns out disadvantageous for dense molecular packing.

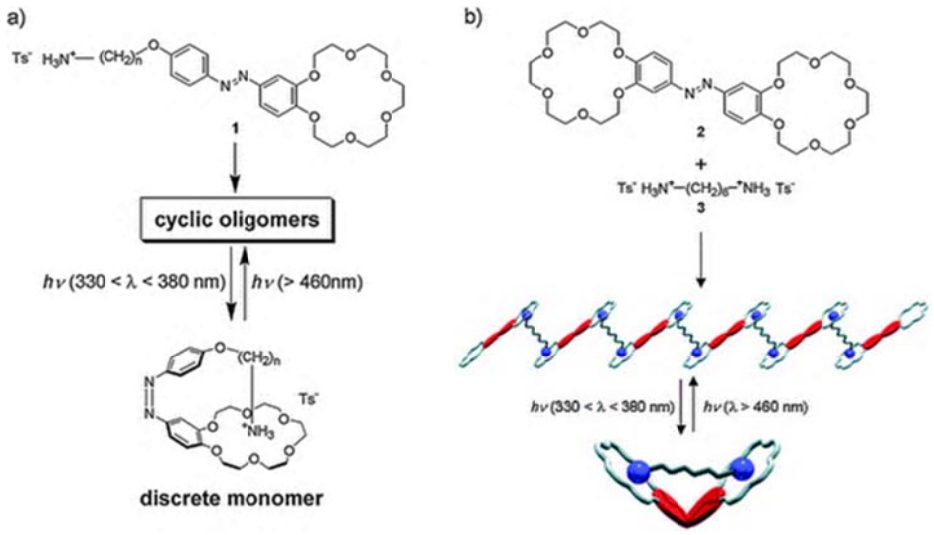

Figure 21: Photoresponsive self-assemblies established by Shinkai et al. (a) One-component system achieved by self-complementary azobenzene functionalized on one end by an ω-ammoniumalkyl and on the other by a crown ether. (b) Two-component system achieved by the mixture of symmetrical azocrown and α,ω-diammoniumalkane.

Sever azobenzene-based molecular devices have been designed for the inclusion and complexation of some ions, such as azophanes, azocrowns[63], azocryptands, azocyclodextrins and

[63] (a) Shinkai, S.; Manabe, O. *Host Guest Complex Chemistry,Macrocycles;* Springer-Verlag: Berlin, **1983**; (b) Kimura, K.; Mizutani, R.; Suzuki, T.;Yokoyama, M. *J. Inclusion Phenom. Mol. Recognit. Chem.* **1998,** *32,* 295–310; (c) Naemura, K.; Ueno, K.; Takeuchi, S.; Tobe, Y.; Kaneda, T.; Sakata, Y.

azocalixarenes[64]. The aza-crown ether showed in Figure 22 when in trans state has an oval-shaped ring structure, with high affinity for small metal ions such as Na^+, whereas the round-shaped ring structure of the cis-form shows greater affinity for larger metal ion K^+.

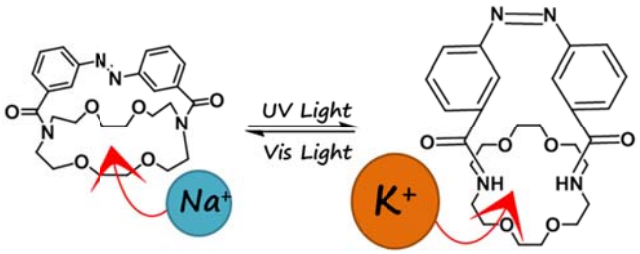

Figure 22: Complexation of metal-alkali ions for different isomers of crown ether.

Another similar system is reported in Figure 23:

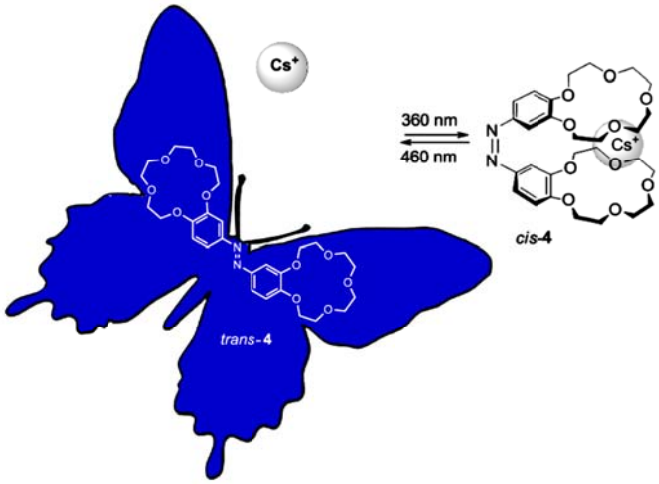

Figure 23: Butterfly-like movement upon irradiation of an azodicrown ether and its ability to complex cations.

This azodicrown ether has been used to remove cations from aqueous solutions, taking advantage of the butterfly motion upon irradiation, where the cis form can trap cations between the two rings in a "sandwich" structure.

J. Am. Chem. Soc. **1993,** *115,* 8475–8476. (d)104.Tamaoki, N.; Wada, M. *J. Am. Chem. Soc.* **2006,** *128,* 6284–6285.

[64] (a) Fujimaki, M.; Matsuzawa, Y.; Hayashi, Y.; Ichimura, K. *Chem. Lett.***1998,** *27,* 165–166. (b).Kim, J. S.; Shon, O. J.; Lee, J. K.; Lee, S. H.; Kim, J. Y.; Park, K.-M.; Lee, S. S. *J. Org. Chem.* **2002,** *67,* 1372–1375. (c) Gu, R.; Depraetere, S.; Kotek, J.; Budka, J.; Wagner-Wysiecka, E.;Biernat, J. F.; Dehaen, W. *Org. Biomol. Chem.* **2005,** *3,* 2921–2923.

Chapter II

Cyclodextrin and azobenzene

1 Photoresponsive supramolecular systems based on host-guest interactions

1.1 Introduction on Cyclodextrins

Among the enormous variety of macrocycles, natural and synthetic, cyclodextrins (CyDs) are the most widely receptors used in inclusion host/guest chemistry, as thet are able to form stable complexes with a great number of guest molecules. CyDs are natural cyclic oligosaccharides, produced from starch by means of enzymatic conversions and are used in a great variety of industrial fields, pharmaceutical[65], in particular drug delivery[66], and chemical industries, as well as agriculture and environmental engineering. CyDs are composed of 5 or more α-D-glucopyranoside units connected through glycosidic α-1,4 bonds, and the most common contain six, seven or eight units of glucose monomers , and are named α-, β- and γ-cyclodextrin, respectively (Figure 24).

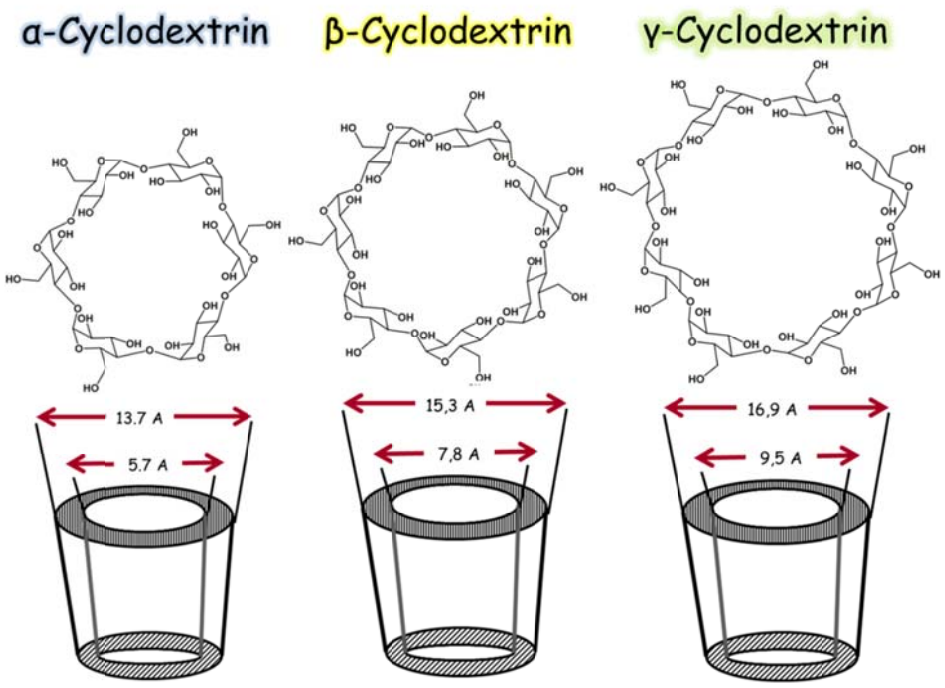

Figure 24: Most readily available cyclodextrins formed by six, seven and eight units, respectively named α-, β- and γ-cyclodextrin.

[65] Kanaka Durga Devi N.et al., *Journal of Global Pharma Technology*, **2010**; 2(11): 1-10

[66] Thatiparti, Thimma R.; Shoffstall, Andrew J.; Von Recum, Horst A., *Biomaterials* 31, **2010**, 2335–47

CyDs containing less than six glucose units are too strained to exists, while those with more than eight units are very difficult to isolate.

CyDs are characterized by a conical cylinder shape, generally pictured as a shallow truncated cone, where all secondary hydroxy groups are situated on one of the two edges of the ring, while on the other edge are situated the primary hydroxyl groups[67], as shown in Figure 25. The primary hydroxy rim of the cavity has a reduced diameter in comparison with the secondary hydroxy groups rim. CyDs cavity results hydrophobic, as a consequence of hydrogen bonds between secondary hydroxy groups in 2 position of each glucopyranoside unit and hydroxyl groups in 3position of the adjacent glucopyranose unit; the hydrophobicity of the cavity makes CyDs ideal hosts with high ability to complex apolar guest molecules in aqueous solution. The dimension of the cavity grows increasing the number of glycosidic units, and intra-molecular hydrogen bonds make these cyclic structures well defined and rigid. Despite the rigidity of these molecules, a significant conformational mobility remains, that is at the basis of the ability of these molecules to fit the size of the guest. In particular it has been established that α and β-cyclodextrins are more flexible than γ-cyclodextrin.

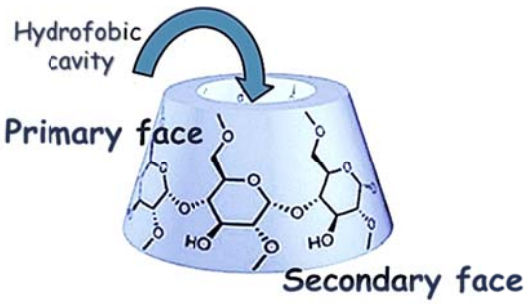

Figure 25: Schematic representation of cyclodextrin, pictured as a shallow truncated cone.

In aqueous solution, the cavity is filled by water molecules, which can be easily replaced by another guest, if less polar than water; so the driving force for the formation of aggregates is represented by the substitution of different "guests", based on a greater affinity for the cavity of cyclodextrins. Besides natural CyDs, widely investigated by Schardinger and Cramer[68], a great number of modified CyDs have been reported in literature. Sever functional group have been used, such as alkyl, hydroxylalkyl, carboxylalkyl, amino, thiol, tosyl groups able to complex organic and inorganic compounds and metal to witness to their huge versatility. The functionalization of hydroxyl groups by ether or ester linkages improves the host solubility and increases the affinity of

[67] J. Szejtli, *Chem. Rev.* **1998,** *98,* 1743-1753

[68] Cramer F., *Angew. Chem.,***1952,** 64 (5),136; (b) Cramer, F., *Chemische Berichte,* **1951,** 84 (9), 851-854

Cyds for a particular target. Several properties have been investigated, such as acid hydrolysis[69], molar volumes[70], activity coefficient, diffusion coefficients[71], and solubility in dimethylformamide[72].

In Table 1 are listed some common properties of the CyDs.

property	cyclodextrin α	β	γ
no. glucose units	6	7	8
empirical formula (anhydrous)	$C_{36}H_{60}O_{30}$	$C_{42}H_{70}O_{35}$	$C_{48}H_{80}O_{40}$
mol wt (anhydrous)	972.85	1134.99	1297.14
cavity length, Å	8	8	8
cavity diameter, Å (approx)	~5.2	~6.6	~8.4
α_D, deg	+150.5	+162.0	+177.4
heat capacity (anhyd solid), J mol^{-1} K^{-1}	1153	1342	1568
heat capacity (infinite diln), J mol^{-1} K^{-1}	1431	1783	2070
pK_a (25°)	12.33	12.20	12.08
$\Delta H°$ (ionization), kcal mol^{-1}	8.36	9.98	11.22
$\Delta S°$ (ionization), cal mol^{-1} K^{-1}	−28.3	−22.4	−17.6
solubility (water, 25°), mol L^{-1}	0.1211	0.0163	0.168
$\Delta H°$ (solution), kcal mol^{-1}	7.67	8.31	7.73
$\Delta S°$ (solution), cal mol^{-1} K^{-1}	13.8[a]	11.7[a]	14.7[a]

[a] Mole fraction standard state.

Table 1: Common properties of α-β- and γ cyclodextrin.

Properties listed in Table 1, show apparently a regular trend increasing the number of glucose units. Focusing on solubility, it is possible to estimate that β-CyD, between all CyDs. results to be less soluble. One explanation of β-CyD low solubility has been proposed by Szejtli, who attributed it as a consequence of intramolecular hydrogen bonds. On the other hand Coleman et al attributed low solubility of β-CyDs to the interruption by aggregated of the hydrogen bond structure of water.

Hydration:

CyDs crystallize from water as hydrates: in particular it has been reported that α-CyD usually exists as hexahydrate form, β-CyD as undecahydrate or dodecahydrate form[73], and γ-CyDs can crystallize

[69] Szejtli, J.; Budai, Z. *Acta Chim. Acad. Sci. Hung*. **1976**, *91*, 73.

[70] Miyajima, K.; Sawada, M.; Nakagaki, M. *Bull. Chem. Soc. Jpn*.**1983**, *56*, 3556.

[71] Craig, L. C.; Pulley, A. O. *Biochemistry* **1962**, *1*, 89.

[72] Danil de Namor, A. F.; Traboulssi, R.; Lewis, D. F. V. *J. Am. Chem. Soc*. **1990**, *112*, 8442.

[73] (a) Lindner, K.; Saenger, W. *Angew. Chem., Int. Ed. Engl*. **1978**, *17*, 694. (b) Fujiwara, T.; Yamazaki, M.; Tomizu, Y.; Tokuoka, R.; Tomita, K.; Matsuo, T.; Suga, H.; Saenger, W. *Nippon Kagaku Kaishi* **1981**, 181.

with from 7 to 18 molecules of water. About α-CyD it has been reported that α-CyD*6H_2O can exist in three different crystal forms. α-CyD*6H_2O form I consist of two water molecules inside the cavity, fixed to each other by hydrogen bonds, and four molecules outside[74], α-CyD*6H_2O form II with one water molecule inside the cavity, whereas the III form, crystallized from an aqueous solution of $BaCl_2$, contains 2.57 water molecules inside the cavity. It has been noticed that in γ and β-CyDs water molecules inside the cavity are distributed among alternate sides, as in the case of α-CyD form III, while the fixed location in α-CyD form I and II is unusual. As consequence, in these crystalline forms, α-CyD's ring has not 6-fold symmetry and consequently shows an higher conformational strain energy. The strain energy seems to be the energy accompanying the inclusion phenomena.

Polarity of the CyDs cavity:

Early studies on CyDs's cavity date back to 1967 when Van Etten et al[75] investigated UV spectra of 4-*tert*-butylphenol in an aqueous solution of α-CyD, in order to determine the polarity of the host cavity. It was found that UV spectra of the complex in aqueous solution did not differ from the one recorded in dioxane. Subsequent studies carried out by the same group, focused just on inclusion phenomena of the aromatic chromophore inside the cavity, but did not justify the results obtained on the various classes of CyDs in different solvents regarding the polarity. Later a great variety of fluorescent molecules and their inclusion complexes have been investigated, because fluorescence quantum yield is sensitive to the polarity of the probe's environment[76].

It was thanks to the studies by Linert et al, that it was possible to determine the polarity of the cavity of the cyclodextrins. Linert et al reported that the cavity of β-cyclodextrins was hydrophobic, while the one of α-cyclodextrin could not be defined as such. Trough Gibbs energy's measurements (carried out by Connors et al as a function of molar ratio of the co-solvent in a binary mixture water-organic solvent) and the affinity constant of the complex in different solvents, it was possible to determine the effective polarity of the cavity of CyDs. Results showed that cosolvents could be divided in two classes: more or less polar than *log P = -0.3,* (P = partition coefficient of 1-

[74] (a) Manor, P. C.; Saenger, W. *Nature* **1972**, *237*, 392. (b) Manor, P. C.; Saenger, W. *J. Am. Chem. Soc*, **1974**, *96*, 3630.

[75] Van Etten, R.L., Sebastian J.F., Clowes, G.A., *J.Am.Chem.Soc.,***1967,** 89,3242.

[76] (a) Turro, N. J.; Okubo, T.; Chung, C. J. *J. Am. Chem. Soc* **1982**, *104*, 3953. (b) Cox, G. S.; Turro, N. J.; Yang, N. C.; Chen, M. J. *J. Am. Chem. Soc* **1984**, *106*, 422. (c) Hamai, S. *J. Phys. Chem*. **1990**, *94*, 2595.

octanol/water, used as a measure of hydrophobicity), that is the effective polarity of the cavity of α-CyD. More polar solvent are less competitive to form complex, while less polar solvent spread easily in the internal cavity[77].

Binding equilibria and Kinetics:

Typically cyclodextrins can form inclusion complexes with different stoichiometric ratios[78]: as a function of the size of the cavity, it can be 1:2, and 1:1 (Figure 26).

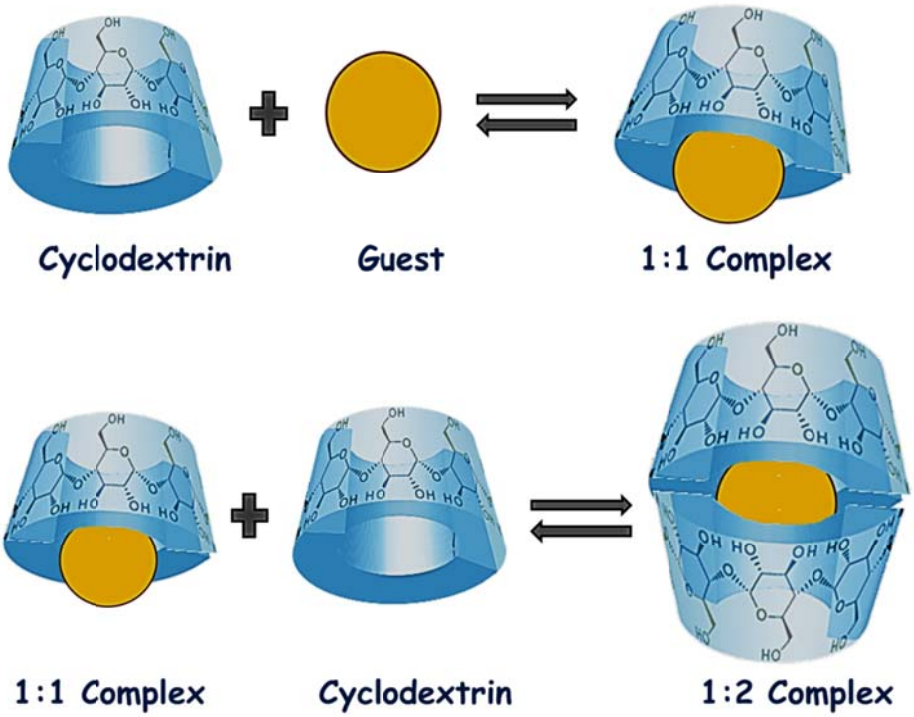

Figure 26: Cyclodextrin's inclusion complexes with different stoichiometric ratio (1:1, 1:2).

CyDs's complexes can form via a bimolecular process, according to the follow equilibria:

$$S + L \leftrightarrows \mathrm{SL}$$

$$SL + L \leftrightarrows SL_2$$

[77] Milski, M.J., Connors, K.A., *Supramol. Chem.,* **1995,** 4, 271

[78] (a) Funasaki, N.; Yodo, H.; Hada, S.; Neya, S. *Bull. Chem. Soc. Jpn*. **1992**, *65*, 1323. (b) Junquea, E.; Tardajos, G.; Aicart, E. *J. Colloid Interface Sci*. **1993**, *158*, 388. (c) Gomez-Orellana, I.; Halle´n, D. *Thermochim. Acta* **1993**, *221*, 183. (d) Hamai, S. *Bull. Chem. Soc. Jpn*. **1982**, *55*, 2721. (e) Buvari, A.; Szejtli, J.; Barcza, L. *Acta Chim. Acad. Sci. Hung*. **1982**, *110*, 51. (f) Kobayashi, N.; Saito, R.; Hino, H.; Hino, Y.; Ueno, A.; Osa, T. *J. Chem. Soc*., *Perkin Trans*. 2 **1983**, 1031.

$$SL + S \leftrightarrows S_2L$$

In which S represents the *guest*, and L is the *host*. The binding constant can be obtained as follows:

$$K_{11}=\frac{[\,\mathrm{SL}]}{[S]\,[L]}$$

$$K_{12}=\frac{[\,\mathrm{SL_2}]}{[SL]\,[L]}$$

$$K_{21}=\frac{[\,\mathrm{S_2L}]}{[SL][S]}$$

It is also common to define a dissociation constant that is the reciprocal of binding constant. Depending on the properties of the guest molecule, it is possible to follow the association process, through several methods, such as optical spectroscopy, (UV absorption, Circular Dichroism, Fluorescence). Upon the formation of a complex, several chemical and physical properties of the guest can change[79], for example:

- *Chemical shift* in NMR spectra;
- *Optical activity* induced on a non-chiral guest after complexation, as consequence of cyclodextrin chirality;
- *Reactivity* of the guest molecule can decrease after the formation of a stable complex; or in other cases, cyclodextrins can act as artificial enzymes, increasing the rate of the reactions or changing their course;
- *Solubility* of the guest molecule can increase in aqueous solution, while *diffusion and volatility* decrease drastically.

In this chapter will be presented the main methods used to confirm the formation of aggregates by optical techniques and calorimetric titration.

[79] Freudenberg, K.; Cramer, F.; Plieninger, H. *Ger. Patent*, 895769, **1953**.

2 Host-guest inclusion complex between azobenzene and cyclodextrins

As described in Chapter I several examples of photo-responsive switches have been reported in literature. One of the most important systems are azobenzene derivatives. It is well known that azobenzene has a great affinity for the cavity of Cyds, in particular for α-CyDs. Photo-responsive self-assemblies of water soluble polymer p(AA/C12) (figure 27) have been reported by Harada et al.[80]. An hydrogel is formed by solvophobic interactions between aliphatic chains of poly(acrylicacid) p(AA/C12) modified with dodecyl groups. After addition of αCD, gel to sol transition occurs, as consequence of the formation of complexes between the aliphatic chain and αCD, disrupting their solvophobic interaction.

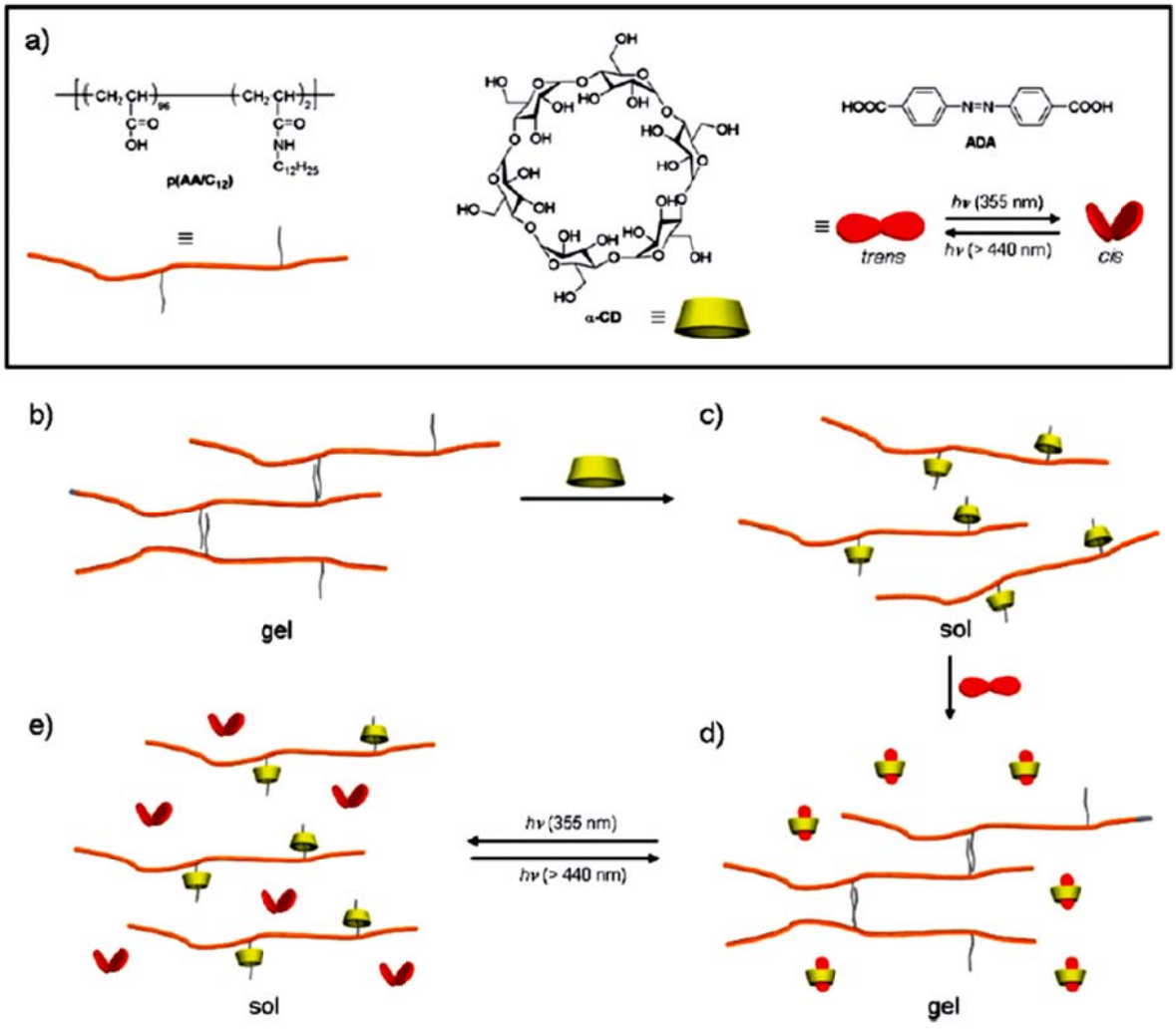

[80] I. Tomatsu, A. Hashidzume and A. Harada, *Macromolecules*, **2005**, *38*, 5223–5227.

Figure 27: (a) Structure and cartoon representations of aqueous polymer p(AA/C12), azobenzene dicarboxylic acid (ADA) and αCD. (b–e) Schematic representation of the self-assembly of aqueous polymer p(AA/C12) controlled by the photoresponsive complexation between ADA and αCD.

When azobenzene dicarboxylic acid is added to the mixture, sol-gel conversion occurs, because αCD has greater affinity for trans azobenzene, so once again the interaction between aliphatic chain afford hydrogels. Upon irradiation with UV light, trans azobenzene is converted to cis isomer, which has less affinity for αCD, thus gel to sol conversion results. This system represents one of the most fascinating photoresponsive self-assemblies of polymer, driven by a photo-responsive key[81]. Another photoresponsive self-assembled system has been reported by the same group[82].

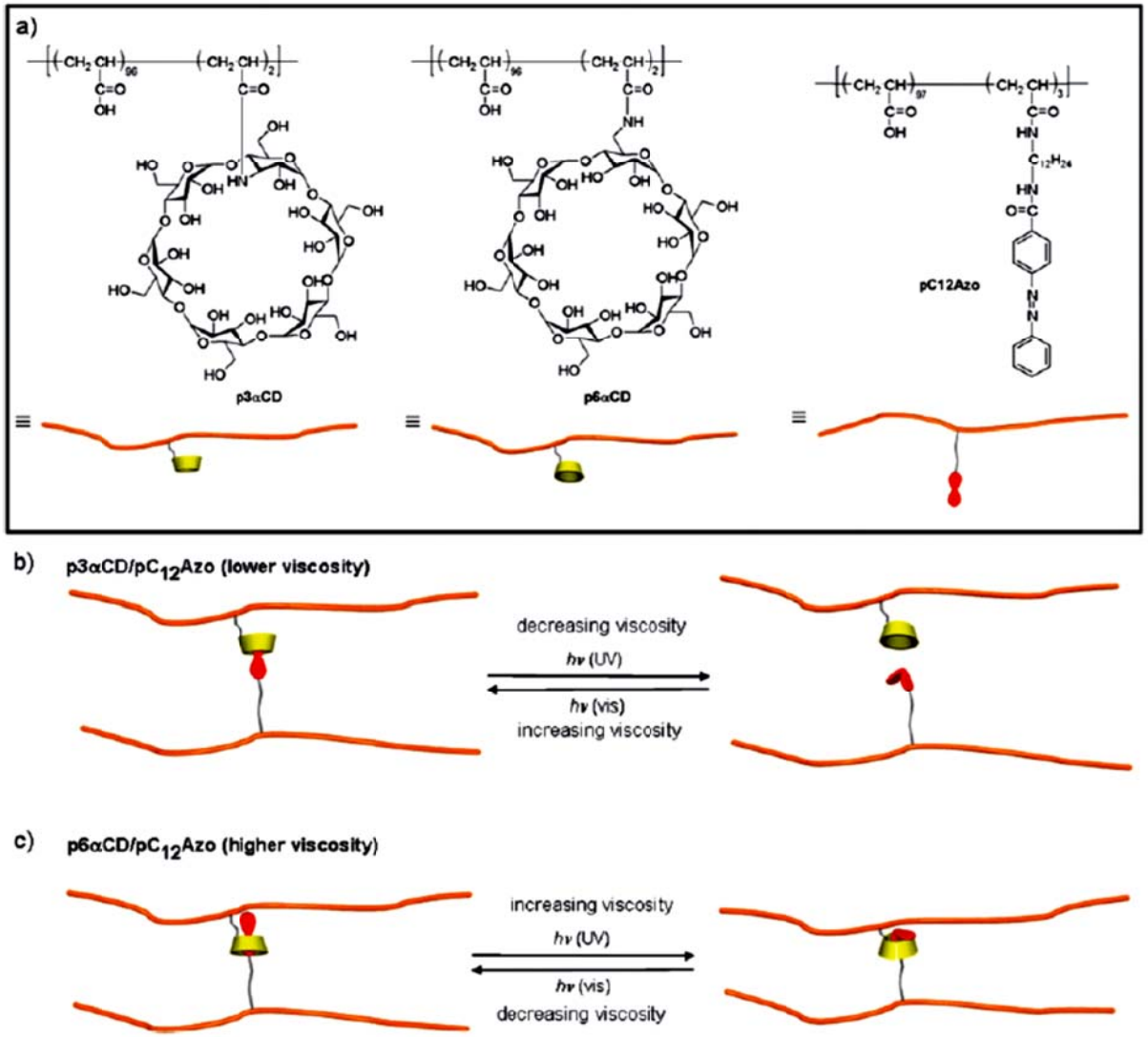

[81] T. Muraoka, K. Kinbara and T. Aida, *J. Am. Chem. Soc*., **2006**, *128*, 11600–11605

[82] I. Tomatsu, A. Hashidzume and A. Harada, *J. Am. Chem. Soc*., **2006**, *128*, 2226–2227.

Figure 28: (a) Structures of crown-appended polymers p6αCD and p3αCD, and azobenzene-C12-modified polymer pC12Azo. (b and c) Schematic representations of photoresponsive self-assemblies of polymer mixtures p3αCD/pC12Azo and p6αCD/pC12Azo, respectively.

Two water soluble polymers, possessing cyclodextrin pendant groups, consisting of either αCD is connected at 3- position of a glucose ring, (p3αCD) or αCD is connected at 6- position of a glucose ring, (p6αCD) have been prepared. Another complementary photoresponsive polymer has been prepared, containing azobenzene-functionalized dodecamethylene pendants. The mixture of the guest and host polymer generate a cross-linked assembly trough the complexation of azobenzene moieties on C12polymer and αCD. The steady state viscosity measurements of semidilute solutions showed that Z value of p6αCD/pC12Azo had a greater value compared to p3αCD/pC12Azo. These results showed the different affinities for the two binary mixtures as function of the local interactions mode. By 2D-NMR Dosy experiments, it was observed that for p3αCD/pC12Azo the interaction occurred mainly between azobenzene and αCD, whereas for p6αCD/pC12Azo interactions involved C12 and αCD. Viscosity measurements after irradiation with UV light, showed an increased Z value for p3αCD/pC12Azo, and a decreased value for p6αCD/pC12Azo. Noesy measurements showed that upon irradiation no more interaction occurred between azobenzene moiety and αCD for p3αCD/pC12Azo, whereas p6αCD and pC12Azo remained interlocked even after trans to cis isomerization.

2.1 Artificial muscles based on azobenzene and αCD

Besides sol-gel switching, a great variety of macroscopic effects can be observed based on interactions between azobenzene and CyDs, such as self-healing and artificial muscles.

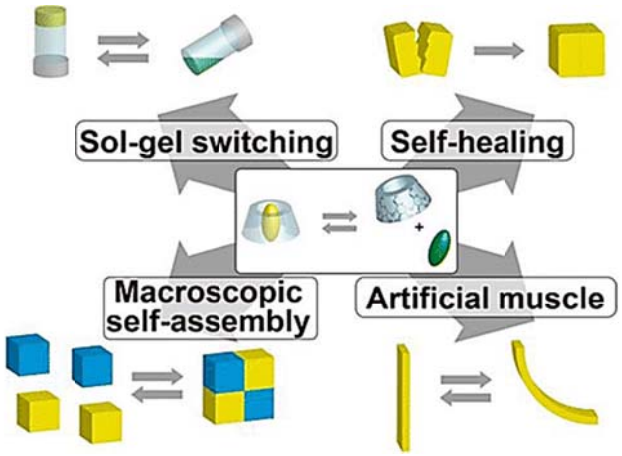

Figure 29: Macroscopic effect observed on interactions between azobenzene and CyDs.

Polymer based actuators, similar to that of actin filaments-based muscle fibrils can be to realized and they show stimuli responsive expansion-contraction properties. A schematic representation of an αCD-azobenzene hydrogels is reported below. Expansion-contraction behavior in hydrogel occurs upon ultraviolet and Vis light irradiation, as consequence of aggregation-disaggregation phenomena between host and trans and cis isomers guest.

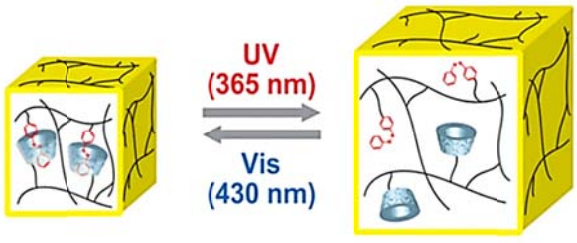

Figure 30: Representative example of an expansion-contraction behavior of αCD-azobenzene hydrogels.

Based on the same systems, it has been noticed that bending phenomena can be correlated to the incident light.

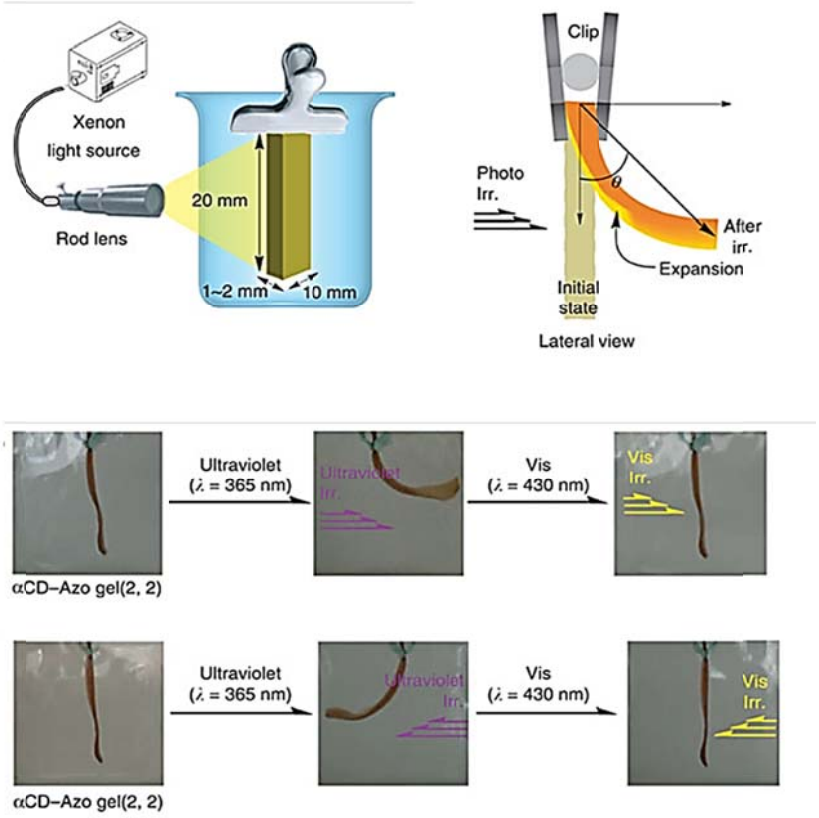

Figure 31: Experimental devices and bending behavior upon photo-isomerization of αCD–Azo gelAzo gel

In particular irradiating the gel at 365 nm from the left side, the gel can bend to the right, whereas irradiating at 430 nm from the same side, the gel returns to its initial condition. It can be summarized that αCD-azobenzene hydrogel bends in the opposite direction of the incident light[83].

2.1.1 Aggregation-disaggregation phenomena monitored via colligative properties

A prototype of a light-powered engine it has been reported by our group in 2008, based on conversion of light into continuous mechanical energy by photo-reversible self-assembly[84]. As reported previously, trans azobenzene isomer has an energy content lower than cis form, thus energy is "harvested" from light and "stored" in the cis isomer. Coupling aggregation and disaggregation phenomena with a change in concentration upon photo-isomerization, the energy

[83] Takashima, Y. et al., *Nat. Commun*., **2012**, 3:1270

[84] Masiero S, Lena S, Pieraccini S, Spada GP, *Angew Chem Int Ed Engl.* **2008**;47(17):3184-7

"harvested" by cis isomer can be converted into a mechanical work, taking advantage from colligative properties, in particular osmosis (Figure 32).

Figure 32: Experimental osmotic cell.

An azodicarboxylic acid derivative, able to aggregate/disaggregate upon photo-isomerization, has been designed. Conformational constrictions make the *Z* isomer exist as an intramolecularly H-bonded, soluble monomer. On the other hand, owing both to the solvent polarity and its ability to compete for H-bonding, the *E* isomer exists in solution as a dynamic distribution of intermolecularly H-bonded, low order supramolecular oligomers. These oligomers, on growing, become insoluble and precipitate to form an extensively H-bonded solid.

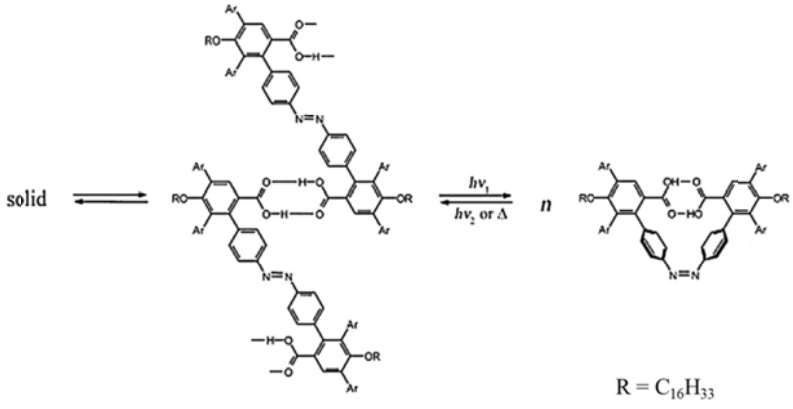

Figure 33: Photoresponsive self-assemblies of azodicarboxylic acid derivative.

In an osmotic cell, both compartments were loaded with a suspension of unirradiated (*E*)-derivative in acetone so that levels were the same. One compartment was alternately irradiated with UV and Vis light, while the opposite was done on the other side. In the compartment where the *E*-

to-*Z* photoisomerization occurs, disaggregation produce an increase in concentration, which makes the solution hypertonic with respect to the solution in the other compartment. In contrast, in the compartment where the *Z*-to-*E* retroisomerization takes place, aggregation and crystallization lower the net concentration of the solution, making it hypotonic with respect to the other. Thus, a flow of solvent takes place from the latter to the first compartment. Inverting the wavelengths shone onto the two compartments reverts the flow, and the overall result is an alternate flow of solvent from one side to the other, with a continuous variation of solvent levels. Thus, the energy harvested from light is transformed continuously into mechanical energy in the form of work necessary to raise and to lower the solvent level.

2.2 Supramolecular photo-responsive polymers: Aim of the project and results

The aim of the project is the design and the characterization of a supramolecular inclusion polymers, able to disaggregate upon photo-isomerization, in order to obtain a photo-controlled concentration change and thus a macroscopic solvent flow through the osmotic cell, previously described.

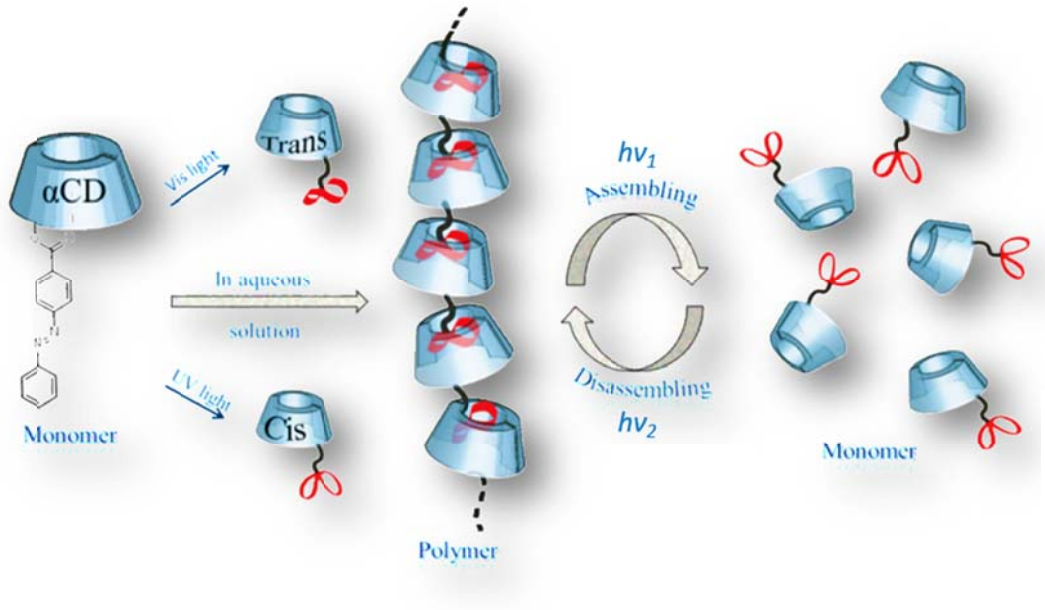

Figure 34: Aim of the project *Photoresponsive supramolecular architecture based on α-cyclodextrin functionalized with azobenene.*

In this project photoresponsive assembling/disassembling behavior of a supramolecular complex based on α-cyclodextrins functionalized with different azobenzene moieties has been studied in

aqueous solution. As reported previously azobenzene undergoes trans to cis isomerization when irradiated with light tuned to an appropriate wavelength, (275–340 nm). The reverse cis to trans isomerization can be driven by light, (245–265 nm or 350–440 nm) or occurs thermally in the dark, Additional substituents on the azobenzene ring system could change the spectroscopic properties and isomerization mechanism. Usually, the photo-stationary state is reached under UV irradiation at 340 nm, and then the back photo-isomerization is carried out under irradiation at 254 nm. Unfortunately αCD-azobenzenene derivatives showed low solubility in aqueous solution, probably due to the formation of the polymer in the trans state, as confirmed by the higher solubility of the cis state. Several techniques, such as two-dimensional NMR, diffusion coefficient measurements, electrospray ionization mass spectroscopy (ESI-MS) and Circular Dichroism, have been used to characterize the formation of a supramolecular oligomer in aqueous solution and its disaggregation upon photo-isomerization. Moreover preliminary study on a model system constituted by Azobenzene carboxylate and cyclodextrines in aqueous solution allow us to obtain information about the constant of association, aggregation/disaggregation phenomena and results obtained have been used to compare data for the linked systems.

2.3 Syntesis of Azo-Cyclodextrins: general mechanism

In this paragraph it is shown the synthetic strategy to obtain mono-functionalization of α-cyclodextrins at the secondary face. As previously reported α-Cyclodextrins can form inclusion complexes with azobenzene in a 1:1 ratio, for this reason it have been synthetized monofunctionalized derivatives. Furthemore in order to avoid the formation of intramolecular complexes, the linker has to be shorter as possible, but flexible, and for this reason the azobenzene moieties have been attached via ester bond.

a) Synthesis of azobenezene

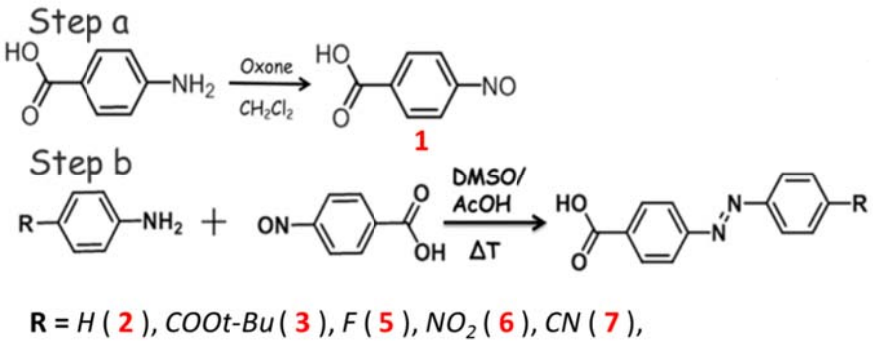

R = *H* (**2**), *COOt-Bu* (**3**), *F* (**5**), NO_2 (**6**), *CN* (**7**),

Azobenzene carboxylic acids have been obtained via condensation reaction between different p-substituted anilines and p-nitrosobenzoic acid, previously obtained by biphasic oxidation of 4-aminobenzoic acid with oxone[85].

[85] a) Estíbaliz Merino**, Chem. Soc. Rev., 2011, 40,** 3835-3853. b) B. Priewisch. K. Rück-Braun, *J. Org. Chem.*, **2005**, *70* (6), pp 2350–2352.

b) Protection of Cyclodextrins

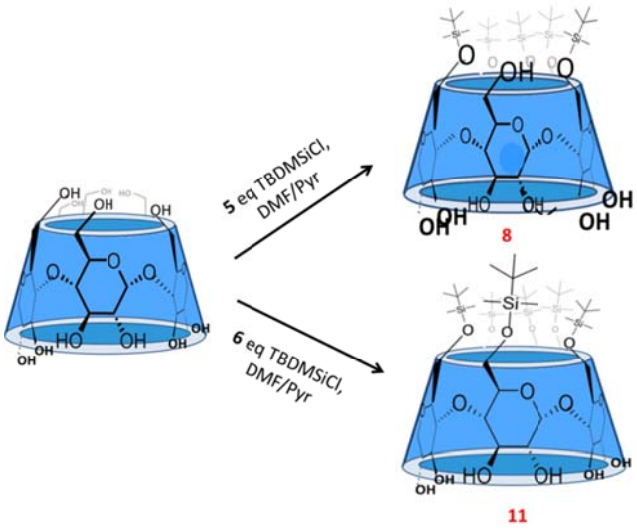

In litterature it is well documented that complexes formed by inclusion of the host from the primary side of αCD are more stable than those arising from secondary side inclusion. On the other hand, the presence of many, more or less, equally reactive hydroxyl groups implies a problem of regioselectivity. In order to obtain a regioselectivity in the synthesis of secondary face mono-functionalized cyclodextrins, and we focused on the use of partially silylated cyclodextrins, in which the primary hydroxyls groups have been converted to silyl ethers. [86] This transformation brings extra advantages, as silylated cyclodextrins are both soluble in various organic solvents and easily purified by common silica gel chromatography. On the other hand in order to obtain di-functionalized αCD, derivative 8 have been designed, where secondary hydroxyl groups and one of the secondary hydroxyl group is not protected.

[86] (a) K. Takeo, K. Uemura, H. Mitoh, *J. Carbohydr. Chem*. **1988**, *7*, 293; (b) K. Takeo, H. Mitoh, K. Uemura, *Carbohydr. Res.* **1989**, *187*, 203; (c) P. Fiigedi, *Carbohydr. Res*. **1989**, *192*, 366; (d) T. J. Michalski, A. Kendler, M. L. Bender, *J. Incl. Phenom*. **1983**, *1*, 125; (e) R. L. Wife, D. E. Reed, D. P. Leworthy, D. M. Barnett, P. D. Regan, H. C. Volger, *Advances in Inclusion Science*, *Proceedings of the 1st International Symposium on Cyclodextrins*; J. Szejtli, Ed.; Akademiai Kiado: Budapest, **1982**; 301.

c) Synthesis of Silylated αCD-azobenzene derivatives

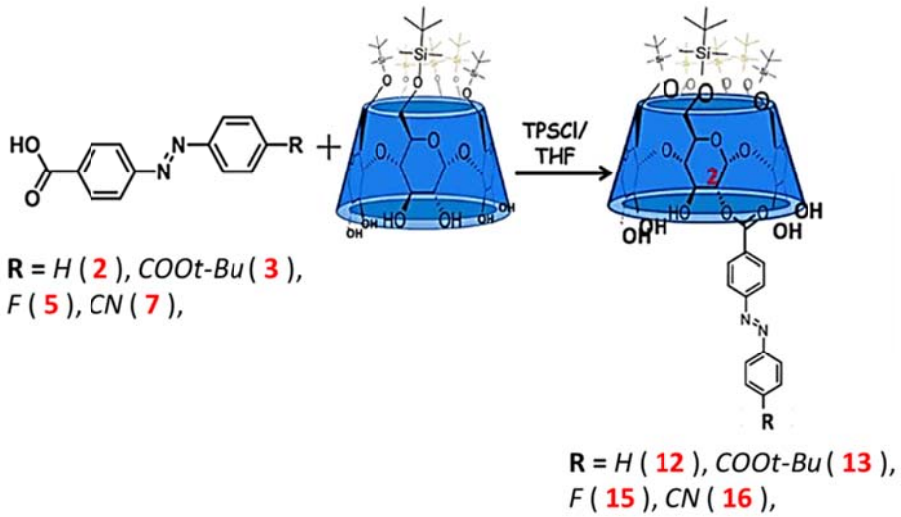

Silylation of primary hydroxyl groups allows to introduce directly and selectively the azobenzene residue on the secondary hydroxyl face of silylated cyclodextrin *via* acylation of the C(2)-hydroxyl, leaving the configuration of all glucose units in the cyclodextrin intact. It has to be noticed that the regioselectivity of the esterification had to be proved, through 2DNMR experiments. Another important aspect to be reckoned with, is to prevent the formation of an intra-molecular complex; thus the bond has to be as short as possible but flexible. In this project photo-responsive azobenzene moieties were attached on the secondary side of αCD via an ester linkage.

d) Deprotection of Sylilated αCD-azobenzene derivatives

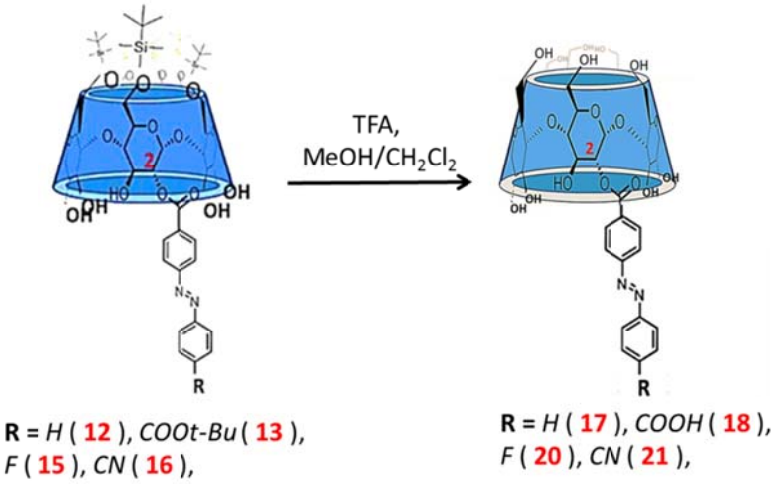

Deprotection of the silylated primary hydroxyls with trifluoro acetic acid yielded αCD monofunctionilized with azobenzene derivatives. Below it is reported the schematic procedure to obtain di-functionalized derivative:

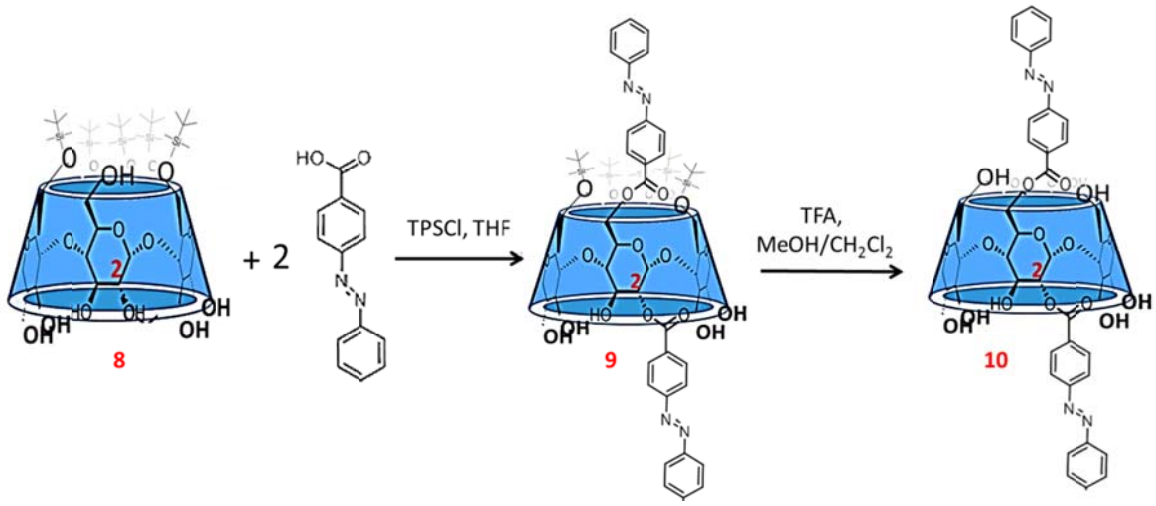

2.4 Methods to study aggregation/disaggregation phenomena

2.4.1 UV titration

For a chromophore located inside the cavity, Benesi Hildebrandt equation can be useful for the determination of the association constant. This method was developed by Benesi and Hildebrand in 1949[87] in order to explain the change of color of iodine in different aromatic solvents. They proposed that a iodine-solvent complex could form through acid-base interactions, and as consequence of aggregation phenomena a shift in the absorption spectrum can be observed. Later, the *Benesi-Hildebrand* method has become one of the most common methods to determine association constants based on absorbance spectra. If H is the host, G is the guest and HG is the complex, the absorbance is the sum of each component, as reported:

$$A = A^{HG}+A^{G}+A^{H}$$

If the initial concentration of the guest is greater than the concentration of the host, then the absorbance referred to the host, (A^{H}), should be negligible.

[87] Benesi H, Hildebrand J, *J. Am. Chem. Soc.* 71(8): **1949,** 2703–07.

$$A = A^{HG} + A^{G}$$

Following the formation of the complex, after several additions of the host, a change in absorbance is what is experimentally recorded, (ΔA), with A_0 corresponding to the initial absorbance before complex is formed, and A the absorbance recorded after each addition.

$$\Delta A = A - A_0$$

Using Lambert-Beer equation, it is possible to write the previous equation as:

$$\Delta A = \varepsilon^{HG}[HG]b + \varepsilon^{G}[G]b - \varepsilon^{G}[G]_0 b$$

where b is the optical path.
Considering, as before, that $[G]_0 >> [H]_0$, it is correct to assume that [G] is equal to $[G]_0$.

$$\Delta A = \Delta\varepsilon\,[HG]b$$

where Δε is the change in value between ε^{HG} and ε^{G}.
The change in concentration as a function of the other component can describe a binding isotherm, as in the following equation.

$$[HG] = \frac{[H]_0 K_a [G]}{1 + K_a [G]}$$

Substituting the binding isotherm equation into the previous equation, the equilibrium constant K_a can be correlated to change in absorbance.

$$\Delta A = b\Delta\varepsilon \frac{[H]_0 K_a [G]}{1 + K_a [G]}$$

And then:

$$\frac{1}{\Delta A} = \frac{1}{b\Delta\varepsilon [G]_0 [H]_0 K_a} + \frac{1}{b\Delta\varepsilon [H]_0}$$

Δε can be obtained from intercept, while K_a can be calculated from the slope.

2.4.2 Circular Dichroism

Different techniques can be applied for the study and characterization of supramolecular architectures, and in particular it results fundamental for reversible systems to verify by these methods all changes in the system, as fluctuations of its physico-chemical characteristics. One of the most advantageous technique used to monitor aggregation/disaggregation phenomena in solution is represented by Circular Dichroism.

The circular dichroism (CD) is a simple variation of the normal absorption spectroscopy: the difference consists in the use of polarized light. The circularly polarized light has an electric vector of constant intensity, which varies in direction in time and space. Through a photo-elastic modulator two right and left circularly polarized components can be generated alternately.

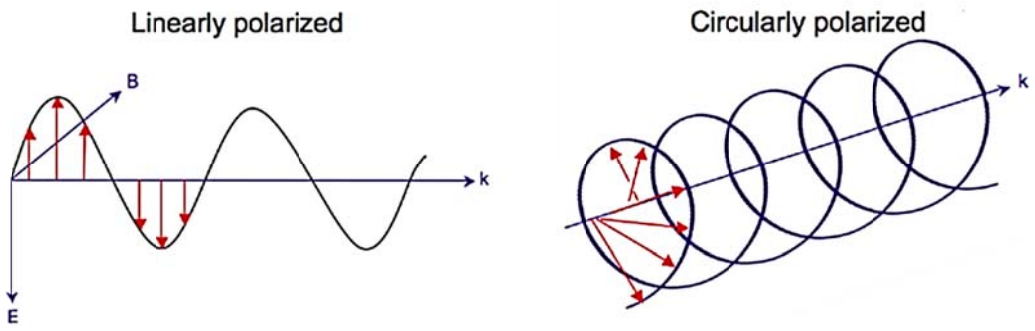

Figure 35: Schematic representation of linearly and circularly polarized light.

When circularly polarized light passes through an absorbing optically active medium, the extent to which right and left polarized lights are absorbed is different ($\varepsilon_L \neq \varepsilon_R$). *Circular dichroism* is the difference $\Delta\varepsilon \equiv \varepsilon_L - \varepsilon_R$. As the light emerging from the sample is thus elliptically polarized, the CD signal can be measured directly by ellipticity (θ) oftransmitted light according to the formula:

$$\theta = arctan\ (b/a)$$

where *a* and *b* are major and minor axis of the ellipse, respectively.

[Θ] it is the molar ellipticity, a parameter expressing the change of ellipticity regardless of the conditions of measurement:

$$[\Theta] = \theta\ \ 100 / cl$$

Where *c* is the concentration of the sample in moles / L and *l* the optical path in cm.
The absorption of these components follows the law of Lambert-Beer, and in the CD spectra two types of absorption can be obtained, one for component

$$A_L - A_R = \Delta A = (\varepsilon_L - \varepsilon_R)\, lc = \Delta\varepsilon_{lc}$$

Where *L* and *R* respectively indicate the rotation levorotatory and dextrorotatory, *A* indicates the absorbance and *Δε* is the molar extinction coefficient differential.
Δε recorded as a function of the wavelength generates a spectrum with bands associated with the electronic transitions of the chromophore. These bands may be positive or negative depending on which circularly polarized radiation is absorbed more, so the sign and the intensity of the bands are directly related to the structure of the substance examined.
It should be noticed that Circular dichroism technique opens up the possibility to detect not only chiral molecules, but also structures created by non chiral chromophores interacting with other chiral molecules. This phenomenon is called induced circular dichroism and results one of the most advantageous methods to determine the structure of supramolecular aggregates. A qualitative information of assembling phenomena and interaction between cyclodextrins and a guest molecule can be obtained from CD spectra. The incorporation of a photocromic moiety converts cyclodextrins into a spectroscopically active system, changing their optical activity. An induced circular dichroism in the absorption region of the chromophore is produced when an achiral azo dye forms complexes with cyclodextrins . For cyclodextrin complexes different rules have been reported by Kodaka and Harata, to correlate the sign of the induced CD (icd) bands with the orientation of the guest chromophore relative to the host. For a chromophore located inside the host cavity, according to their theoretical treatment,, a positive Cotton band is produced when the electronic transition moment of the guest is nearly parallel to the molecular axis of αCD.. On the contrary,a perpendicular transition dipole moment will give rise to a negative band, . These rules are inverted in the case of a chromophore located outside the cavity[88] (Figure 36).

[88] Masato Kodaka et Al. J. Am. Chem. Soc., 1993, 115 (9), pp 3702–3705

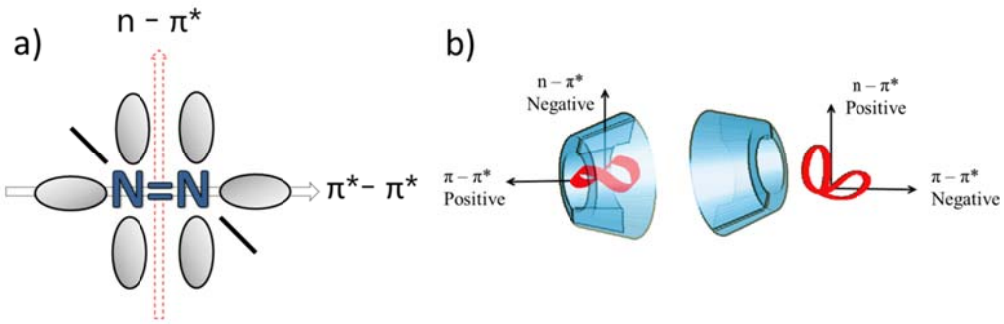

Figure 36: a) Illustration of the electric transition dipole for the π-π* (black vector) and n-π* (red vector) for azobenzene moiety; b) schematic illustration of Kodaka and Harata rules for CyD's complexes.

2.5 Determination Binding Costant αCD and Sodium Azobenzene carboxylate (AzoCOONa) by UV, CD and ITC

Preliminary studies on a model system, consisting of a mixture of azobenezene carboxylate sodium salt and α-cyclodextrin in aqueous solution have been performed, in order to obtain the value of the association constant. In particular UV titrations, Isothermal Calorimetry Titrations and circular dichroism have been used for this purpose.

2.5.1 UV Titration

In a quartz cell (optical path 0,5 cm), a 0,08 mM solution of AzoCOONa in water was titrated with a solution 1 mM of αCD. The UV-Vis spectra were recorded with a Jasco V-650 spectrometer in water with a 0.5 cm quartz cell at room temperature.

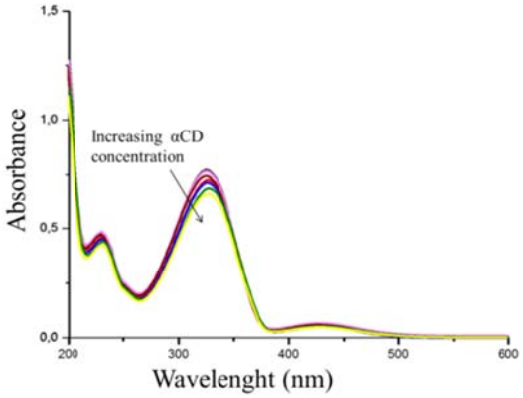

Figure 37: UV-Vis absorption spectra of 0.09 mM *trans*-AzoCOONa in aqueous solution in the presence of varying concentrations of αCD.

The absorbance at 325 nm, maximum absorption wavelength for *trans* AzoCOONa, decreases with increasing αCD concentration (Figure 38), and does not change up to 1 equivalent of native αCD. Figure 39 shows the Benesi-Hildebrand plot for αCD and trans AzoCOONa: the good linearity is indicative of one-to-one complex formation. The K value was evaluated to be 3×10^3 M^{-1}.

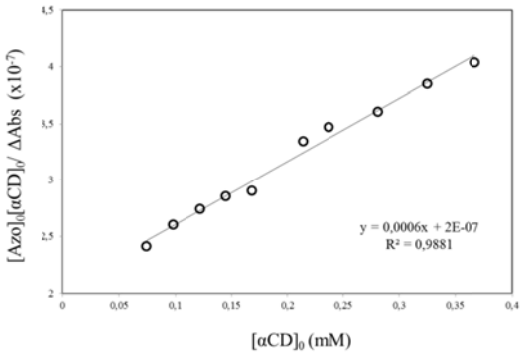

Figure 38: Benesi-Hildbrand plot for AzoCOONa and αCD.

Azobenzene carboxylate sodium salt (0.09 mM) was isomerized by photo-irradiation using a 300 W Xenon lamp (Asahi spectra MAX-301) lambda and then it have been titrated with native αCD, to evaluate the association constant for the cis isomer. Unlike the trans isomer, no absorbance shift was observed for the *cis*-isomer, as reported in figure 39, indicative of no or only a weak interaction. For the cis state it was not possible to evaluate the *K* value.

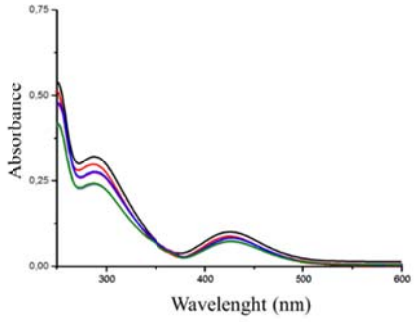

Figure 39: UV-Vis absorption spectra of 0.09 mM *cis*-AzoCOONa in aqueous solution in the presence of varying concentrations of αCD.

2.5.2 Isothermal titration calorimetry[89]

Heats of dissociation were measured using a MicroCal VP-ITC titration microcalorimeter in water at 30°C. The binding isotherms were analyzed by the non linear fitting model with a one binding site model, assuming the formation of one-to-one inclusion complexes of αCD and AzoCOONa, using Origin Software. In figure 40 and 41 are reported the isothermal titration calorimetric thermograms obtained from titrating 10 mM αCD aqueous solution with **a**) water, and **b**) 0.67 mM *trans*-AzoCOONa **c**) cis-AzoCOONa (0,67 mM) in aqueous solution. It can be seen that the fitting curves show a good agreement with experimental data, indicating that the fitting model is adapted and the thermodynamics parameters extracted are reliable.

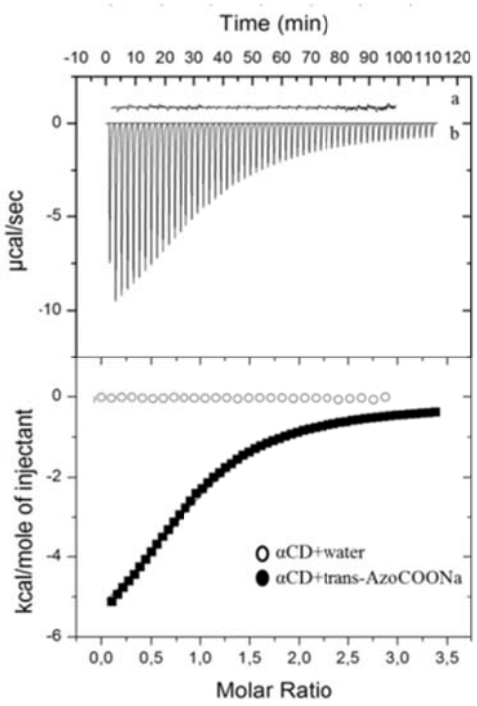

Figure 40: Cell feedback vs time for titrating 10 mM αCD aqueous solution with water (a), and *trans*-AzoCOONa aqueous solution (0,67 mM) (b) at 303 K . Curve (a) is shifted up for clarity.

[89] P. J. Zheng, C. Wang, X. Hu, K. C. Tam, and L. Li, *Macromolecules*, Vol. 38, No. 7, **2005**

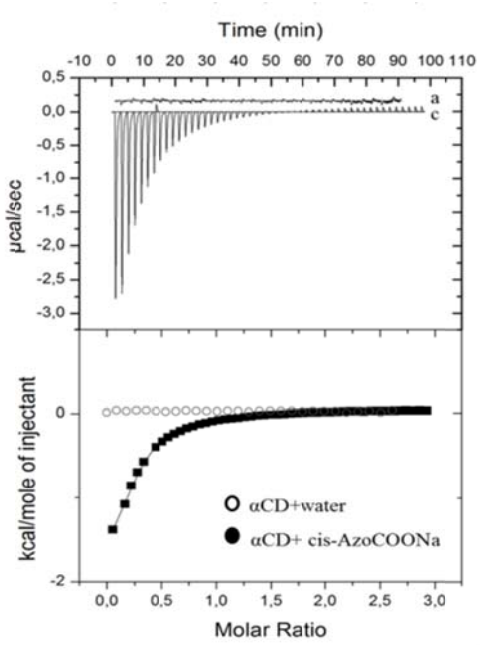

Figure 41: Cell feedback vs time for titrating 10 mM αCD aqueous solution into water (a), and *cis*-AzoCOONa aqueous solution (0,67 mM) (b) at 303 K.

The thermodynamic parameters extracted from the model fitting are reported in Table 2.

	N	K ($mol^{-1} \cdot L$)	ΔH (KJ/mol)	ΔS (J/mol·K)
Trans Isomer	1.00	2.83E3 ± 156	-7029 ± 71	-6.5
Cis Isomer	0.25	1.42E4 ± 1.53E3	-2103 ± 129.5	12.1

Table 2: Thermodynamic parameters of complexation behaviour between □CD and AzoCOONa (trans and cis isomers) in aqueous solution at 303 K.

Concerning the *trans*-isomer, the *K* value obtained with ITC is comparable with the one obtained by UV-Vis titration. The inclusion complex formation is exothermic. Both negative and enthalpy changes were observed suggesting that inclusion complex formation is enthalpy-driven and entropy opposed for the *trans*-isomer. When α-CD and AzoCOONa form inclusion complexes, their degree of freedom of motion decrease. This effect contributes to a negative entropy change. ITC data obtained from titrating 10 mM α-CD aqueous solution with a *cis*-AzoCOONa aqueous solution (under the same conditions) indicate that inclusion complexes are not formed. Enthalpogram shows that saturation of UV-irradiated AzoCOONa takes place at a lower concentration, confirming that less αCD molecules are bound to AzoCOONa. It should be noticed that *trans-cis*

photoisomerization is not quantitative, but the system reaches a photostationary equilibrium under irradiation. However, due to the incomplete isomerization, the UV-irradiated AzoCOONa still exhibits its ability to bind α-CD molecules. Therefore the system is composed partially of the *trans*-isomer, but the stoichiometric number *n* is significantly reduced from 1 to 0.25 upon *trans*-to-*cis* isomerization of AzoCOONa. The positive value entropy for the *cis*-isomer suggests a more disordered system due to disassembling process after photo-isomerization. It has to be noticed that the results are affected by a great value, thus data obtained for *cis*-isomer are not completely faithful.

2.5.3 Circular Dichroism

In Figure 42 are reported the CD spectra of AzoCOONa in water before and after addition of 10 eq of native αCD.

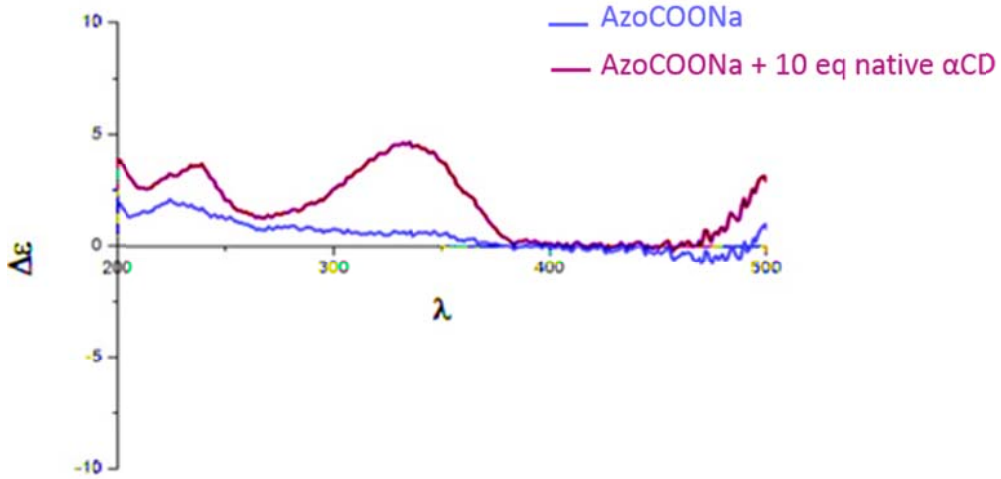

Figure 42: CD Spectra AzoCOONa, in H_2O (0.08 mM, cell 0.5 cm) before and after addition of 10 eq of native αCD.

As expected, no ICD signals are observed for AzoCOONa, thus ICD signal arise after complexation with αCD. The positive ICD sign observed for the π-π* transition of the azo group is correctly predicted by the Kodaka general rule, confirming the formation of the complex after addition of 10 equivalent of αCD, with a π-π* transition aligned along with the CD's axis.

2.6 Supramolecular and photocromic behavior of αCD-Azobenzene derivatives

2.6.1 αCD-AzoCN (21)

- *UV and CD Spectra in MeOH*

UV spectrum of trans-2-αCD-AzoCN in MeOH (0.03 mM) shows two absorption bands, located at 328 and 230 nm while for the cis-isomer these two bands appear at 263 and 436 nm. In Figure 43 are reported UV spectra obtained during irradiation of trans-2-AzoCN-αCD at 340 nm in MeOH. The trans-to-cis photo-isomerization is complete within 40 min. The reverse cis-to-trans isomerization is complete within 15 min under photo-irradiation at 254 nm, but more than 18 h are necessary in the dark. Several irradiation cycles can be repeated without loss of performance.

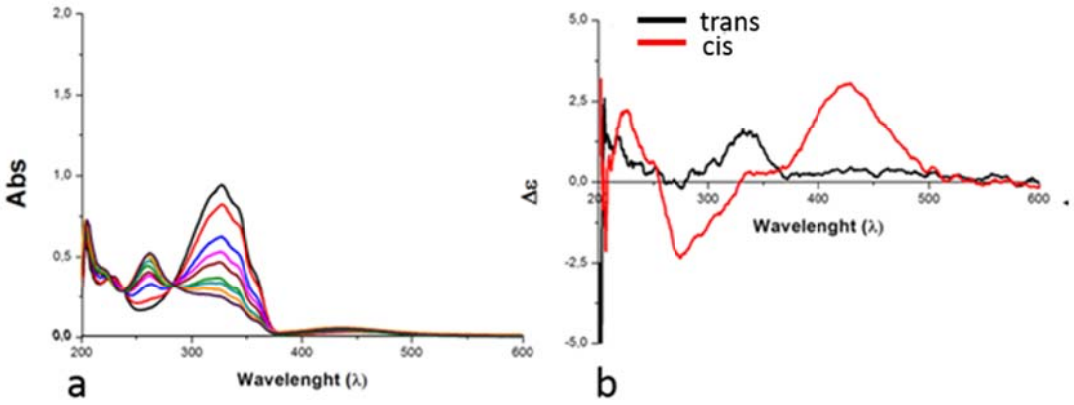

Figure 43: a) Absorption and b) CD spectra of 2-AzoCN-αCD in MeOH upon irradiation at 340 nm.

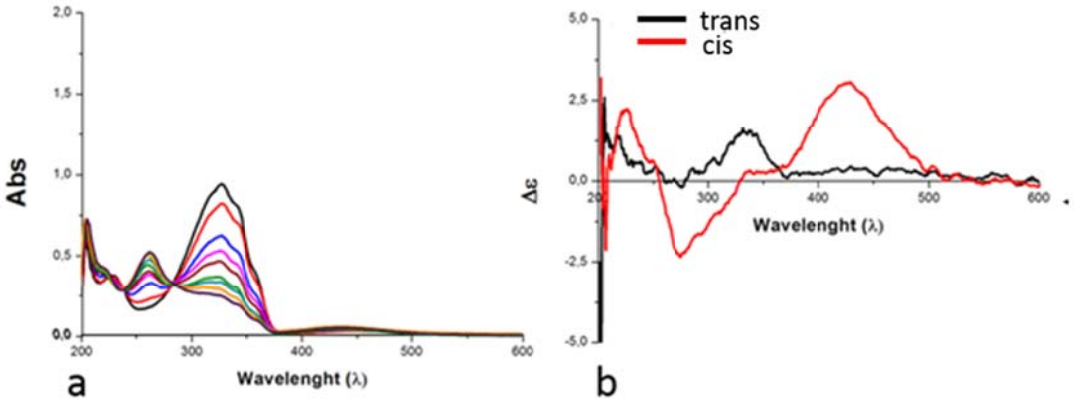

Figure 43b shows the circular dichroism spectra obtained in MeOH for the trans-isomer (black) and for the cis photostationary state (red). ICD spectra in MeOH show an induced positive band for the trans-isomer around 332 nm, corresponding to the π-π* transition band of the N=N group, but no optical activity related to the n-π* is observable. Taking into account the good solubility of this azo moiety in methanol, it seems unlikely that 2-AzoCN-αCD forms inclusion complexes in this solvent and the positive CD band at 332 nm can be ascribed to an induced CD on the achiral azobenzene chromophore by the covalently bound cyclodextrin moiety. On the contrary, a positive and a negative signal, respectively at 427 and 286 nm, are indicative of no aggregation for the cis-isomer.

- *UV and CD Spectra in H_2O*

UV spectra of αCD-AzoCN in water (0.6 mM) show two absorption bands located at 334 and 234 nm for trans isomer, and at 437 and 253 nm for cis isomer. In Figure 44 are reported the UV and CD spectra obtained during irradiation of 2-AzoCN-αCD at 340 nm in water. The trans-to-cis photo-isomerization performed at 340 is partially complete within 28 min in water. The reverse cis-to-trans isomerization under photo-irradiation at 254 nm is completed within 15 min or more than 18 h in the dark. Several irradiation cycles can be repeated without loss of performance.

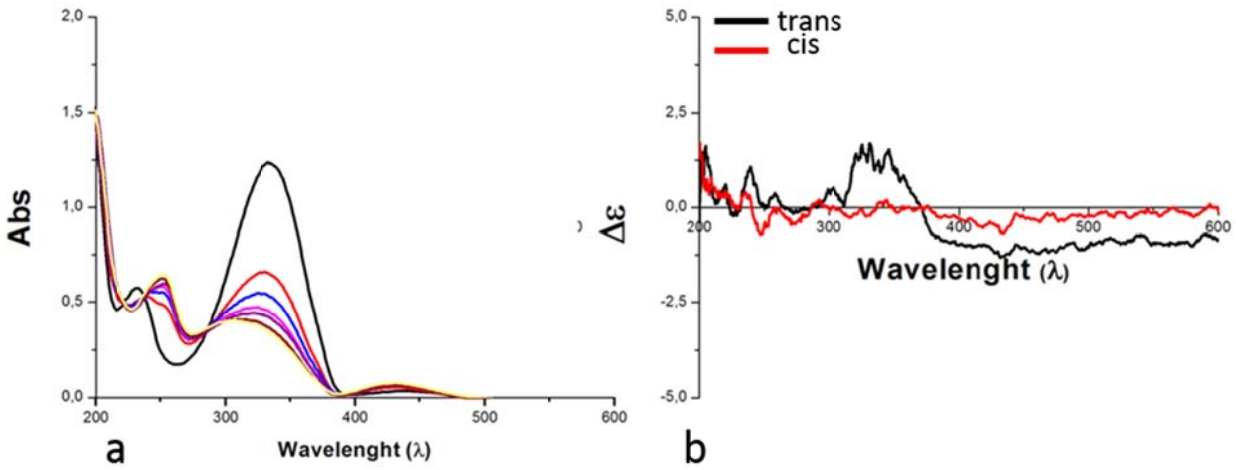

Figure 44: a) Absorption and b) CD spectra of 2-AzoCN-αCD in H_2O upon irradiation at 340 nm.

In Figure 44b are reported circular dichroism spectra for trans-isomer and after reaching the photostationary state of a solution of 2-AzoCN-αCD in water. CD spectra show a weak induced positive band for the trans-isomer around 340 nm, corresponding to the π-π* transition band of the N=N group: this suggests the existence of inclusion complexes. On the contrary, no signal was observed for the cis-isomer. This results can be explained as consequence of the sum of two opposite trend, due to the presence of a mixture of trans and cis isomers in solution, as far as the photo-isomerization is not quantitative.

2.6.2 αCD-AzoF (20)

- *UV and CD Spectra in MeOH*

UV spectrum of trans αCD-AzoF in MeOH (0.06 mM) exhibits two absorption bands located at 327 and 229 nm, whereas for the cis-isomer the two bands move to 435 and 260 nm, respectively. in Figure 45 are reported UV spectra obtained during irradiation of the sample 2-AzoCN-αCD at 340 nm in MeOH (Figure 45). The trans-to-cis photoisomerization performed at 340 is complete within 20 min. The reverse cis-to-trans isomerization under photoirradiation at 254 nm is completed within 50 min or more than 18 h in the dark.

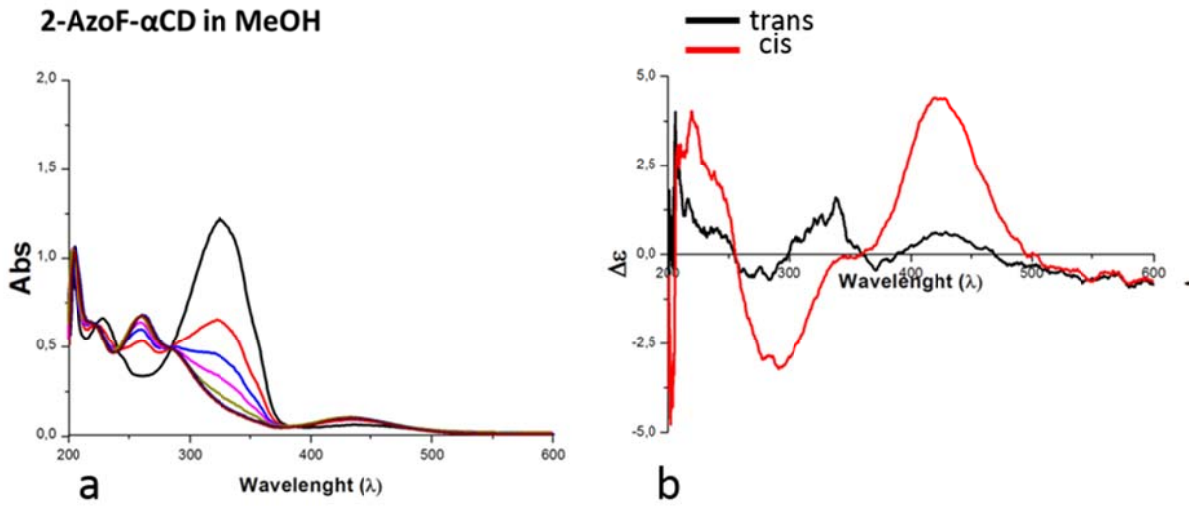

Figure 45: a) Absorption and b) CD spectra of 2-AzoF-αCD in MeOH upon irradiation at 340 nm.

CD spectra in MeOH show a weak induced positive band for the trans-isomer around 326 and 420 nm, indicative of low aggregation. A positive and a negative signal, respectively at 425 and 289 nm, are indicative of no aggregation for cis-isomer.

- *UV and CD Spectra in H_2O*

UV spectra of αCD-AzoF in water (0.08 mM) exhibit an absorption band due to trans-2-AzoF-αCD, located at 332 and 230 nm for trans isomer and at 428 and 251 nm for cis isomer. In Figure 46a are reported UV spectra obtained during irradiation of the sample 2-AzoCN-αCD at 340 nm in water. The trans-to-cis photoisomerization performed at 340 is complete within 20 min. The reverse cis-to-trans isomerization under photoirradiation at 254 nm is complete within 50 min or more than 18 h in the dark.

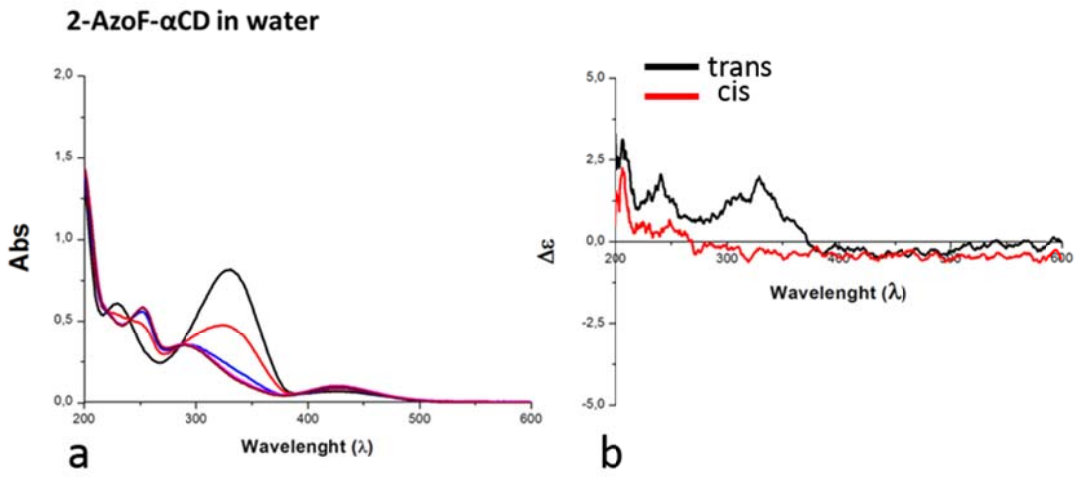

Figure 46: a) Absorption and b) CD spectra of 2-AzoF-αCD in H_2O upon irradiation at 340 nm.

Figure 46b shows the CD spectra of 2-AzoF-αCD in water before and after photo-isomerization. A weak induced positive band for the trans-isomer around 328 nm suggests a weak complexation. On the contrary, no signal was observed for the cis-isomer. This results can be explained as consequence of the sum of two opposite trend, due to the presence of a mixture of trans and cis isomers in solution, as far as the photo-isomerization is not quantitative.

2.6.3 αCD-AzoCOOH (18)

- *UV and CD Spectra in MeOH*

UV spectra of αCD-AzoCOOH in MeOH (0.059 mM) exhibits an absorption band due to trans-2-AzoCOOH-αCD, located at 331 and 232 nm, then for the cis-isomer at 436 and 262 nm. In Figure 47 are reported spectra obtained during irradiation of the sample 2-AzoCOOH-αCD at 340 nm.

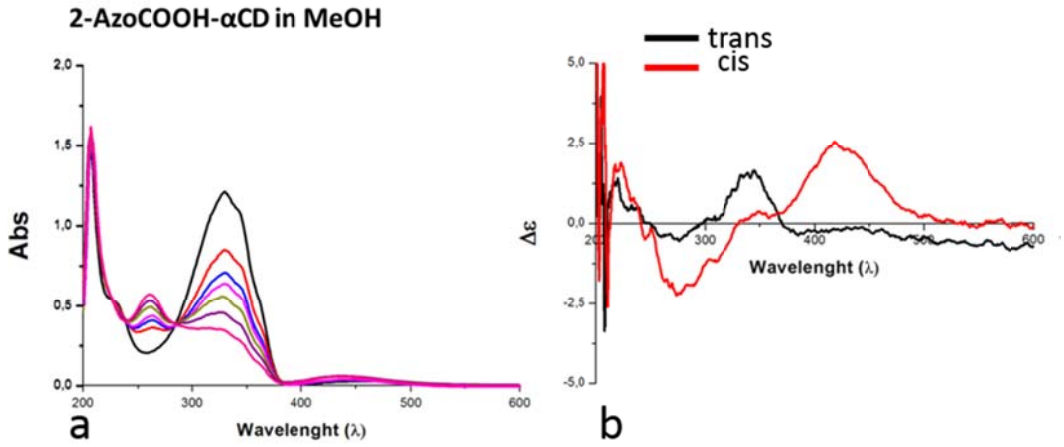

Figure 47: a) Absorption and b) CD spectra of 2-AzoCOOH-αCD in MeOH upon irradiation at 340 nm.

The trans-to-cis photoisomerization performed at 340 is not complete, even after prolonged irradiation. The reverse cis-to-trans isomerization under photoirradiation at 254 nm is completed within 30 min or more than 18 h in the dark. ICD spectra, (Figure 47b), show an induced positive band for the trans-isomer around 342 nm. On the contrary, a positive and a negative signal, respectively at 429 and 280 nm, are indicative of no aggregation for the cis-isomer.

- *UV and CD Spectra in H_2O*

A solution of αCD-AzoCOOH in water (0.08 mM) was prepared. The absorption band due to trans-2-AzoCOOH-αCD are located at 341 and 234 nm for trans isomer, at 436 and 256 nm for cis isomer. In Figure 48 are reported the spectra obtained during irradiation of the sample 2-AzoCOOH-αCD at 340 nm.

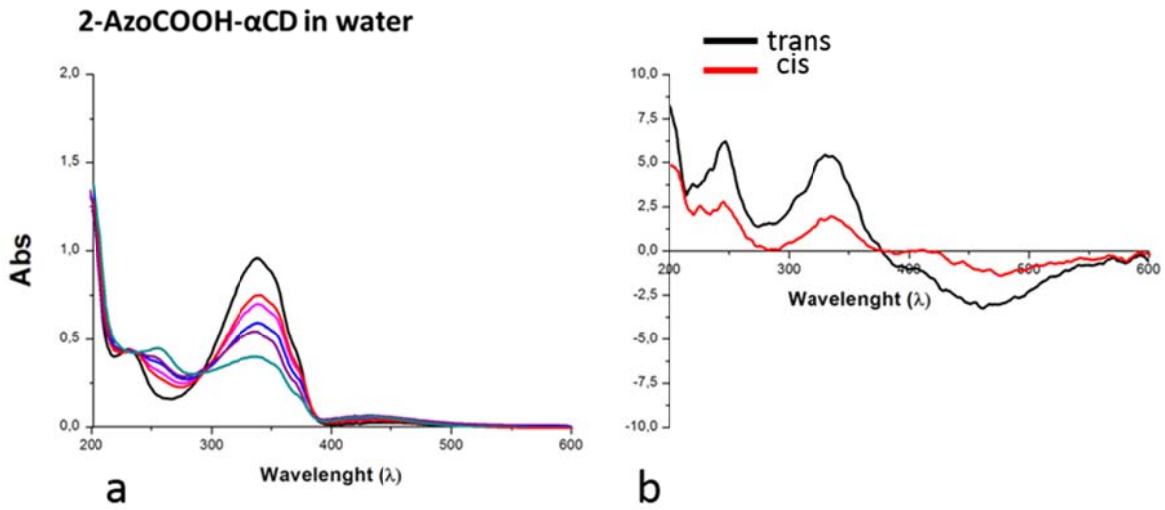

Figure 48: a) Absorption and b) CD spectra of 2-AzoCOOH-αCD in H_2O upon irradiation at 340 nm.

Also in water the trans-to-cis photoisomerization performed at 340 is not complete even after prolonged irradiation. The reverse cis-to-trans isomerization under photo-irradiation at 254 nm is completed within 30 min or more than 18 h in the dark. ICD spectra recorded, (Figure 48b), show a negative band for the trans-isomer from 510 to 425 nm, and two positive around 334 and 246 nm. This signal are agree with the formation of aggregates. Since the photo-isomerization is not complete, ICD signal after irradiation is due to trans isomer still present in the mixture.

2.6.4 αCD-AzoCOONa

A solution of αCD-AzoCOONa was prepared adding 1 eq of $NaHCO_3$ in phosphate buffer (pH 7.4) to αCD-azoCOOH, and irradiated in a quartz cell (b=1cm, 0.04 mM) at 340 nm. The absorption bands due to trans-2-AzoCOONa-αCD are located at 343 and 233 nm, and for the cis-isomer at 430 and 259 nm (Figure 49).

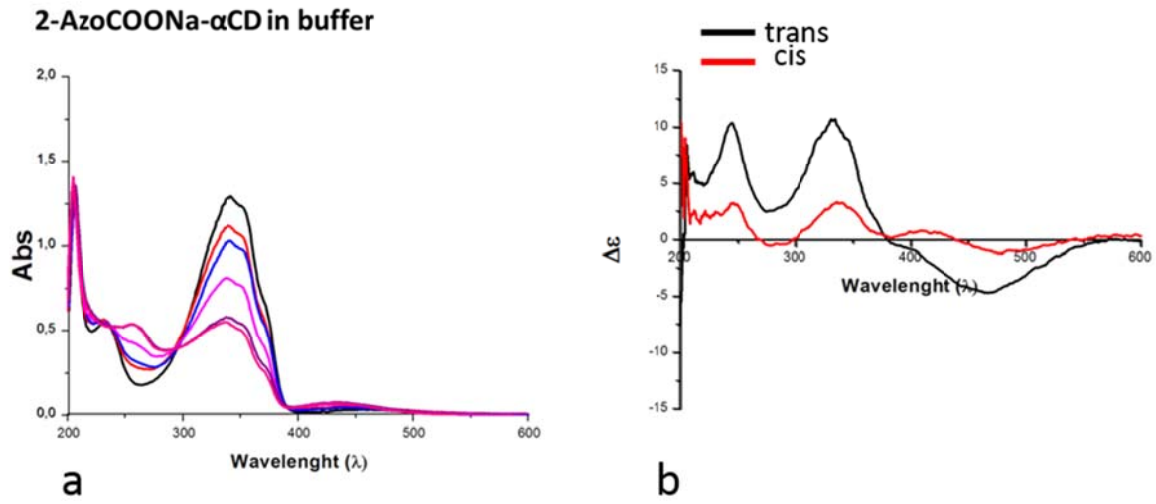

Figure 49: a) Absorption and b) CD spectra of 2-AzoCOONa-αCD in buffer upon irradiation at 340 nm.

The trans-to-cis photoisomerization performed at 340 is not complete, even after three hours. The reverse cis-to-trans isomerization under photoirradiation at 254 nm is complete within 30 min or more than 18 h in the dark. Figure 49b exhibits CD spectra for the trans-isomer before and after reaching the photostationary state of a solution of 2-AzoCOONa-αCD, in which a strong induced positive band for the trans-isomer around 340 and a negative one at 468 nm is shown, in agreement with the presence of inclusion complexes. Since the photoisomerization is not complete, aggregation form is observed not only for trans isomer, but also for the trans-cis mixture obtained after irradiation.

2.6.5 αCD-AzoH (17)

- *UV and CD Spectra in MeOH*

UV spectra of trans αCD-AzoH in MeOH (0.18 mM) show two absorption band located at 324 and 227 nm. For the cis-isomer the two bands appear at 433 and 263 nm. In Figure 50a are reported spectra upon irradiation of the sample 2-AzoH-αCD at 340 nm. Trans-to-cis photoisomerization is complete within 15 min. The reverse cis-to-trans isomerization under photoirradiation at 254 nm is complete within 15 min or more than 18 h in the dark. Several irradiation cycles can be repeated without loss of performance.

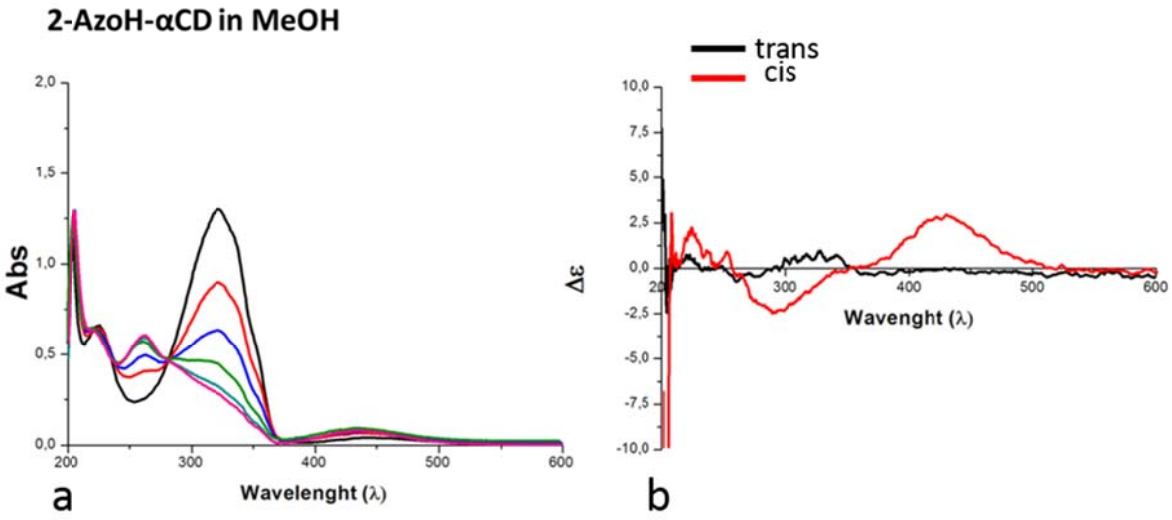

Figure 50: a) Absorption and b) CD spectra of 2-AzoH-αCD in MeOH upon irradiation at 340 nm.

Figure 50b exhibits CD spectra for the trans-isomer before and after reaching the photostationary state of a solution of 2-AzoH-αCD. CD spectra show very weak signal for trans-isomer, significative of dimer. A positive and a negative signal, respectively at 429 and 291 nm for cis isomer, in agreement with Kodaka and Harata's rule, is indicative of absence of aggregates.

- *UV and CD Spectra in H_2O*

UV spectra of αCD-AzoH, (0.04 mM), exhibit an absorption band due to trans-2-AzoH-αCD located at 332 and 431 nm (π-π* and n-π* transition, respectively), then for the cis-isomer at 260 and 426 nm. In Figure 51a are reported UV spectra obtained upon irradiation of the sample at 340 nm.

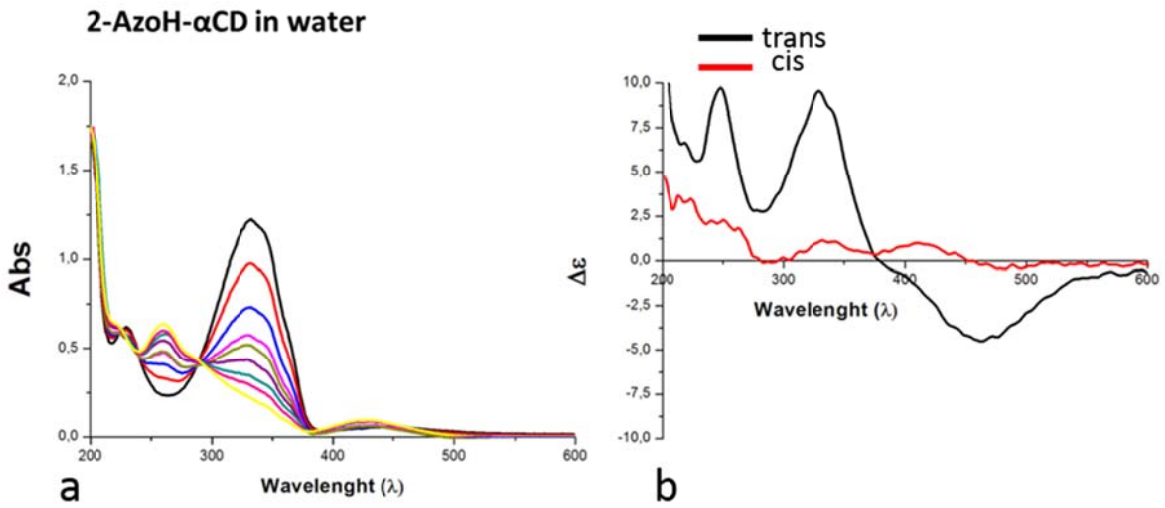

Figure 51: a) Absorption and b) CD spectra of 2-AzoH-αCD in H_2O upon irradiation at 340 nm.

The trans-to-cis photo-isomerization performed at 340 is complete within 15 min. The reverse cis-to-trans isomerization under photo-irradiation at 254 nm is complete within 15 min or more than 18 h in the dark. Several irradiation cycles can be performed without loss of performance. CD spectra, figure 51b, show a strong induced positive band for the trans-isomer around 340 nm, corresponding to the π-π* transition band of the N=N group, and this is indicative of strong aggregation. On the contrary, very weak signals are observed for the cis-isomer, as consequence of the sum of opposite trends, due to the presence of a mixture of trans and cis isomers.

2.7 Supramolecular and photocromic behavior of γCD-Azobenzene derivatives

Compared to α-Cyclodextrin, γ-Cyclodextrin has a larger cavity, so it can form complexes with azobenzene in a 1:2 ratio and its solubility in water is higher, (solubility in water, , α-CD 129.5 g/kg H_2O, γ-CD 249.2 g/kg H_2O). In order to obtain more soluble polymers, also γCD-Azobenzene derivatives have been synthetized. In particular were prepared a γCD mono-functionalized on the secondary rim with an azobenzene carboxylic acid moiety, and a difunctionalized γCD, where one azobenzene unit is attached on the primary rim while the second one is attached on the secondary rim. Aggregation/disaggregation phenomena in aqueous solution have been monitored for both compounds. While, on one hand, γCD offers the advantage of an higher solubility, on the other hand one possible drawback is its lower affinity for azobenezene. The synthetic strategy to obtain

γCD derivatives is the same reported previously for α-CDs. In the case of the di-functionalized derivative, the protection of the primary rim of γCD was carried out with 7 equivalents of TBDMSiCl, so that one hydroxyl group on the primary rim was left unproctected and could be functionalized in the subsequent step, as reported in the following scheme:

a) Protection of Cyclodextrins

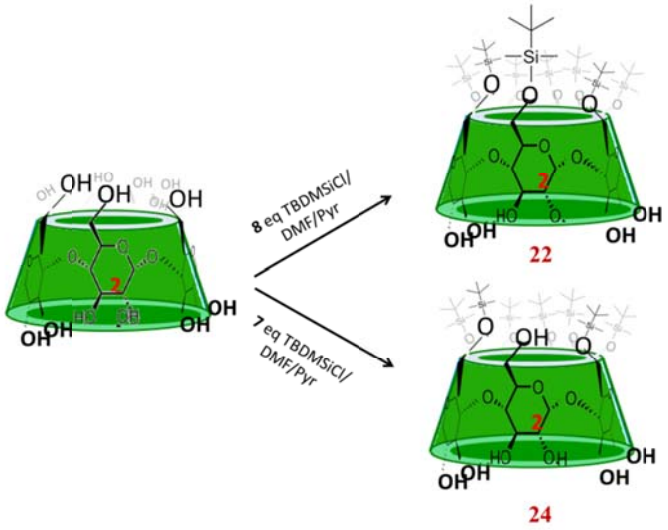

b) Synthesis of Silylated αCD-azobenzene

- Derivative **23**

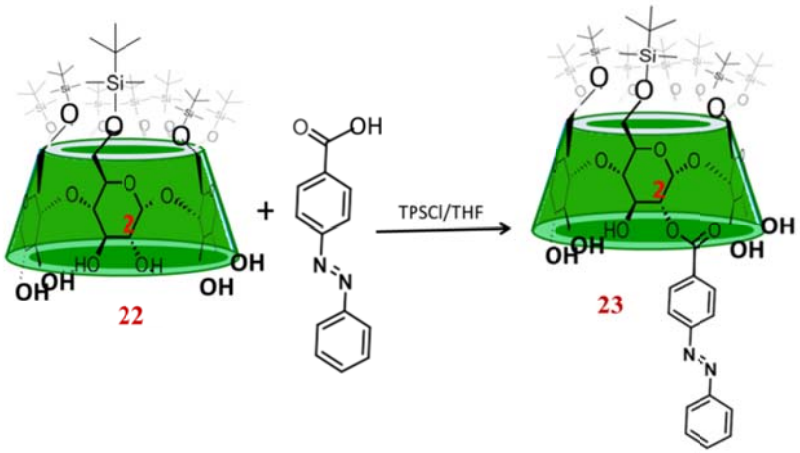

- Derivative **25**

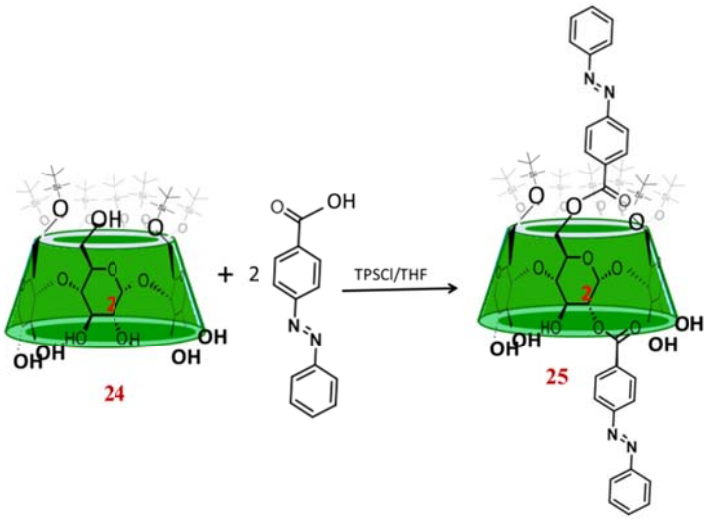

c) Deprotection of Sylilated αCD-azobenzene derivatives

- Derivative **26**

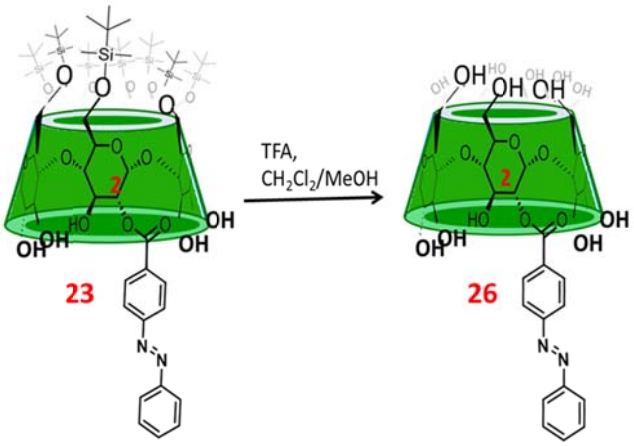

- Derivative **27**

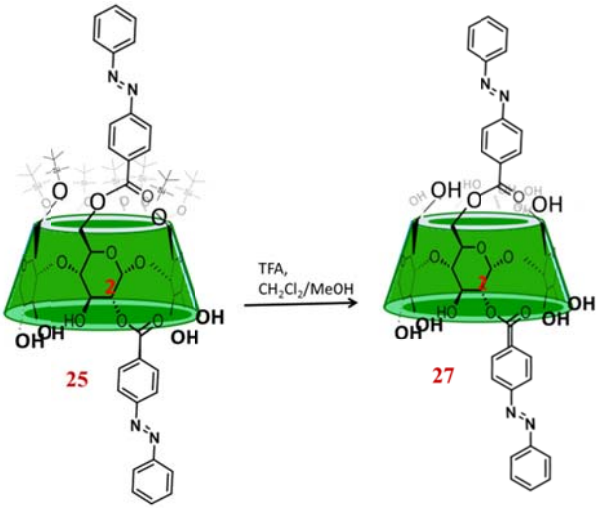

Figure 52: Synthesis procedure to obtain mono and di-functionalized γCD with azobenzene.

2.7.1 Mono-functionalized compound: 2azoH-γCD (26)

- *UV and CD spectra in H_2O*

In Figure 53 are reported the UV and CD spectra obtained from a 0.09mM solution of the mono-functionalized compound. The total trans-cis photo-isomerization occurs in about 1 hour. According to Kodaka rule, CD Spectra show an aggregate system for trans isomer and a disaggregate one for cis isomer.

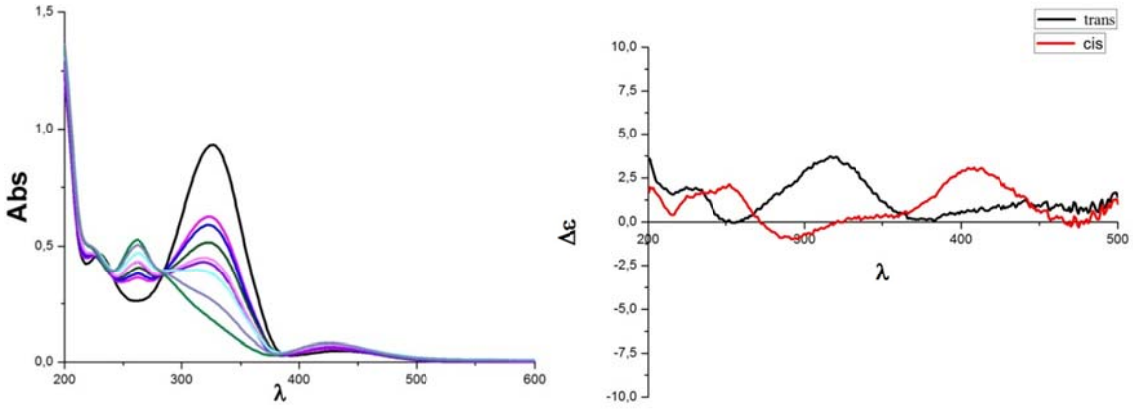

Figure 53: a) Absorption spectra b) CD spectra of 2AzoH-*γCD* in aqueous solution, before and after irradiation at 340 nm.

CD spectra obtained for cis-2AzoH-γCD show a positive signal located at c.a. 400 nm and a negative signal located at c.a. 280 nm. This confirms that in the cis state there is complete disaggregation of the polymers, while for cis-2AzoH-αCD the spectrum does not give such a clear evidence.

2.7.2 Di-functionalized compound: 2-3-AzoH-γCD (27)

In Figure 54 are reported the UV and CD spectra obtained for the di-functionalized compound. The photoisomerization of a 0.06 mM aqueous solution was incomplete even after 2 h of irradiation. Despite the good solubility of native γCD, the bis-azo derivative showed the lowest solubility (less than 1 mM) among the azocyclodextrins prepared.

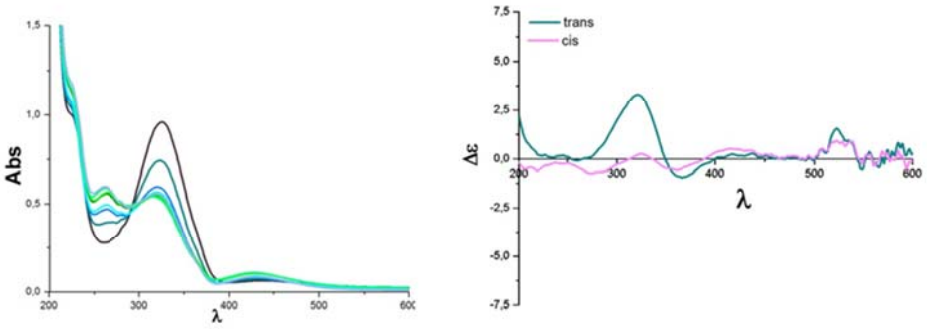

Figure 54: a) Absorption spectra b) CD spectra of 2,3AzoH-*γCD* in aqueous solution, upon irradiation at 340 nm.

2.8 AzoH-αCD: best candidate for osmotic cell

In general, all the derivatives so far presented showed a poor to modest solubility in water.

The highest solubility has been obtained for derivative 2-AzoH-αCD, (trans isomer's solubility has been estimated c.a. 6.3 mM in water). CD spectra reported in the previous paragraph confirm the existence of a supramolecular oligomer for the trans state, which is converted into a monomer or dimer upon isomerization at 340 nm, while UV spectra showed an excellent photo-isomerization yield in water, (almost 90%). Therefore it was decided to focus on this compound for further studies.

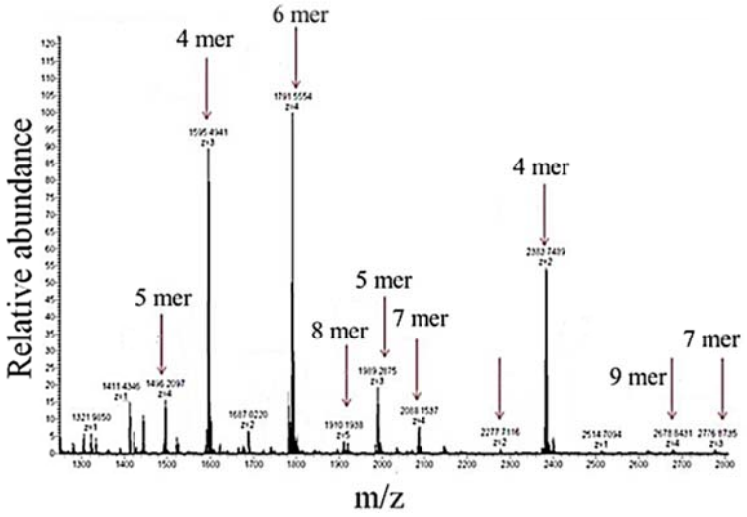

Figure 55: ESI-MS spectrum of 2-AzoH-α-CD in H_2O, 1 mM.

The low solubility, with respect to native αCD, of 2-AzoH-αCD trans-isomer is probably the combined outcome of the presence of the hydrophobic Azo group and the formation of supramolecular oligomers large enough to possess low solubility. On the other hand, the higher solubility of cis-isomer could be ascribed both to the greater polarity of the cis-azo moiety and to disaggregation phenomena.

In order to estimate the molecular size of the supramolecular complexes formed by the trans isomer, several techniques were employed. The degree of polymerization for trans-isomer has been investigated by ESI-MS analysis. As shown in figure 55, polymeric inclusion complexes up to a nonamer can be observed even at lower concentrations (< 1 mM). Diffusion coefficient have been determined by pulse field-gradient spin-echo (PGSE) DOSY NMR. Slow back photo-isomerization in the dark allowed us to perform PGSE NMR measurements also for the *cis*-isomer. In figure 56 is reported the plot of the diffusion coefficients for 2-AzoH-αCD in D_2O (*trans*- and *cis*-isomers) and in DMSO (*trans*-isomer) in the concentration range 0.5 - 6.3 mM.

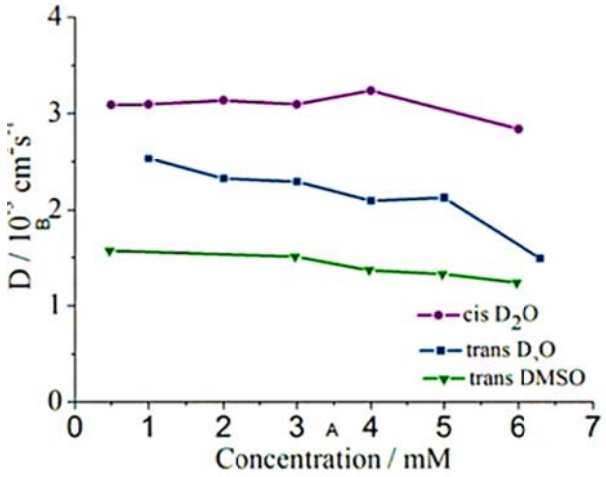

Figure 56: Plot of diffusions coefficients of trans 2-AzoH-αCD in D2O (blue line) and in DMSO (green line) and cis isomer in D2O (violet line), (8.5 ppm for trans and 7.9 ppm for cis).

The two plots for the compound in water show that the size of intermolecular complexes formed by trans 2-AzoH-αCD in D_2O increases with an increase in concentration. Analogously to what is observed in the disgregating solvent DMSO, no change occurs for the diffusion coefficient of *cis*-isomer, as function of concentration. For the *cis*-isomer, the dimension of molecules seems to be coherent with dissociated compound. Table 3 reports the measured diffusion coefficients, together with the calculated hydrodynamic radii. The average radius for trans in water rougly doubles with concentration and is always higher than both the radius of cis and trans in DMSO. The radius of cis remains constant and is very close to the value measured for DMSO.

Trans 2-AzoH-αCD in D_2O				
Conc (mM)	1	2	4	6,3
D (x 10^6 cm^2s^{-1})	2.54	2.33	2.10	1.58
Rh nm	1.09	1.19	1.33	1.85

Cis 2-AzoH-αCD in D_2O				
Conc (mM)	0,5	1	2	4
D (x 10^6 cm^2s^{-1})	3.09	3.1	3,14	3,24
Rh nm	0.9	0.9	0,89	0,86

Trans 2-AzoH-αCD in DMSO					
Conc (mM)	0.5	3	4	5	6
D (x 10^6 cm^2s^{-1})	1.6	1.54	1.4	1.36	1.27
Rh nm	0.7	0.73	0.8	0.8	0.88

Table 3: Diffusion coefficients and and hydrodynamic radii (R_H) as function of concentration for *trans*-2-AzoH-αCD in D_2O and DMSO, and for *cis*-2-AzoH-αCD in D_2O.

The 2D ROESY spectrum (Figure 57) of *trans*-2- AzoH-αCD in D_2O, shows strong correlation signals between C(5)-H and C(3)-H in the αCD cavity and phenyl protons **a** and **b** of the Azo moiety and weak correlation signals with phenyl protons **c** and **d**. This is a clear evidence of the formation of an inclusion complex .

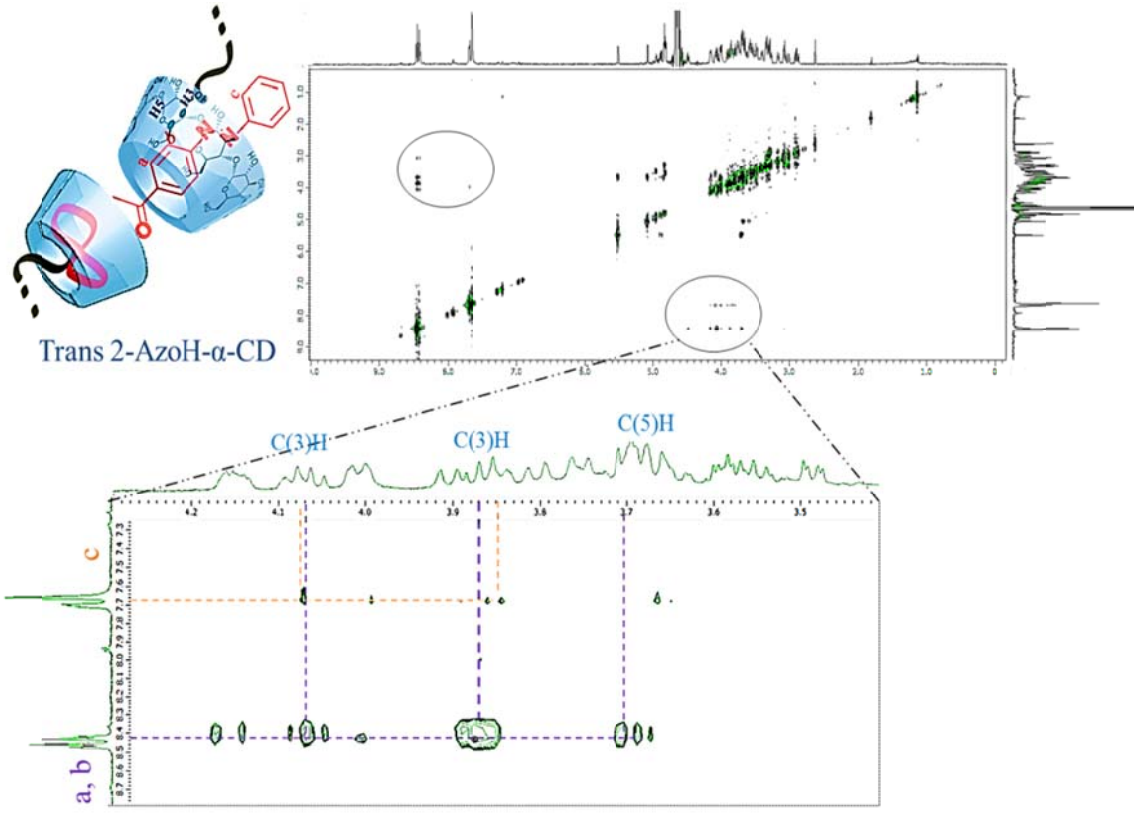

Figure 57: 2D ROESY NMR spectrum of trans 2-AzoH-αCD in D_2O, 2 mM, at 25 ° C.

On the contrary, the 2D ROESY spectrum of the *cis*-isomer does not show significant correlation signals (Figure 58), ruling out the existence of complexed species, as already suggested by CD spectra and DOSY data.

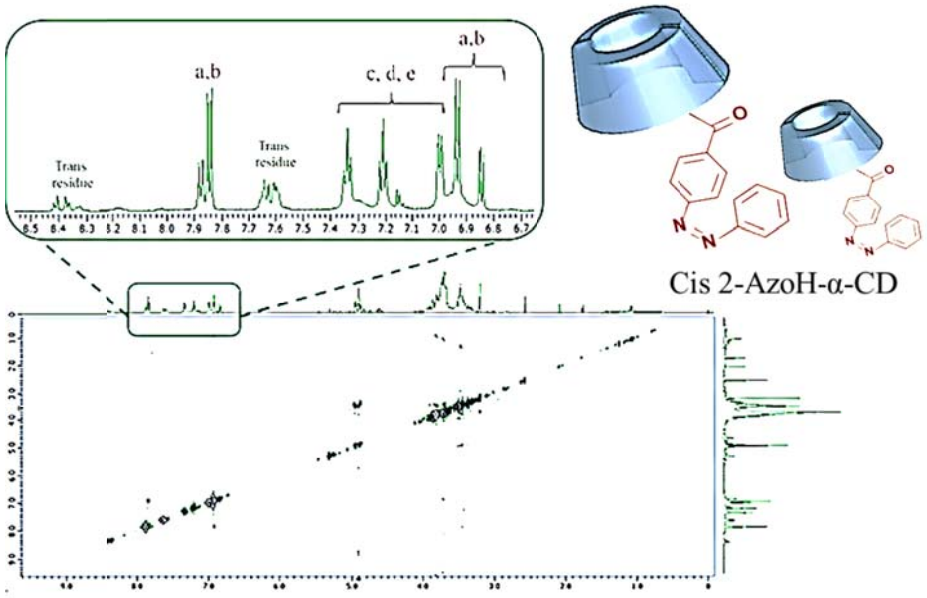

Figure 58: 2D ROESY NMR spectrum of cis 2-AzoH-αCD in D_2O, 2 mM, at 25 ° C.

3 Osmotic cell

As already mentioned previously, the main aim of this project was to obtain a macroscopic effect, via an external stimulus, by controlling aggregation/disaggregation phenomena of a supramolecular polymer based on αCD-azobenezene derivatives. To this purpose we planned to take advantage from osmosis. For these experiments we designed and had built the osmotic cell shown in Figure 59. In this cell photo-isomerization could be carried out in both compartments independently, thanks to quartz windows.

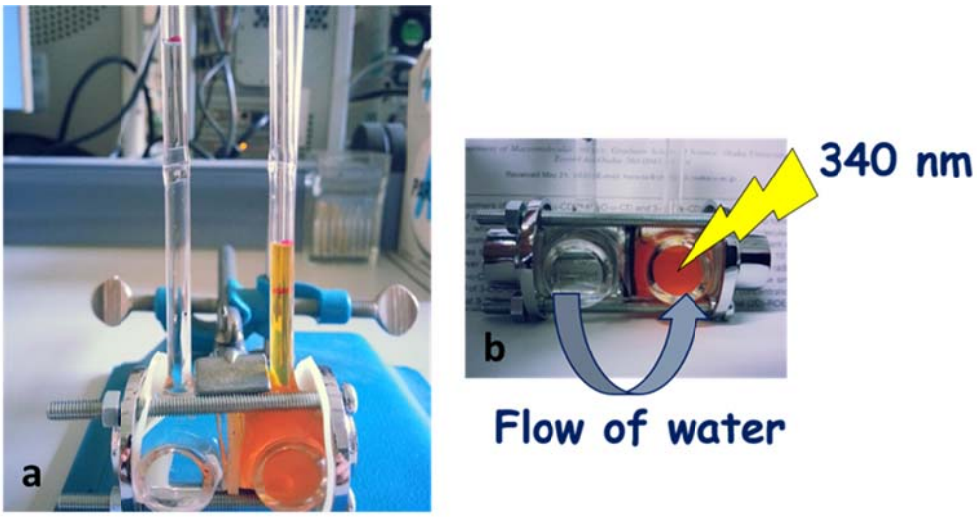

Figure 59: Osmotic cell.

One compartment was loaded with a suspension in water of unirradiated trans- 2AzoH-αCD derivative, while the other compartment was loaded with pure water (Figure 59a). After equilibration between the two compartments (Figure 59b), the 2AzoH-αCD solution was irradiated at 340 nm.

While trans to cis photo-isomerization occurred, disaggregation produced an increase in concentration in the right compartment and, thus, a flow of solvent from the compartment containing pure water took place (Figure 60 inset).

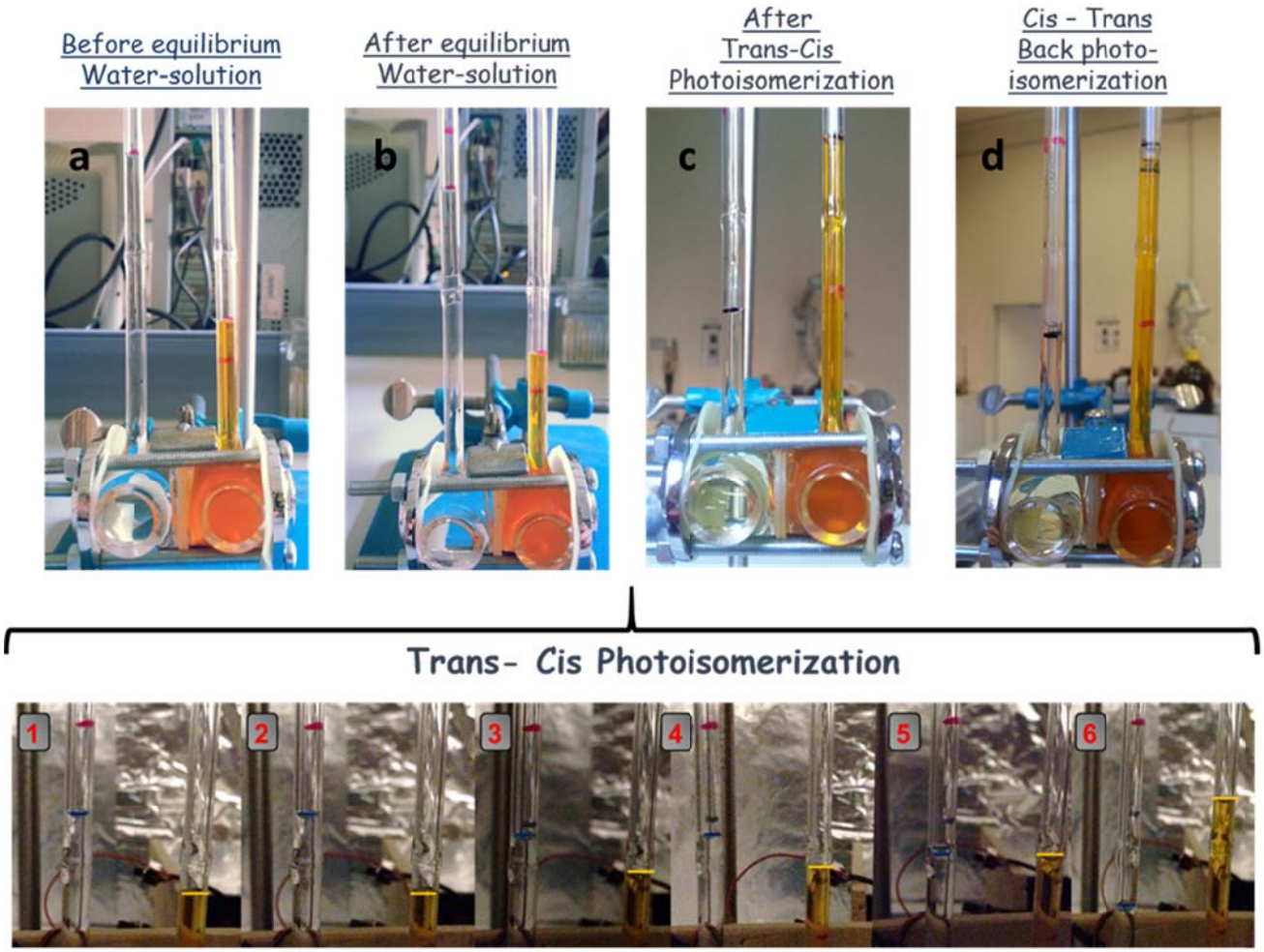

Figure 60: Irradiation with visible light reverted the supramolecular process: the trans isomer, thus reformed, recreated the inclusion complex, and this in turn produced a flow of water from the right to the left compartment (Figure 60d).

4 Conclusion

In this device, by means of a reversible supramolecular process, light is directly converted into mechanical energy. Given the known photochemical stability of azobenzenes, the process can be repeated many times without loss of performance. Experiments are in progress to confirm this point. With respect to the molecular system employed in the previous example of direct light-to-mechanical energy conversion, the present system offers two main advantages: the molecular unit is simpler to make and water is used as the solvent in place of organic solvents. From the practical standpoint, this broadens the range of suitable, commercially available membranes and, in perspective, renders the process more environmental friendly.

Chapter III

Supramolecular architectures based on Azoguanosine

1 Supramolecular organization of guanosine derivatives

1.1 Introduction

In the last decades, natural and unnatural nucleobases have been deeply investigated. Since they can participate to a great variety of cooperative non-covalent interactions, they have been considered as basic units for a variety of supramolecular motifs, and proposed as potential building blocks for highly ordered nanostructured materials. The five natural nucleobases, *i.e.*, adenine (A), guanine (G), cytosine (C), thymine (T), and uracil (U) (Figure 61), are the main components of the most important examples of self-assembled biopolymers, DNA and RNA. It is well known that the formation of the duplex DNA/RNA from their single-stranded components results from non-covalent interactions, and the code sequence is mainly due to molecular recognition between nucleobases through hydrogen bonding.[90,91]

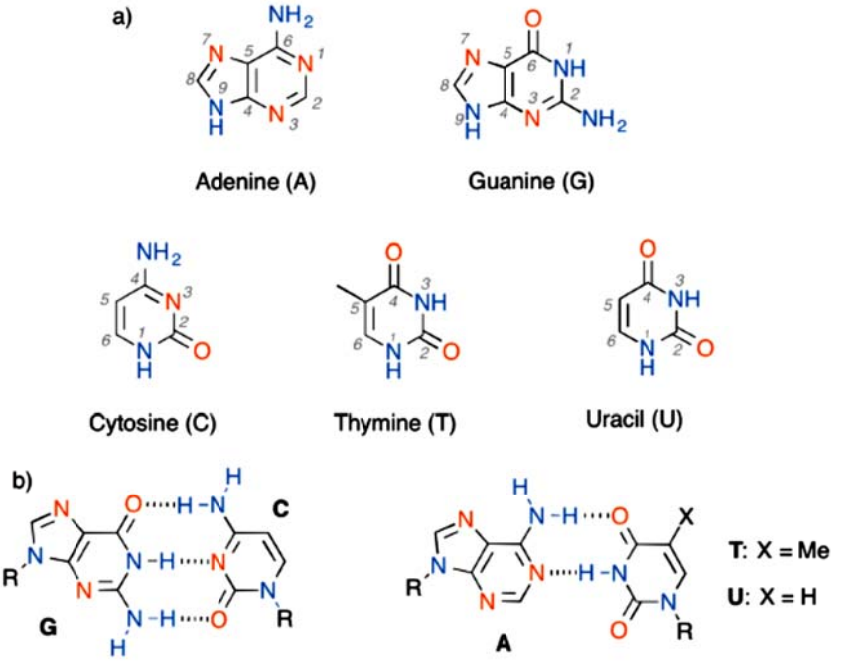

Figure 61: The five natural nucleobases adenine (A), guanine (G), cytosine (C), thymine (T), and uracil (U).

The formation of intermolecular hydrogen bonds is considered the most important tool to obtain supramolecular architectures.[92] Indeed, among nucleobases, guanine is the most widely investigated

[90] Saenger, W., *Principles of Nucleic Acid Structure*, Springer-Verlag: New York, **1984**.

[91] Ciesielski, A., El Garah, M., Masiero, S. and Samorì, P. (**2016**), Small, 12: 83–95. doi:10.1002/smll.201501017

and reported in the literature thanks to its ability to self-assemble via multiple H-bonding. Due to the presence of both a Watson-Crick edge and a Hoogsteen edge its self-assembly may result in several different superstructures, and it is thus considered the most versatile nucleobase. Linear polymers (ribbons) have been observed in the absence of metal ions, while tetrads (G-quartets) form in the presence of salts. The stacking interaction among G-quartets generates the G-quadruplex structure, showing a potential role in DNA transcription processes[93].

The formation of intermolecular hydrogen bonds is considered the most important tool to obtain supramolecular architectures.[94] Indeed, among nucleobases, guanine is the most widely investigated and cited in the literature thanks to its ability to self-assemble via multiple H-bonding. Due to the presence of both a Watson-Crick edge and a Hoogsteen edge, its self-assembly may result in several different structures, and it is thus considered the most versatile nucleobase. Linear polymers (ribbons) have been observed in the absence of metal ions, while tetrads (G-quartets) form in the presence of salts. The stacking interaction among G-quartets generates the G-quadruplex structure, showing a potential role in DNA transcription processes[95].

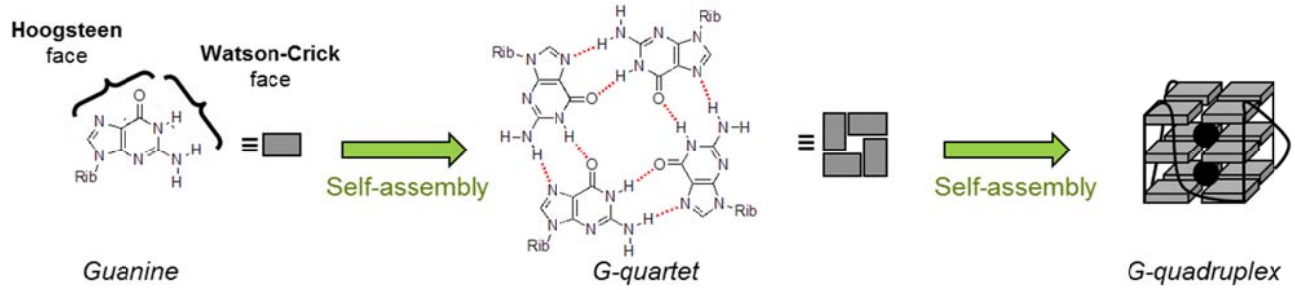

Figure 62: Watson-Crick and Hoogsten interactions

The capacity of guanine derivatives to form aggregates in water is well known since 1910, when Bang noticed that a highly concentrated solution of guanylic acid (5'-GMP) can form a gel. Fifty years later these structures have been described by Gellert by diffraction experiments as originated

---

[93] (a) Zhou, S. Y.; Liu, D. *Crit. Rev. Eukaryot. Gene Expr.* **2006**, *16*, 103-118. (b) McEachern, M. J.; Krauskopf, A.; Blackburn, E. H. *Annu. Rev. Genet.* **2000**, *34*, 331-358. (c) Collins, K. *Curr. Opin. Cell Biol.* **2000**, *12*, 378-383. (d) Greider, C. W. *Annu. Rev. Biochem.* **1996**, *65*, 337-365. (e) Bailey, S. M.; Murnane, J. P. *Nucleic Acids Res.* **2006**, *34*, 2408-2417.

by square planar G-quartets[96]. Since then, in the last decades, several guanine-related molecules have been synthesized and deeply investigated in different areas, from medicinal chemistry to nanotechnology. The use of guanine opens up the possibility to design functional materials with tailored physical properties, that can be easily manipulated thanks to the reversible nature of the interactions.

1.2 Guanosine architectures in non-polar solvents

Until the early 1990s G-quartets have been studied only in aqueous media. Indeed, Guschlbauer reported in his review that *"water appears to be an indispensable solvent for the autoassociation of guanosine [...] organic solvents give rise to poorly organized aggregates"*. At that time the appropriate conditions to characterize G-quadruplexes in organic media were not yet identified. It was just few years later, in 1995, that our group in Bologna[97], and in the same years independently the Davis's[98] group in Maryland, reported that lipophilic guanosine derivatives could form G-quartet structures also in organic media, in presence of alkali-metal cations. The possibility to work in organic media opened up the possibility to design a great variety of functionalized guanosines, both in the sugar hydroxyl groups both in the aromatic base, and unlike in water, it was possible to observe not only supramolecular architectures based on the metal-ion template G-quartet motif, but also ribbon-like, sheet like and continuous helical architectures.[99] In order to study the guanosine behavior in absence of H-bonding competitors, like water molecules, our group started to synthesize lipophilic derivatives (LGs). In these derivatives the donor and acceptor groups in the nucleobase were still present, while aliphatic chains attached to the sugar moiety increased the solubility in organic media. Few examples of LG derivatives are reported below.

[96] M. Gellert, M. N. Lipsett, D. R. Davies, *Proc. Natl. Acad. Sci. USA* **1962**, 48, 2013.

[97] G. Gottarelli, S. Masiero, G. P. Spada, *J. Chem. Soc. Chem. Commun.* **1995**, 2555.

[98] J. T. Davis, S. Tirumala, J. Jenssen, E. Radler, D. Fabris, *J. Org. Chem*. **1995**, *60*, 4167.

[99] J. T. Davis, S. Tirumala, J. Jenssen, E. Radler, D. Fabris, *J. Org. Chem*. **1995**, *60*, 4167.

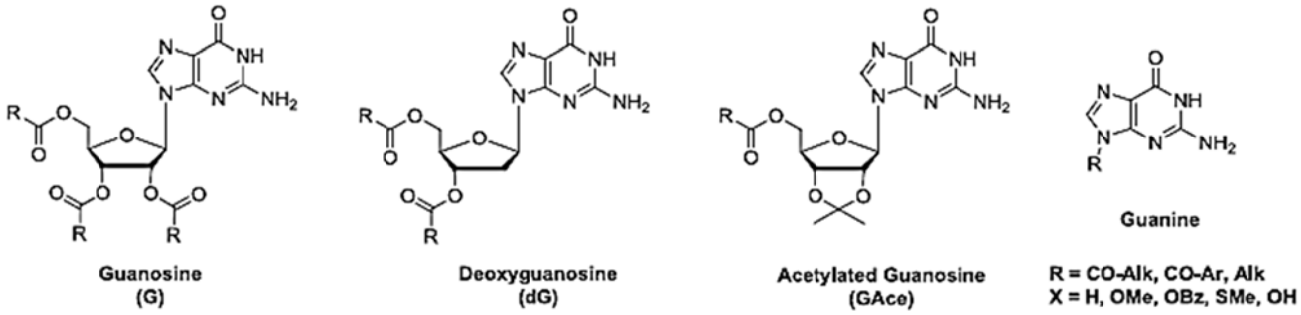

Figure 63: Structures of some lipophilic guanosines and guanines (LGs).

Depending on the experimental conditions different self-assembly pathways were observed. In absence of cations LGs can form, in solution and in the solid state, ribbon-like structures, while in the presence of cations G-quartets are formed, as schematically pictured in figure 64.

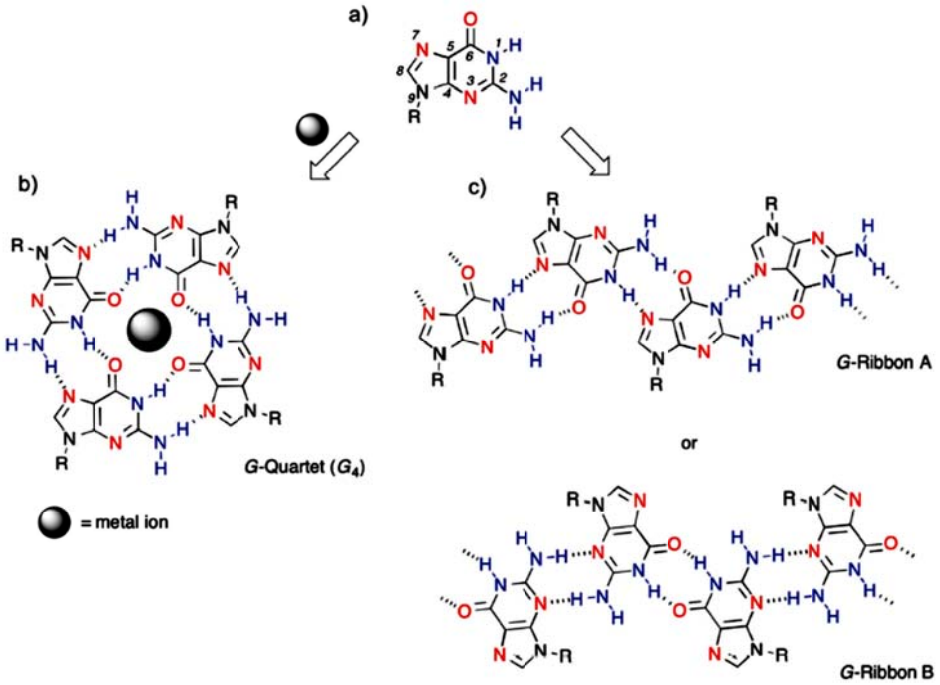

Figure 64: Supramolecular architecture based on guan(os)ine derivatives, template or not by metal-alkali ions

1.3 Supramolecular assemblies mediated by alkali metal ions

In organic media, as well in water, cations are essential to promote the formation of G-quartets. LGs can capture ions from water and transfer them into the organic phase. In particular, performing an extraction of K^+ picrate (Kpic) from water to an organic solution of **dG 1** (figure 65a), a discrete

and highly stable octamer, $[dG\ 1]_8 \cdot K^+$, or columnar polymeric aggregates, $[dG\ 1]_n \cdot nK^+$, can be formed as pictured in Figure 65b.

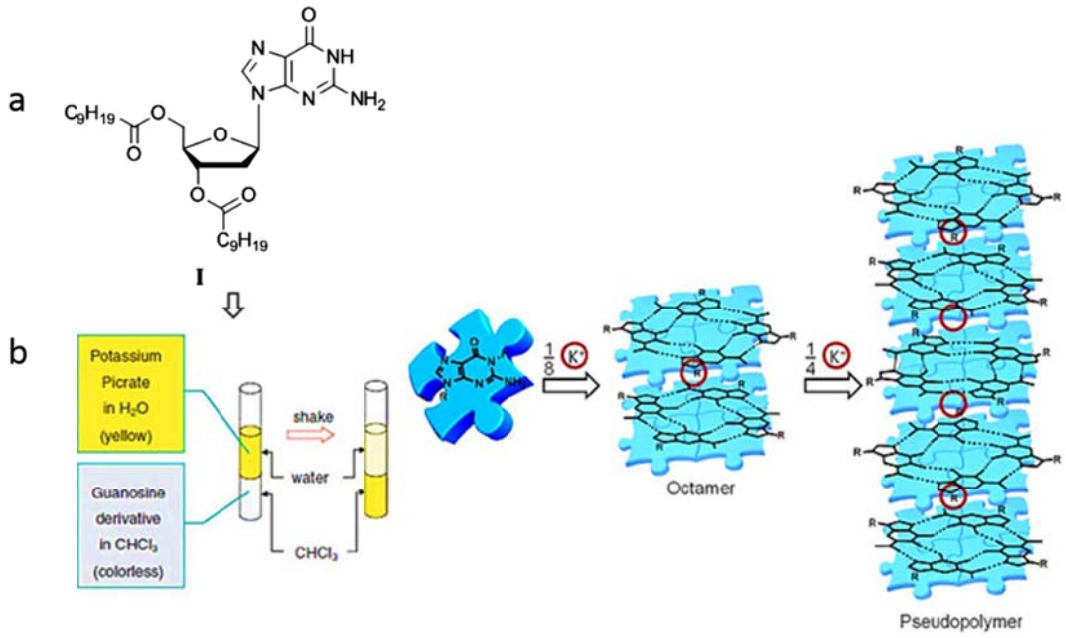

Figure 65: a) Structure of dG1, b) The set-up of the extraction experiment and consequent cation directed self-assembly of a lipophilic guanosine.

Following the extraction it is possible to observe macroscopically the ionophoric behavior of LGs. In fact, at the beginning a yellow water solution of KPic and a colorless chloroform solution of LG are observed, while, as the extraction proceeds, the organic phase increases its yellow color. Circular Dichroism and NMR spectra recorded on the LG solution before and after extraction, evidence the aggregation phenomena mediated by metal alkali ions. In addition, through NMR it is also possible to determine the stoichiometry of the complex. Thus, it has been demonstrated that when a small quantity of Kpic is added, a 8:1 LG/K^+ ratio (the octamer) is obtained; when more Kpic is added, a 4:1 LG/K+ structure (the *pseudo*-polymer) is formed. Stabilization of G-quartets is driven by the coordination of carbonyl oxygens by alkali metal ions and the ionic radius of the cations determines its position between two quartets and its ability to stabilize G-quartets. As shown in the Figure 66, K^+, with bigger ionic radius, it is found between two tetrads, whereas Na^+, with a smaller ionic radius, it has been found in the same layer of G-quartet. In this case the stabilization of the aggregates increases by increasing the ionic radius:[100]

K+ (1.38 A) > Rb+ (1.49 A) ~ Na+ (1.02A) > Cs+ (1.70 A) > Li+ (0.74 A).

[100] Hardin, C. C.; Watson, T.; Corregan, M.; Bailey, C., *Biochemistry* **1992,** *31* (3), 833-41.

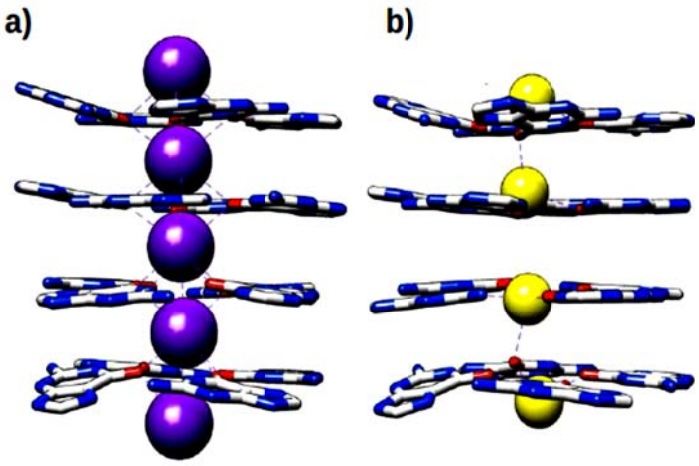

Figure 66: a) K^+ and b) Na^+ location in a G-quadrupelx

Furthermore, the picrate anion is not passive, as it contributes to keep together the complex structure by means of hydrogen bonds. A stereochemical consequence to the cation-templated self-assembly of guanosines and guanosine derivatives is costituted from the mutual orientation of the stacked G-quartets. They have diasterotopic faces, known as head (H) and tail (T), as pictured in figure 67b:

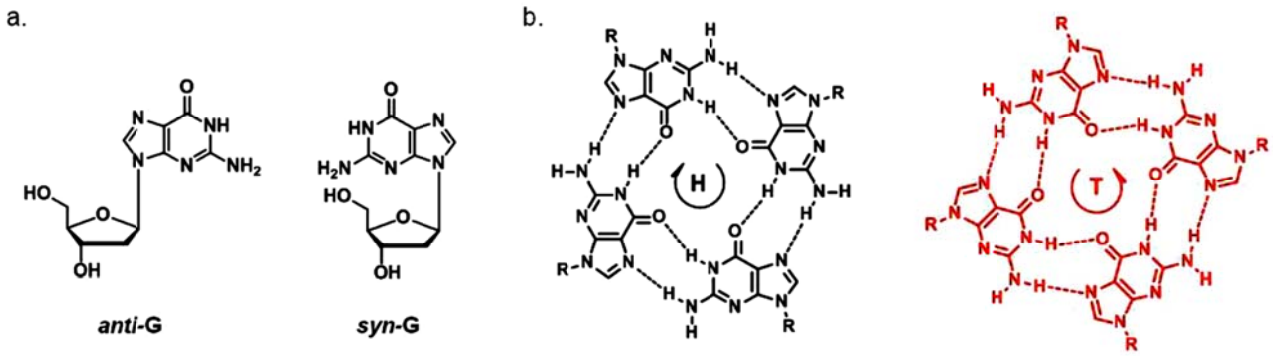

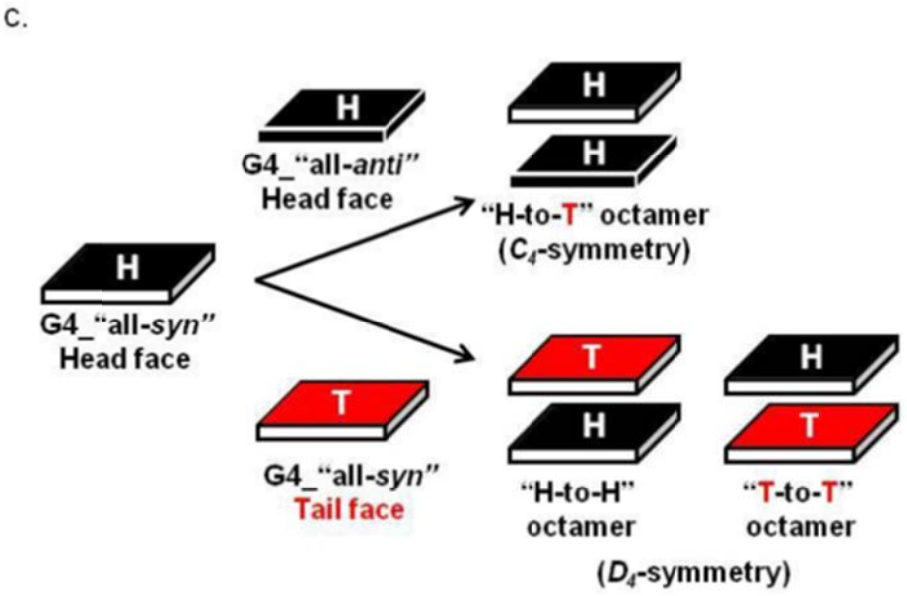

Figure 67: a) Glicosidic *syn* and *anti* conformations of guanosine **dG**; b) Two diasterotopic faces of a G-quartet: while the head (H) face shows a clockwise direction of H-bondings, the tail (T) face shows an anti-clockwise direction; c) Schematic drawing of a *C4*-symmetric octamer (in which an all-*syn* G-quartet stacks with its tail-side on the head-side of an all-*anti* G-quartet), and a *D4*-symmetric octamer (where two all-*syn* G-quartets stack facing their tail sides).

The two quartets in the octameric aggregates can be arranged in three different ways, leading to different symmetries (figure 67c):

- H-to-T (*C4* symmetry, homopolar stacking),
- H-to-H (*D4* symmetry, heteropolar stacking)
- T-to-T (*D4* symmetry, heteropolar stacking)

Information about the symmetry of the aggregates can be obtained by NMR spectra. In fact, while for C4 symmetry two sets of signals are observed in the 1H-NMR spectrum (the two G-quartets are diastereotopic), in the case of D4 symmetry only a single set of signals is observed for the two homotopic G-quartets. Furthermore, as it will be better explained in the next paragraph, Circular Dichroism is a diagnostic way to confirm the stacking polarity of two contiguous G-quartets. At 230–300 nm, region characteristic of the π–π* transitions of guanine chromophore, a double-signed exciton-like signal can be observed in the CD spectrum, due to the rotation of the two tetrads to each other. This couplet, the sign of which allows the assignment of the stacking helicity

(handedness), exhibits opposite signed bands at about 260 and 240 nm for the head-to-tail (*C4*-symmetric) stacking, while both bands are blue-shifted by 20–30 nm in the *D4*-symmetric stacking, as shown in figure 68.[101,102]

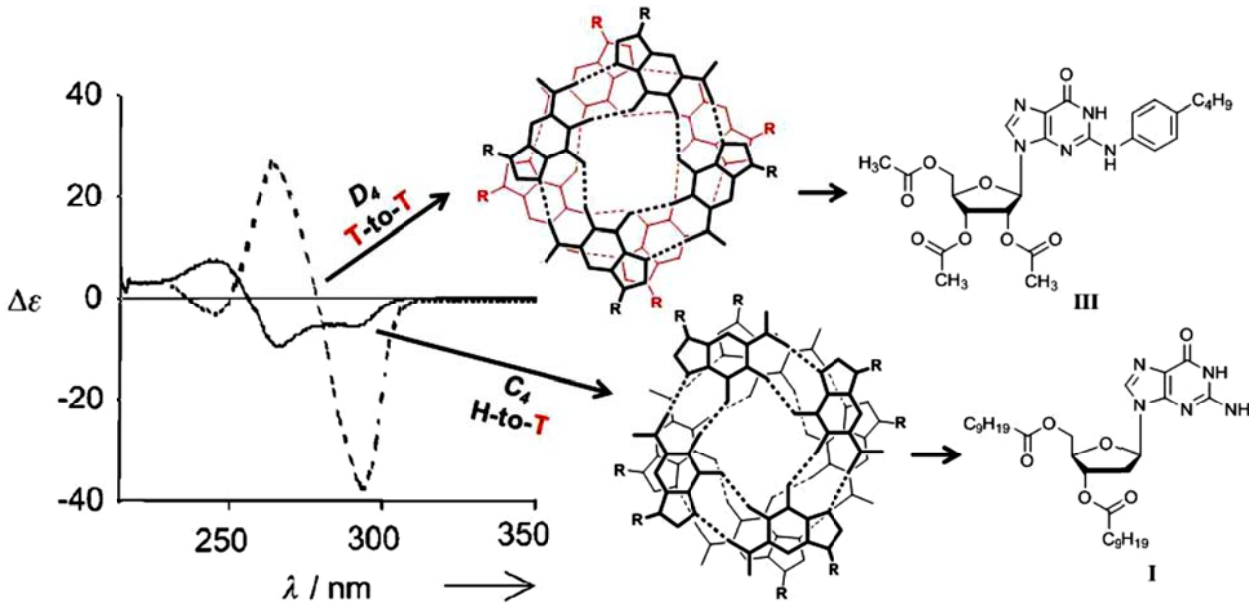

Figure 68: Comparison between CD spectra of *C4*- (solid line) and *D4*-symmetric (dashed line) octamers G8·M+ obtained from derivatives **I** and **III**, respectively.

1.3.1 C_4-Symmetry octamer $G_8{\cdot}M^+$

In collaboration with the Davis's group (University of Maryland)[103] it was possible to determine the structure of the octameric form of **dG 1**, figure 69a, through NMR spectroscopy.[104] The complex resulted to be very stable and robust. NMR spectra showed two sets of signals in a 1:1 ratio, corresponding to two different conformations of the glycosydic moiety, a *syn*-like and an *anti*-like.

[101] Gottarelli, G.; Masiero, S.; Spada, G. *Journal Of The Chemical Society-Chemical Communications* **1995**, 2555.

[102] Graziano, C.; Masiero, S.; Pieraccini, S.; Lucarini, M.; Spada, G. *Organic Letters* **2008**, *10*, 1739.

[103] Davis, J.; Tirumala, S.; Jenssen, J.; Radler, E.; Fabris, D. *Journal Of Organic Chemistry* **1995**, *60*, 4167.

[104] A. Marlow, E. Mezzina, S. Masiero, G. P. Spada, J. T. Davis, G. Gottarelli, *J. Org. Chem.* **1999**, *64*, 5116.

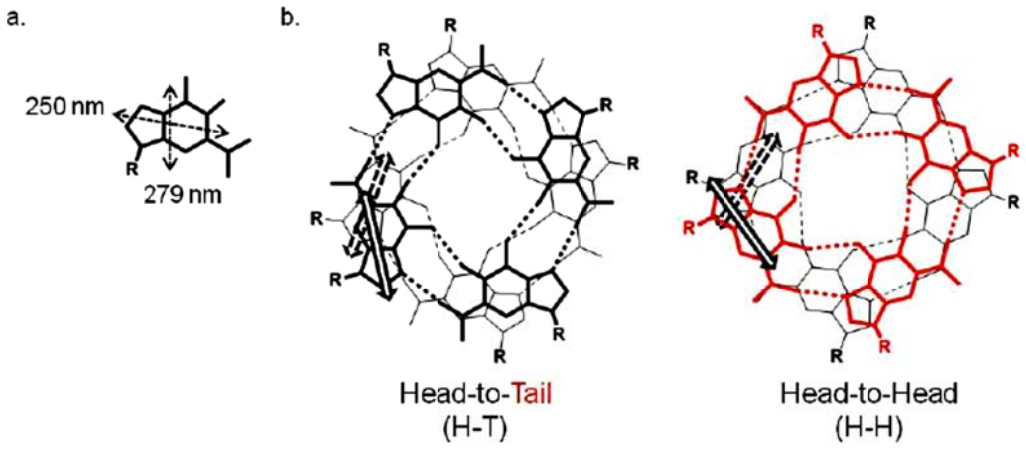

Figure 69: a) Representation of π-π* axis polarized transitions in guanine structure; b) Two possible stacking modes of guanine octamers.

NMR spectra indicated that this octamer was a single diastereomer of C4 symmetry. In one G-quartet, all monomers had a *syn* conformation, while the other tetramer had an "all-*anti*" conformation. NOE interactions indicated a relative orientation with the head-side of the "all-*anti*" G-quartet facing to the tail-side of the "all-*syn*" G-quartet.

1.3.2 D4-symmetric "polymer", (G4.M+)n

With an excess of Kpic columnar polymeric aggregates of **dG1** have been observed, $[dG1\ ]_n \cdot nK^+$, and this structure was resolved in our group by NMR and SANS (Small Angle Neutron Scattering) spectroscopy[105]. For this system NMR spectra showed three sets of signals, in a 1:1:1 ratio, in which each set corresponds to guanosines with different conformations (one *anti* and two different *syn* conformers). NMR data were consistent with the formation of a polymer constituted by dodecamer building blocks. Each dodecamer is composed by three stacked G-quartets: an all-*anti* (A), an all-*syn1* (S_1), an all-*syn2* (S_2). Even if three possible sequential arrangements could be possible, AS1S2, AS2S1, S1AS2, only the first have been observed, and once again considering the diastereotopicity of the quartet's face, eight (2^3) different relative orientations of A, S1 and S2 were possible (Figure 70).

In excess of potassium picrate, columnar polymeric aggregates of dG1 have been observed, $[dG1\ ]_n \cdot nK^+$, and this structure was solved in our group by NMR and SANS, (small angle neutron

[105] E. Mezzina, P. Mariani, R. Itri, S. Masiero, S. Pieraccini, G. P. Spada, F. Spinozzi, J. T. Davis, G. Gottarelli, *Chem. Eur. J.* **2001**, *7*, 388.

scattering), spectroscopy[106]. For this system, NMR data showed three sets of signals, in a 1:1 ratio, in which each set correspond to guanosine monomers with a different conformation (one *anti*, and two different *syn* conformers). NMR data are consistent with the formation of a polymer consisting of a dodecamer building block with three different arrangments of stacked G-quartets: all-*anti* (A), all-*syn1*, (S_1), all-*syn2*, (S_2). Even if three possible sequential arrangments could be possible, AS1S2, AS2S1, S1AS2, only the first have been observed, and once again considering the diastereotopicity of the quartet's face, eight, (2^3), different relative orientations of A, S1, and S2 are possible.

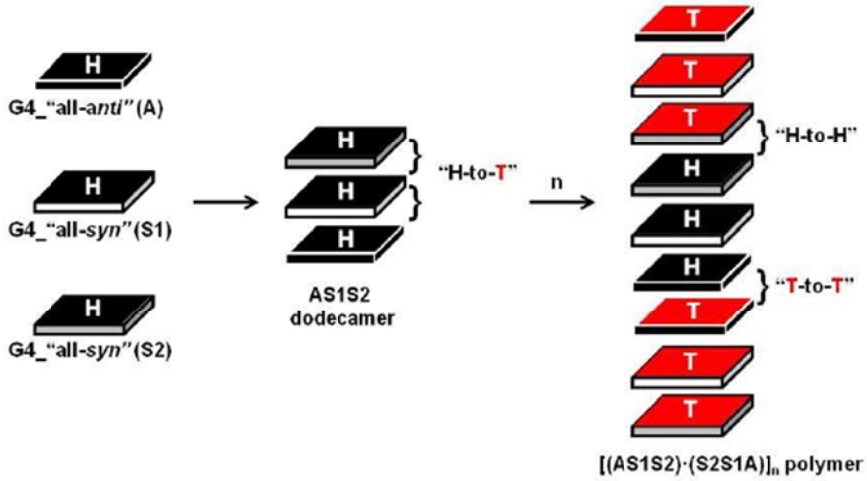

Figure 70: Formation of [(AS1S2) (S2S1A)]n polymer, composed of all-anti (A, all-syn1 (S1) and all-syn2 (S2) quartets.

NOESY experiments confirmed that the AS1S2 dodecamer consists of a unique stereoisomer, and the repetition of dodecamer can be reported as: [AS1S2] [S2S1A] [AS1S2] [S2S1A] [AS1S2], wherein two all-*anti* quartets A and two all-*syn*2 quartets S2 are close together, arranged in a tail-to-tail and a head-to-head orientation, respectively.

Moreover, it was found that both ribbon-like structures and supramolecular polymeric assemblies can self-correlate forming lyotropic liquid-crystalline phases of the cholesteric and hexagonal types in hydrocarbon solvents above a critical concentration[107].

1.3.3 D_4-symmetric octamer $G_8{\cdot}M^+$ and D_4-symmetric hexadecamer $G_{16}{\cdot}4M^+$

[106] E. Mezzina, P. Mariani, R. Itri, S. Masiero, S. Pieraccini, G. P. Spada, F. Spinozzi, J. T. Davis, G. Gottarelli, *Chem. Eur. J.* **2001**, *7*, 388.

[107] S. Pieraccini, G. Gottarelli, P. Mariani, S. Masiero, L. Saturni, G. P. Spada, *Chirality* **2001**, *13*, 7.

While dG(C10) forms the K^+-templated C4-symmetric octamer or the polymeric assembly $(G4 \cdot M^+)n$ in solution, other LG derivatives can give a different octamer with a D4-symmetry. In the presence of Na^+ ions, N2-modified guanosine derivatives, like N2-(4-butylphenyl)-2‘,3‘,5‘-O-triacetylguanosine (II), are found to self-associate into discrete octamers with D4 symmetry. Indeed, 1H spectrum reveals only one set of signals, corresponding to a syn glycosidic conformation for all eight guanosine molecules in each octamer, while correlation studies demonstrate that the two G-quartets are stacked in a tail-to-tail fashion.

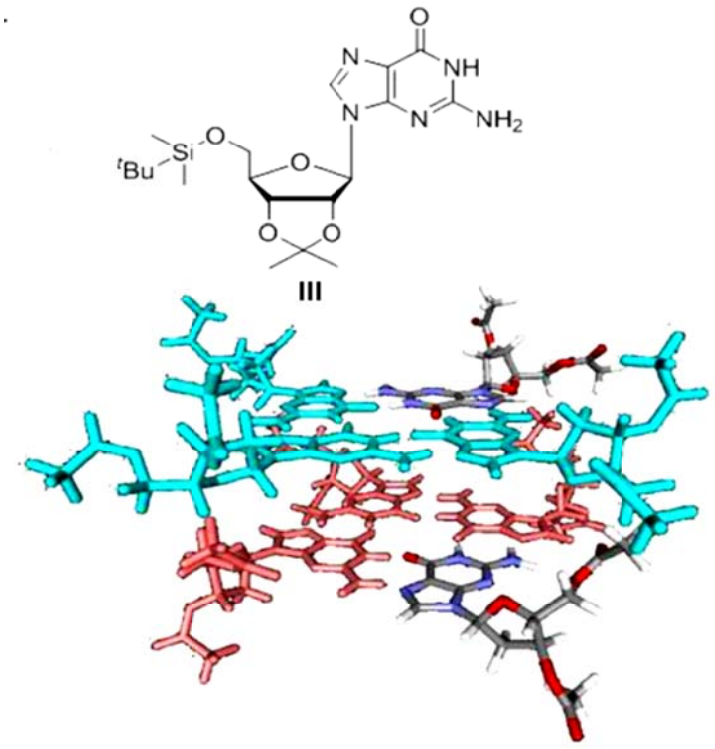

Figure 71: The structure of the LG(III)8.K^+ octameric complex (the metal ion at the center is not shown for clarity): an all-anti G-quartet (three molecules are colored in light blue) with its head side stacks on the tail side of an all-syn G-quartet (three molecules are colored in red).

Other types of G4-aggregates can be obtained in solution from other LGs.I A hexadecamer is formed by the lipophilic derivative 5‘-tertbutyldimethylsilyl-2‘,3‘-isopropylideneguanosine (II) in presence of equimolar potassium and cesium picrates, as pictured below.

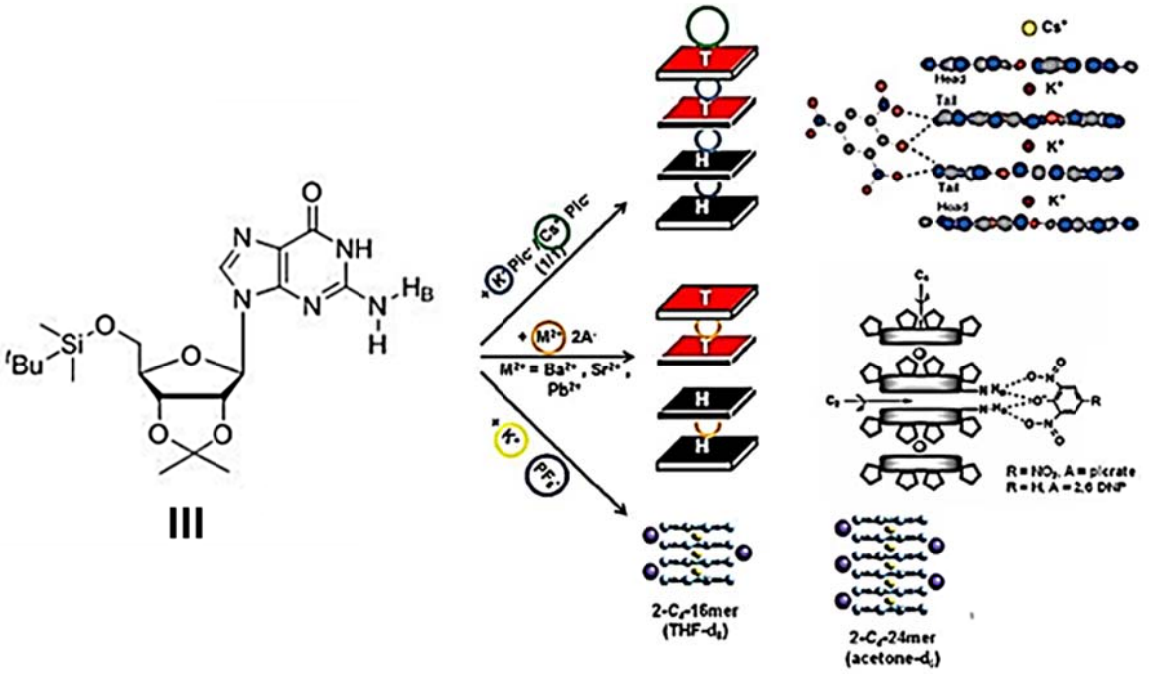

Figure 72: Aggregates formed by **III** with different cations and solvent: hexadecameric ions channel *D4*-symmetric hexadecamer *C4*-symmetric 16-mer and 24-mer.

The structure of the hexadecamer G16·3K^+/1Cs^+·4Pic^-, characterized by X-ray chrystallography,[108]consists of two C4-symmetric G8·K^+ octamers linked together by four picrate anions H-bonded to the N2-HB amino protons that project from the two inner G4-quartets. The resulting D4-symmetric hexadecamer represents a fully occupied cation channel, with three collinear K^+ ions located between the adjacent G-quartet planes, and one Cs^+ ion capping this ion channel. Hexadecameric aggregates were detected also in the presence of bivalent cations, such as Ba^{2+}, Sr^{2+}, Pb^{2+}. Compared to G16 4K^+·4Pic^- these latter complexes display a higher stability due to the greater charge density of the divalent cations. It has to be noticed that also the anion has an important role to determine the nature and stability of guanosine aggregates. More chelating and basic anions, like 2,6-DNP, allow a stabilization ofresence of bivalent cations, such as Ba^{2+}, Sr^{2+}, Pb^{2+}. Compared to G16 4K^+·4Pic^-, the higher stability of G16·2Ba^{2+}·4Pic^- is due to divalent cation, which has a greater charge density that held together the picrate. The presence of bivalent cations, leads to homochiral G-hexadecamers by enhancement of cation-dipole interactions, G-quartet hydrogen bonds, and G-quadruplex-picrate interactions. on-coordinating anions, such as PF^{6-} or BF^{4-}, favoured the growth of the G-quadruplexes, while the use of bulky (BPh^{4-}) anions leads to the formation of smaller species. Finally an important role is played by the solvent: more polar

[108] Forman, S.; Fettinger, J.; Pieraccini, S.; Gottareli, G.; Davis, J. *Journal Of The American Chemical Society* **2000**, *122*, 4060.

solvents, which can solvate the dissociated anion more efficiently, favor the formation of larger assemblies. In the case of III, for example, 16mers are formed in THF, 24mers in acetone, whereas the use of more polar solvents, (i.e. DMSO) resulted in no complexation because they are strongly competing solvents for hydrogen bonding.

1.4 Methods for studying G-quadruplexes

Circular Dicroism spectroscopy is widely used to study G-quadruplex self-assembly in solution.[109] In CD spectra a diagnostic exciton CD signal arises when two or more chromophores are chirally oriented with respect to each other. The exciton coupling is characterized by two opposite signed CD bands in the absorption region, while the λ max absorption corresponds, or nearly corresponds, to a zero CD intensity[110]. In the case of G-quadruplexes the chromophores are the guanine moieties that exhibit two absorption bands located at around 250 and 290 nm, corresponding to π-π^* transitions (short axis polarized at *ca.* 290 nm, long axis polarized at *ca.* 250 nm). An exciton coupling between the transition dipole moments located in near-neighbour guanines is generated by the mutual rotation of piled G-tetrads. Homopolar stacking (head-to-tail configuration) or heteropolar stacking (head-to-head or tail-to-tail) origin different excitonic bands at the 250 nm transition, arising from the relative orientation of the transition moments located in the closest guanines in stacked tetrads. The CD signal intensity is related to the rotational strength R*0a*, which is the product of the electric and magnetic transition moments associated to a specific electronic transition (from the ground state *0* to the excited state *a*), therefore to be CD active a transition must have both electric and magnetic moment. When two G-tetrads are stacked to each other, the magnetic moment arises from the coupling of two non-coplanar electric moments of guanine in adjacent quartets (Figure 73a.). Two non-degenerative coupling modes are possible, parallel or antiparallel, for the magnetic moment with respect to the electric one, thus, the product of electric and magnetic moments gives rise to one positive (parallel mutual orientation) and one negative (antiparallel orientation) rotational strength, with the lower energy coupling at higher wavelength.

[109] a) Masiero, S.; Trotta, R.; Pieraccini, S.; De Tito, S.; Perone, R.; Randazzo, A.; Spada, G., *Organic & Biomolecular Chemistry* **2010,** *8* (12), 2683-2692. b) Randazzo, A.; Spada, G.; Da Silva, M.; Chaires, J.; Graves, D., *Quadruplex Nucleic Acids* **2013,** *330*, 67-86.

[110] Superchi, S.; Giorgio, E.; Rosini, C., *Chirality* **2004,** *16* (7), 422-451.

For heteropolar stacking a positive exciton couplets is expected, while a negative exciton couplets is predicted for homopolar stacking (Figure 73 c.).

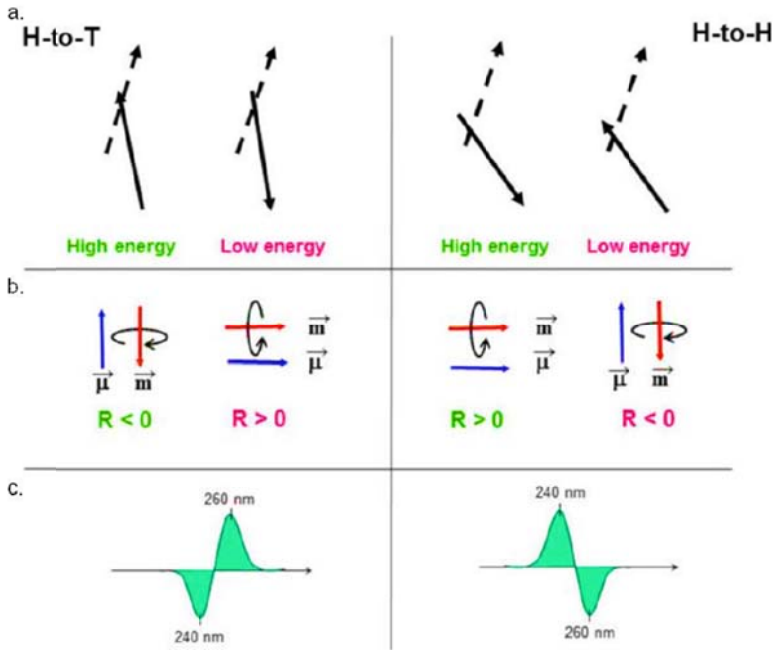

Figure 73: Origin of the exitonic CD signal in stacked G quartets.

1.5 Self assembly non mediated by alkali metal ions

All the supramolecular architectures described so far are promoted by the presence of alkali metal ions, which stabilize via dipole-ion interactions the formation of G-quartets that in turn can stack forming G-quadruplexes. In the absence of metal cations, guanosines can polymerize via hydrogen bonding forming supramolecular linear ribbons which have been deeply investigated. In 1998 our group isolated and characterized these aggregates both in organic solution and in the solid state.[111] Two different ribbon-like aggregates can be obtained, which differ for the patterns of hydrogen bonds and posses different symmetry. Thus, while ribbon B has no dipole, the ribbon A structure possess a permanent dipole moment. In addition, at the solid state ribbons An arrange in parallel fashion making polar the whole bulk.

[111] Gottarelli, G.; Masiero, S.; Mezzina, E.; Spada, G.; Mariani, P.; Recanatini, M. *Helvetica Chimica Acta* **1998**, *81*, 2078.

a.

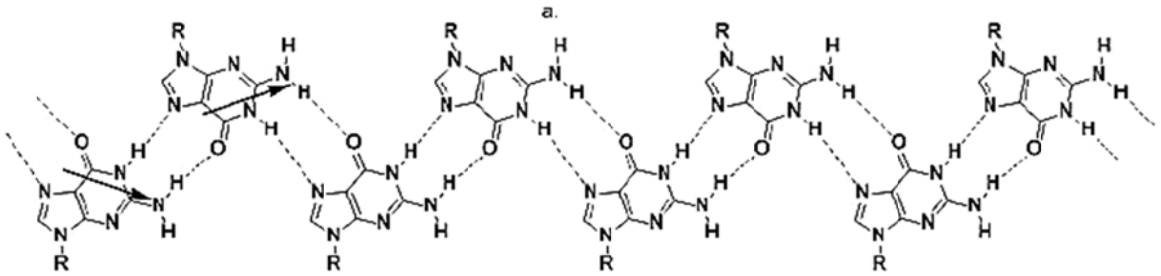

b.

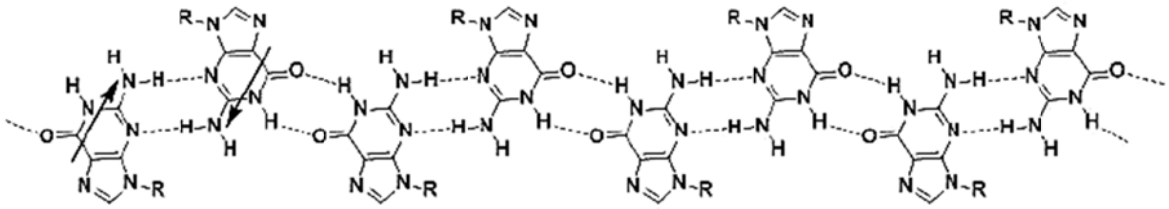

Figure 74: H-bond pattern of ribbon-like assemblies: ribbon A (a.), ribbon B (b.). Arrows indicate molecular dipoles.

Ribbon A was found to be more stable in the solid state and is held together by an intermolecular N^2H-–O^6 and N^1H—N^7 hydrogen bond network. In solution, the ribbon A slowly converts to a thermodynamically more stable form (ribbon B), characterized by N^1H-–O^6 and N^2H –N^3 intermolecular cyclic hydrogen bonds. A back rearrangement of ribbon B-type to the A-type ribbon occurs upon adsorption at the solid–liquid interface. In both ribbon-like polymers the glycosydic bonds adopt an *anti* conformation. A change of the guanosine backbone may lead to different aggregates. For example, formation of "bare" G-quartet structures without any templation effect by cations[112] can be obtained by introducing a bulky substituent (like 4-NMe_2-Ph, SMe or Br) in the C8 position of guanine. Resulting conformational constrained nucleoside adopts a *syn*-glycosidic bond conformation that forces the exocyclic amino group on top of the sugar ring, preventing ribbon formation both in the solid state and in solution. Moreover, the introduction of an hydroxyl group in C^8 promotes the tautomerization to the more stable 8-oxo-guanosine. The relative disposition of the two amide groups opens up new possibilities for the formation of strong amide-amide hydrogen bonding pairing, resulting in continuous helical architectures observed in solution,

[112] Sessler, J.; Sathiosatham, M.; Doerr, K.; Lynch, V.; Abboud, K. *Angewandte Chemie-International Edition* **2000**, *39*, 1300.

in the liquid crystalline phase,[113] and also at the solid-liquid interface on graphite (as shown by STM images).[114]

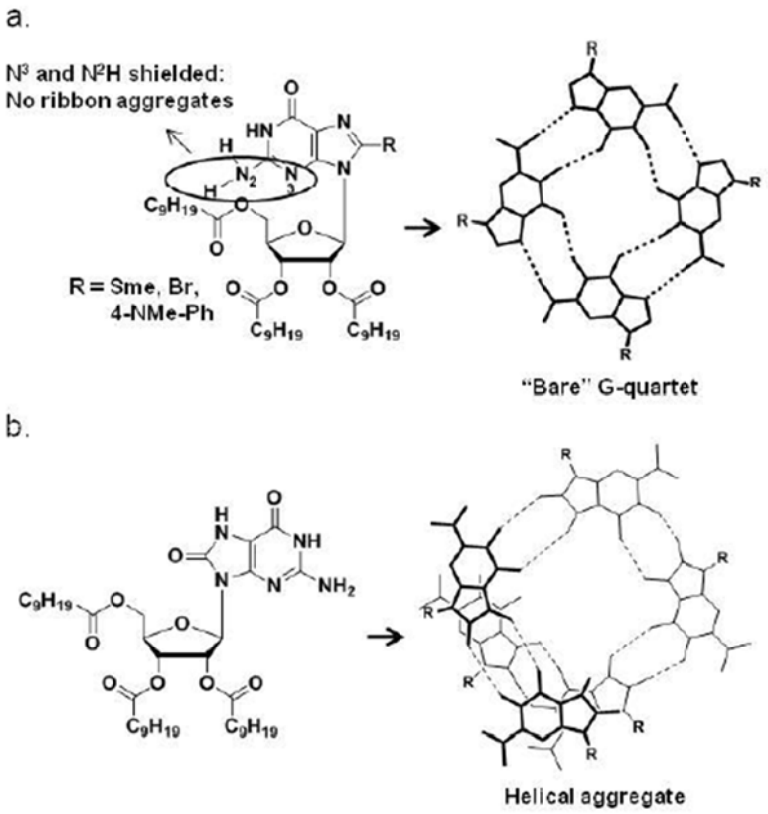

Figure 75: a) C^8 substitued lipophilic guanosines which form "*bare*" G-quartets; b) a lipophilic 8-oxo-guanosine self-assembling in helical aggregates.

1.6 Guanosine as organogelators

Low molecular-weight organogelators (LMOGs) have been subject of constant attention over the past few decades, because they represent potential systems for the applications on smart materials, drug delivery, agents, sensors, or water purification.[115] LMOGs can self-assemble into various

[113] Lena, S.; Cremonini, M.; Federiconi, F.; Gottarelli, G.; Graziano, C.; Laghi, L.; Mariani, P.; Masiero, S.; Pieraccini, S.; Spada, G. *Chemistry-A European Journal* **2007**, *13*, 3441.

[114] Giorgi, T.; Lena, S.; Mariani, P.; Cremonini, M.; Masiero, S.; Pieraccini, S.; Rabe, J.; Samori, P.; Spada, G.; Gottarelli, G. *Journal Of The American Chemical Society* **2003**, *125*, 14741.

[115] a) N.M. Sangeetha, U. Maitra, *Chem. Soc. Rev*. 34, **2005**, 821. b) M. Suzuki, Y. Sakakibara, S. Kobayashi, M. Kimura, H. Shirai, K. Hanabusa, *Polym. J.* 34, **2002**, 474. c) S. Kobayashi, N. Hamasaki, M. Suzuki, M. Kimura, H. Shirai, K. Hanabusa, *J. Am. Chem. Soc*. 124, **2002**, 6550. d)

three-dimensional structure like strands, ribbons, fibers, rods, tubules and helices. Different physico-chemical and mechanical properties can be monitored, such as reversible changes in volume and surface properties, in response to a variety of environmental stimuli, such as temperature, pH, ionic strength, electric field, light irradiation and solvent composition.[116] Guanylic nucleotides and oligonucleotides can form hydrogels or liquid-crystalline phase in aquesous solution, as a consequence of the formation of self-assembled G-quartet based chiral columnar aggregates, held together by non-covalent interactions[117].

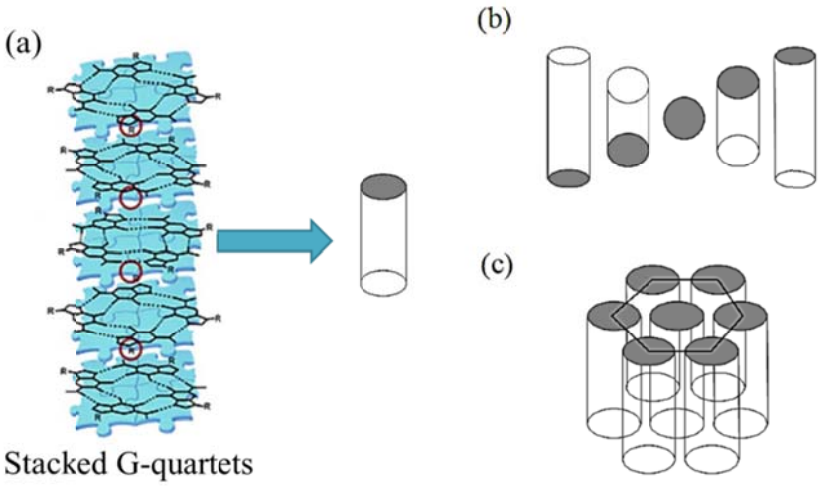

F.S. Schoonbeek, J.H. van Esch, B. Wagewijs, D.B.A. Rep, M.P. de Haas, T.M. Klapwijk, R.M. Kellog, B.L. Feringa, *Angew. Chem., Int. Ed*. 38, **1999**, 1393. e) S. Bhattacharya, Y.K. Ghosh, *Chem. Commun*., **2001**, 185. f) V. Bekiari, P. Lianos, *Chem. Mater*. 18, **2006**, 4142. g) S. Ray, A.K. Das, A. Banerjee, *Chem. Mater*. 19, **2007**, 1633.

[116] a) Y. Hirokawa, T. Tanaka, *J. Chem. Phys*. 81, **1984**, 6379. b) G.M. Eichenbaum, P.F. Kiser, S.A. Simon, D. Needham, *Macromolecules* 31, **1998**, 5084. c) F.M. Winnik, M.F. Ottaviani, S.H. Bossmann, M. Garciagaribay, N.J. Turro, *Macromolecules* 25, **1992**, 6007. d) F.M. Winnik, H. Ringsdorf, J. Venzmer, *Macromolecules* 23, **1990**, 2415. e) Y. Osada, H. Okuzaki, H. Hori, *Nature* 355, **1992**, 242. f) A. Suzuki, T. Tanaka, *Nature* 346, **1992,** 345.

[117] a) G. Gottarelli, G. P. Spada, A. Garbesi in *Comprehensive Supramolecular Chemistry: Templating, Self-assembly and Self-organisation, Vol. 9* (Eds.: J. M. Lehn, J.-P. Sauvage, M. W. Hosseini), Pergamon, Oxford, **1996**, Chapter 13. b) The serendipitous discovery of the self-assembly of simple guanilates leading to liquid-crystal phases was narrated in: G. Gottarelli, G. P. Spada, *Chem. Rec.* **2004**, *4*, 39. c)W. Guschlbauer, J. F. Chantot, D. Thiele, *J. Biomol. Struct. Dyn.* **1990**, *8*, 491.

Figure 76. Lyotropic liquid crystals from (a) self-assembled guanosines. The symmetry of the (b) cholesteric and (c) hexagonal phase.

Changing different conditions, such as temperature or equivalents of added salts, these aggregates can originate viscous gel-like phases or self-correlate to generate mesophases of either cholesteric or hexagonal type, as pictured in Figure 76. Not only template aggregates, but also in the absence of cations, lipophilic guanosine supramolecular aggregates can form lyotropic mesophases also in organic media,[118].

1.7 Liquid Crystals

In this section it will be described general informations about liquid crystals (LCs), useful to better understand the behavior of guanosine aggregates, starting from classification to general characteristics. The three well-defined states of matter are represented by solids, liquids and gases, that differ each others from a different amount of order. The solid state exhibits a rigid arrangement of the molecules, that are oriented in a fixed way and highly ordered. In the liquid state molecule are not constrained to occupy a specific position, thus are free to diffuse in a random fashion. Attractive forces in the liquid state still exist, but result to be weaker than in solids. In gas phase the degree of order is therefore much less than in the liquid state, and more molecules move quickly in all directions. LCs are matter in a state that has properties intermediate between those of conventional liquid and those of solid crystal. For example, LCs can flow like a liquid, but its molecule are oriented as in the solid state. To the typical properties of the solid state (optical anisotropy and electric) and of the liquid state (fluidity and molecular mobility), are added peculiar characteristics of the liquid crystal itself: such as the ability to vary the degree of order by means of magnetic and electric fields , or change of color as function of the temperature and so on.This has made of the liquid crystal a class of compounds that are now widely used for the construction of objects of daily use such as the LCD display.

[118] G. Gottarelli, S. Masiero, E. Mezzina, S. Pieraccini, G. P. Spada, P. Mariani *Liq. Cryst.* **1999**, *26*, 965.

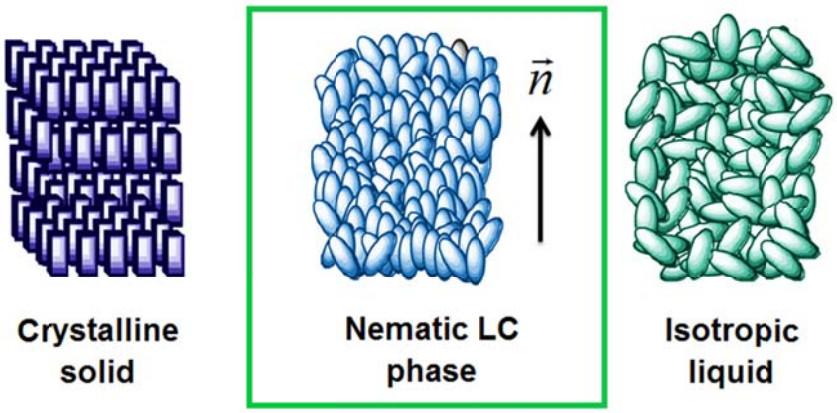

Figure 77: Schematic representation of solid, liquid crystal and liquid phase.

It is possible to define different type of LCs, as function of their different optical properties; LCs can be divided into three phase: *lyotropic*, *thermotropic* and *metallotropic* phases. *Thermotropic* and *Lyotropic* LCs consist of organic molecules, and while the first one exibits phase transitions as a function of temperature, the latter is dependent from temperature and also concentration in a solvent. *Metallotropic* LCs are composed of both organic and inorganic molecules, and phase transition depends not only on temperature and concentration, but also on inorganic-organic composition ratio.

1.7.1 Thermotropic mesophases

The order of a thermotropic LC can be changed by temperature; when the temperature is too high the LC convert to an isotropic liquid, as consequence of motion of the components, whereas if the temperature is too low, the LC turns into a glass phase. Upon the transition from glass state to isotropic liquid, LCs display different "subphases" of growing degree of order, *nematic, smectic* and *colesteric,* and considering the shape they can be divided in disco-shaped and rod-shaped molecules. One of the most common LC phases is the *nematic* one. In a nematic phase, the *calamitic* or rod-shaped organic molecules have no positional order, so they are free to flow, but they self-align to have long-range directional order with their long axes roughly parallel, maintaining their long-range directional order[119]. Nematics exhibit fluidity similar to that of ordinary (isotropic) liquids, but they can be easily aligned by an external magnetic or electric field. Aligned nematics have the optical properties of uniaxial crystals and this makes them extremely

[119] Rego, J.A.; Harvey, Jamie A.A.; MacKinnon, Andrew L.; Gatdula, Elysse *Liquid Crystals* **37** (1), **2010,** 37–43.

useful in liquid crystal displays (LCD). The *smectic* phases, found at lower temperatures than the nematic, form well-defined layers, which can slide over one another. The smectic phases are exibit positional ordered along one direction. Different smectic phase can be observed, characterized by different types and degrees of positional; thus, in the Smectic A phase, the molecules are oriented along the layer normal, while in the Smectic C phase they are shifted away from the layer normal. These phases are liquid-like within the layers.

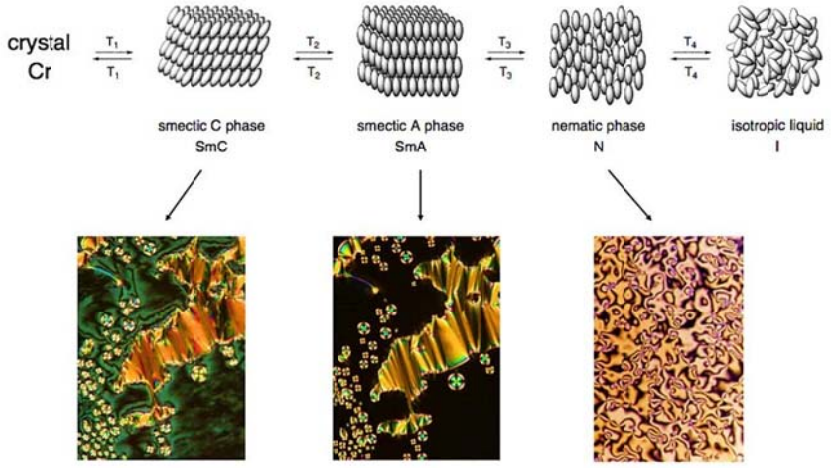

Figure 78: Liquid crystal phase sequence for calamitic molecules, and the textures observed for each mesophase by polarized optical microscopy.

The *cholesteric* phase, observed for the first time for cholesterol derivatives exhibits chirality (handedness), and only chiral molecules can give rise to such a phase. This phase exhibits a twisting of the molecules perpendicular to the director, with the molecular axis parallel to the director. The finite twist angle between adjacent molecules is due to their asymmetric packing, which results in longer-range chiral order. Thus, the director is not a constant vector, but it rotates around a direction perpendicular to the long axis of the molecule. As consequence an helical structure can be observed, that determine a strong influence on the polarization of light passing through it.

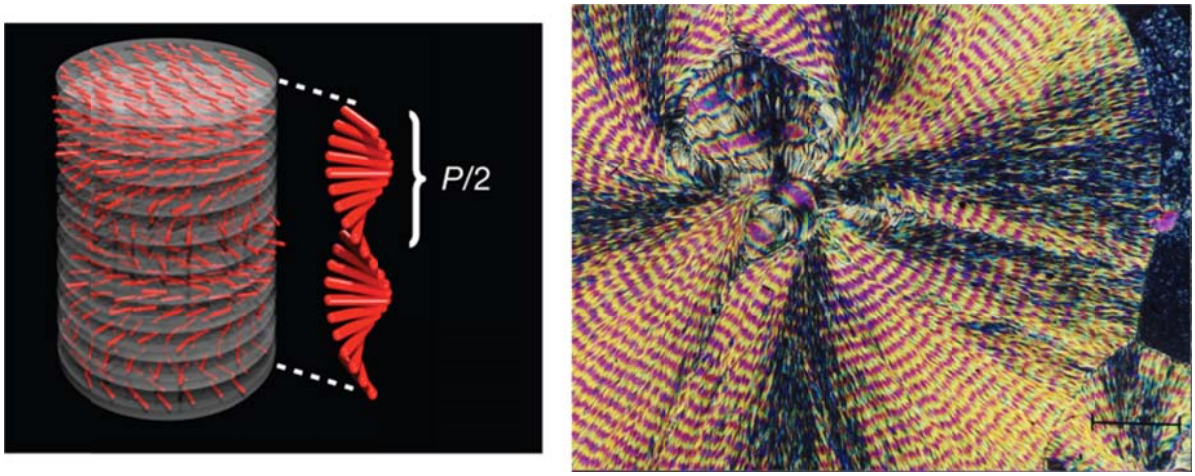

Figure 78: Cartoon of cholesteric phase phase and the textures observed by polarized optical microscopy.

1.7.2 Lyotropic mesophases

A lyotropic liquid crystal is dependent not only by temperature, but also by concentration ranges. In the lyotropic phases, solvent molecules fill the space around the compounds increasing fluidity to the system. Contrary to thermotropic liquid crystals, these lyotropics have another degree of freedom of concentration, that enables them to induce a variety of different phases. The content ratio of the solvent molecules may change the self-assembled structures. At very low concentration, the molecules are dispersed randomly without any ordering, increasing the concentration (but still low), molecules assemble into micelles or vesicles, however still not having an high order. At higher concentration, the assemblies become ordered. A typical phase is a hexagonal columnar phase, long cylinders arrange themselves into a roughly hexagonal lattice. A generic progression of phases, going from low to high concentration, is:

1 Discontinuous cubic phase (micellar cubic phase)
2 Hexagonal phase (hexagonal columnar phase) (middle phase)
3 Lamellar phase
4 Bicontinuous cubic phase
5 Reverse hexagonal columnar phase
6 Inverse cubic phase (Inverse micellar phase)

1.8 From guanosines gels to liquid crystalline mesophases

Lipophilic guanosine derivatives, with two long alkyl chain can form liquid crystal phases both in absence and in presence of alkali metal ions. In absence of metal ions, the gelation process is mediated by the formation of ribbon-like aggregates and a lyotropic phase have been observed by X-ray diffraction studies, where solvent (hexadecane, heptane) penetrates the structure dissolving long alkyl chain. In chloroform instead the solvent is not able to penetrate the structure, generating a new different structure, in which the rods, packed in a two-dimensional square cell, are composed of multiple (two to four) stacked ribbons[120] (Figure 79 a). Adding potassium picrate to a chloroform solution of derivative in 1:4 ratio in heptane, X-ray diffraction studies demonstrated that the aggregate formed, according to NMR spectroscopy studies, is a columnar polymer, made of piled G-quartets with an internal channel of K^+ ions. Increasing the concentration of the aggregate, the liquid crystalline phase, initially a cholesteric phase, became an hexagonal phase[121](Figure 79 b).

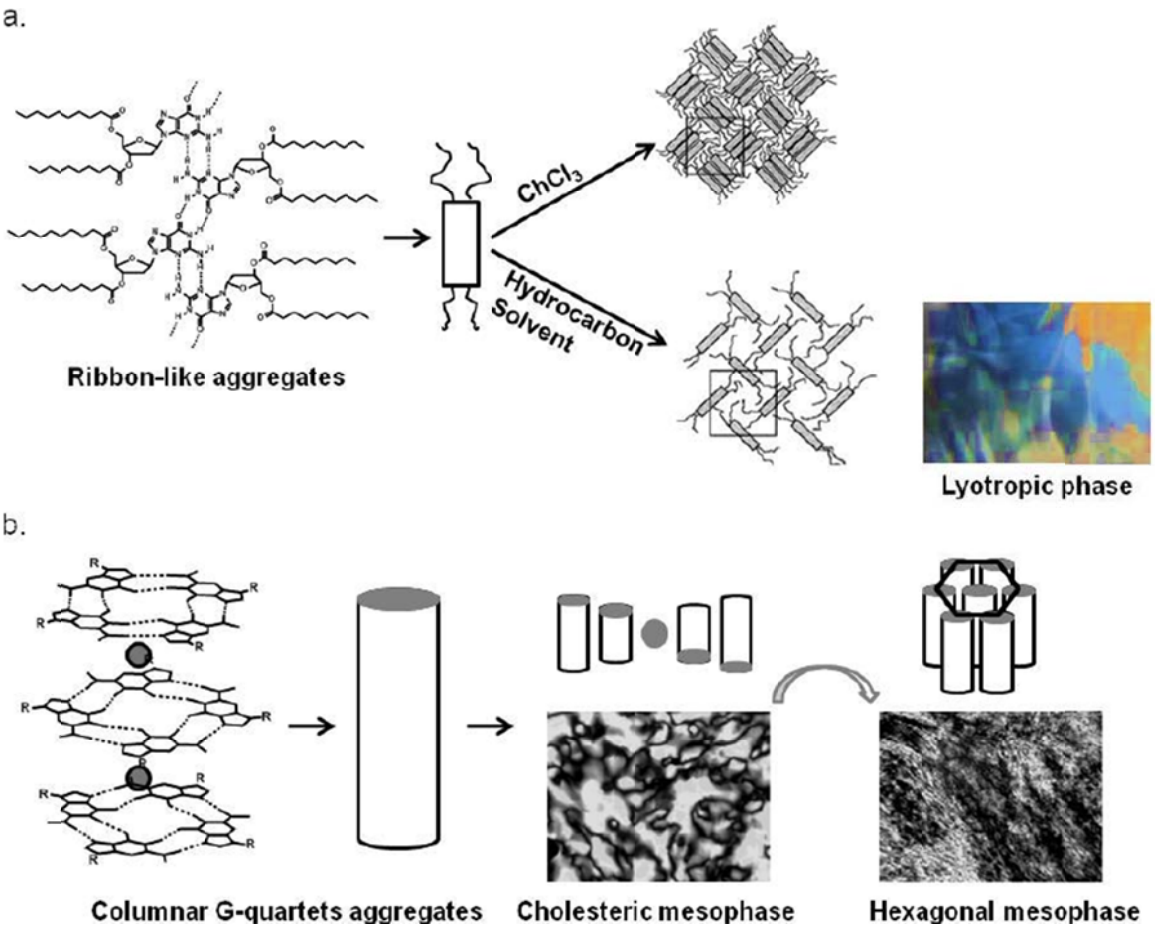

[120] Giorgi, T.; Grepioni, F.; Manet, I.; Mariani, P.; Masiero, S.; Mezzina, E.; Pieraccini, S.; Saturni, L.; Spada, G.; Gottarelli, G. *Chemistry-A European Journal* **2002**, *8*, 2143.

[121] Pieraccini, S.; Gottarelli, G.; Mariani, P.; Masiero, S.; Saturni, L.; Spada, G. *Chirality* **2001**, *13*, 7.

Figure 79: Different type of liquid crystalline mesophases formed by Lipophilic guanosine derivatives, with two long alkyl chain,: in absence of cations (a.) the specie responsible for mesophases is a ribbon-like structure, while with Kpic (b.) the formation of a columnar G-quartet aggregates lead to a cholesteric phase and, increasing the concentration, to a hexagonal phase[122].

Another example of lipophilic guanosine derivatives, figure 80a, forming a gel when in ribbon-like structure is reported below, and in particular its ability to display gel-to-sol conversion[123]. Gelation occurs in some aprotic solvents, such as toluene, after the concentration reached a definite value. The ribbon-like structure is able to change to G-quartets in the presence of K^+, which led to the transformation from a gel to a solution. Upon the addition of the cryptand [2.2.2], G-quartets reverted to the original ribbon-like structure and the gel is recovered. Subsequently, upon the addition of acids, K^+ was released from the cryptate with the transformation of gel-to-sol simultaneously. Finally, upon the addition of bases which deprotonated the gel was regenerated again.

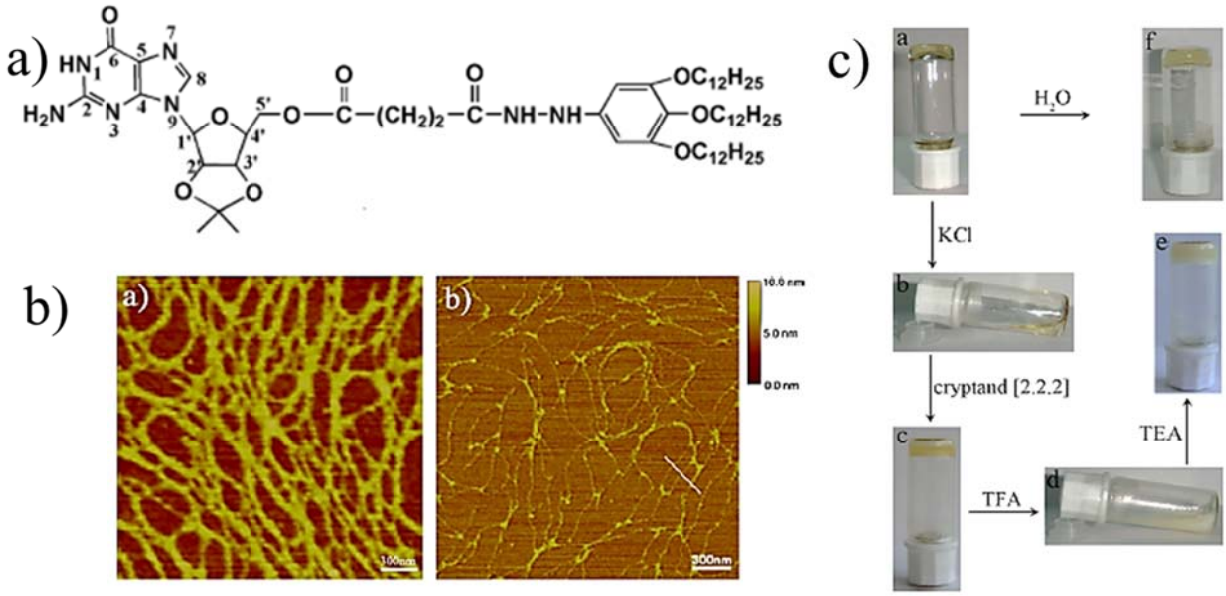

Figure 80. a) structure of lipophilic guanosine derivatives, b) AFM tapping mode height images of 1 on mica. (a) 10 mM in toluene, (b) 1 mM in toluene, c) visual observation of the reversible gel–sol interconversion of the organogel formed by compound 1. TFA: trifluoroacetic acid. TEA: triethylamine.

[122] Pieraccini, S.; Gottarelli, G.; Mariani, P.; Masiero, S.; Saturni, L.; Spada, G. *Chirality* **2001**, *13*, 7.

[123] X. Wang et al. / Journal of Colloid and Interface Science 353 (2011) 412–419

1.9 Switching between assemblies

1.9.1 Alkali metal ions templation

Reversibility is a basic aspect of the supramolecular chemistry. On this issue, lipophilic guanosines represent unique building blocks in which it is possible to switch from G-quartets or G-quadruplexes to ribbon-like structures. Indeed, few years ago our group reported the interconversion between G-quartets and G-ribbons by sequential addition and removal of cations.[124]

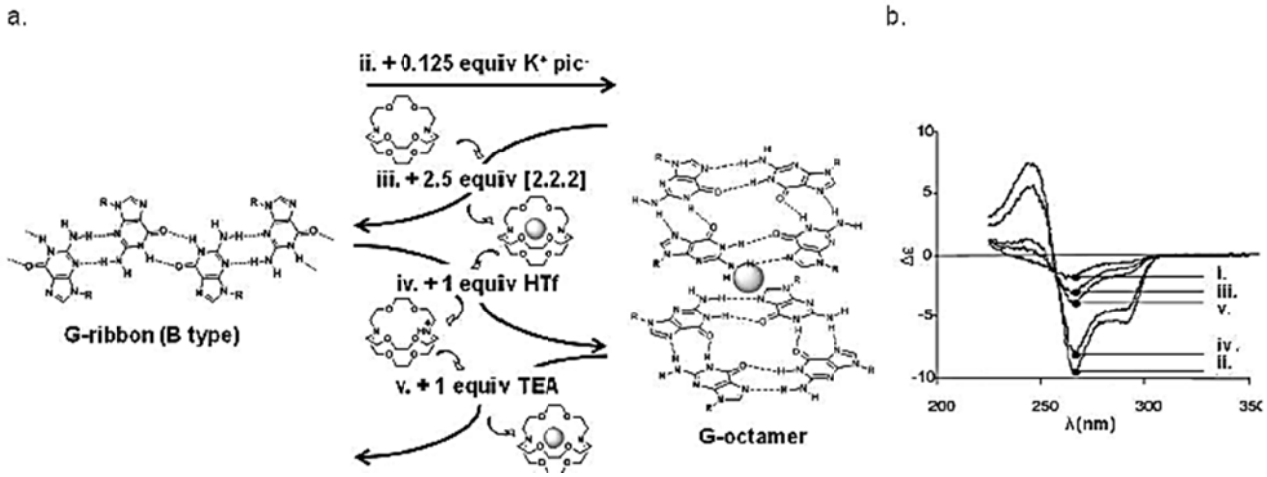

Figure 82: a)Switching between ribbon and octameric species mediated by cation addition and removal and b) the corresponding CD spectra.

Ribbon-like aggregates of the B-type in chloroform convert to the octameric complex by addition of 1/8 equivalent of potassium picrate. Subsequent addition of 2.5 equivalent of cryptand [2.2.2], which offers an efficient complexation of potassium, $[K^+ \cap 2.2.2]$, reverts the potassium complex to the ribbon-type structure. Upon protonation with 1 equivalent of triflic acid of one of the bridgehead nitrogen atoms of the cryptate, $[H^+ \cap 2.2.2]$, the bound K^+ can be released reforming the octamer structure. Once again the ribbon-type structure can be regenerated by addition of 1 equivalent of triethylamine (TEA), that promotes the deprotonation of the cryptand. Several cycles of protonation/deprotonation can be repeated monitoring the ribbon/octamer intervonversion via Circular Dichroism (CD) and ^{1}H-NMR in solution. The switching process can be observed also at the solid/liquid interface trough STM (Scanning Tunneling Microscopy), Figure 83, on highly oriented pyrolitic graphite (HOPG), using an octadecyl guanine derivative.[125] Compared to the

[124] Pieraccini, S.; Masiero, S.; Pandoli, O.; Samori, P.; Spada, G. *Organic Letters* **2006**, *8*, 3125.

[125] Ciesielski, A.; Lena, S.; Masiero, S.; Spada, G.; Samori, P. *Angewandte Chemie-International Edition* **2010**, *49*, 1963.

characterization in solution, reproducibility of STM imaging of the interconversion from ribbons to G4-based architectures requires strict experimental conditions.

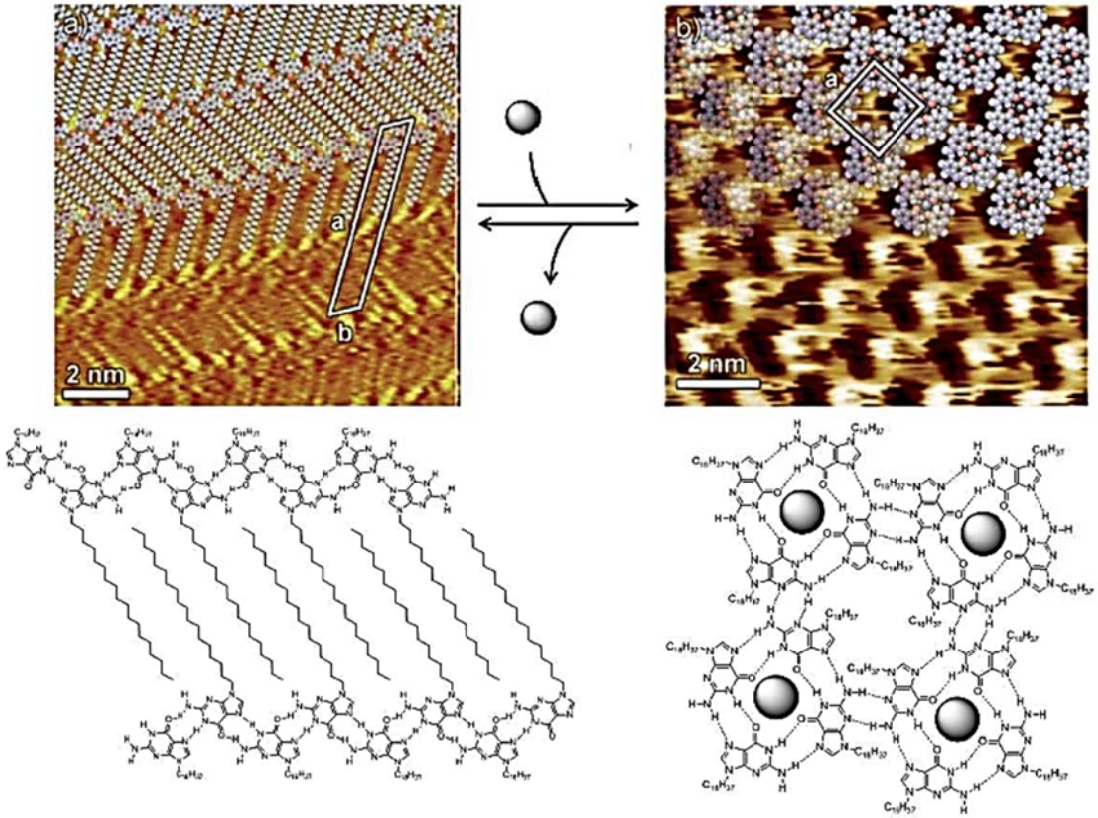

Figure 83: STM images of monolayers of supramolecular architectures of octadecyl guanine derivative at the solid-liquid interface self-assembled from TCB solution; ribbonlike structure (left) and G4-based architecture (right).

1.9.2 Light as external stimuli

Light can be a usefull external stimuli to control guanosine molecular self-assembly. Inspired from Ogasawara work,[126] our group reported the photocontrolled self-assembly of a guanosine nucleobase where an arylvinyl moiety had been introduced at the 8 position. In the presence of a measured amount of KI a self-assembled D4-symmetric octamer is formed. Photoisomerization to the *Z* isomer determines the decomposition of the complex, which is re-formed when the molecule is reverted to the *E* form either by thermal or photochemical back isomerization.

[126] a) S. Ogasawara, M. Maeda, *Angew. Chem. Int. Ed.* **2008**, *47*, 8839-8842; b) S. Ogasawara, M. Maeda, *Angew. Chem. Int. Ed.* **2009**, *48*, 6671-6674.

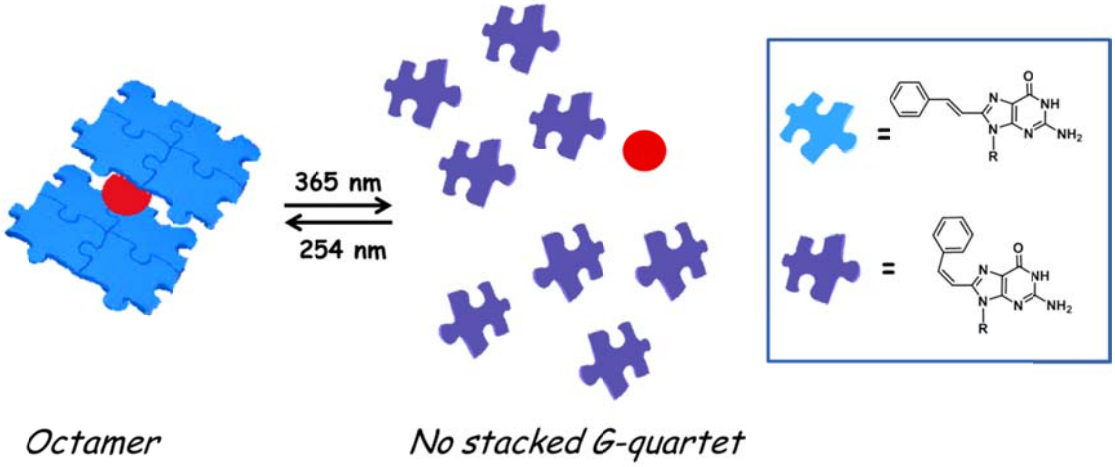

Figure 84: Triggering of guanosine self-assembly by light

The MeCN solution of LG without any added salts shows a CD spectrum profile superimposable to the one recorded in MeOH, a strong competing solvent, suggesting the presence of a disaggregate form (Figure 85).

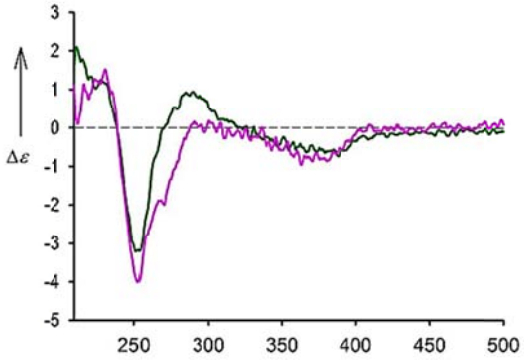

Figure 85: CD spectra of a 5 mM solution of (C8)arylvinyl guanosine derivative in acetonitrile (violet line) and in methanol (green line).

When 1/8 equivalent of KI is added to the MeCN solution of the G-derivative in the trans state, CD spectrum changes dramatically, as expected when the formation of stacked G-quartets templated by the cation occurs. In the CD spectrum (Figure 86a) of the octameric complex, a positive band at 255 nm and a very strong, positive band at 350 nm can be observed. Upon irradiation at 365 nm, photoconversion to the *Z* isomer takes place, and the CD spectrum shows very weak signals, superimposable to the ones corresponding to the *trans-derivative* withouth KI. CD spectrum is similar to that of uncomplexed structure: stacked G-quartets no longer exist in solution.

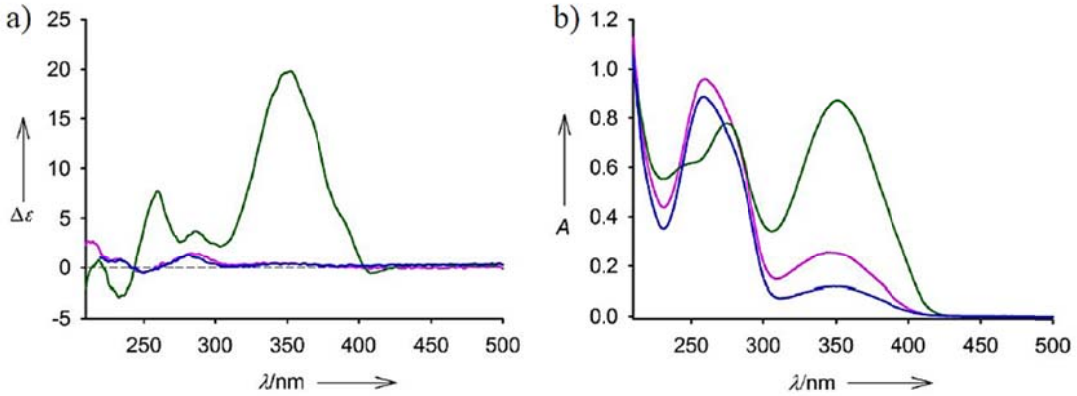

Figure 86. a) CD spectra and b) UV-Vis of a 5 mM solution of ***E*-derivative**/KI (green line), of ***Z*-derivative**/KI (blue line) and ***Z*-derivative** (violet line) in acetonitrile.

Thus, the G-quartet based complex can be cyclically assembled and disassembled by light. As shown in Figure 87, the process is perfectly reversible: no change in molar absorptivity was observed for both *E* and *Z* states after five cycles.

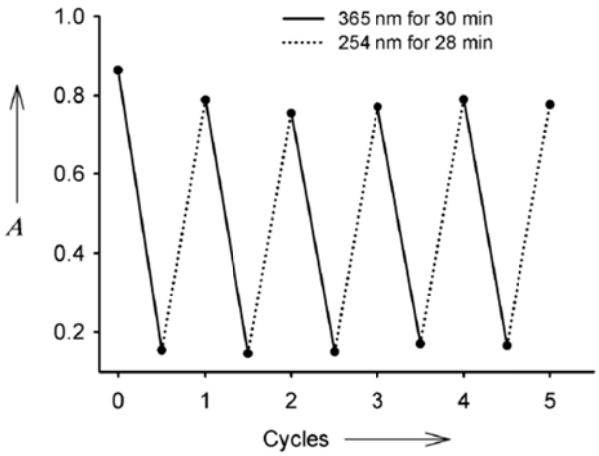

Figure 87: Switching cycles between ***E*-derivative**/KI and ***Z*-derivative**/KI by alternate irradiation with 365 nm and 254 nm light.

In conclusion, by the introduction of a photoactive moiety at C8 in a lipophilic guanosine derivative it is possible to operate a photo-control over the self-assembly of the molecule, where the existence of G-quartets can be alternately switched on and off.

1.10 Aim of the project

Inspired by a previous work on triggering of guanosine self-assembly by light, guanosines derivatives functionilized with azobenzene moieties have been prepared. We questioned if the presence of an azo-substituent could hinder or break the aggregates. For this reason we have synthesized different azoderivates of guanosine (Figure 88), and studied their aggregation in function of an external stimuli, light in this case.

NMR experiments provided a characterization of the obtained compounds. In order to obtain information about supramolecular structures, all compounds were studied by CD/UV spectroscopy in different solvents, in the presence and in the absence of added salts. UV spectra gave us informations about times and yields of photo-isomerization, while CD spectra gave us information about changes of superstructures upon irradiation at 340 nm.

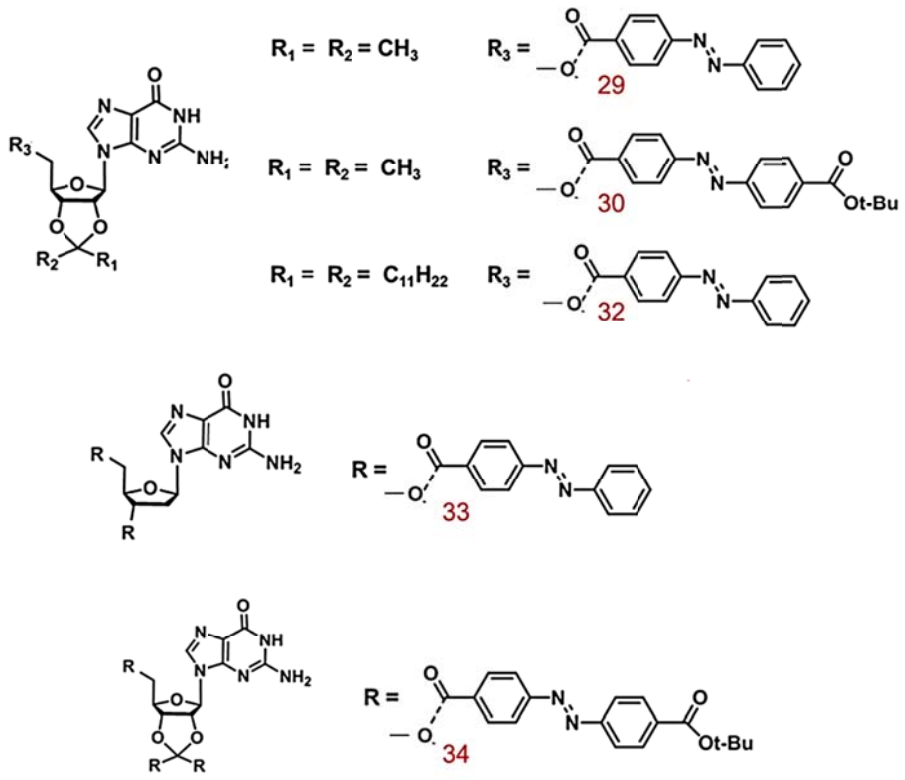

Figure 88: Azoguanosine derivatives

1.10.1 Synthesis of liponucleosides

It is possible to modulate the lipophilicity of guanosine, and therefore its solubility in various organic solvents, by introducing suitable substituents on the guanosine. The functionalizations have

been carried out exclusively on the hydroxyl functions of the glycosidic portion. In order to obtain molecules with different lipophilicity, two guanosine acetals have been prepared, using two different symmetrical aliphatic ketones: acetone and tricosanone.

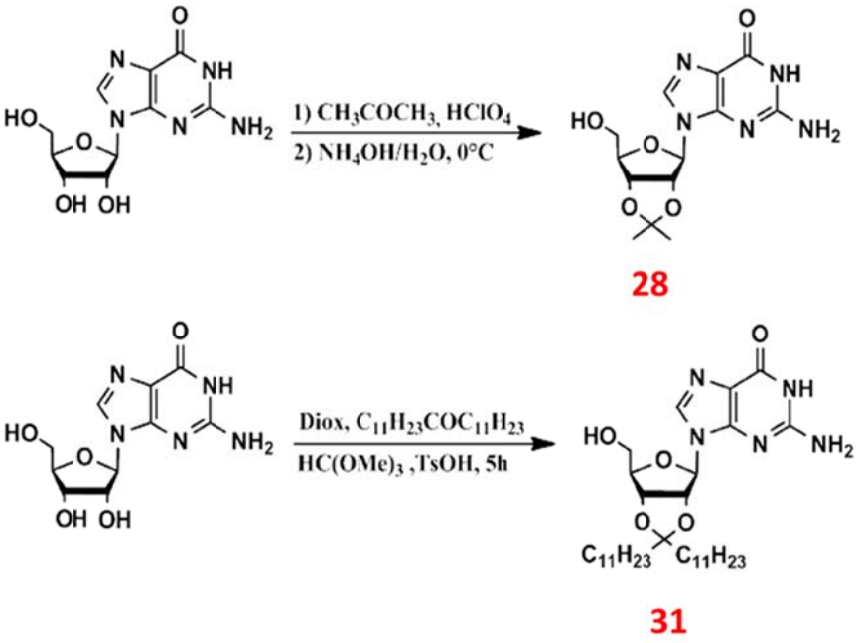

Figure 89: General mechanism for synthesis of derivative **28** and **31**

While for acetone the reaction works smoothly, thanks to the fact that acetone can be used as the solvent, the use of other higher molecular weight aldehydes or ketones proved troublesome. A satisfactory solution to shift the equilibrium towards the formation of the product was found by employing trimethyl orthoformate, which acts as a scavenger, forming methanol and the methyl methanoate.

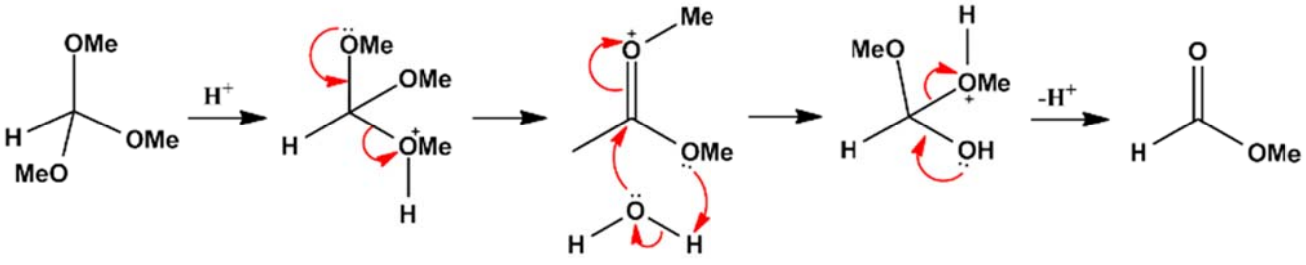

Figure 90: Scavenger mechanism actuated by trimethyl orthoformate.

1.10.2 Synthesis of azoguanosine

The last step in the synthesis of azoguanosine is a Steglich esterification with azobenzene carboxylic acid derivatives.[127] In Steglich esterification dicyclohexylcarbodiimide (DCC) is used in order to form an aduct with the carboxylic acid, which offers a reactivity similar to the corresponding anhydride. The carbonyl is thus activated and can undergo nucleophilic attack by hydroxyl groups.

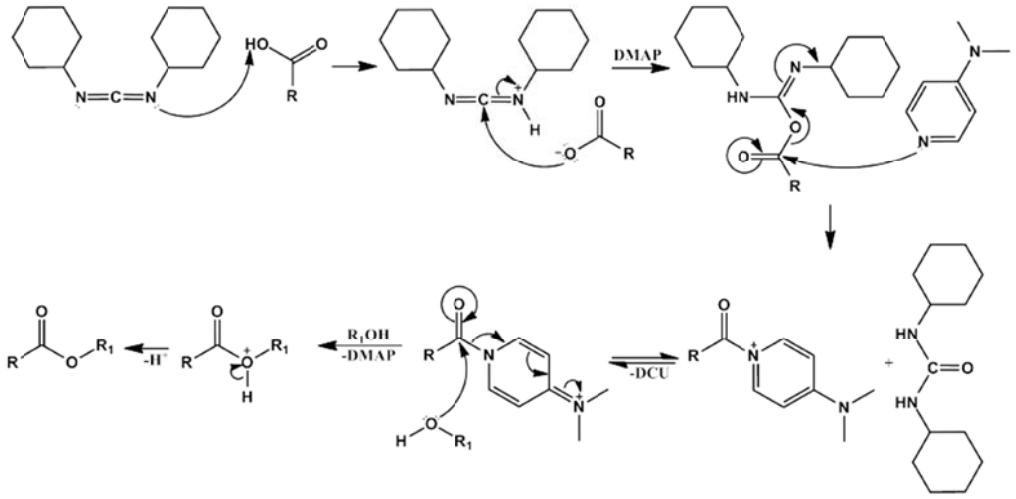

Figure 91: Steglich esterification mechanism, to obtain derivatives **30, 32, 33**

1.10.3 Synthesis of derivative 34

Derivative 34, differently from the azoguanosine reported until now, contains three azobenzene ester moieties, attached in position 2', 3' and 5' of the sugar. Steglich esterification has been used, but produced the compound in low yield. The reaction has been carried out, via generating in situ a mixed anhydride with $MeSO_2Cl$ and Et_3N, as reported in the figure 92.

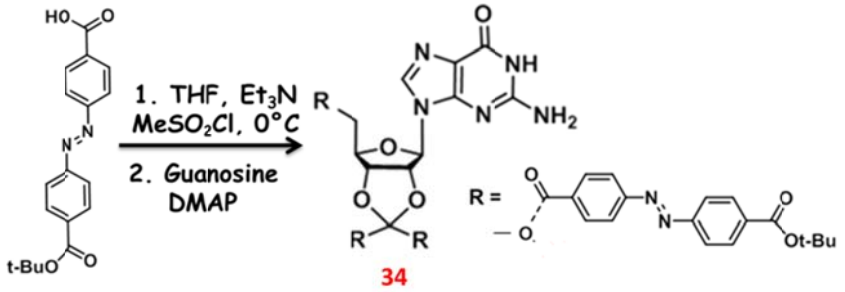

Figure 92: Synthesis of derivative 34

[127]B. Neises, W. Steglich, *Angew. Chem. Int. Ed.*, **1978**, 17, 522-524

1.11 Azoguanosine: Photochemical and supramolecular behavior

This section lists the photochemical studies performed on azoguanosines, and the experimental conditions that have been used. CD spectra were recorded with a Jasco J-710 spectropolarimeter. UV-Vis spectra were recorded with a Jasco V-550 spectrometer. UV/CD spectra were measured in THF and $CHCl_3$ at concentrations between 0.039 and 0.016 mM, in a 1 cm quartz cell at room temperature. Azobenzene moieties were isomerized by photoirradiation using a 340nm UV Led.

1.11.1 GaceazoH (29)

- *Tetrahydrofuran*

A solution of GaceazoH in THF, 0.035 mM, was prepared and added with 1/8 potassium picrate. The sample was stirred for3 days. The main absorption band of the trans isomer is located at 325 nm, while the one for the cis isomer at 258 nm. In Figure 93 are reported spectra obtained during irradiation of the sample at 340 nm in THF and CD spectra recorded before and after irradiation.

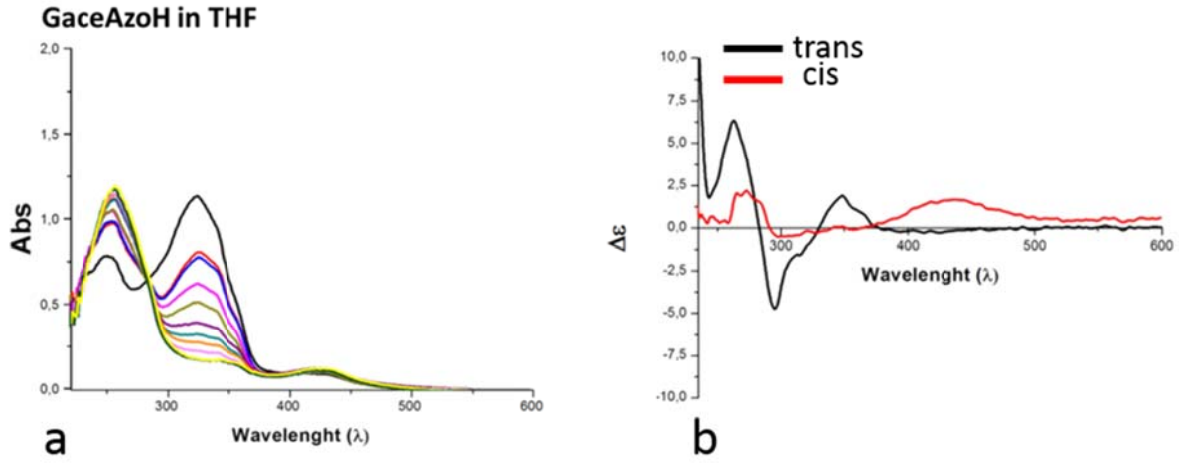

Figure 93: a) Absorption and b) CD spectra of GaceazoH in THF upon irradiation at 340 nm.

The trans-to-cis photoisomerization performed at 340 nm is complete within 20 min in THF. The thermal reverse cis-to-trans isomerization is partially completed, (almost 50%), in 24 h in the dark. Several irradiation cycles can be repeated without loss of performance. CD spectrum of derivative **29** (trans isomer) upon Kpic complexation, showed in the region of the π- π transitions of the guanine at *ca.* 260 nm a strong exciton signal, typical of a D_4-simmetric octamer. Upon irradiation

at 340 nm, the conversion of the trans isomer into the cis leads to the disaggregation of the G-quartet based structure, and a positive signal at ca. 425 nm due to the cis-azobenzene moiety appears.

- *Chloroform*

A solution of GaceazoH in $CHCl_3$, 0.02 mM, was prepared, then added with 1/8 potassium picrate and stirred for 3 days. The main absorption band due to the trans isomer is located at 324 nm, while for the cis isomer it appears at 261 nm. In Figure 94a are reported spectra obtained during irradiation of the sample at 340 nm in $CHCl_3$ and in figure 94b CD spectra recorded before and after irradiation.

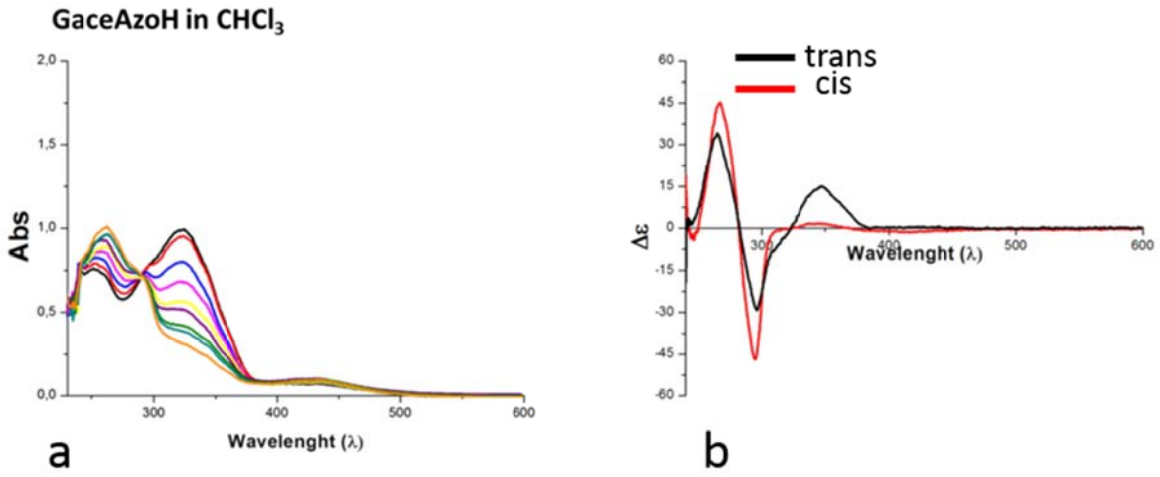

Figure 94: Absorption and CD spectra of GaceazoH in $CHCl_3$ upon irradiation at 340 nm.

The trans-to-cis photo-isomerization performed at 340 is complete within 20 min in $CHCl_3$. The thermal reverse cis-to-trans isomerization is completed in 24 h in the dark. Several irradiation cycles can be repeated without loss of performance. CD spectrum of derivative **29** showed a strong excitone signal, typical of a D_4-simmetric octameric species induced by the presence of potassium picarate for trans isomer, and a intense positive band due to azobenzene motifs at 340 nm. Upon irradiation at 340 nm the exciton still persists and only the signal coupled to trans-azobenze disappears.

1.11.2 Gacetrico-azoH (32)

- *Tetrahydrofuran*

A solution of GacetricoazoH in THF, 0.039 mM, was prepared and added with 1/8 potassium picrate, and stirred for 3 days. The absorption band due to trans isomer is located at 326 nm, while for cis isomer at 257 nm. In Figure 95 are reported spectra obtained during irradiation of the sample at 340 nm in THF and CD spectra recorded before and after irradiation.

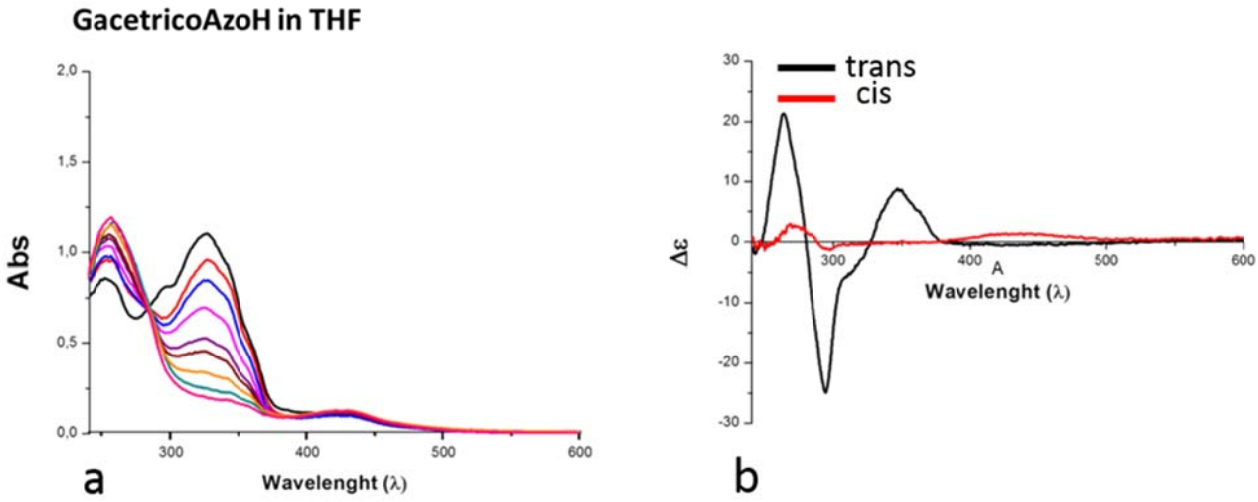

Figure 95: a) Absorption and b) CD spectra of GacetricoazoH in THF upon irradiation at 340 nm.

The trans-to-cis photo-isomerization performed at 340 is complete within 10 min in THF. The thermal reverse cis-to-trans isomerization is partially completed, (almost 25%), in 15 h in the dark. Several irradiation cycles can be repeated without loss of performance. CD spectrum of derivative **32** (trans isomer) in the region of the π- π transitions of the guanine chromophore at *ca.* 260 nm showed a strong exciton signal, typical of a D_4-simmetric octamer species induced by the the presence of potassium picrate. Upon irradiation at 340 nm, the conversion of the trans isomer into the cis leads the disaggregation of the G-quartet structure, and a small positive signal at *ca.* 425 nm due to the cis-azobenzene moiety appears.

- *Chloroform*

A solution of GacetricoazoH in $CHCl_3$, 0.037 mM, was prepared, then added with 1/8 potassium picrate and stirred for 3 days. The absorption band due to the trans isomer is located at 326 nm, while for the cis isomer at 262 nm. In Figure 96 are reported spectra obtained during irradiation of the sample at 340 nm in $CHCl_3$ and CD spectra recorded before and after irradiation.

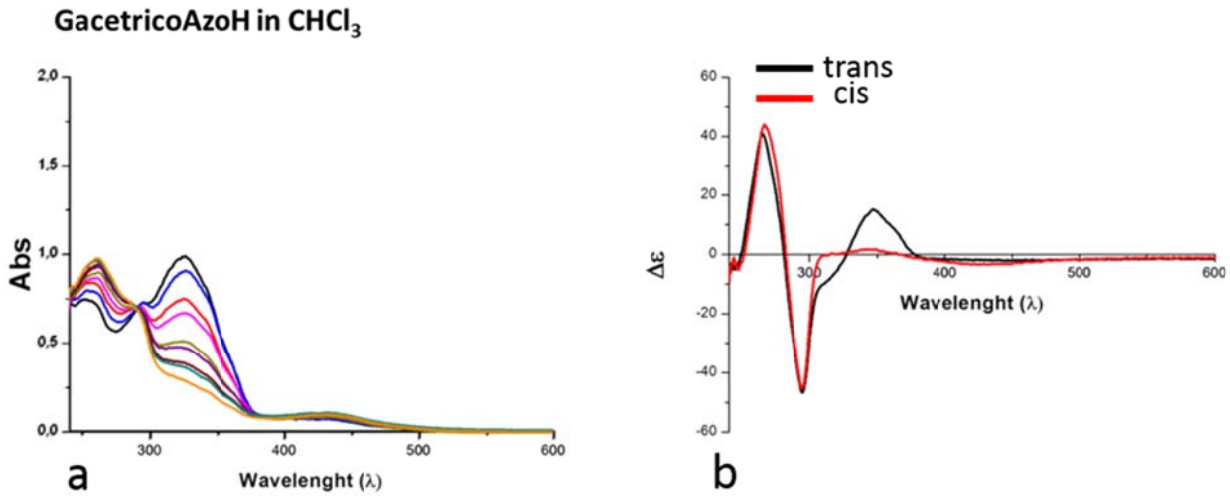

Figure 96: a) Absorption and b) CD spectra of GacetricoazoH in $CHCl_3$ upon irradiation at 340 nm.

The trans-to-cis photo-isomerization performed at 340 is complete within 20 min in $CHCl_3$. The thermal reverse cis-to-trans isomerization is completed in 24 h in the dark. Several irradiation cycles can be repeated without loss of performance. CD spectrum of derivative **32** (trans isomer) showed a strong excitone signal, typical of a D_4-simmetric octameric species induced by the presence of potassium picrate, and an intense positive band due to azobenzene motifs at 340 nm. Upon irradiation at 340 nm the exciton still persists and only the signal coupled to the trans-azobenze disappears.

1.11.3 Gace-azoTertBu (30)

- *Tetrahydrofuran*

A solution of GaceazoTertBu in THF, 0.039 mM, was prepared and added with 1/8 potassium picrate within 3 days. The absorption band due to trans isomer is located at 331 nm, while for cis isomer at 259 nm. In Figure 97 are reported spectra obtained during irradiation of the sample at 340 nm in THF and CD spectra recorded before and after irradiation.

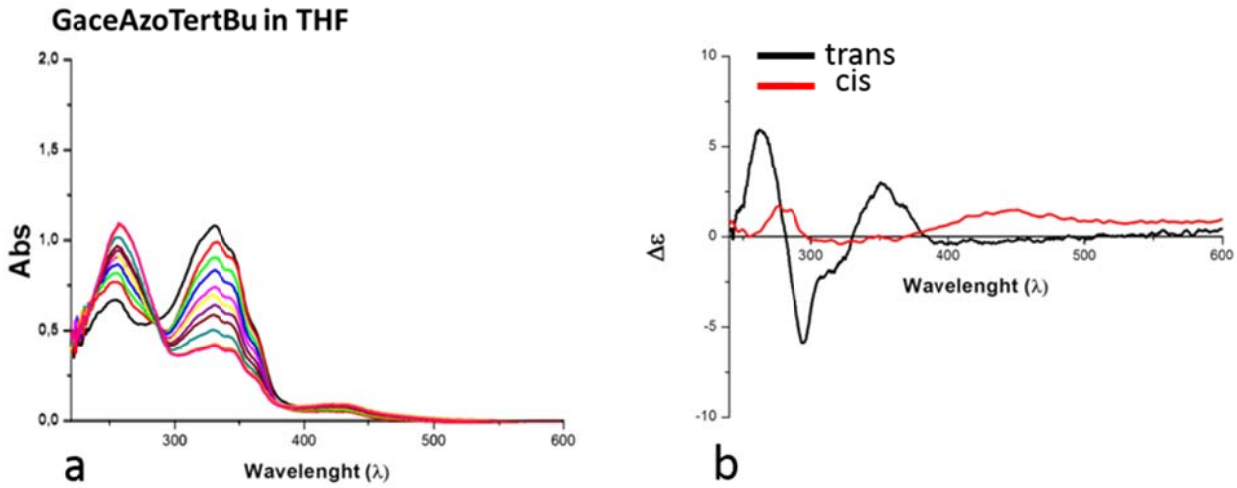

Figure 97: a) Absorption and b) CD spectra of Gaceazot-Bu in THF upon irradiation at 340 nm.

The trans-to-cis photoisomerization performed at 340 is partially complete within 60 min in THF. The thermal reverse cis-to-trans isomerization is partially completed, (25% ca), in 15 h in the dark. Several irradiation cycles can be carried out without loss of performance. CD spectrum of derivative **30** in the region of the intense π- π transitions of the guanine chromophore at *ca.* 260 nm showed an exciton signal, typical of a D_4-simmetric octamer species induced by the presence of potassium picrate for trans isomer. Upon irradiation at 340 nm, the conversion of trans isomer in to cis leads the disaggregation of G-quartet structure, and a small positive signal at ca. 425 nm due to cis-azobenzene moiety appears.

- *Chloroform*

A solution of GacetertBu in $CHCl_3$, 0.037 mM, was prepared, then added with 1/8 potassium picrate and stirred for 3 days. The absorption band due to trans isomer is located at 326 nm, while for cis isomer at 262 nm. In Figure 98 are reported UV spectra obtained during irradiation of the sample at 340 nm in $CHCl_3$, (fig 98a), and CD spectra, (fig 98b), recorded before and after irradiation.

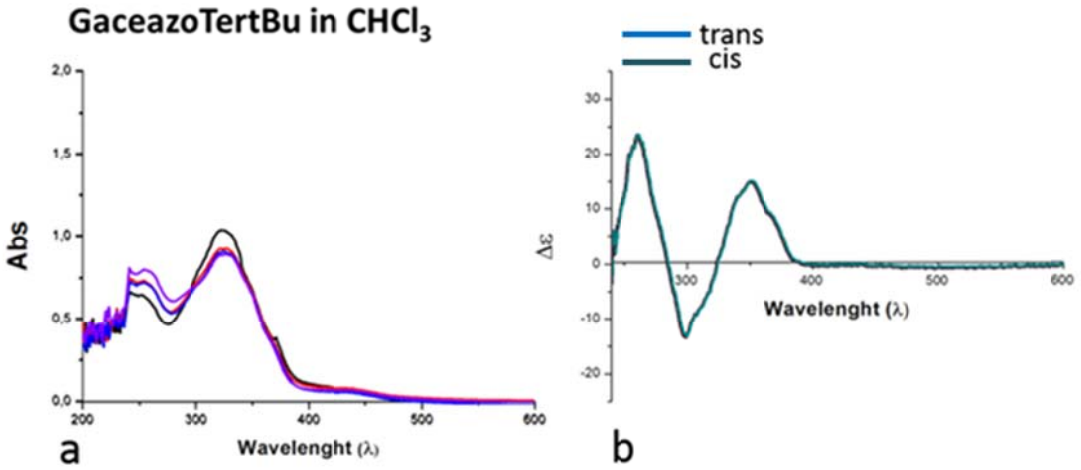

Figure 98: a) Absorption and b) CD spectra of Gaceazot-Bu in $CHCl_3$ upon irradiation at 340 nm.

The trans-to-cis photo-isomerization performed at 340 is not complete even after prolonged irradiation in $CHCl_3$. CD spectrum of derivative 30 showed a strong exciton signal, typical of a D_4-simmetric octameric species induced by the presence of potassium picrate for trans isomer, and an intense positive band due to azobenzene motifs at 340 nm. Upon irradiation at 340 nm the exciton still persists, indicating that disassembly is not taking place in this case.

1.11.4 Ribo-3(azoTertBu) (34)

A solution of GacetertBu in $CHCl_3$, 0.07 mM, was prepared, then added with 1/8 potassium picrate and stirred for 3 days. UV and CD spectra during irradiation of the sample at 340 nm in THF (Figure 99) and in $CHCl_3$ (Figure 100) are reported:

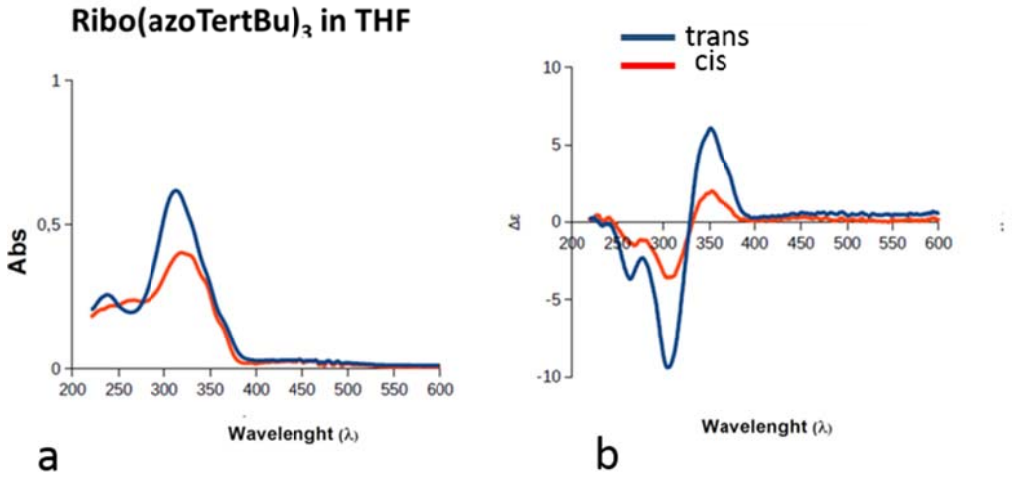

Figure 99: a) Absorption and b) CD spectra of Ribo(azoTertBu)$_3$ in THF upon irradiation at 340 nm.

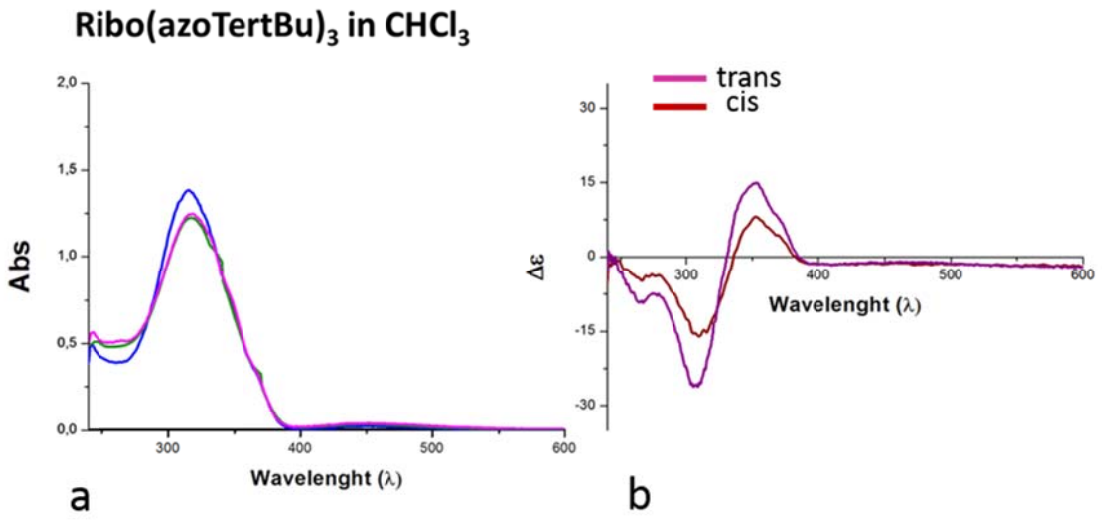

Figure 100: a) Absorption and b) CD spectra of Ribo(azoTertBu)$_3$ in $CHCl_3$ upon irradiation at 340 nm.

The trans-to-cis photo-isomerization performed at 340 is not complete neither after prolonged irradiation in THF and in $CHCl_3$. CD spectrum of derivative 34 showed a strong exciton signal, and upon irradiation at 340 nm the exciton still persists.

1.12 Liquid crystals based on not ions templated aggregates of GacetricoazoH

Derivative **32**, GacetricoAzoH, in absence of ions, has been shown a peculiar characteristic to form "gel" in organic solvents, such as THF and $CDCl_3$. Once again we have been questioned if the photo-isomerization could have some consequence, such as gel to sol transition. Starting from the studies carried out in solution, and monitoring by CD spectra the full absence of cations, it can be possible to presume that the formation of liquid crystal can be attributed to ribbon-like structure.

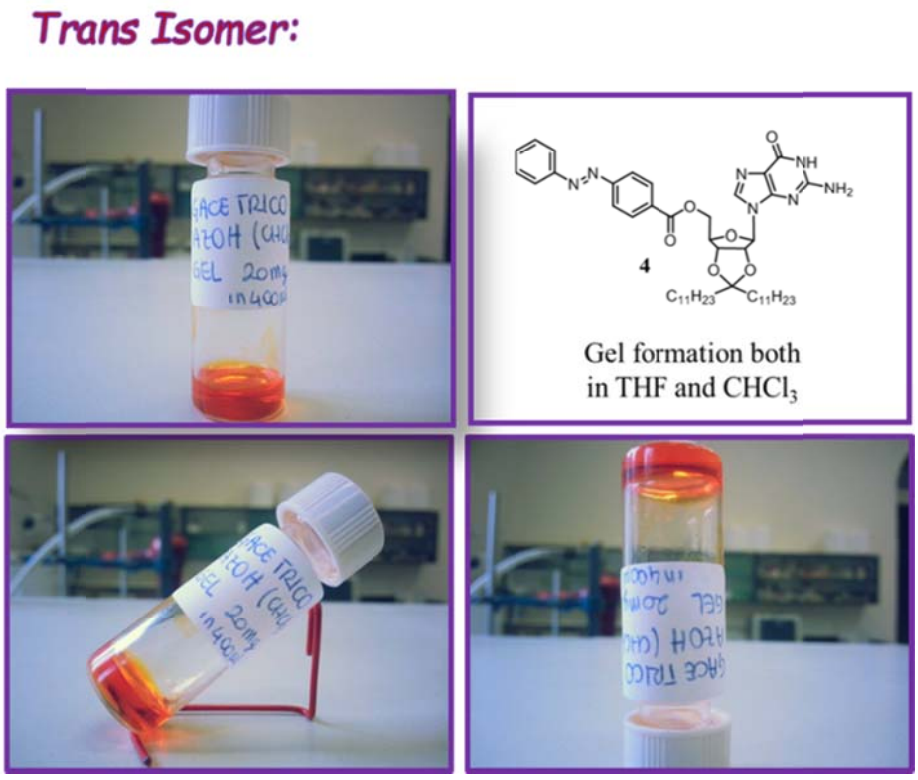

Figure 101: Derivative 32 forming a gel in THF

1.13 Conclusions

Azo-Guanosine derivatives showed clearly to originate octameric structures in the trans state in the presence of cations. The photo-isomerization yields depend on the number of azobenzene units, as the presence of any substituent in the azobenzene moieties and also on the solvent. For all derivatives CD spectra have been showed that in $CDCl_3$, the octameric structure is particular strong, and it was not possible to monitorate any change as consequence of the photoisomerization; this aspect has been confirmed also by NMR experiments. On the other hand in THF, CD spectra of all derivatives have showed a change in the supramolecular structure upon photoisomerization, and NMR experiments are still in progress. In particular derivative **32,** Gacetrico-AzoH, represents the most interesting derivative, both for the good photo-isomerization yield, (almost 90%), both for its ability to form gel in organic solvent in absence of cations. In particular in THF the *trans-to-cis* isomerization leads to the disaggregation of "gel", to convert to a solution.

Chapter IV

Oligoazobenzene for photovoltaic applications

1 Organic solar Cells

1.1 Introduction

In the last decades materials bearing a delocalized π electron system, which can absorb sunlight, create photo-generated charge carriers, and transport these charge carriers, have attracted considerable attention not only from academic research, but also from industrial field, as potential materials for organic solar cells[128,129]. Nowadays the chance to use sustainable, clean and secure energy source has became more and more a must to ensure a future for coming generations. If we consider that a great amount of energy arises from sunlight ($4.3x10^{20}$ J per 1 h), it is consequential to consider solar energy as the most likely possible renewable energy resource[130]. Recently a huge number of systems and materials has been proposed, in order to improve the efficiency or reduce the total cost of photovoltaic converters[131]. One of the most representative examples, the "Gratzel cell", is constituted by a mesoporous n-type TiO_2 coated with a photosensitizer dye and a p-type conducting electrolyte[132,133]. In general, dye sensitized solar cells, DSSCs, are regenerative photo-electrochemical cells based on the sensitization of a nanocrystalline semiconductor with a dye able to absorb a wide range of the solar spectrum[134]. In figure 102a is reported a general scheme of the operating principle and energy level diagram of a dye-sensitized solar cell. The first event (1) consists of the photoexcitation of the dye, followed by electron injection from the dye excited state into the conduction band of the semiconductor, TiO_2, supported onto transparent fluorine-doped tin oxide (FTO) conducting glass. An external circuit allows the electrons to flow to the counter electrode, where they are transferred to a redox pair present in the electrolyte. Holes created at the dye ground state can be regenerated through reduction by the hole-transport material. The most common transport material is of $I/I3^-$ redox couple: at the counter electrode triiodide is converted to iodide. Once the oxidized dye is regenerated by electron donation from the electrolyte, the cycle is complete. It is fundamental that sensitizer regeneration of the by a hole transporter occurs faster than the recombination of the conduction band electrons with the oxidized sensitizer. In addition,

[128] S. Gunes, H. Neugebauer, and N. S. Sariciftci*, Chem. Rev*. **2007**, 107, 1324−1338

[129] Hoppe, H.; Sariciftci, N. S. *J. Mater. Chem*. **2004**, 19, 1924

[130] N. S. Lewis, D. G. Nocera, *Proc. Natl. Acad. Sci. USA* **2006**, *103*, 15729

[131] M. A. Green, *Phys. E* **2002**, *14*, 11.

[132] Hagfeld, A.; Gratzel, M. Acc. Chem. Res. 2000, 33, 269-277

[133] A. Reynal, E. Palomares *Eur. J. Inorg. Chem.* **2011**, 4509–4526

[134] A. Hagfeldt, G. Boschloo, L. Sun, L. Kloo, H. Pettersson, Chem. Rev. 2010, 110, 6595.

the highest occupied molecular orbital (HOMO) of the dye has to be lower than the energy level of the hole transporter, so that the oxidized dyes formed after electron injection into the conduction band of TiO_2 can be effectively regenerated by accepting electrons from the hole transporter materials[135]. The sequence of steps involved in the cycle can be resumed as follows:

1) Photo-excitation: $S + h\nu \rightarrow S^*$
2) Electron injection: $S^* + TiO_2 \rightarrow S^+ + e^-\text{-}TiO_2$
3) Electrolyte regeneration: $I_3^- + 2e^- \rightarrow 3I^-$
4) Oxidized dye regeneration: $2S^+ + 3I^- \rightarrow 2S + I_3^-$

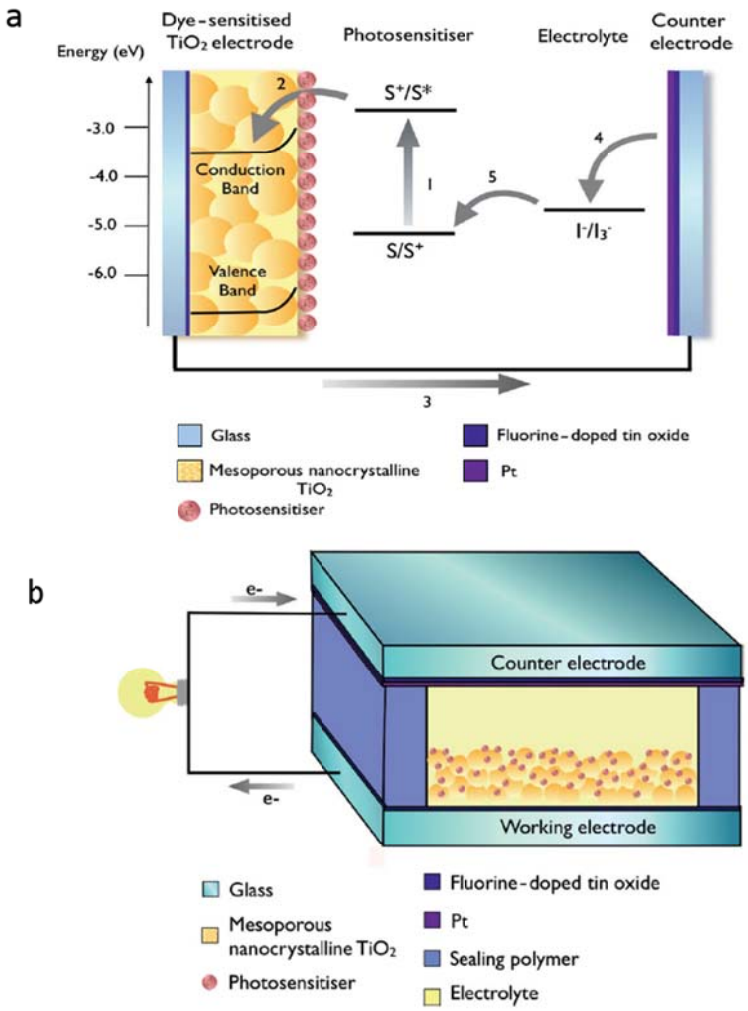

Figure 102: a) Scheme of dye-sensitized solar cell based on mesoporous TiO_2, b) Schematic representation of the cross-section of a DSSC

The total efficiency of this system can be lowered by some undesirable loss mechanisms, such as:

- deactivation of the dye excited state

[135]A. Mishra, M. K. R. Fischer, and P. Buerle, *Angew. Chem. Int. Ed.* **2009**, 48, 2474 – 2499

- recombination of the photo-injected electrons in the semiconductor with the dye
- recombination of the photo-injected electrons in the semiconductor with the oxidized form of the redox mediator, also called "dark current".

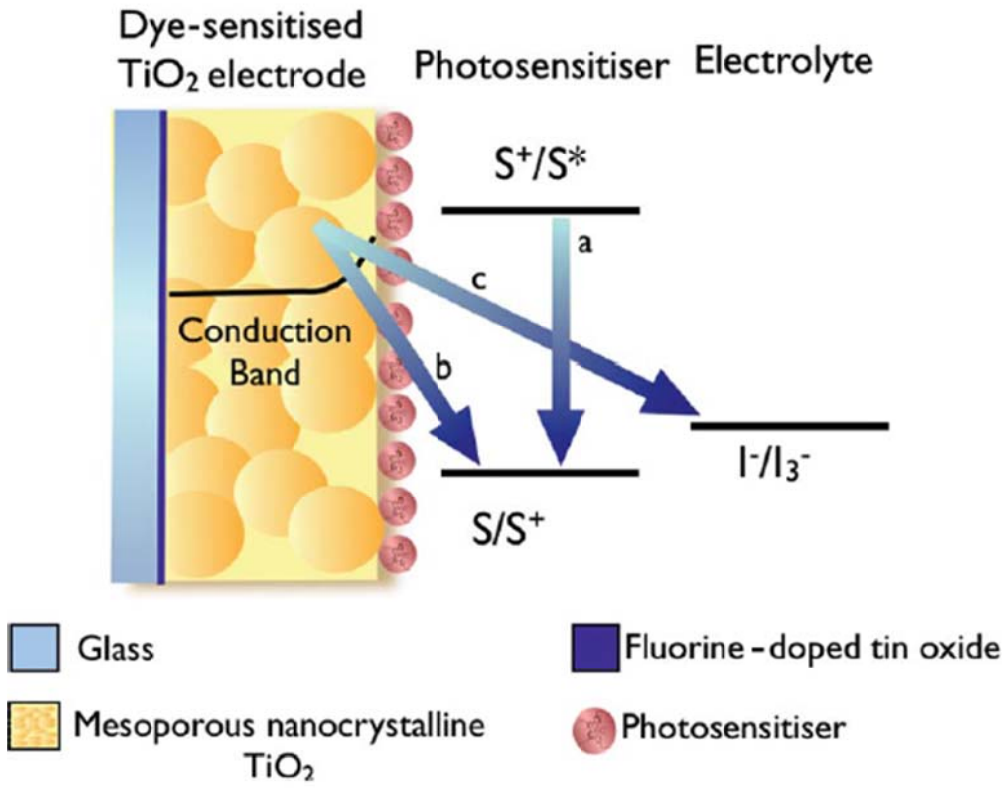

Figure 103: Scheme of the loss reactions in a DSSC. (a) Dye excited state deactivation, (b) e^--TiO_2/S^+ back electron transfer, and (c) e^--TiO_2 /I_3^- recombination reaction.

1.2 Molecular Sensitisers[136]

To date a great number of compounds has been designed for solar cell applications. The most important examples can be grouped as follows: metal-containing complexes[137], organic dyes[138] and natural compounds[139]. In figure 104 are reported some of the most used metal complexes used as photosensitizers[140], based on different metal ions such as RuII [141], OsII[142] PtII[143] ReI[144] CuI[145] or

[136] A. Reynal, E. Palomares *Eur. J. Inorg. Chem*. **2011**, 4509–4526

[137] A. S. Polo, M. K. Itokazu, N. Y. Murakami Iha, Coord. Chem. Rev. 2004, 248, 1343.

[138] a) A. Mishra, M. K. R. Fischer, P. Bäuerle, Angew. Chem. Int. Ed. 2009, 48, 2474; b) Y. Ooyama, Y. Harima, Eur. J. Org. Chem. 2009, 2903.

[139] G. P. Smestad, M. Gratzel, *J. Chem. Educ*. **1998**, *75*, 752.

[140] C. A. Bignozzi, R. Argazzi, C. J. Kleverlaan, *Chem. Soc. Rev*. **2000**, *29*, 87.

FeII.[146] The introduction of different anchoring ligands allows the formation of covalent bonds with the hydroxyl groups present on the TiO_2 semiconductor nanoparticle surface. Furthermore, this method increases the amount of absorbed dye, the stability of the cell and the strength of the electronic coupling between the π* molecular orbital of the dyes and the orbitals of TiO_2 and decreases the rate of dye desorption[147].

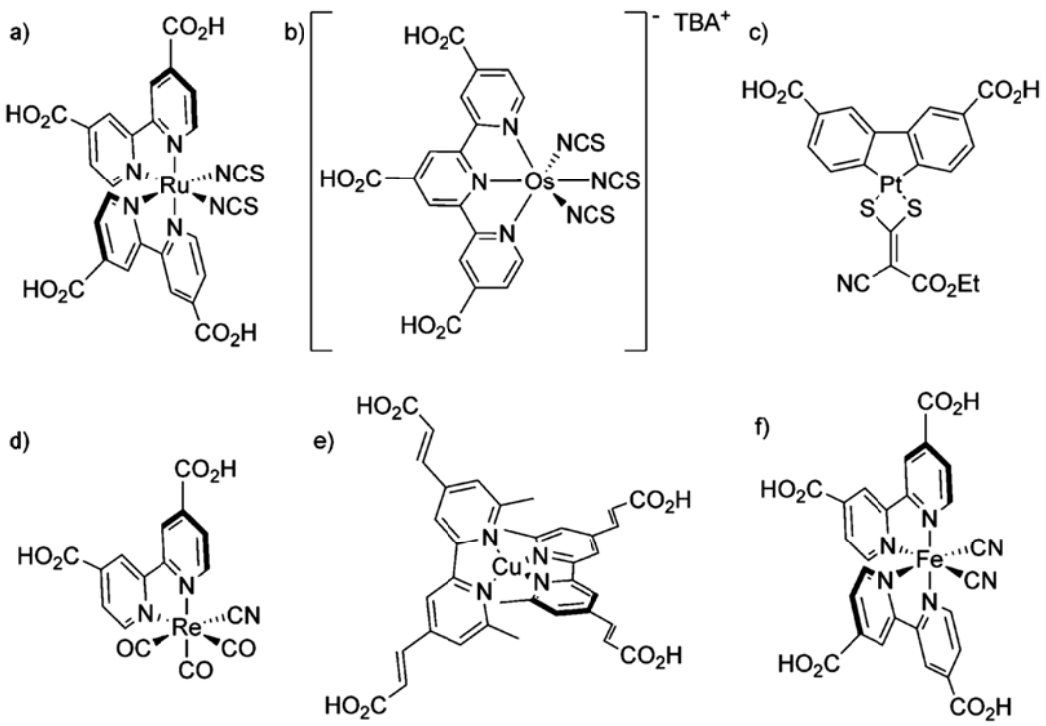

[141] a) M. K. Nazeeruddin, S. M. Zakeeruddin, J. J. Lagref, P. Liska, P. Comte, C. Barolo, G. Viscardi, K. Schenk, M. Grätzel, Coord. Chem. Rev. 2004, 248, 1317; b) A. Islam, H. Sugihara, H. Arakawa, J. Photochem. Photobiol. A: Chem. 2003, 158, 131.

[142] a) T. A. Heimer, C. A. Bignozzi, G. J. Meyer, *J. Phys. Chem.* **1993**, *97*, 11987; b) D. Kuciauskas, M. S. Freund, H. B. Gray, J. R. Winkler, N. S. Lewis, *J. Phys. Chem. B* **2001**, *105*, 392; c) S. Altobello, R. Argazzi, S. Caramori, C. Contado, S. Da Fre, P. Rubino, C. Chone, G. Larramona, C. A. Bignozzi, *J. Am. Chem. Soc.* **2005**, *127*, 15342.

[143] a) A. Islam, H. Sugihara, K. Hara, L. P. Singh, R. Katoh, M. Yanagida, Y. Takahashi, S. Murata, H. Arakawa, G. Fujihashi, *Inorg. Chem.* **2001**, *40*, 5371; b) E. A. M. Geary, L. J. Yellowlees, L. A. Jack, I. D. H. Oswald, S. Parsons, N. Hirata, J. R. Durrant, N. Robertson, *Inorg. Chem.* **2005**, *44*, 242.

[144] G. M. Hasselmann, G. J. Meyer, *J. Phys. Chem. B* **1999**, *103*, 7671.

[145] a) N. Alonso-Vante, J.-F. Nierengarten, J.-P. Sauvage, *J. Chem. Soc., Dalton Trans.* **1994**, 1649; b) T. Bessho, E. C. Constable, M. Grätzel, A. H. Redondo, C. E. Housecroft, W. Kylberg, M. K. Nazeeruddin, M. Neuburger, S. Schaffner, *Chem. Commun.* **2008**, 3717.

[146] a) S. Ferrere, *Chem. Mater.* **2000**, *12*, 1083; b) S. Ferrere, B. A. Gregg, *J. Am. Chem. Soc.* **1998**, *120*, 843.

[147] E. Galoppini, *Coord. Chem. Rev.* **2004**, *248*, 1283.

Figure 104: Molecular structures of metal-based sensitisers. (a) Octahedral RuII complex (b) octahedral OsII complex, (c) squareplanar PtI complex, (d) octahedral ReI complex, (e) tetrahedral CuII complex and (f) octahedral FeII complex.

As well as metal complex sensitizers, several examples of organic dyes have been studied. Compared to metal-containing analogues, these dyes exhibit several advantages, such as higher molar extinction coefficients, a large variety of different structures as chromophoric groups and, last but not least, they do not contain precious metals. Among organic dyes, porphyrins, phthalocyanines, perylenes, squaraines, conjugated donor–acceptor moieties, etc., have been explored[148]. The main disadvantages of organic dyes can be ascribed to a) the narrow absorption bands, as in the case of phthalocyanines, and thus in poorer sunlight harvesting; b) the possibility to form aggregates, e.g. in the case of perylenes, which prevents electron injection into the TiO_2 conduction band; c) a lower stability relative to metal complexes (squaraines). Although in the majority of cases the efficiency of these devices still results lower than ruthenium-based DSSCs, recent publications reported efficiencies of up to 10% with organic photosensitisers[149].

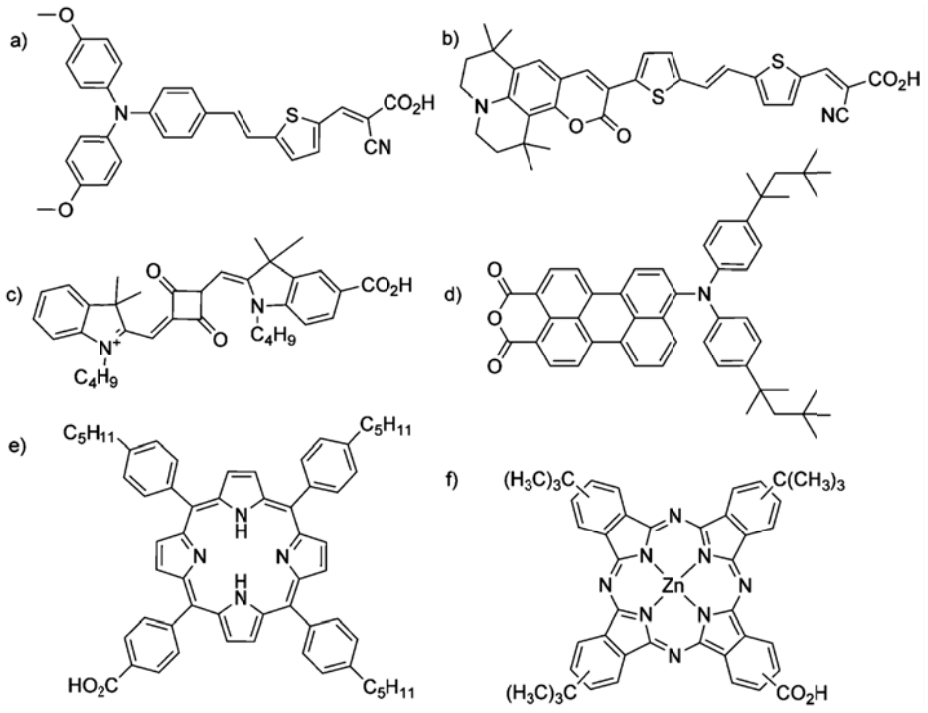

[148] a) H. Imahori, T. Umeyama, S. Ito, *Acc. Chem. Res.* **2009**, *42*, 1809; b) M. V. Martinez-Diaz, G. de la Torre, T. Torres, *Chem. Commun.* **2010**, *46*, 7090.

[149] a) W. Zeng, Y. Cao, Y. Bai, Y. Wang, Y. Shi, M. Zhang, F. Wang, C. Pan, P. Wang, *Chem. Mater.* **2010**, *22*, 1915; b) T. Bessho, S. M. Zakeeruddin, C.-Y. Yeh, E. W.-G. Diau, M. Grätzel, *Angew. Chem. Int. Ed.* **2010**, *49*, 6646.

Figure 105: Molecular structures of a series of organic dyes. (a) Donor–π-acceptor dye with a triphenylamine donor moiety, (b) donor–π-acceptor dye with a coumarin donor moiety, (c) squaraine dye, (d) perylene dye, (e) porphyrin dye and (f) phthalocyanine dye.

Finally, in addition to organic dyes and metal complex sensitizers also natural photosensitizers can be used in photovoltaic devices. This class includes pigments extracted from plants, flowers and fruits.

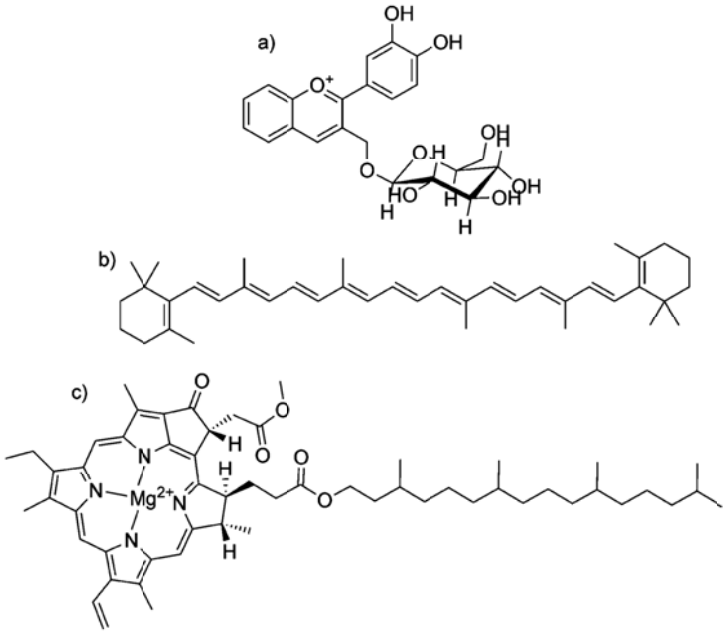

Figure 106: Molecular structures of natural dyes used in DSSCs. (a) Anthocyanin dye, (b) β-carotene dye, and (c) chlorophyll dye.

1.3 Organic Photovoltaic Cell (OPV) based on Metal-free Organic Dyes

While in Dye Solar Cells Based on Mesoporous TiO_2, the dye and the semiconductor nanoparticle are covalently linked, another important example of solar cell is represented by OPV (Organic Photovoltaic Cell) cells, consisting of electron acceptor and donor species generally mixed. Once the light is absorbed by the electron donor material, consisting of a π-conjugated polymer or a small molecule capable of leading the positive charges, excitons photo-generated pass from the valence state to the conducting state and reach the acceptor molecules, capable to capture electrons. In order to obtain high efficiency for this kind of solar cells, it is mandatory that the photo-physical and electrochemical properties of donor and acceptor materials respond to certain parameters: a) it is fundamental that the donor material possesses high absorption coefficients; b) the acceptor should be an electron-poor material and its band gap has to be superimposable with the one of the

acceptor. For efficient photovoltaic devices, transport of the created charges to the appropriate electrodes within their lifetime is one of the main steps, as far as the driving force to reach the electrodes. Most of the cases in literature, report that the driving force is represented by a gradient in the chemical potentials of electrons and holes built up in a donor-acceptor junction, as difference between the highest occupied molecular (HOMO) level of the donor and the lowest unoccupied molecular orbital (LUMO) level of the acceptor. Another common driving force is dependent on the concentration gradients of the respective charges, which leads to a diffusion current. It has to be noticed that to improve solar cells performance, interfacial area between donor and acceptor has to be large, so it is important to reduce the distance between donor-acceptor interfaces to a value lower than exciton diffusion length from the absorption site.

The architecture in OPV devices can be schematically described as follows:

- **DONOR**: it is a *p*-type hole conducting polymer (usually PPV derivatives);
- **ACCEPTOR**: it is a *n*-type electron conducting compound (usually fullerene derivatives);
- **HOLE TRASPORTER LAYER**: it is composed of poly(3,4-ethylendioxythiohene)-polystyrene-para-sulphonic acid, *i.e* PEDOT-PSS);
- **ELECTRODES**

Important representatives of hole conducting donor-type semiconducting polymers are:

- derivatives with phenylenevinylene backbones, such as poly[2-methoxy- 5-(3,7-dimethyloctyloxy)]-1,4-phenylenevinylene) (MDMOPPV),
- derivatives of thiophene, such as poly(3- hexylthiophene) (P3HT)
- derivatives with fluorene backbone, such as (poly(9,9′-dioctylfluorene-co-bis-N,N′-(4-butylphenyl-1,4-phenylenediamine) (PFB).

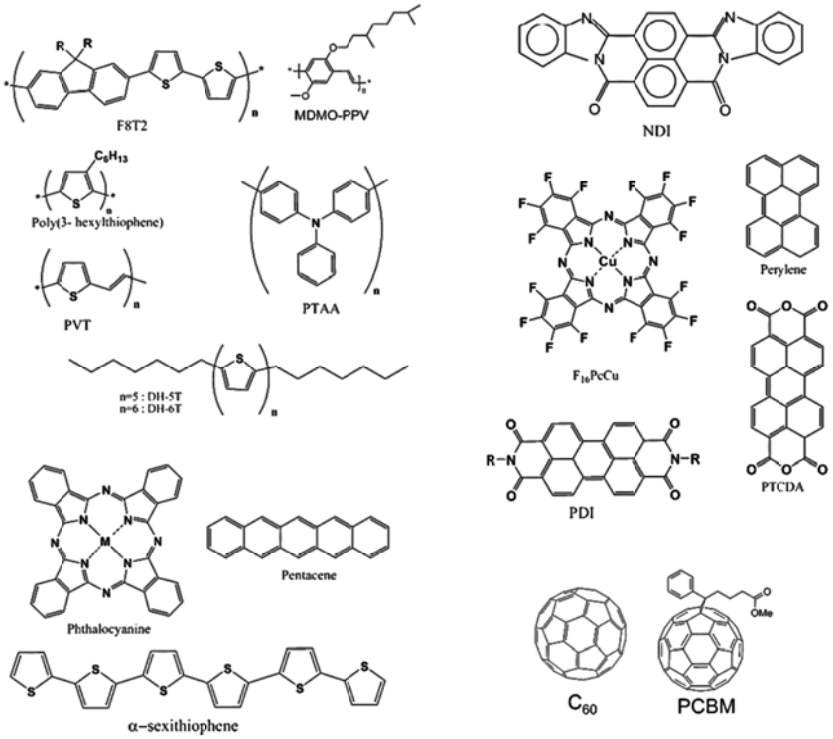

Figure 107: examples of conducting donor-type semiconducting polymers.

Also for these systems the process of conversion of light into electrical energy can be resumed as follows[150]:

- *light absorption and exciton formation;*
- *exciton migration;*
- *exciton dissociation at donor/acceptor interface;*
- *charge transport.*

Different OPV architectures have been exploited, as listed as follow.

- *Bilayer heterojunction devices*

In a bilayer heterojunction device[151], p-type and n-type semiconductors are sequentially stacked on top of each other. In such devices, low quantum efficiency is attributed to the limited charge generation; only excitons created within the distance of 10-20 nm from the donor-acceptor interface can reach the heterojunction interface: this creates a loss of absorbed photons[152].

[150] Brédas, J.-L.; Norton, J.E.; Cornil, J.; Coropceanu, V., *Acc. Chem. Res*., **2009**, 42,11, 1691-1699.

[151] (a) Nelson, J. Curr. Opin. Solid State Mater. Sci. 2002, 6, 87-95. (b) Brabec, C. **J**.; Winder, C.; Sariciftci, N. S.; Hummelen, J. C.; Dhanabalan, A.; van Hal, P. A.; Janssen, R. A. J. AdV. Funct. Mater. 2002, 12, 709-712.

[152] Winder, C.; Sariciftci, N. S. J. Mater. Chem. 2004, 14, 1077

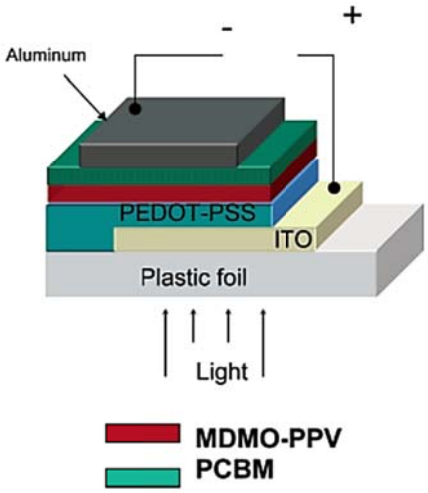

Figure 108: Bilayer configuration in organic solar cells.

1.3.1 Bulk heterojunction devices

To improve the efficiency of the solar cells, it is necessary to increase the interfacial area between the donor and the acceptor. In bulk heterojunction devices, the donor and acceptor components are intimately intermixed (Figure 109), and the phase separation results in a 10-20 nm length scale, that is less than the exciton diffusion length from the absorbing site.

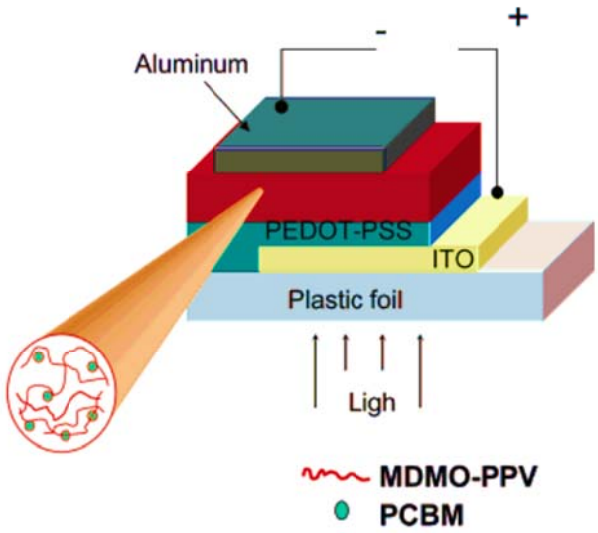

Figure 109: Bulk heterojunction configuration in organic solar cells.

1.4 Aim of the project: Conjugated oligoazobenzenes in the development of OPV

The molecular structure of p-conjugated oligoazobenzene derivatives resembles the one of PPV derivatives, so that oligoazobenzenes can be considered the azo-analogues of this latter family of organic compounds[153]. On the other hand, the strong withdrawing character of the azo group makes these derivatives good candidates as acceptor-type p-conjugated systems. In addition, the structural similarity between PPVs and oligoazobenzenes could lead to a very good miscibility. Starting from 2009, our group, in collaboration with Prof. Credi and ISOF-CNR, Bologna, designed different conjugated oligo-azobenzenes, testing their performance as electron acceptor materials for photovoltaic applications. In figure 110 are reported some of the formulae of derivatives studied in this project.

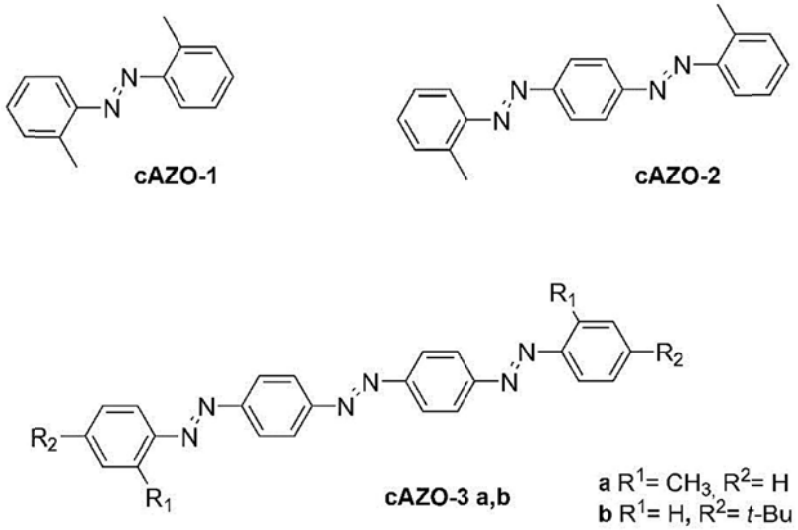

Figure 110: Structure of conjugated oligoazobenzenes.

In particular we have been focusing on the relationship between the number of azobenzene units and the electrochemical properties observed. Increasing the number of azobenzene units a shift of the reduction potential towards more positive values occurs, allowing to test their application as electron acceptors in photovoltaic cells. In the next paragraphs it will be discussed the synthetic strategy to obtain oligo-azobenzenes and their photo-physical and electrochemical properties.

1.5 Synthesis of oligo-azobenzene: general mechanism

A general scheme to obtain azobenzene derivatives is reported in Figure 111:

[153] Moneo, A.; Justino, G.C.; Carvalho, M.F.N.N.; Oliveira, M.C.; Antunes, A.M.M.;Bléger, D.; Hecht, S.; Telo, J.P., *J. Phys. Chem. A*, **2013**, 117,51,14056-14064.

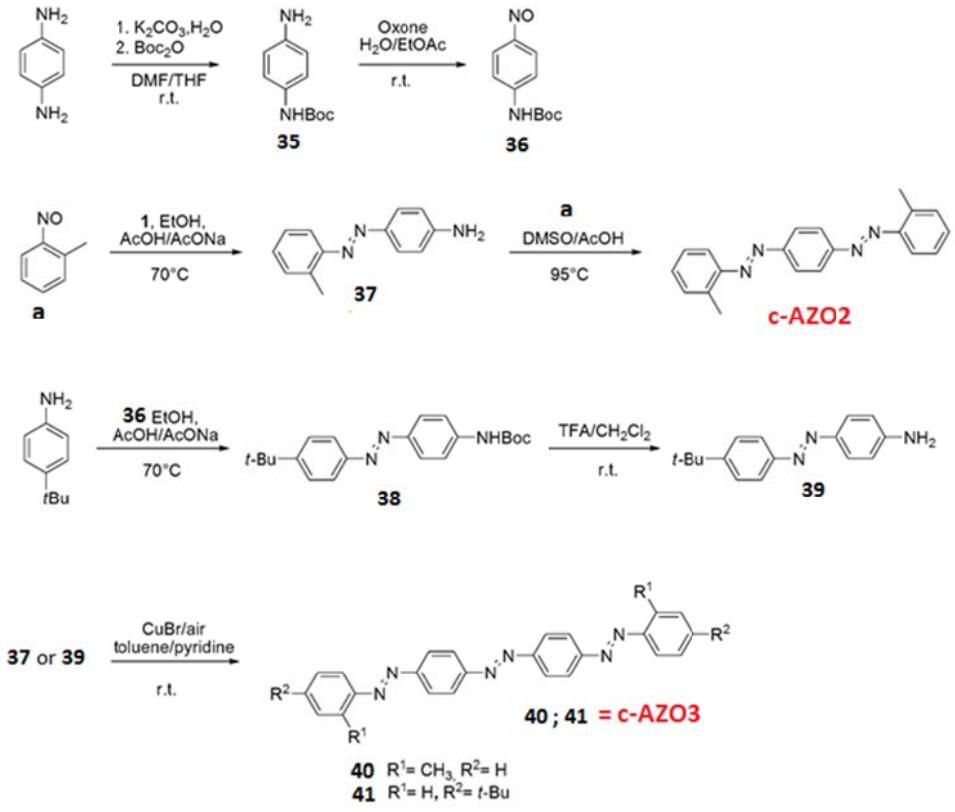

Figure 111: general scheme for synthesis of derivative cAZO2, cAZO3.

Substituted azobenzenes have been obtained by two methods:

- oxidation of anilines, (with Oxone, a stable triple salt, $2KHSO_5,KHSO_4,K_2SO_4$) to form nitrosoarenes and subsequent condensation reactions with anilines[154]. The condensation reaction can be carried out in acetic acid or in buffer solution, (AcOH/AcONa).
- Dimerization of anilines catalyzed by CuBr[155] or HgO/I_2[156]

Azobenzene derivatives **42** and **43**, (Figure 112), have been obtained through electrophilic aromatic substitution of diazonium salts with m-phenylediamine, in which the diazonium ion acts as an electrophile, attacking an aromatic ring activated by strong electrodonor groups, (as $-NH_2$ or $-NR_2$).

[154] B. Priewisch, K. Ruck-Braun *J. Org. Chem*. **2005**, 70, 2350-2352

[155] C. Zhang, N, Jiao *Angew. Chem. Int. Ed*. **2010**, 49, 6174 –6177

[156] K. Orito et al. *Tetrahedron* 54, **1998**, 8403-8410

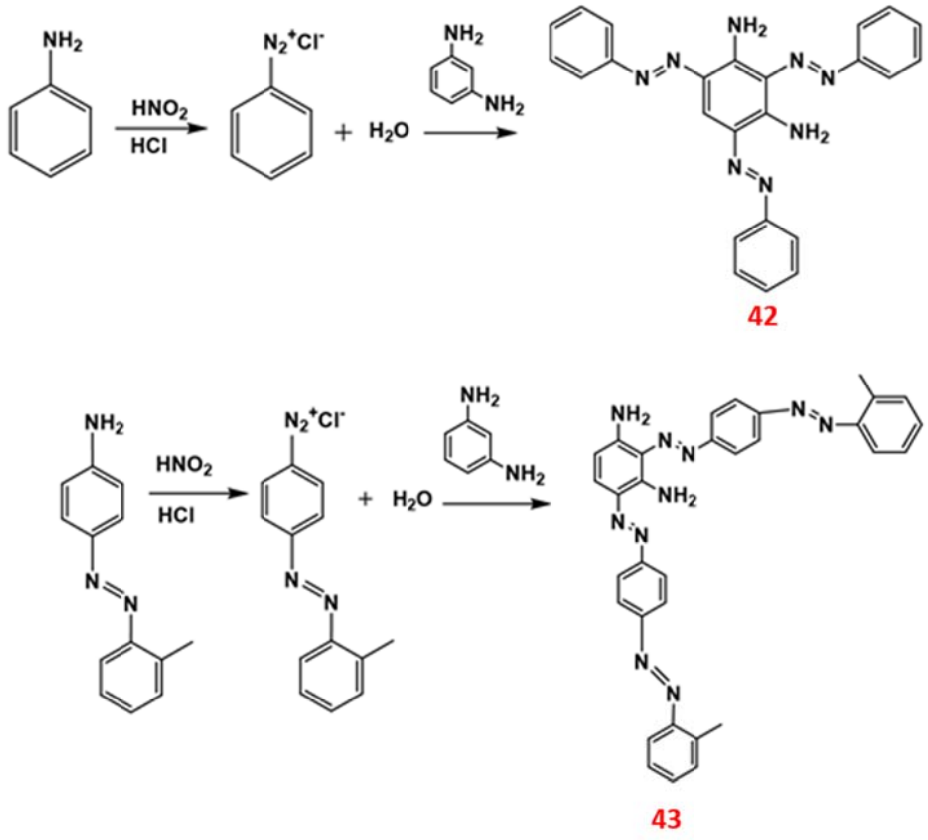

Figure 112: general scheme for synthesis of derivative 42 and 43.

1.6 Electrochemical characterization

1.6.1 A brief introduction on the technique

- **Cyclic voltammetry**

Cyclic voltammetry or CV is a type of potentiodynamic electrochemical measurement, and is generally used to study the electrochemical properties of an analyte in solution. CV technique consist on the application of a potential scan to the working electrode, linearly versus time, and then the current response of the cell is measured. After the set potential is reached, the working electrode's potential return to the initial potential, ramped in the opposite direction. These cycles of ramps in potential can be performed as well as desired. The cyclic voltammogram trace is obtained from the current at the working electrode plotted versus the applied voltage.

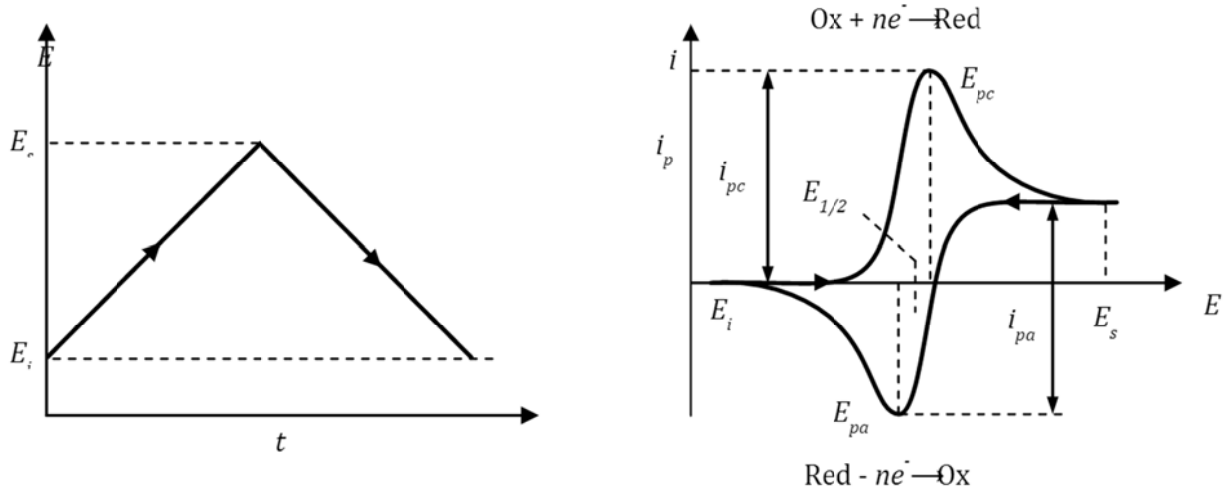

Figure 113: Potential excitation function and current vs potential response for cyclic voltammetry

For an electrochemically reversible redox process in an unstirred solution containing a supporting electrolyte, the difference between the two peak potentials (E_p), ΔE_p, is of particular interest.

$$\Delta E_p = |E_{pc} - E_{pa}|$$

This difference mainly results from the effects of analyte diffusion rates. In the ideal case of a reversible 1e- couple, ΔE_p is 59 mV at 298 K. Typical values observed experimentally are greater, often approaching 70 or 80 mV. The waveform is also affected by the rate of electron transfer, usually discussed as the activation barrier for electron transfer. Moreover for a ideal reversible couple, the values of the couple peak are characterized by $i_{pa}/i_{pc} = 1$, and generally semi-reversible (i_{pa}/i_{pc} is close but not equal to 1). Many redox processes observed by CV are quasi-reversible or non-reversible. In such cases the peak potential does not remain fixed by changing the scan rate and the irreversibility is indicated by $i_{pa}/i_{pc} \neq 1$. Deviations from unity are attributable to a subsequent chemical reaction that is triggered by the electron transfer.

- **Differential pulse voltammetry**

In contrast to cyclic voltammetry, differential pulse voltammetry (DPV) is a more sensitive technique, where a series of regular potential pulses over a base potential are applied: in this case small increments of the applied voltage is stepped from the imposed potential range, having the same height respect to the base potential and the same time duration, as pictured in Figure 114.

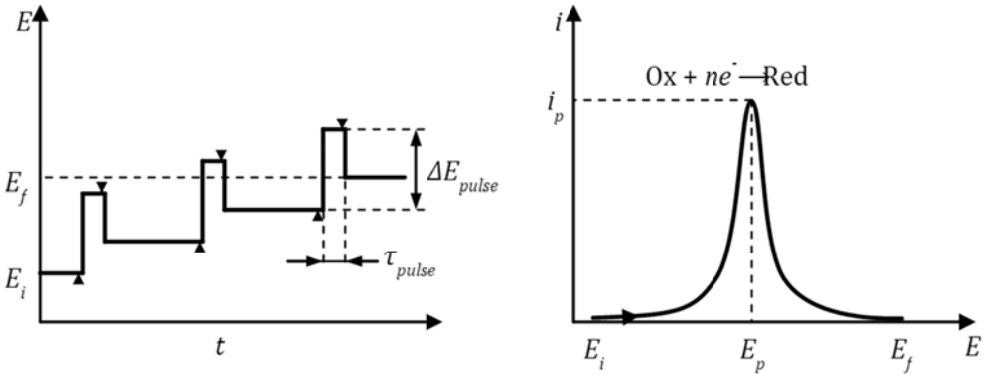

Figure 114: Potential excitation function and current vs potential response for differential pulse voltammetry.

The most important parameters for DPV are: modulation amplitude (Ep), the height of the potential pulse, and modulation time (p), the duration of the potential pulse. In this case, the scan rate is defined as the ratio between the potential increment and the period of the cycle.In the case of a reversible process, the potential corresponding to the peak in the voltammogram is independent on the scan rate and is related to the half wave potential, and voltammogram exhibits a symmetrical shape. In the case of irreversible processes (chemically or electrochemically), the DPV peak is weaker and broader and its shape is not symmetric anymore.

1.6.2 Electrochemical characterization of oligoazobenzene

Concerning derivatives cAZO1, cAZO2 and cAZO3 two irreversible oxidation processes can be observed for all compounds.

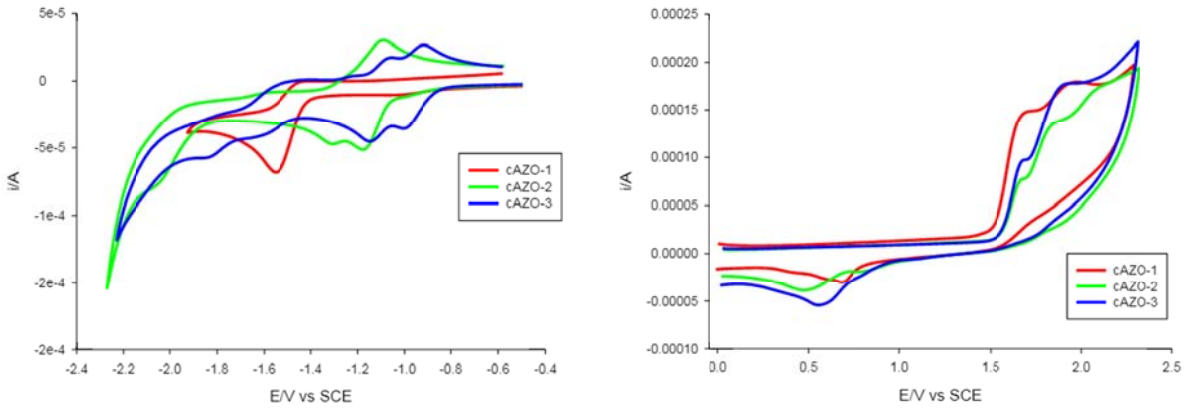

Figure 115: Cyclic voltammograms of deoxygenated solutions (1 mM) of the conjugated oligoazobenzene derivativesin CH_2Cl_2. Supporting electrolyte: $TBAPF_6$; internal reference: decamethylferrocene; scan rate: 200 mV/s; working electrode: glassy carbon.

It is important to focus the attention on the reduction processes, in order to state if these derivatives can be employed as electron conducing materials. We found that increasing the number of azobenzene units, the process becomes more reversible and occurs at less negative potentials.

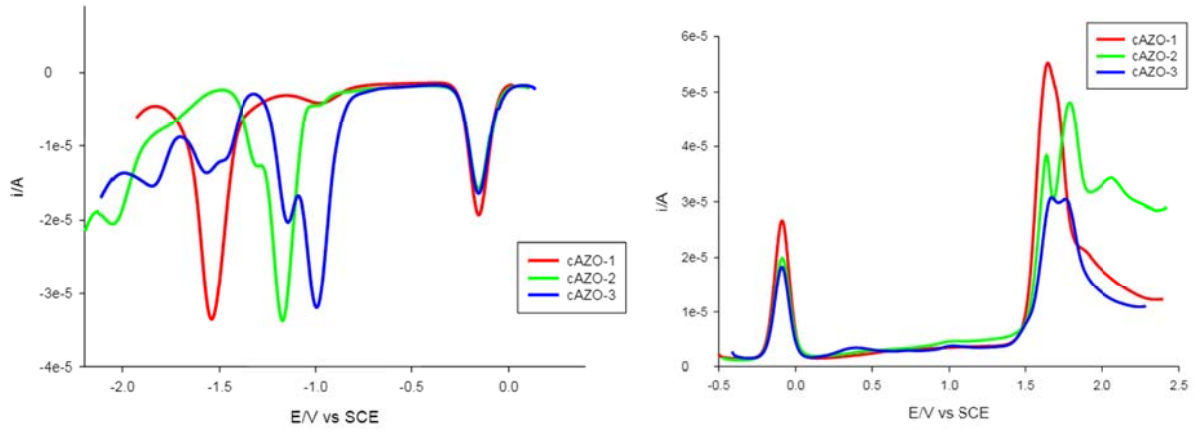

Figure 116: DPV of deoxygenated solutions (1 mM) of conjugated oligoazobenzene derivatives in CH_2Cl_2.Supporting electrolyte: $TBAPF_6$; internal reference: decamethylferrocene; modulationtime: 40 ms; modulation amplitude: 75 mV; scan rate 20 mV/s; working electrode: glassy carbon.

Resumed in Table **5**, are the electrochemical parameters obtained for **t**he conjugated oligo-azobenzenes derivatives:

	E_{OX}(V)	E_{RED}(V)	N° e^-_{RED}
cAZO-1	1.65	-1.54	/
cAZO-2	1.66 1.77	-1.16	0.6
cAZO-3	1.65 1.78	-0.99	0.7

Table 5: Electrochemical parameters for conjugated oligoazobenzenes.

The increasingly positive reduction potential value, increasing the number of azobenzene units, can be explained looking at the energy of their frontier orbitals. The energy of the LUMO lowers considerably moving from cAZO-1 to cAZO-3, and as consequence the reduction potential will move towards more positive values.

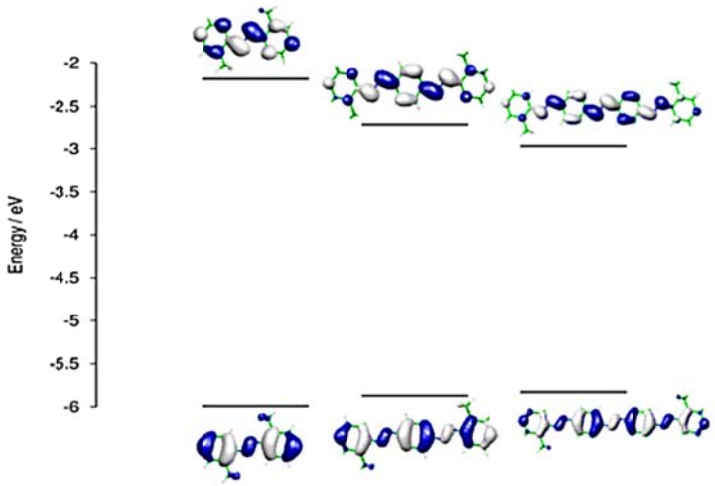

Figure 117: Frontier molecular orbitals and B3LYP/6-31G* computed orbital energies of conjugated oligoazobenzenes.

1.6.3 Photochemical quantum yield

Increasing the number of azobenzene units, a linear auxochromic effect in the absorption spectra has been observed. Moreover, increasing conjugation in the system results in a bathochromic effect for the absorption band referring to π-π* transitions and in cAZO-3 the bands referring to π-π* and n-π* transitions are superimposed.

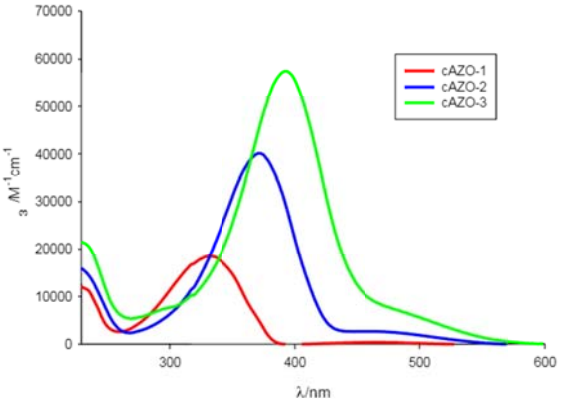

Figure 118: Absorption spectra of conjugated oligoazobenzenes in CH_2Cl_2 at r.t.

Also the photo-reactivity decreases by increasing the number of azobenzene units: thus cAZO-1 shows the typical spectral variations of azobenzene upon irradiation at 365 nm. In particular, a decrease of the band located at 332 nm and an increase of the one at 468 nm is observed, with the presence of isosbestic points at 280 and 290 that remain fixed for the whole irradiation time.

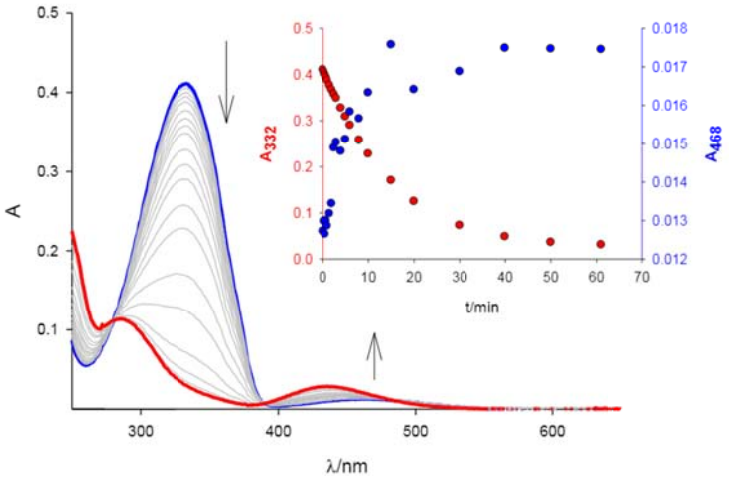

Figure 119: Changes in the absorption spectra of cAZO-1 upon irradiation at 365 nm. Inset: time dependent absorption changes in the π-π* and n-π* bands upon irradiation.

As it has been reported previously, increasing the number of azobenzene units decreases the photo-reactivity and as consequence also the E-Z photochemical quantum yield;

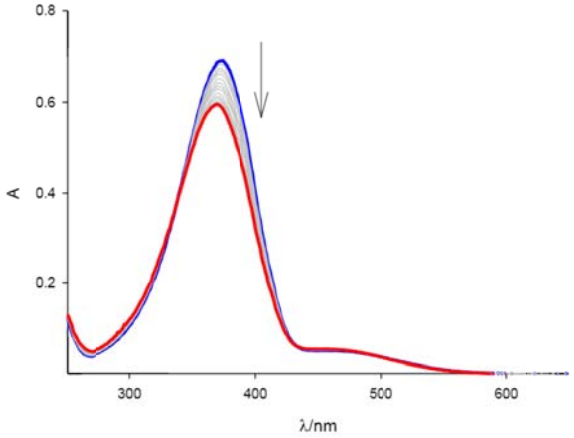

Figure 120: Changes in the absorption spectra of cAZO-2 upon irradiation at 365 nm.

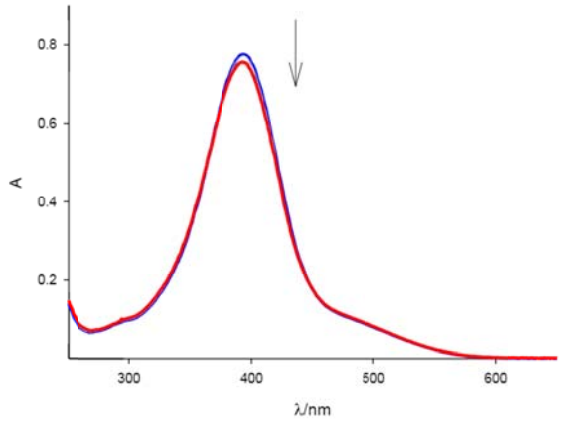

Figure 121: Changes in the absorption spectra of cAZO-3 upon irradiation at 365 nm.

These data confirm that conjugation of azobenzene units is responsible for suppression of photo-reactivity.

1.7 Oligoazobenzenes as electron acceptor materials

Results obtained for cAZO-3 have been considered promising for its use as an electron acceptor material. The compound was blended with electron donating materials to check the quality of the mixtures thus obtained. Commercially available electron-donating polymers, listed below, were used as electron-donors counterparts:

- P3HT (poly-3-hexylthiophene),
- PTB7 (poly{4,8-bis[(2-ethylhexyl)oxy]benzo[1,2-b:4,5-b']dithiophene-2,6-diyl-alt-3-fluoro-2-[(2-ethylhexyl) carbonyl]thieno[3,4-b]thiophene-4,6-diyl})
- MDMO-PPV (poly[2-methoxy-5-(3′,7′-dimethyloctyloxy)-1,4-phenylenevinylene])

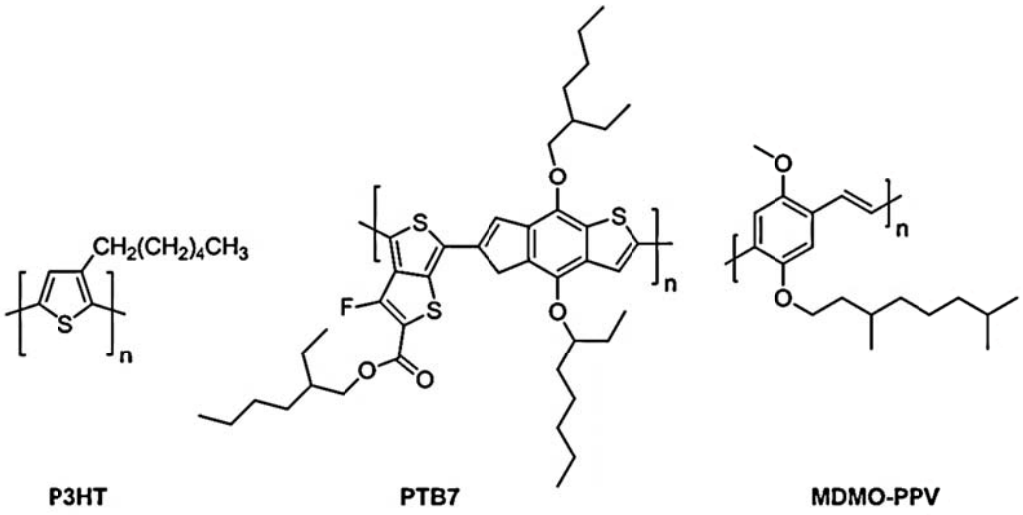

Figure 122: Structure of donor polymers.

The energy levels of the materials used are reported below, together with the energy levels of cAZO3:

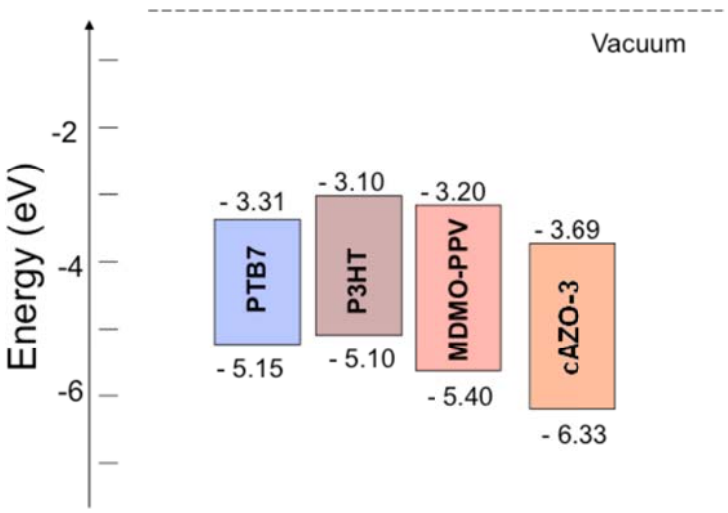

Figure 123: Energy levels for donor polymers and cAZO-3

The energy offset for LUMO orbitals for acceptor and donors is between 0.4 and 0.6 eV; the found energy offset could be sufficient for the photoinduced electron transfer from donors to cAZO-3. Optical microscopy images of composite films of PTB7/cAZO-3, P3HT/cAZO-3 and MDMO-PPV/cAZO-3 unfortunatelly showed an high phase segregation between donor and acceptor, ascribable to cAZO-3 aggregation.

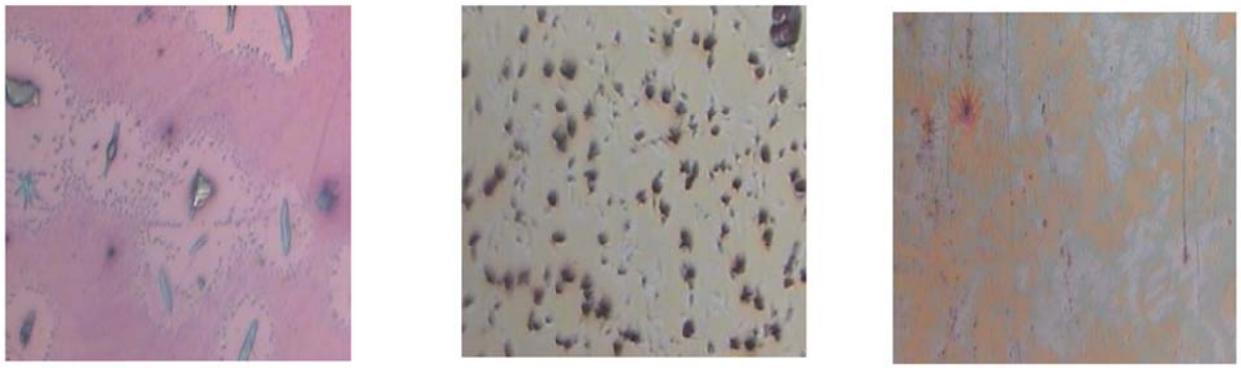

Figure 124: Optical microscopy images of composite films of PTB7/cAZO-3 (left), P3HT/cAZO-3 (middle) and MDMO-PPV/cAZO-3(right) deposited on quartz (561x457 m).

Futhemore, the blends have been deposed on quartz and their absorption and emission spectra have been compared with those obtained for pure acceptor polymers (Figure 124). In all cases, a negligible quenching of the donor emission has been observed, suggesting an insufficient acceptor activity of c-AZO3 derivative. This observation leads to the consideration that the microstructure of the obtained blend is an important parameter to take into account in order to increase the overall efficiency of these systems.

Blend	PL quenching
PTB7:cAZO-3	1.6
P3HT:cAZO-3	2.8
MDMO-PPV:cAZO-3	1.6

Table 6: Photoluminescence quenching of polymer/cAZO-3 blends

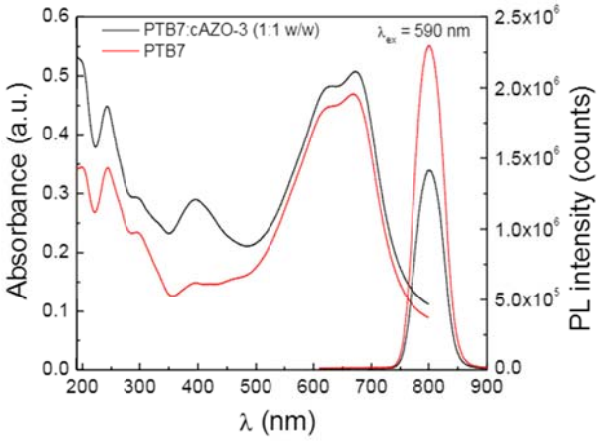

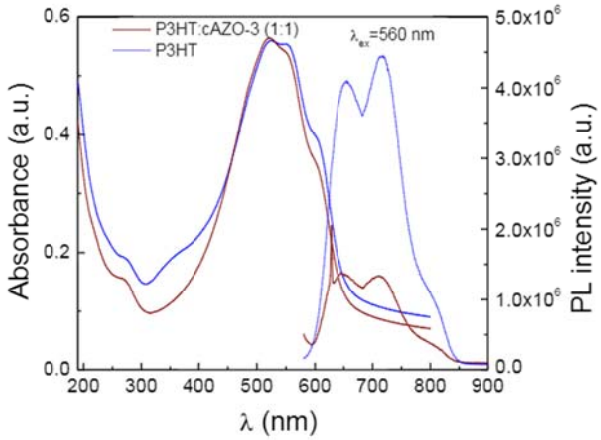

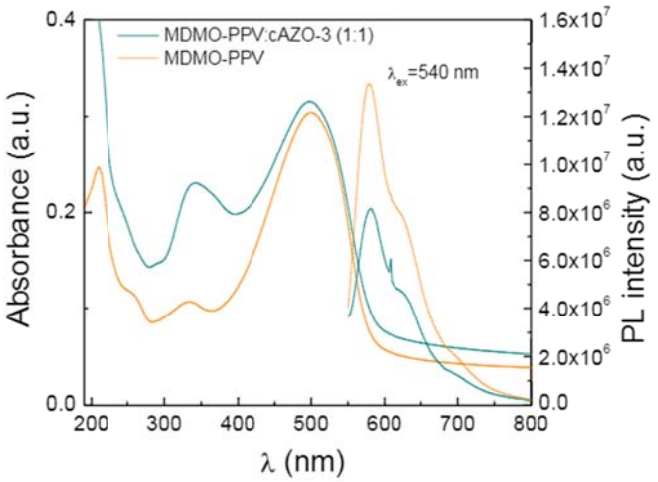

Figure 125: Absorption and emission spectra of cAZO-3/polymer blends and pure polymer deposited on quartz.

Moreover, the low miscibility of azobenzene-based acceptor materials and polymeric donors has to be addressed: in order to obtain a good candidate. Other oligoazobenzenes have been synthetized and characterized. In particular it was designed oligoazobenzene, cAZO-4, with 3 azo units and with higher solubility in organic solvents.

1.8 cAZO-4

In order to overcome the above-mentioned solubility issues, photochemical and electrochemical properties of another conjugated oligo-azobenzene derivatives have been investigated. Tert-butyl terminal groups can increase its miscibility in the final polymeric blend.

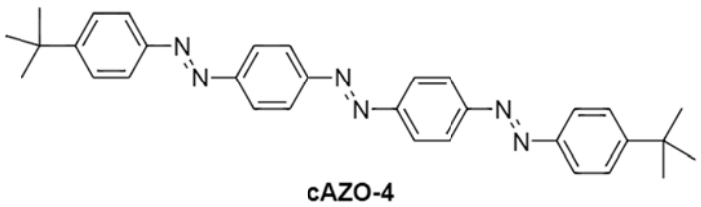

Figure 126: Structure of cAZO-4.

As reported already for other conjugated oligoazobenzene derivatives, cAZO-4 exhibits an almost total suppression of its photoreactivity, thus confirming that its photophysical and photochemical properties are comparable with those found for cAZO-3.

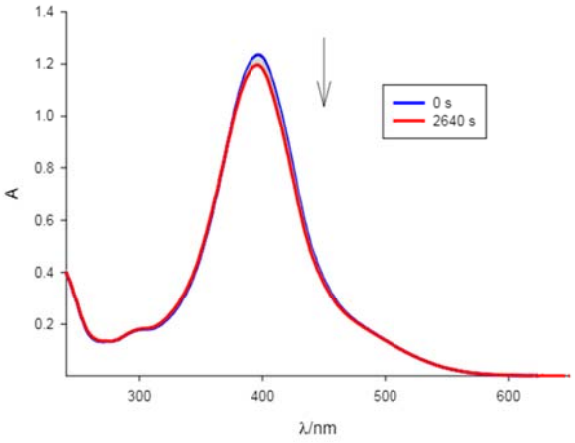

Table 6.4 **- Photophysical and photochemical parameters for cAZO-3 and cAZO-4.**

	ε/M⁻¹cm⁻¹	Φ
cAZO-3	57500	/
cAZO-4	53500	/

Figure 127: Changes in the absorption spectra of cAZO-4upon irradiation at 365 nm.

Also electrochemical behavior is confrontable with the one found for cAZO-3: two irreversible oxidation processes and quasi-reversible reduction processes can be observed and the value of the first reduction process is comparable with that of cAZO-3.

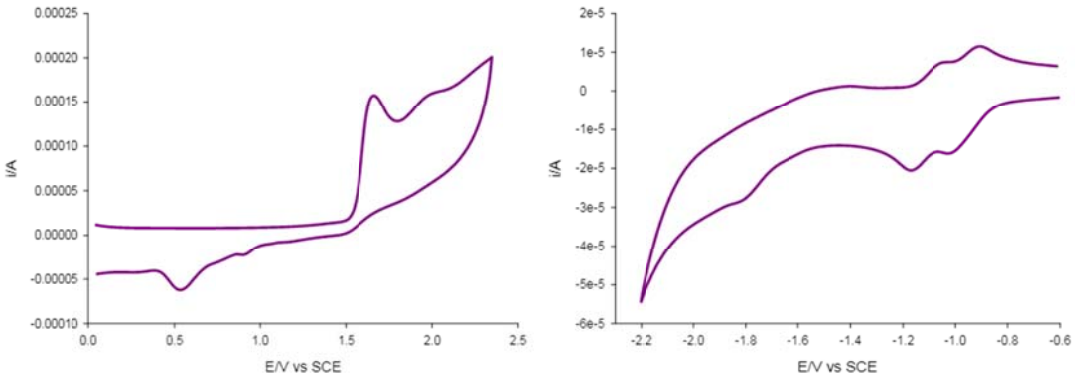

Figure 128: Cyclic voltammograms of a deoxygenated solution (0.5 mM) of cAZO-4 in CH_2Cl_2. Supporting electrolyte: $TBAPF_6$; internal reference: decamethylferrocene; scan rate: 200 mV/s; working electrode: glassy carbon.

	E_{OX} (V)	E_{RED} (V)
cAZO-3	1.65 1.78	-0.99
cAZO-4	1.74 2.00	-1.00

Table 7: Electrochemical parameters for cAZO-3 and cAZO-4.

By comparing the potential values for oxidation, it can be observed that electron-donor substituents shift the two processes towards higher potential values, whereas no effect is exerted on the value of reduction potential. Since the value referring to the first reduction process is comparable with that found for cAZO-3 and PCBM, the next step will be to test this compound as an electron acceptor material, when blended with a donor species.

1.9 Conclusions

Conjugation of azobenzene photochromic units leads to the development of rigid molecular structures and the structure of these organic compounds resembles that of oligo (p-phenylenevinylene) (PPV) derivatives and they can be considered their electron poor counterparts. In fact, their reduction potential shifts to more positive values upon increasing of azo units and the linear trend found for the redox potential and computed LUMO energy levels suggests that the addition of more azo units will lower further LUMO energy, thus moving the reduction potential towards more positive values. This makes these molecules potential electron acceptor materials in the development of organic solar cells. Preliminary tests did not a show a significant reduction of donor materials photoluminescence and this can be ascribable to high phase segregation between donor and acceptor, due to aggregation of acceptor material. The obtained results suggest that an improvement in the design of conjugated oligo-azobenzene has to focus on molecular functionalization, in order to avoid phase segregation and to tune the electrochemical properties.

Chapter V

Experimental Section

1 General considerations

All reactions were carried out under magnetic or mechanical stirring. For anhydrous reactions oven-dried glassware under dry argon atmosphere was used. Column chromatography was performed on Aldrich silica gel 230-400 mesh. Reagents and solvents were purchased from Aldrich, Fluka, TCI or Alfa Aesar. NMR spectra were recorded with Varian (Gemin 200, Inova 300 or 400, Mercury 600 MHz) instruments. Electron spray ionization mass spectra were obtained with a Micromass ZMD 4000.

2 Azobenzene derivatives

4-Nitrosobenzoic acid (1)

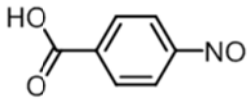

1

An aqueous solution (65 mL) of oxone, (1.5 eq, 12.93 g, 21 mmol) was added dropwise to a solution of 4-aminobenzoic acid (1.92 g, 14 mmol) in CH_2Cl_2 (23 mL). The yellow suspension was stirred for 1 hour at room temperature. The reaction mixture was then filtered through a Buckner, the precipitate was washed several times with water and dried under vacuum for one week. The product was obtained as a yellow solid, (1.79 g, 11.85 mmol, yield = 84.6 %) and was used for the next step without any further purification.

^{1}H-NMR Spectra (DMSO, 200 MHz):

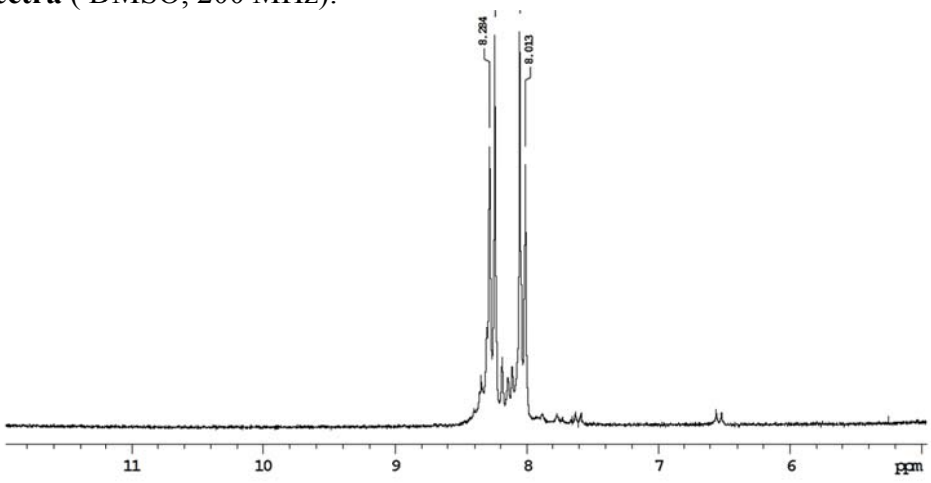

(E)-4-(phenyldiazenyl)benzoic acid (2)

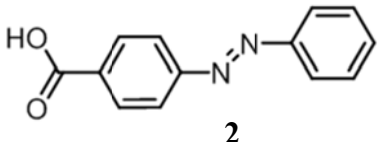

2

A mixture of nitrosobenzene (2.3 g, 21.4 mmol) and 4-amino benzoic acid, (2.14 g, 23.2 mmol) in 40 mL of acetic acid was stirred overnight at 90 °C. The crude product was filtered and the precipitate was washed with EtOH and crystalized from acetone to afford 2.2 g of (E)-4-(phenyldiazenyl) benzoic acid **2**, (yield 45.5 %), as an orange solid.

Rf: 0.4 Dichloromethane/methanol, 92:8

ESI-MS: calculated m/z: 225.03 $[M+H]^+$; found 225 $[M-H]^-$

^{1}H-NMR Spectra (CD_3OD, 200 MHz):

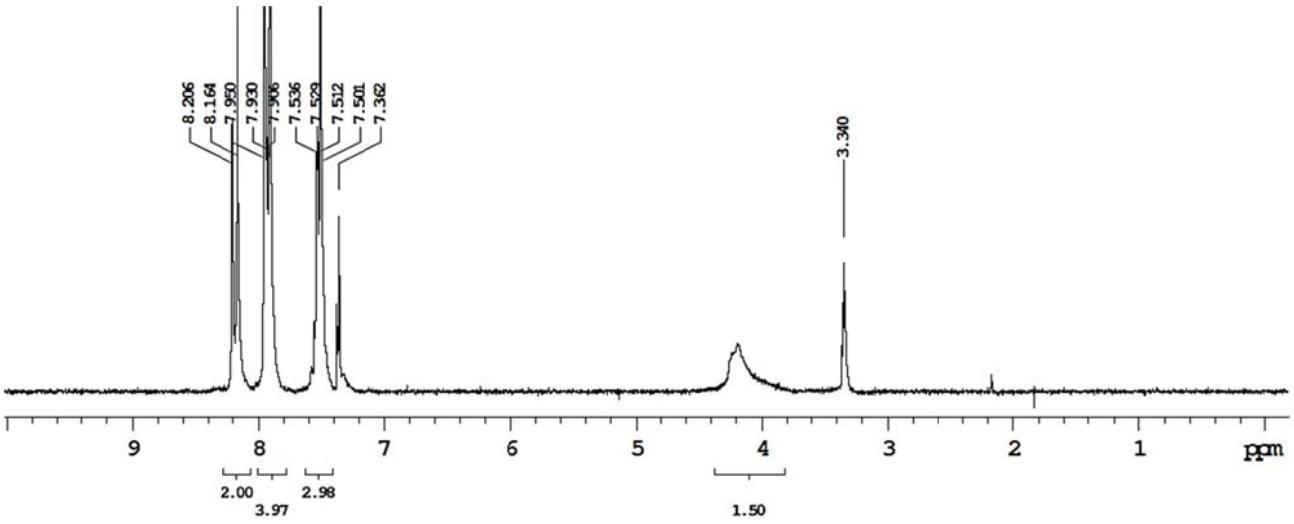

(E)-4-((4-(tert-butoxycarbonyl)phenyl)diazenyl)benzoic acid (3)

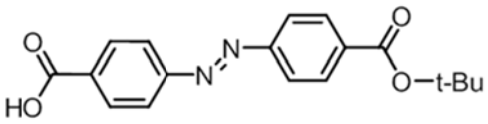

3

Dried 4-nitrosobenzoic **1**, (0.5 g, 3.31 mmol) was suspended in a mixed solvent of DMSO/AcOH (0.5 M). 1.2 equivalent of tert-butyl-4-aminobenzoate, (0.77 mg, 3.97 mmol), was added to the suspension and stirred for 4 days, refluxing at 90 °C. The crude product was filtered and washed with EtOH, then purified by silica gel chromatography (dichloromethane/methanol, 95:5), affording 0.377 g, (yield = 35 %) of the title compound as an orange solid.

Rf : 0.43 Dichloromethane/Methanol, 95:5

ESI-MS: calculated m/z: 326.35 $[M+H]^+$; found 324.9 $[M-H]^-$

^{1}H-NMR Spectra (CD_3OD, 600 MHz)

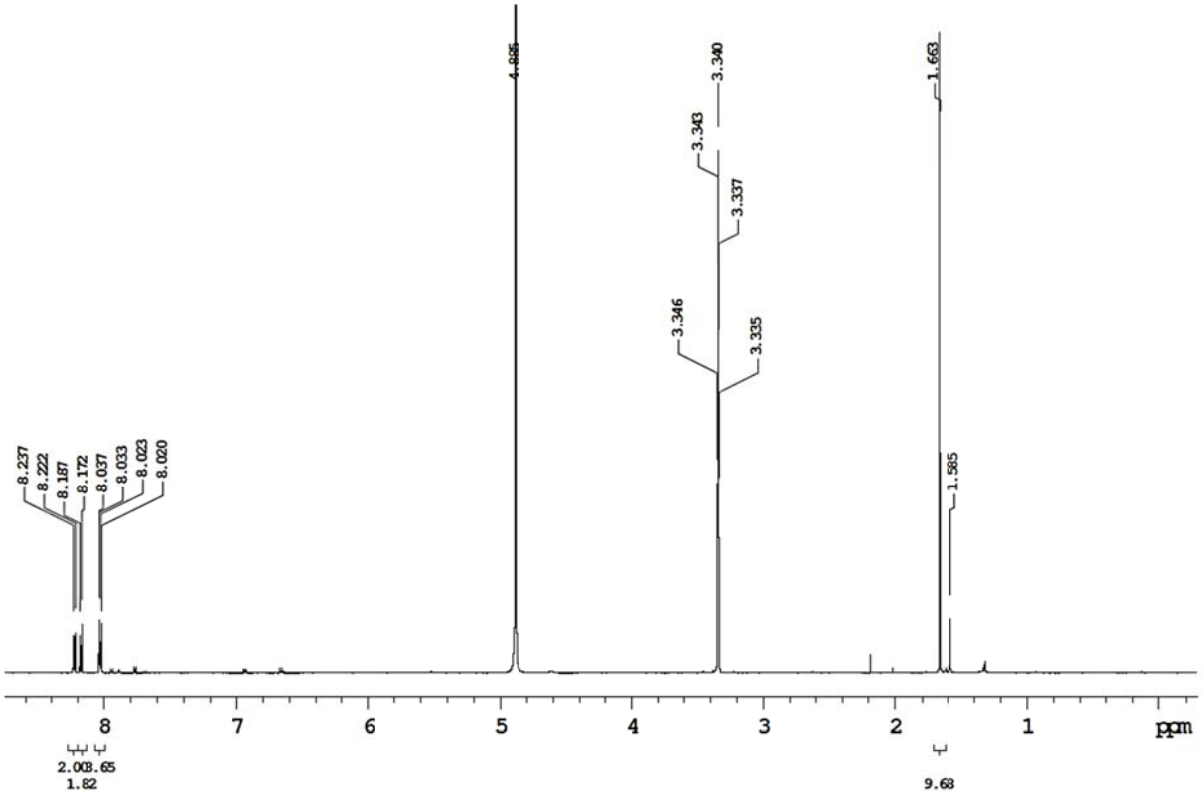

(E)-4-(pyridin-3-yldiazenyl)benzoic acid (4)

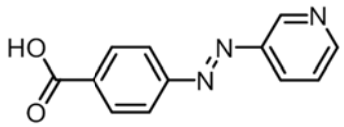

4

Dried 4-nitrosobenzoic acid **1**, (0.32 g, 2.06 mmol) was suspended in AcOH (10 mL). 1.2 equivalents of 3-aminopyridine (0.215 mg, 2.28 mmol) were added and the suspension was stirred for 4 days at 90 °C. The crude product was filtered and washed several times with water, then it was purified by chromatography on silica gel (dichloromethane/methanol, 95:5, affording **4** (200 mg, yield = 42.7 %) as an orange solid.

Rf : 0.43 Dichloromethane/Methanol, 95:5

ESI-MS: calculated m/z: 228, $[M+H]^+$; found 226 $[M-H]^-$

^{1}H-NMR Spectra (DMSO, 200 MHz):

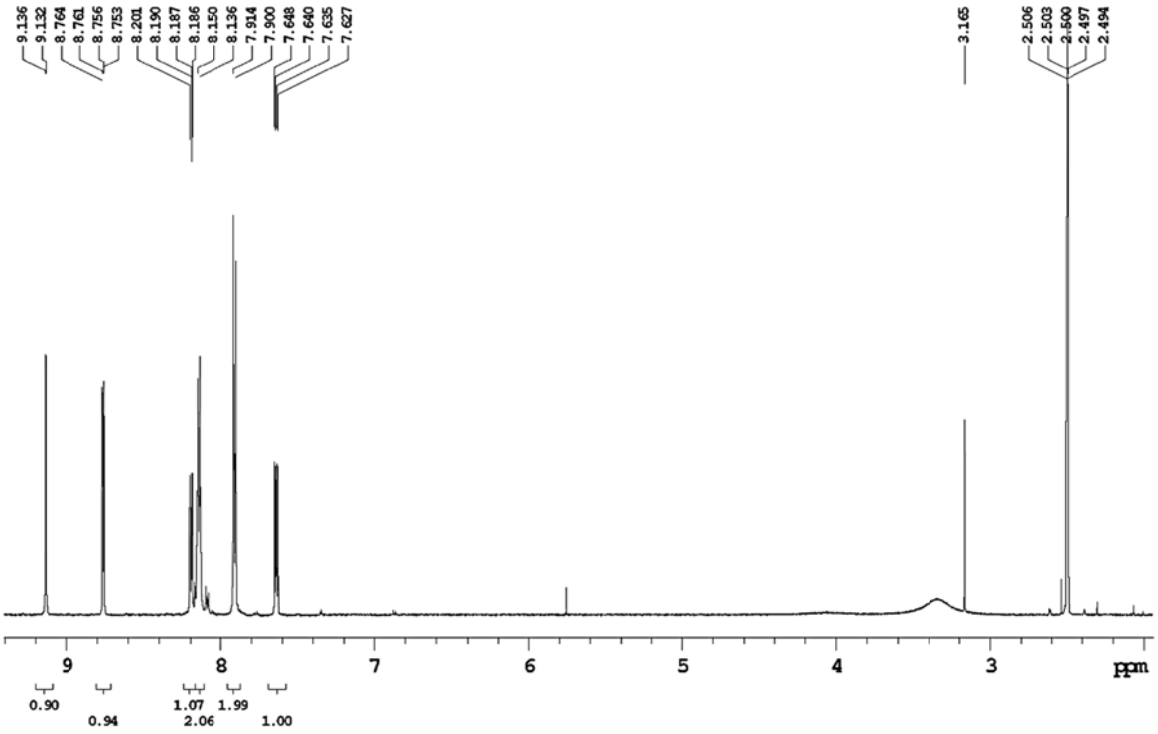

(E)-4-((4-fluorophenyl)diazenyl)benzoic acid (5)

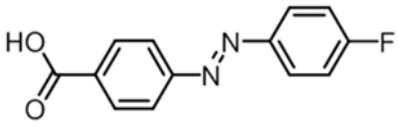

5

Dried 4-nitrosobenzoic acid **1**, (0.3 g, 1.9 mmol) was suspended in a mixture EtOH/H_2O 4:1 (5 mL). A buffer solution (AcOH/AcONa) and 4-nitroaniline, (0.22 mg, 1.9 mmol, 0.188 mL), were added and the suspension was stirred for 4 days at 80 °C. The crude product was filtered and washed several times with EtOH, then it was purified by silica gel chromatography (dichloromethane/methanol, 95:5), affording **5** (0.087 g, yield = 18.8 %) as a yellow solid.

Rf : 0.36 Dichloromethane/Methanol, 92:8

ESI-MS: calculated m/z: 244.06, $[M+H]^+$; found 242 $[M-H]^-$

^{1}H-NMR Spectra (CD_3OD, 600 MHz):

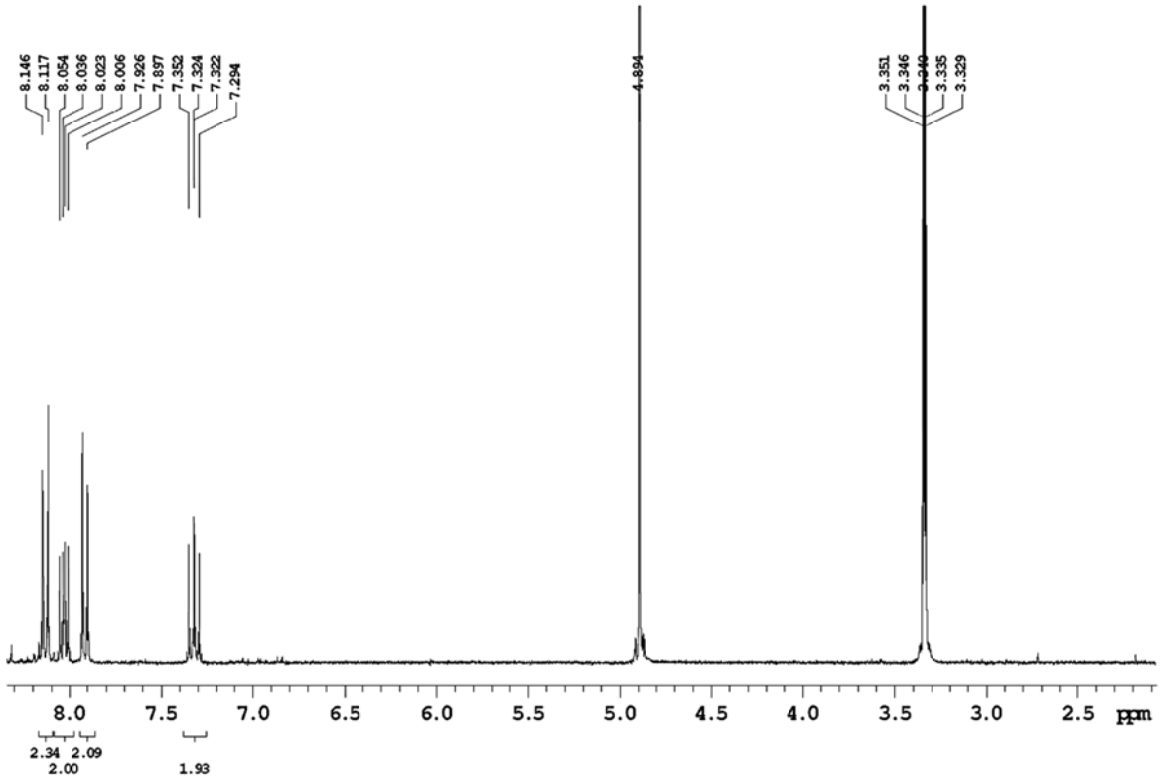

(E)-4-((4-nitrophenyl)diazenyl)benzoic acid (6)

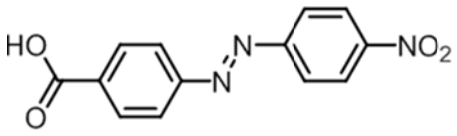

6

Dried 4-nitrosobenzoic acid **1**, (0.22 g, 1.43 mmol) was suspended in a mixture EtOH/H_2O 4:1 (5 mL). A buffer solution AcOH/AcONa and 4-nitroaniline, (0.2 g, 1.45 mmol) were added and the suspension was stirred for 4 days at 80 °C. The crude product was filtered and washed several times with EtOH, then it was purified by silica gel chromatography (dichloromethane/methanol, 95:5), affording **6** (0.103 g, yield = 26.5 %) as a brownish solid.

Rf : 0.38 dichloromethane/ Methanol, 92:8

ESI-MS: calculated m/z: 272.06, $[M+H]^+$; found 270 $[M-H]^-$

(E)-4-((4-cyanophenyl)diazenyl)benzoic acid (7)

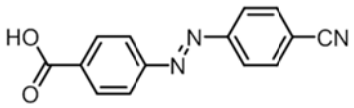

7

Dried 4-nitrosobenzoic acid **1**, (1 g, 6.6 mmol) was suspended in a 1:1 mixture of AcOH/DMSO (90 mL). 4-Aminobenzonitrile (0.2 g, 6.6 mmol) was added and the suspension stirred for 8 days at 100 °C. The reaction progress was monitored by TLC (dichloromethane). Water was added to the reaction mixture and the orange precipitate thus formed was filtered and washed several times with water. The crude was purified by silica gel chromatography (petroleum ether/ethyl acetate 1:1), affording **7** (0.450 g, yield = 28 %) as an orange solid.

Rf : 0.36 Dichloromethane/Methanol, 92:8

ESI-MS: calculated m/z: 25.07, $[M-H]^-$; found 250 $[M-H]^-$

^{1}H-NMR Spectra (DMSO, 600 MHz):

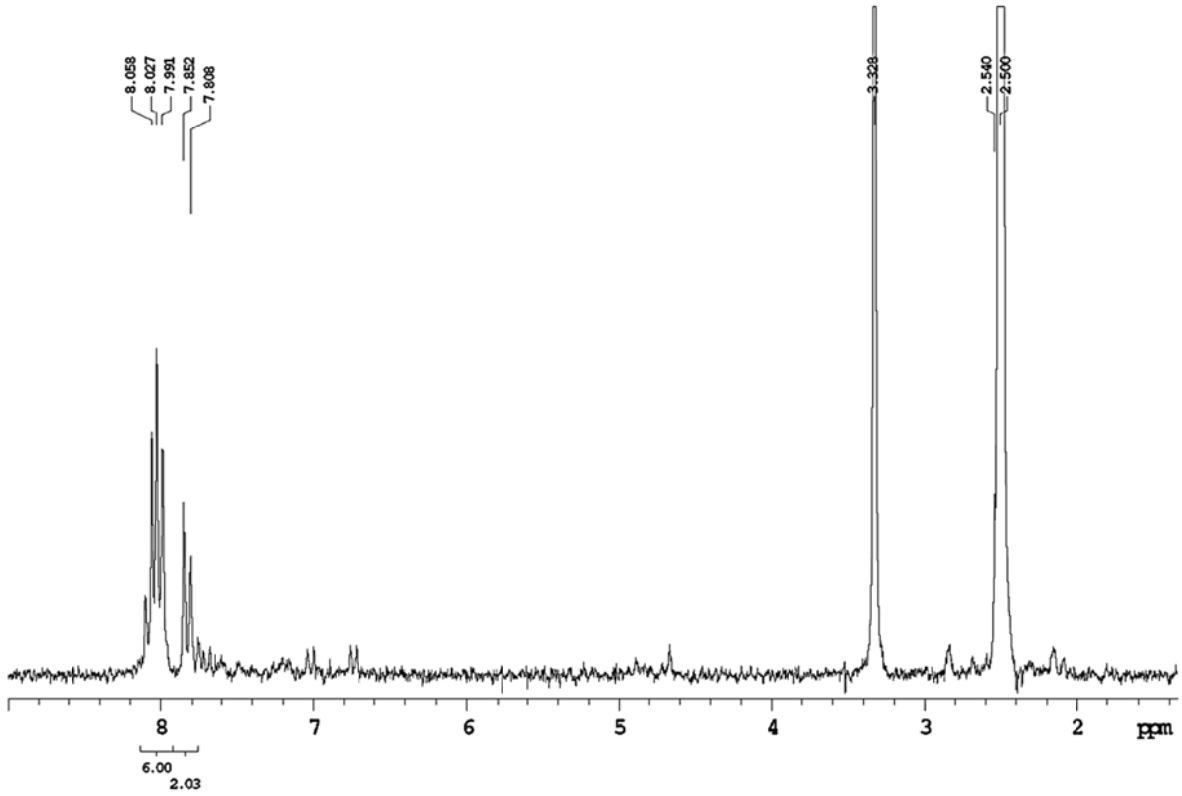

3 α-Cyclodextrin derivatives

Pentakis(6-*O*-*tert*-butyldimethylsilyl)-α-CD (8)

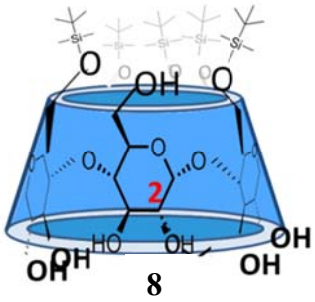

8

To dried α-cyclodextrin (1 eq, 3.1 g, 3.19 mmol) in dry DMF/Pyridine (ratio 7.5/4, 34 mL) at 0 °C was added tert-butyldimethylsilyl chloride (5.2 eq, 2.49 g, 16.6 mmol.). After stirring for 3 days at room temperature, the reaction mixture was poured into ice/water (350 mL) and stirred for 15 min. The resulting white precipitate was filtered, washed with ice-cold water, and dissolved in Et_2O (70

mL). The organic solution was washed with 5% aqueous HCl (3 x 50 mL), aqueous saturated $NaHCO_3$ (50 mL), and saturated brine (50 mL). Finally, the solution was dried over anhydrous Na_2SO_4, filtered, and concentrated. The crude product was purified by flash chromatography using CH_2Cl_2/MeOH 9/1 as eluent, to afford 4.58 g silylated cyclodextrin as a white solid.

Rf : 0.23 dichloromethane/ Methanol, 93:7

ESI-MS: calculated m/z: 1543 $[M+H]^+$; found 1544 $[M+H]^+$.

^{1}H-NMR Spectra ($CDCl_3$, 600 MHz):

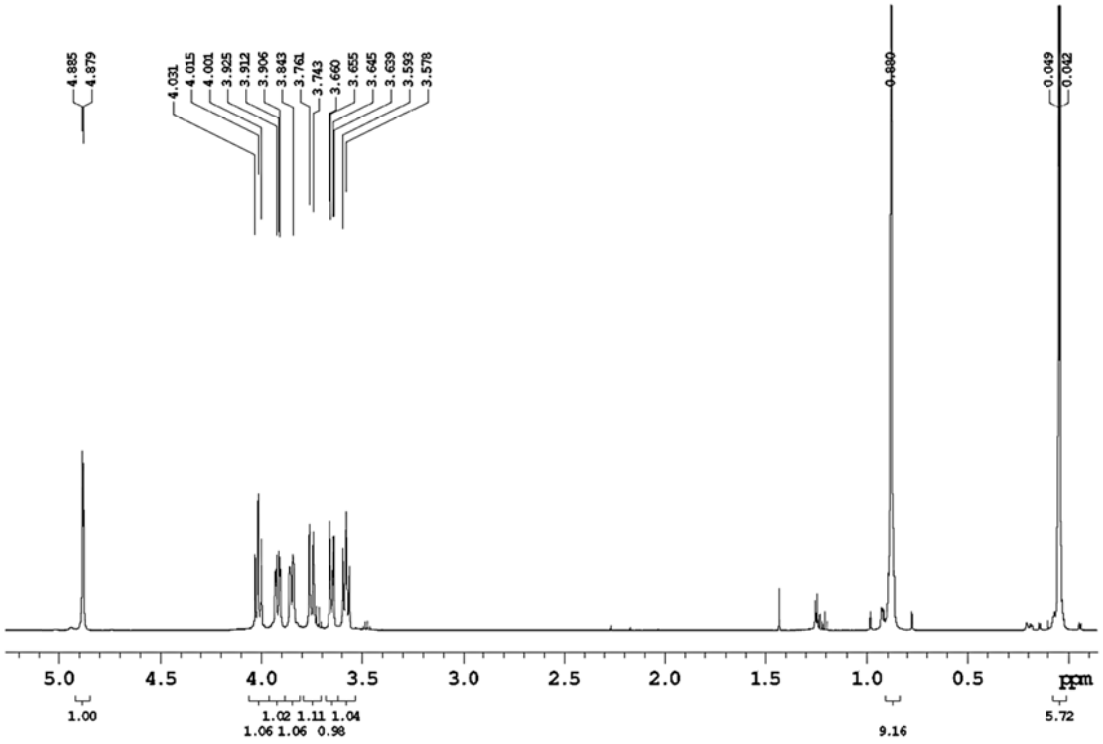

2,6-*O*-di-[pentakis(6-*O*-*tert*-butyldimethylsilyl)-α-CD]-bis-4'-phenylazobenzoate (9)

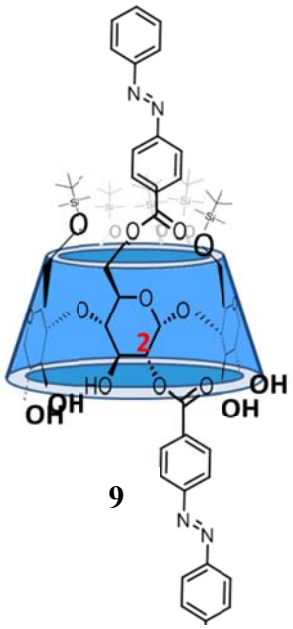

9

2,4,6-Triisopropylbenzenesulfonyl chloride (2.4 eq, 72 mg, 0.48 mmol) was added to a solution of 4-(phenylazo)benzoic acid (2.4 eq, 108 mg, 0.48 mmol) in anhydrous THF (10 mL) and redistilled triethylamine (5.5 eq, 1.1 mmol, 152 μL) at 0 °C. The resulting solution was stirred for two hours then allowed to reach room temperature and stirred for additional 20 minutes. Silylated cyclodextrin (0.312 g, 0.2 mmol), dried over P_2O_5 under vacuum for 2 h at 55 °C, and a catalytic amount of DMAP were then added and the mixture was stirred under argon overnight. After evaporation of the solvent in vacuo, chloroform (40 mL) was added and the organic layer was washed with water (3 x 20 mL) and 5 % $NaHCO_3$ aqueous solution (3 x 20 mL). The organic layer was dried over Na_2SO_4 and concentrated in vacuo. The crude material was partially purified by flash column chromatography on silica gel (eluent: dichloromethane/methanol 95:5) to afford 0.091 g (yield = 22.7 %) of compound **9** as a pale orange solid.

Rf: 0.32 dichloromethane/methanol 95/5

ESI-MS: calculated m/z: 1959 $[M+H]^+$; found 1959 $[M-H]^-$

2-*O*-mono-α-CD-bis-4'-phenylazobenzoate (10)

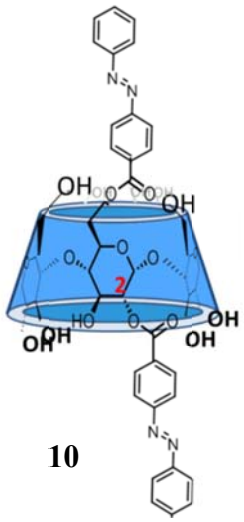

10

Trifluoroacetic acid (1.2 mL) was added to cyclodextrin diester **9** dissolved in MeOH (1 mL). The solution was stirred at room temperature for 1 h, monitoring desilylation process by ESI. The solvent was removed in vacuo. Methanol was added and evaporated in vacuo for azeotropic removal of any residual trifluoroacetic acid. The residue was dissolved in water and washed three times with Et_2O. After freeze-drying, compound **10** was obtained not perfectly pure as a pale orange solid in quantitative yield.

ESI-MS: calculated m/z: 1389 $[M+H]^+$; found 1389 $[M+H]^+$, 1412 $[M+Na]^+$,

Hexakis(6-*O*-*tert*-butyldimethylsilyl)-α-CD (11)

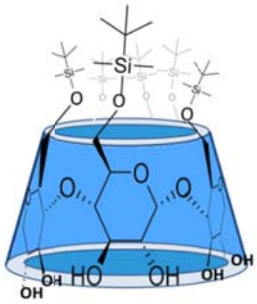

11

To dried α-cyclodextrin (1 eq, 3.05 g, 3.14 mmol) in dry DMF/Pyridine (ratio 7.5/4, 34 mL) was added, at 0 °C, tert-butyldimethylsilyl chloride (6.2 eq, 2.93 g, 19.5 mmol.). After stirring for 3 days at room temperature, the reaction mixture was poured into ice/water (350 mL) and stirred for 15 min. The resulting white precipitate was filtered, washed with ice-cold water, and dissolved in Et_2O (70 mL). The organic phase was washed with a 5 % aqueous HCl (3 x 50 mL), saturated aqueous $NaHCO_3$ (50 mL) and brine (50 mL). Finally, the solution was dried over anhydrous Na_2SO_4,

filtered, and concentrated. The crude product was purified by flash chromatography using $Et_2O/EtOH/H_2O$ (10/0.9/0.3) as eluent, to afford 4.58 g of silylated cyclodextrin **11** (yield 88 %) as a white solid.

Rf : 0.21 Dichloromethane/Methanol, 95:5

ESI-MS: calculated m/z: 1659.42 $[M+H]^+$; found 1659 $[M+H]^+$, 1655.9 $[M-H]^-$;

^{1}H-NMR Spectra ($CDCl_3$, 600 MHz):

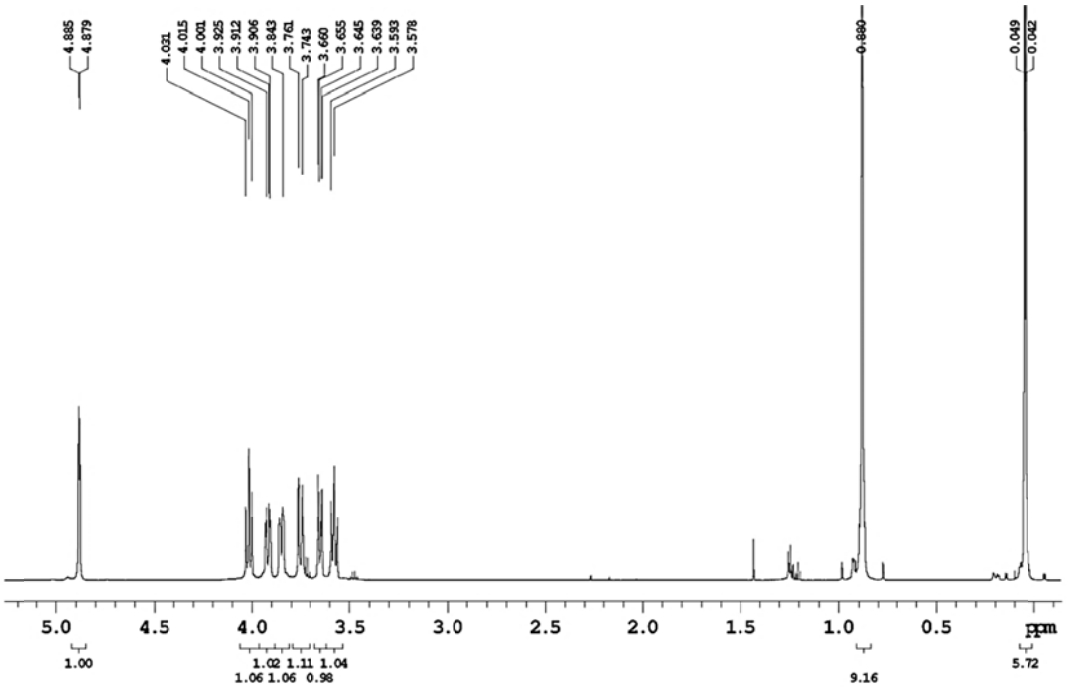

2-*O*-mono[hexakis(6-*O*-*tert*-butyldimethylsilyl)-α-CD]-4'-phenylazobenzoate (12)

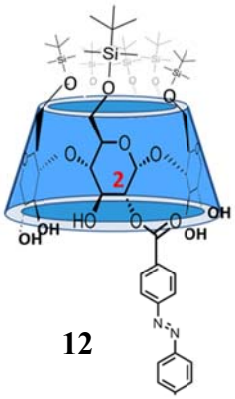

12

2,4,6-Triisopropylbenzenesulfonyl chloride (1.17 eq, 42 mg, 0.114 mmol) was added to a solution of 4-(phenylazo)benzoic acid **2** (1.4 eq, 33 mg, 0.144 mmol) in anhydrous THF (10 mL) and redistilled triethylamine (2.75 eq, 100 µL) at 0 °C. The resulting solution was stirred for two hours

then allowed to reach room temperature and stirred for additional 20 minutes. Silylated cyclodextrin **11** (0.2 g, 0.12 mmol), dried over P_2O_5 under vacuum for 2 h at 55 °C, and a catalytic amount of DMAP were then added and the mixture was stirred under argon overnight. After evaporation of the solvent in vacuo, chloroform (40 mL) was added and the organic layer was washed with water (3 x 20 mL) and 5 % $NaHCO_3$ aqueous solution (3 x 20 mL). The organic layer was dried over Na_2SO_4 and concentrated in vacuo. The crude material was purified by flash column chromatography on silica gel (eluent: dichloromethane/methanol 95:5) to afford 0.096 g (yield = 43 %) of compound as a pale orange solid.

Rf: 0.33 Dichloromethane/Methanol, 92:8

ESI-MS: calculated m/z: 1886.6 $[M+H]^+$; found 1887 $[M-H]^-$

^{1}H-NMR Spectra (CD_3OD, 600 MHz):

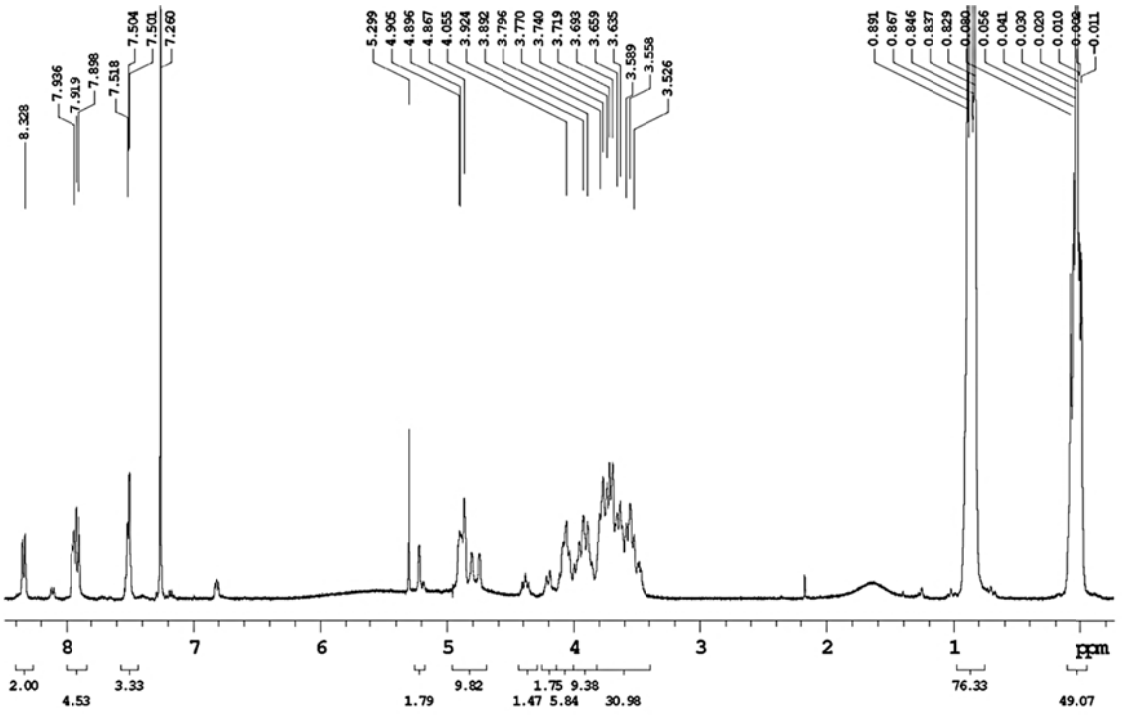

2-*O*-mono[hexakis(6-*O*-*tert*-butyldimethylsilyl)-α-CD]-4-(tert-butoxycarbonyl) phenylazobenzoate (13)

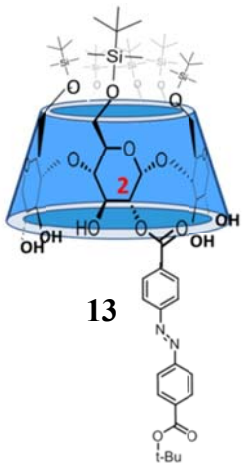

13

2,4,6-Triisopropylbenzenesulfonyl chloride (0.046 g, 0.15 mmol, 1.17 eq.) was added to a solution of 4-(tert-butoxycarbonyl)phenyl diazenyl benzoic acid **3** (0.059 g, 0.18 mmol, 1.4 eq.) in anhydrous THF (18 mL) and redistilled triethylamine (50 µL, 2.75 eq.) at 0 °C. The resulting solution was stirred for two hours then allowed to reach room temperature and stirred for additional 20 minutes. Silylated cyclodextrin **11** (0.219 g, 0.13 mmol), (dried over P_2O_5 under vacuum for 2 hours at 55 °C), and a catalytic amount of DMAP were then added and the mixture was stirred under argon overnight. After evaporation of the solvent in vacuo, chloroform (40 mL) was added and the organic layer was washed with water (3 x 20 mL) and 5 % $NaHCO_3$ aqueous solution (3 x 20 mL). The organic layer was dried over Na_2SO_4 and concentrated in vacuo. The crude material was purified by flash column chromatography on silica gel (eluent: dichloromethane/methanol 95:5) to afford 0.062 g (yield = 21 %) of compound as a pale orange solid.

Rf: 0.28 dichloromethane/methanol, 95:5

ESI-MS: calculated m/z: 1967.8 $[M+H]^+$; found 1988.2 $[M+Na]^+$

^{1}H-NMR Spectra (CD_3OD, 600 MHz):

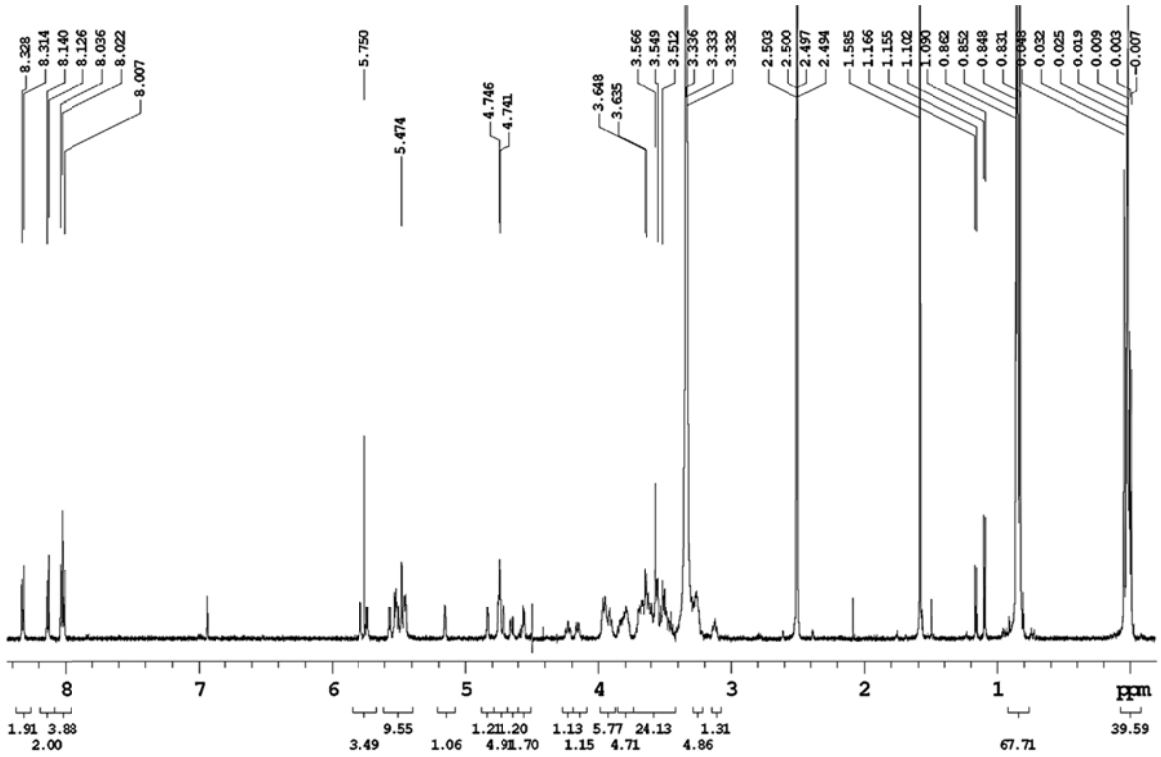

2-*O*-mono[hexakis(6-*O*-*tert*-butyldimethylsilyl)-α-CD]-(E)-4'-(pyridin-3-yldiazenyl)benzoate (14)

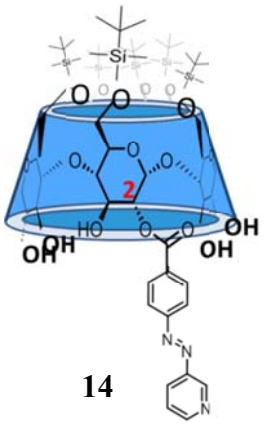

14

2,4,6-Triisopropylbenzenesulfonyl chloride (1.2 eq, 13 mg, 0.043 mmol) was added to a solution of (E)-4-(pyridin-3-yldiazenyl benzoic acid **4** (1.2 eq, 10 mg, 0.043 mmol) in anhydrous THF (7 mL) and redistilled triethylamine (2.75 eq, 14 μL) at 0 °C. The resulting solution was stirred for two hours then allowed to reach room temperature and stirred for additional 20 minutes. Silylated

cyclodextrin **11** (0.060 g, 0.036 mmol, dried over P_2O_5 under vacuum for 2 h at 55 °C) and a catalytic amount of DMAP were then added and the mixture was stirred under argon overnight. After evaporation of the solvent in vacuo, chloroform (40 mL) was added and the organic layer was washed with water (3 x 20 mL) and 5 % $NaHCO_3$ aqueous solution (3 x 20 mL). The organic layer was dried over Na_2SO_4 and concentrated in vacuo. The crude material was purified by flash column chromatography on silica gel (eluent: dichloromethane/methanol 95:5) to afford 0.026 g (yield = 38.4 %) of compound as a pale orange solid.

Rf: 0.37 dichloromethane/methanol 94:6.

ESI-MS: calculated m/z: 1867.6 $[M+H]^+$; found 1867 $[M-H]^-$

2-*O*-mono[hexakis(6-*O*-*tert*-butyldimethylsilyl)-α-CD]-(E)-4'-(fluoro)-phenylazobenzoate (15)

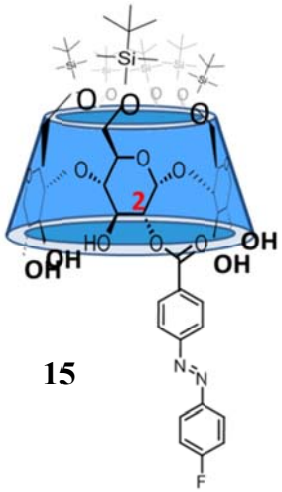

15

2,4,6-Triisopropylbenzenesulfonyl chloride (1.2 eq, 0.043 g, 0.141 mmol) was added to a solution of (E)-4-((4-fluorophenyl)diazenyl benzoic acid **5** (1.2 eq, 0.035 g, 0.141 mmol) in anhydrous THF (7 mL) and redistilled triethylamine (2.75 eq, 50 µL) at 0 °C. The resulting solution was stirred for two hours then allowed to reach room temperature and stirred for additional 20 minutes. Silylated cyclodextrin **11** (0.060 g, 0.036 mmol), dried over P_2O_5 under vacuum for 2 h at 55 °C, and a catalytic amount of DMAP were then added and the mixture was stirred under argon overnight. After evaporation of the solvent in vacuo, chloroform (40 mL) was added and the organic layer was washed with water (3 x 20 mL) and 5 % $NaHCO_3$ aqueous solution (3 x 20 mL). The organic layer was dried over Na_2SO_4 and concentrated in vacuo. The crude material was purified by flash column chromatography on silica gel (eluent: dichloromethane/methanol 97:3) to afford 0.026 g (yield = 38.4 %) of compound as a pale orange solid.

Rf: 0.38 dichloromethane/methanol 97:3.

ESI-MS: calculated m/z: 1883.89 $[M+H]^+$; found 1907 $[M+Na]^+$

^{1}H-NMR Spectra (CD_3OD, 600 MHz):

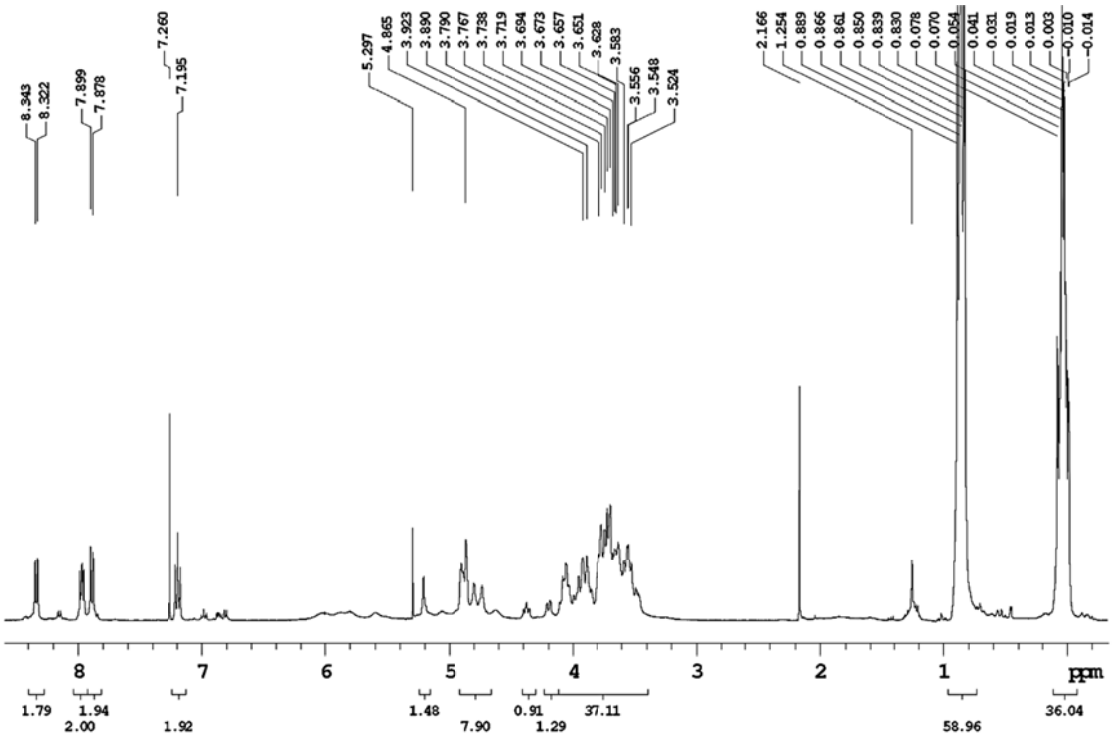

2-*O*-mono[hexakis(6-*O*-*tert*-butyldimethylsilyl)-α-CD]-(E)-4'-(cyano)-phenylazobenzoate (16)

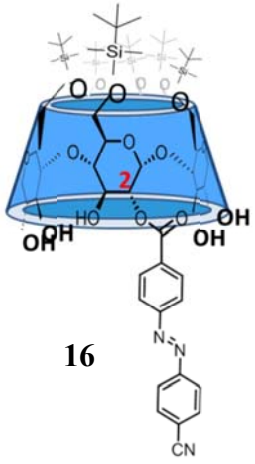

16

2,4,6-Triisopropylbenzenesulfonyl chloride (1.2 eq, 0.103 g, 0.47 mmol) was added to a solution of (E)-4-(4-cyanophenyl)diazenyl benzoic acid **7** (1.4 eq, 0.1 g, 0.04 mmol) in anhydrous THF (7 mL) and redistilled triethylamine (2.75 eq, 0.113 mL) at 0 °C. The resulting solution was stirred for two hours then allowed to reach room temperature and stirred for additional 20 minutes. Silylated cyclodextrin **11** (0.473 g, 0.28 mmol), dried over P_2O_5 under vacuum for 2h at 55 °C, and a

catalytic amount of DMAP were then added and the mixture was stirred under argon overnight. After evaporation of the solvent in vacuo, chloroform (40 mL) was added and the organic layer was washed with water (3 x 20 mL) and 5 % $NaHCO_3$ aqueous solution (3 x 20 mL). The organic layer was dried over Na_2SO_4 and concentrated in vacuo. The crude material was purified by flash column chromatography on silica gel (eluent: dichloromethane/methanol 95:5) to afford 0.163 g (yield = 22 %) of compound as a pale orange solid.

Rf: 0.57 dichloromethane/methanol 97:3.

ESI-MS: calculated m/z: 1889.89 $[M+H]^+$; found 1913 $[M+Na]^+$

^{1}H-NMR Spectra (CD_3OD, 600 MHz):

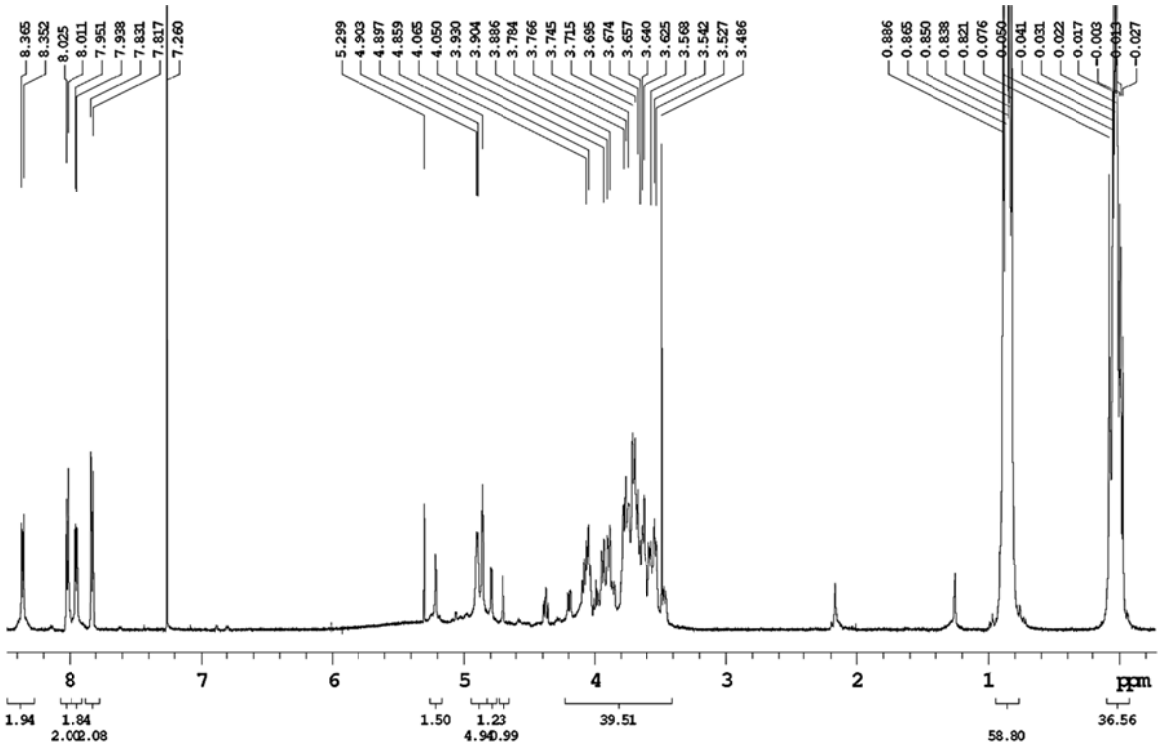

2-*O*-mono-α-CD-4'-phenylazobenzoate (17)

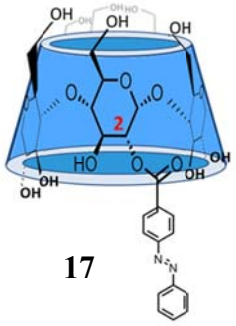

17

To TBDMS-protected α-cyclodextrin **12** dissolved in MeOH, (1 mL) was added trifluoroacetic acid (1.2 mL). The solution was stirred at room temperature for 1 h, monitoring the desilylation process by ESI. The solvent was removed in vacuo. Methanol was added and evaporated in vacuo for azeotropic removal of any residual trifluoroacetic acid. The residue was dissolved in water and washed three times with Et_2O. After freeze-drying, compound **17** was obtained as a pale orange solid in 100 % yield.

ESI-MS: calculated m/z: 1181.07 $[M+H]^+$; found 1181 $[M+H]^+$, 1204 $[M+Na]^+$,

^{1}H-NMR Spectra (D_2O, 600 MHz)

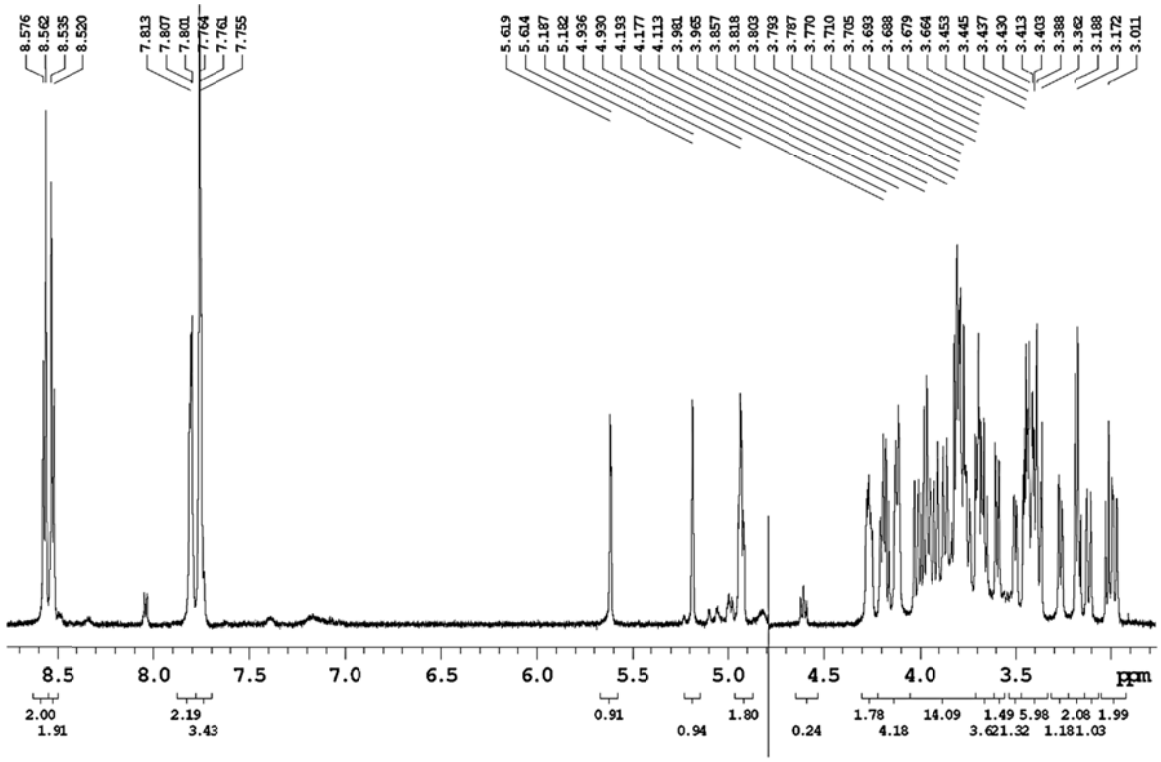

2-*O*-mono-α-CD-4'- carboxy-azobenzene (18)

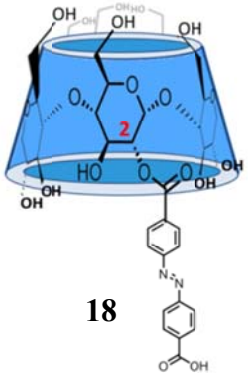

18

To TBDMS-protected cyclodextrin, **13,** (0.100 g, 0.06 mmol) dissolved in MeOH (1 mL) was added trifluoroacetic acid (5 mL). The solution was stirred at room temperature for 3 h, monitoring the desilylation process by ESI analysis every 15 minutes. The solvent was removed in vacuo. Methanol was added and evaporated in vacuo for azeotropic removal of any residual trifluoroacetic acid. The residue was dissolved in water and washed three times with Et_2O. After freeze-drying, compound **18** was obtained as a pale orange solid in 100 % yield.

ESI-MS: calculated m/z: 1224.6 $[M+H]^+$; found 1224 $[M+H]^+$, 1247.6 $[M+Na]^+$,

^{1}H-NMR Spectra (D_2O, 600 MHz):

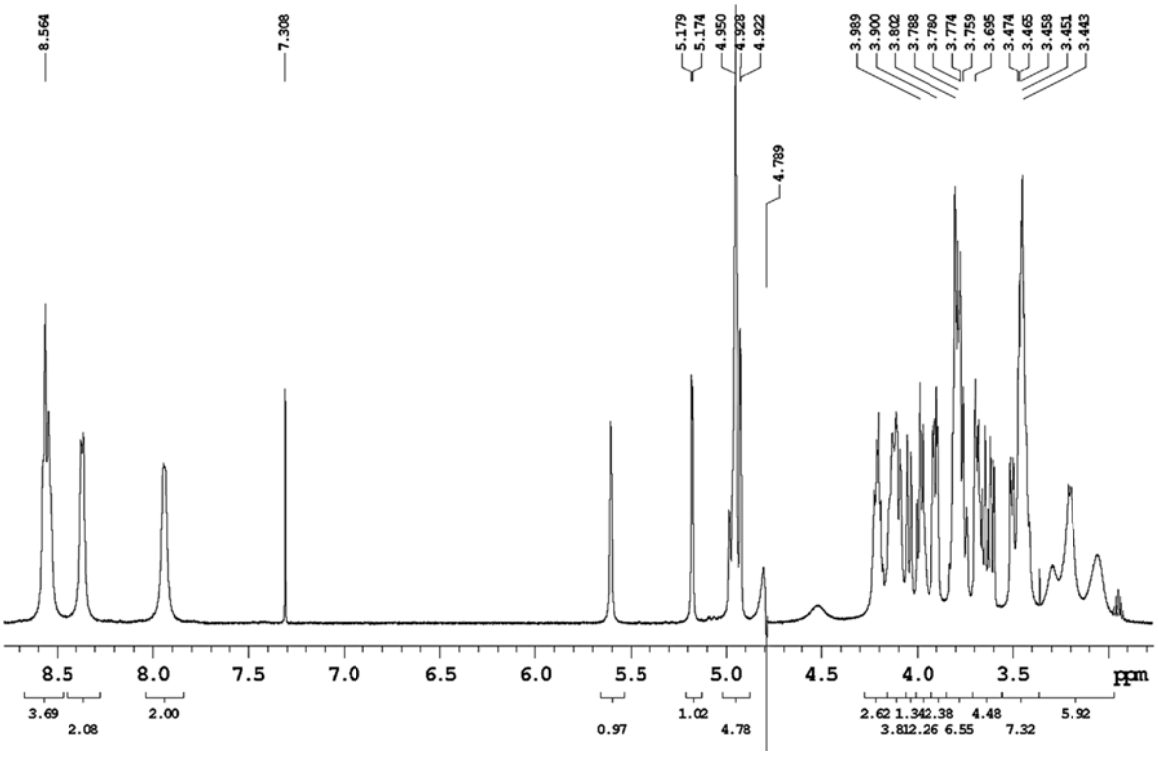

2-*O*-mono-α-CD-4'- E)-4'- (pyridin-3-yldiazenyl)benzoate (19)

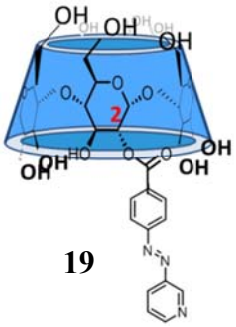

19

To TBDMS-protected cyclodextrin **13**, dissolved in MeOH, (1 mL), was added trifluoroacetic acid (1.2 mL). The solution was stirred at room temperature for 1 h, monitoring the desilylation process by ESI. The solvent was removed in vacuo. Methanol was added and evaporated in vacuo for azeotropic removal of any residual trifluoroacetic acid. The residue was dissolved in water and washed three times with Et_2O. After freeze-drying, compound **19** was obtained as a pale orange solid in 100 % yield.

ESI-MS: calculated m/z: 1181.38 $[M+H]^+$; found 1182 $[M+H]^+$, 1205 $[M+Na]^+$.

2-*O*-mono-α-CD-4'-(fluoro)-phenylazobenzoate (20)

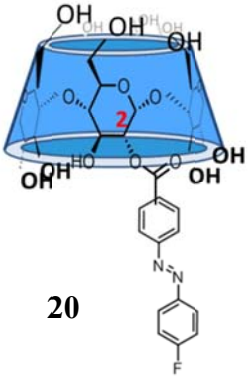

20

To TBDMS-protected cyclodextrin **15**, dissolved in MeOH, (1 mL) was added trifluoroacetic acid (1.2 mL). The solution was stirred at room temperature for 1 h, monitoring the desilylation process by ESI. The solvent was removed in vacuo. Methanol was added and evaporated in vacuo for azeotropic removal of any residual trifluoroacetic acid. The residue was dissolved in water and washed three times with Et_2O. After freeze-drying, compound **20** was obtained as a pale orange solid in 100 % yield.

ESI-MS: calculated m/z: 1198.38 $[M+H]^+$; found 1221 $[M+Na]^+$,

^{1}H-NMR Spectra (D_2O, 600 MHz):

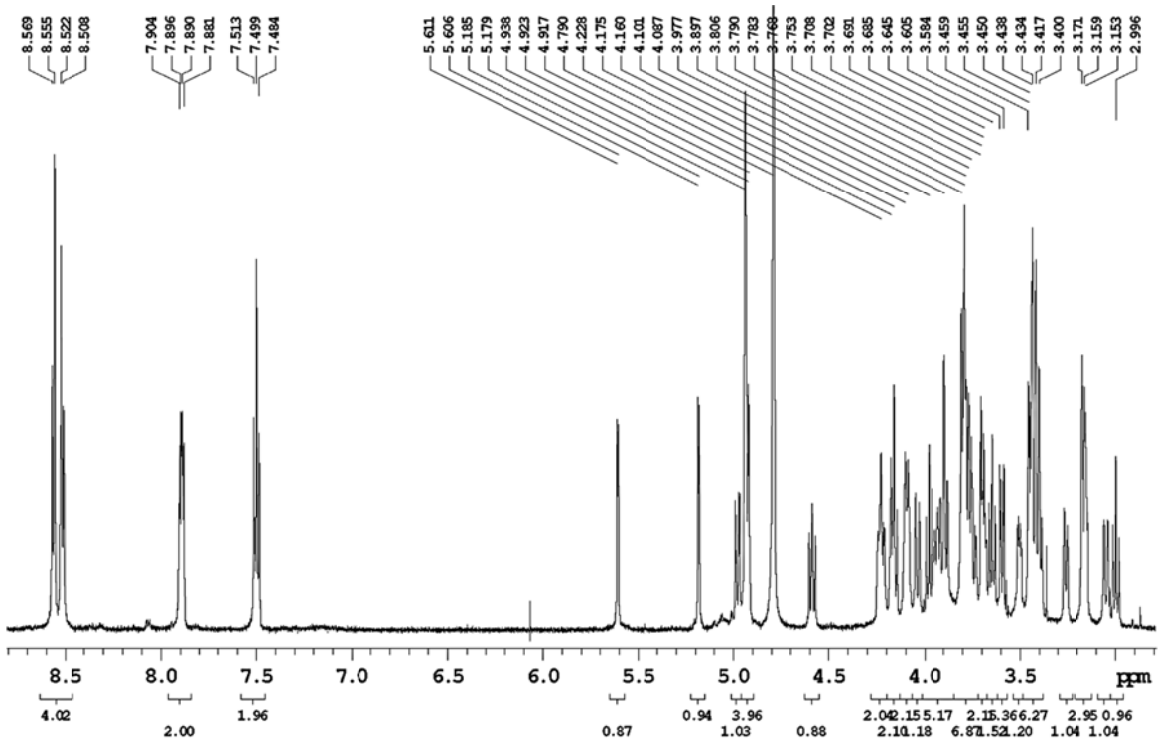

2-*O*-mono-α-CD-4'-(cyano)-phenylazobenzoate (21)

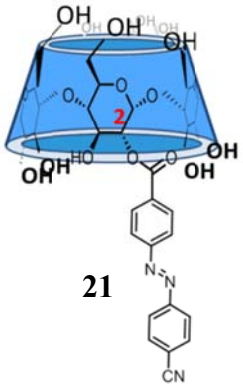

21

To TBDMS-protected cyclodextrin **16**, dissolved in MeOH (3.5 mL), was added trifluoroacetic acid (1.2 mL). The solution was stirred at room temperature for 1 h, monitoring desilylation process by ESI. The solvent was removed in vacuo. Methanol was added and evaporated in vacuo for azeotropic removal of any residual trifluoroacetic acid. The residue was dissolved in water and washed three times with Et_2O. After freeze-drying, compound **21** was obtained as a pale orange solid in 100 % yield.

ESI-MS: calculated m/z: 1205.38 $[M+H]^+$; found 1228 $[M+Na]^+$,

^{1}H-NMR Spectra (D_2O, 600 MHz):

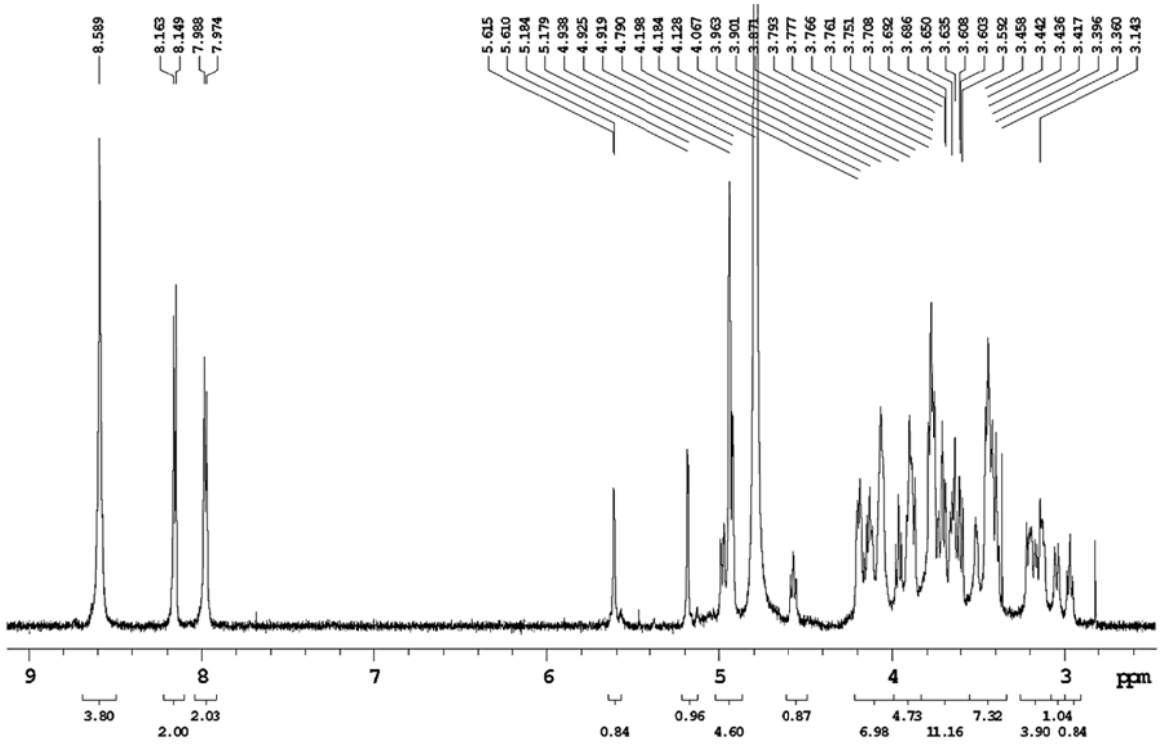

4 γ-Cyclodextrin derivatives

Octakis(6-*O*-*tert*-butyldimethylsilyl)-γ-CD (22)

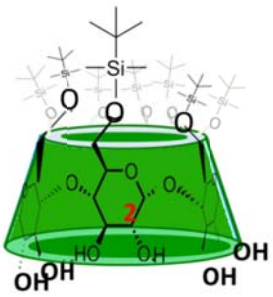

22

To dried γ-cyclodextrin (1 eq, 3.0 g, 2.3 mmol) in dry DMF/Pyridine (ratio 7.5/4, 34 mL) was added, at 0 °C, tert-butyldimethylsilyl chloride (8.2 eq, 2.84 g, 18.9 mmol.). After stirring for 3 days at room temperature, the reaction mixture was poured into ice/water (350 mL) and stirred for 15

min. The resulting white precipitate was filtered off, washed with ice-cold water, and dissolved in Et_2O (70 mL). The solution was washed with a 5 % aqueous HCl solution (3 x 50 mL), a saturated aqueous $NaHCO_3$ solution (50 mL), and saturated brine (50 mL). Finally, the solution was dried over anhydrous Na_2SO_4, filtered, and concentrated. The crude product was purified by flash chromatography using CH_2Cl_2/MeOH (9:1) to afford 4 g of silylated γ-cyclodextrin **22** (yield 78.6 %) as a white solid.

Rf : 0.53 dichloromethane/ Methanol, 92:8

ESI-MS: calculated m/z: 2211 $[M+H]^+$; found 2212 $[M+H]^+$

2-*O*-mono[octakis(6-*O*-*tert*-butyldimethylsilyl)-γ-CD]-4'-phenylazobenzoate (23)

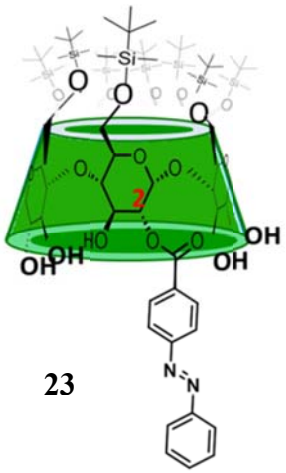

23

2,4,6-Triisopropylbenzenesulfonyl chloride (1.17 eq, 51 mg, 0.168 mmol) was added to a solution of 4-(phenylazo)benzoic acid (1.2 eq, 38 mg, 0.172 mmol) in anhydrous THF (10 mL) and redistilled triethylamine (2.75 eq, 55 µL) at 0 °C. The resulting solution was stirred for two hours then allowed to reach room temperature and stirred for additional 20 minutes. Silylated γ-cyclodextrin **22** (0.3 g, 0.14 mmol, dried over P_2O_5 under vacuum for 2 h at 55 °C) and a catalytic amount of DMAP were then added and the mixture was stirred under argon overnight. After evaporation of the solvent in vacuo, chloroform (40 mL) was added and the organic layer was washed with water (3 x 20 mL) and 5 % $NaHCO_3$ aqueous solution (3 x 20 mL). The organic layer was dried over Na_2SO_4 and concentrated in vacuo. The crude material was purified by flash column chromatography on silica gel (eluent: dichloromethane/methanol 96:4) to afford 0.130 g (yield = 38 %) of compound **23** as a pale orange solid.

Rf: 0.29 dichloromethane/methanol 92/8

ESI-MS: calculated m/z: 2418 $[M+H]^+$; found 2418 $[M+H]^+$;

^{1}H-NMR Spectra (D_2O, 600 MHz):

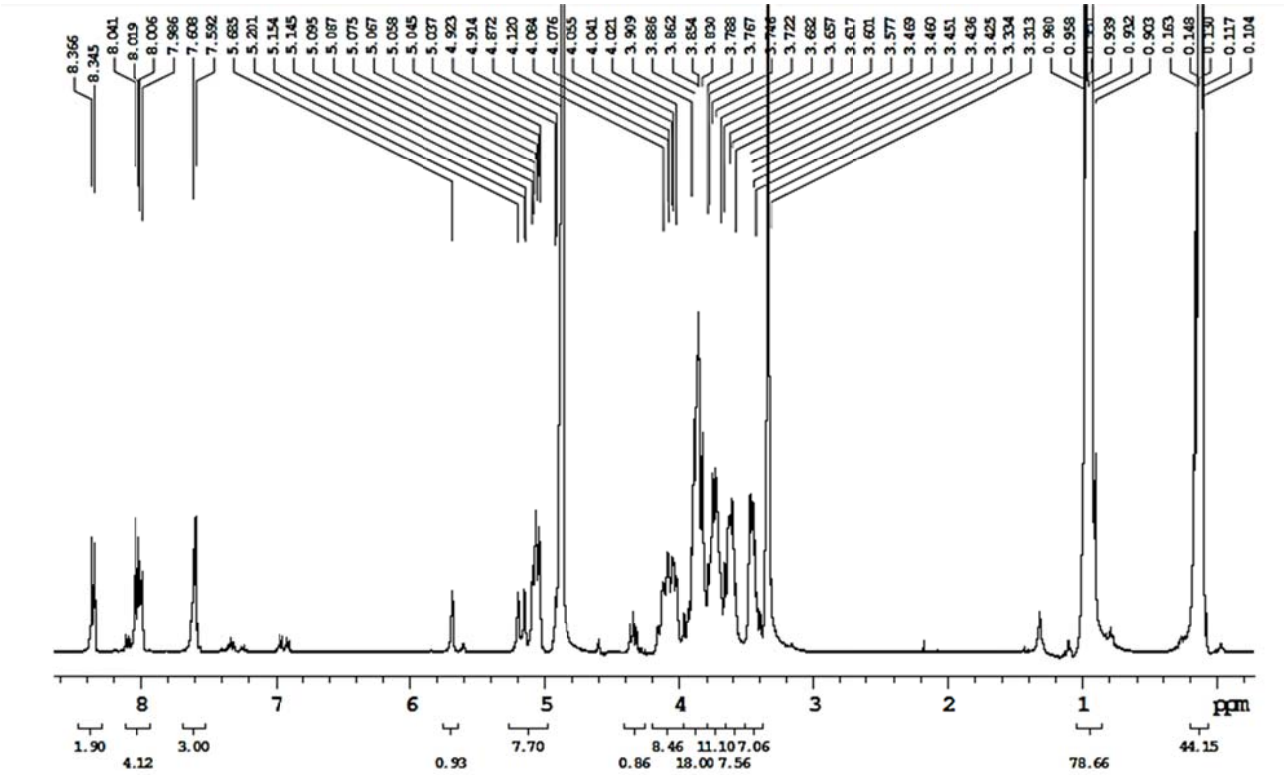

Eptakis(6-*O*-*tert*-butyldimethylsilyl)-γ-CD (24)

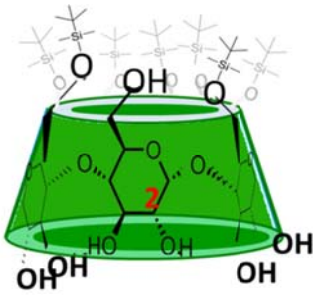

24 **24**

To dried **γ** -cyclodextrin (1 eq, 3.0 g, 2.3 mmol) in dry DMF/Pyridine (ratio 7.5/4, 34 mL) was added, at 0 °C, tert-butyldimethylsilyl chloride (7 eq, 2.4 g, 16 mmol.). After stirring for 3 days at room temperature, the reaction mixture was poured into ice/water (350 mL) and stirred for 15 min. The resulting white precipitate was filtered off, washed with ice-cold water, and dissolved in Et_2O (70 mL). The solution was washed with a 5 % aqueous HCl solution (3 x 50 mL), a saturated aqueous $NaHCO_3$ solution (50 mL), and saturated brine (50 mL). Finally, the solution was dried over anhydrous Na_2SO_4, filtered, and concentrated. The crude product was purified by flash

chromatography using Et_2O/EtOH/H_2O (10/0.9/0.3) to afford 1.2 g of silylated cyclodextrin **24** (yield 24.8 %) as a white solid.

Rf : 0.33 dichloromethane/ Methanol, 92:8

ESI-MS: calculated m/z: 2096 $[M+H]^+$; found 2096 $[M+H]^+$

^{1}H-NMR Spectra ($CDCl_3$, 600 MHz):

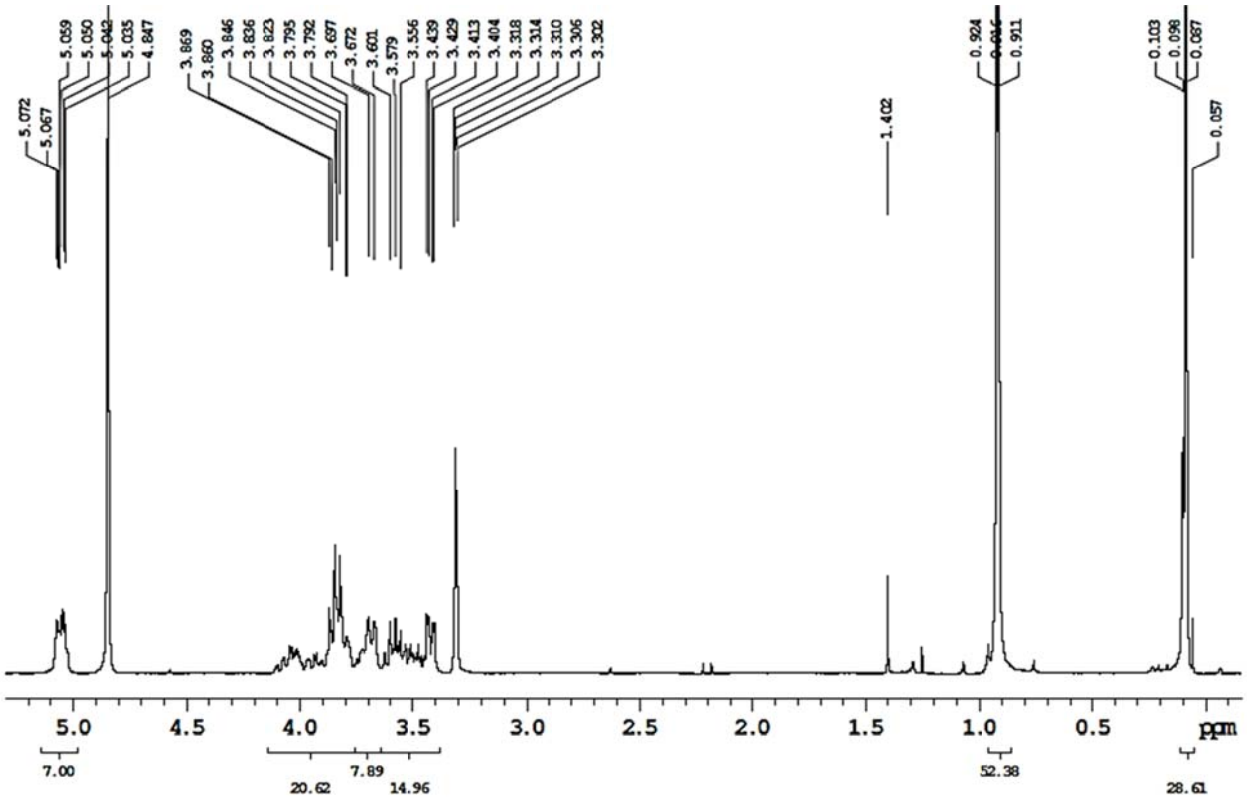

2,6-*O*-di[octakis(6-*O*-*tert*-butyldimethylsilyl)-γ-CD]-4'-phenylazobenzoate (25)

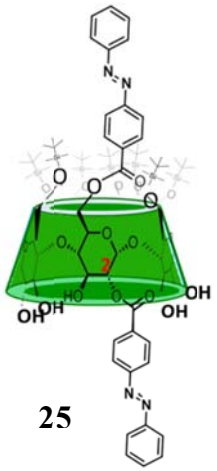

25

2,4,6-Triisopropylbenzenesulfonyl chloride (2.4 eq, 104 mg, 0.34 mmol) was added to a solution of 4-(phenylazo)benzoic acid **2** (2.4 eq, 77 mg, 0.34 mmol) in anhydrous THF (10 mL) and redistilled triethylamine (5.5 eq, 107 μL) at 0 °C. The resulting solution was stirred for two hours then allowed to reach room temperature and stirred for additional 20 minutes. Silylated cyclodextrin **24** (0.3 g, 0.14 mmol, dried over P_2O_5 under vacuum for 2 h at 55 °C) and a catalytic amount of DMAP were then added and the mixture was stirred under argon overnight. After evaporation of the solvent in vacuo, chloroform (40 mL) was added and the organic layer was washed with water (3 x 20 mL) and 5 % $NaHCO_3$ solution (3 x 20 mL). The organic layer was dried over Na_2SO_4 and concentrated in vacuo. The crude material was partially purified by flash column chromatography on silica gel (eluent: dichloromethane/methanol 96:4) to afford 0.08 g (y= 23 %) of compound **25** as a pale orange solid.

ESI-MS: calculated m/z: 2513 $[M+H]^+$; found 2514 $[M+H]^+$.

2-*O*-mono-γ-CD-4'-phenylazobenzoate (26)

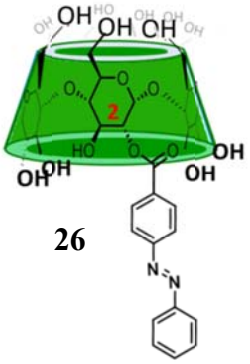

26

To TBDMS-protected cyclodextrin **23**, dissolved in MeOH (1 mL) was added trifluoroacetic acid (1.2 mL). The solution was stirred at room temperature for 1 h, monitoring the desilylation process by ESI. The solvent was removed in vacuo. Methanol was added and evaporated in vacuo for azeotropic removal of any residual trifluoroacetic acid. The residue was dissolved in water and washed three times with Et_2O. After freeze-drying, compound **26** was obtained as a pale orange solid in 100 % yield.

ESI-MS: calculated m/z: 1504.49 $[M+H]^+$; found 1505 $[M+H]^+$

^{1}H-NMR Spectra (D_2O, 600 MHz):

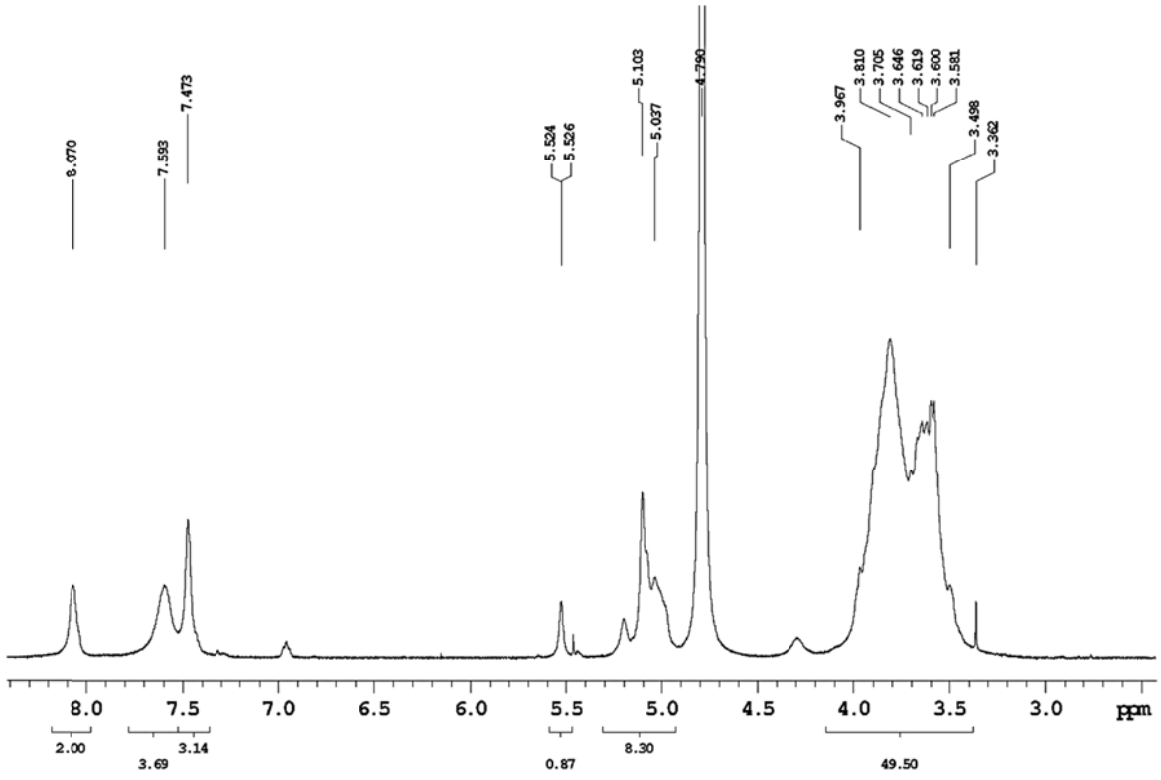

2,6-*O*-di-γ-CD-4'-phenylazobenzoate (27)

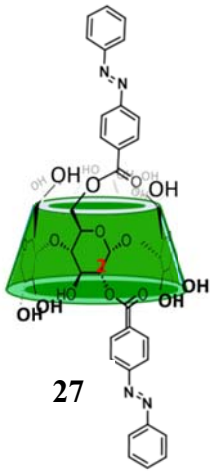

27

To TBDMS-protected cyclodextrin **25**, dissolved in MeOH (1 mL), was added trifluoroacetic acid (1.2 mL). The solution was stirred at room temperature for 1 h, monitoring the desilylation process by ESI. The solvent was removed in vacuo. Methanol was added and evaporated in vacuo for azeotropic removal of any residual trifluoroacetic acid. The residue was dissolved in water and washed three times with Et_2O. After freeze-drying, compound **27** was obtained as a pale orange solid in 100 % yield.

ESI-MS: calculated m/z: 1712.55 $[M+H]^+$; found 1713 $[M+H]^+$

^{1}H-NMR Spectra (D_2O, 600 MHz):

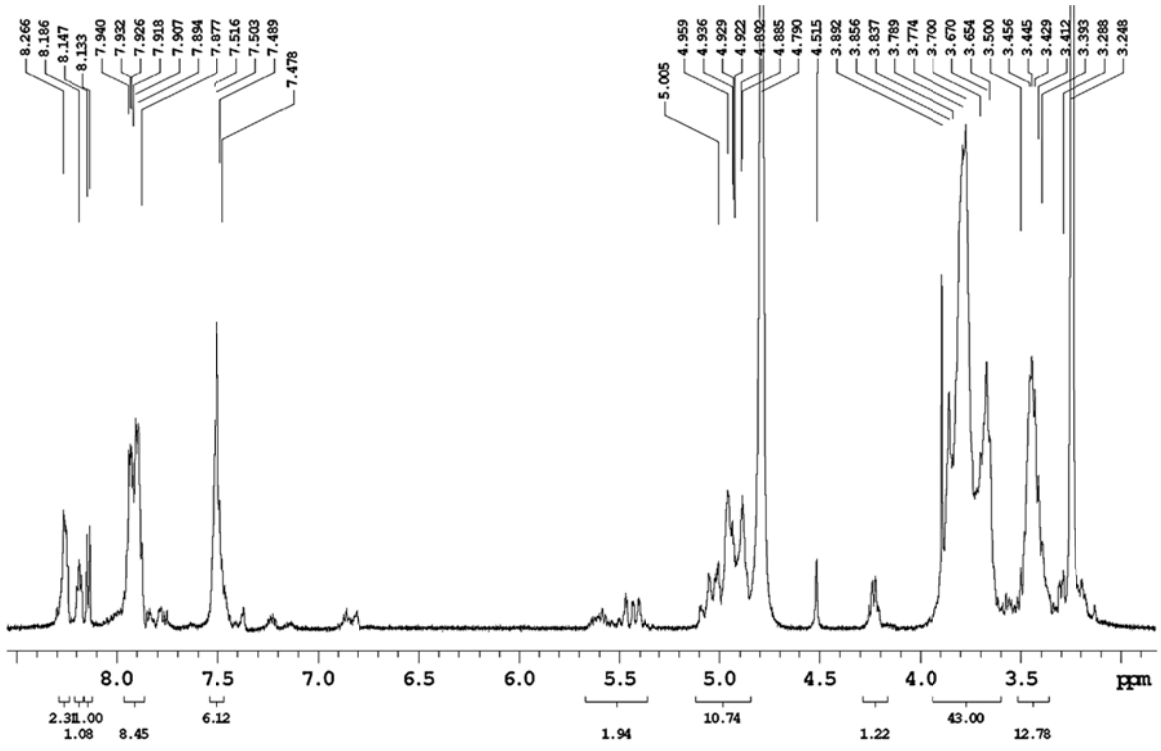

5 Azobenzene guanosine

2'-3'-Isopropylideneguanosine (28)

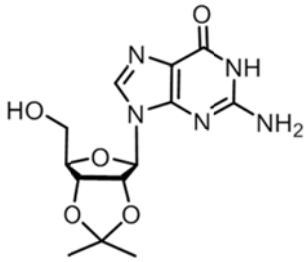

28

To a suspension of guanosine (1 g, 3.53 mmol) in 60 mL of acetone was added 70 % perchloric acid (0.41 mL, 4.75 mmol). After 70 minutes, concentrated ammonium hydroxide (0.67 mL, 4.98 mmol) was added to the reaction mixture and cooled down with ice-water bath. Water (60 mL) was added and the solution was concentrated under reduce pressure until the formation of a white precipitate. The solid was then filtered out and dried over vacuum to afford 0.95 g (y = 83.2 %).

Rf: 0.28 dichloromethane/ Methanol, 9:1.

ESI-MS: calculated m/z: 324.32 $[M+H]^+$; found 321.9 $[M-H]^-$, 346 $[M+Na]^+$;

^{1}H-NMR Spectra (DMSO, 600 MHz):

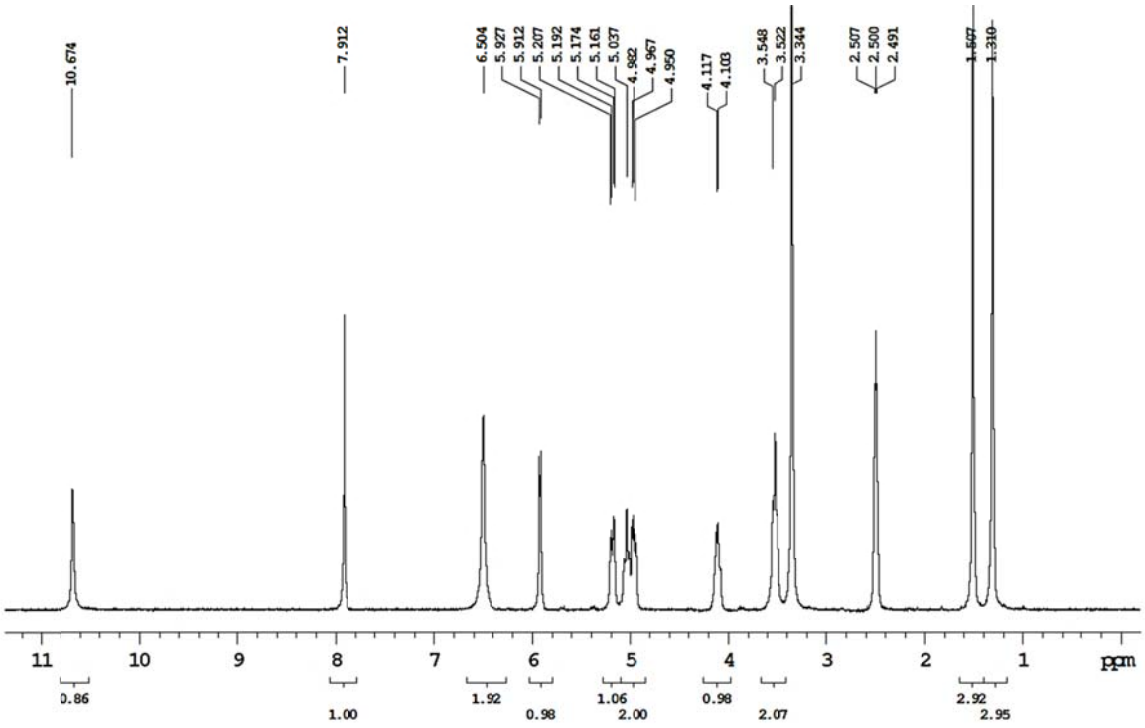

^{13}C-NMR Spectra (DMSO, 600 MHz):

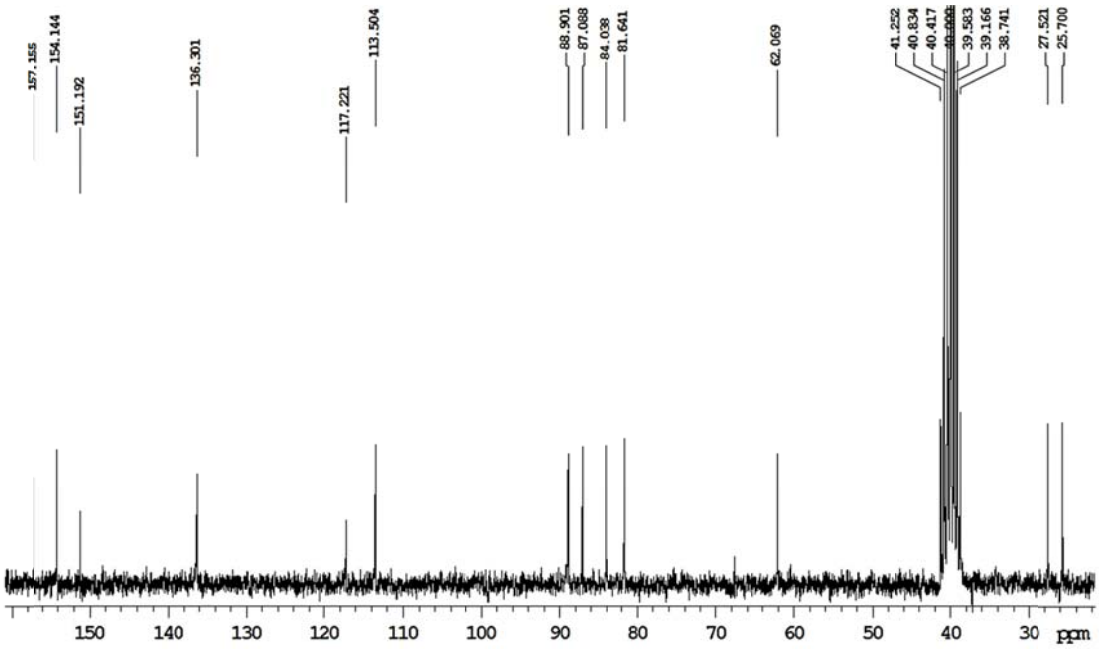

5'-O-(E)-carboxy-azobenzene-2'-3'-O-Isopropylideneguanosine (29)

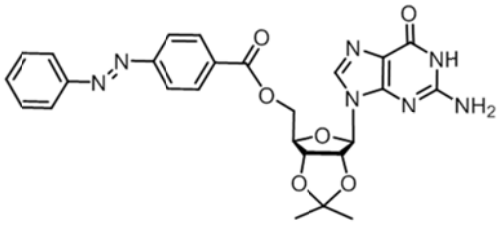

29

N,N'-Dicyclohexylcarbodiimide, (2.4 eq, 0.527 g, 2.4 mmol) was added to a solution (E)-4-(phenyldiazenyl)benzoic acid **2**, (1.2 eq, 0.278 g, 1.23 mmol) in dry DMF, 10 mL, under nitrogen. After stirring the mixture for 30 minutes at room temperature, 2'-3'-O-Isopropylideneguanosine, (0.328 g, 1.0 mmol) and 1 eq of DMAP as catalyst (0.123 g, 1.0 mmol) were added. All reagents were previously vacum dried over P_2O_5 at 50 °C for 12 hours. Then, after evaporating the solvent, the crude was dissolved in CH_2Cl_2 and extracted with water . The organic layer was dried over $MgSO_4$, filtered and concentrated; the crude product was purified through chromatography on silica gel (dichloromethane/ methanol, 96:4) to afford 0.323 g (0.61 mmol) of 5'-O-(E)-carboxy-azobenzene-2'-3'-O-Isopropylideneguanosine as an orange solid (yield = 61%).

Rf: 0.24 dichloromethane/methanol, 96:4.

ESI-MS: calculated m/z: 531.19 $[M+H]^+$; found 531.2 $[M+H]^+$;

^{1}H-NMR Spectra (DMSO, 600 MHz):

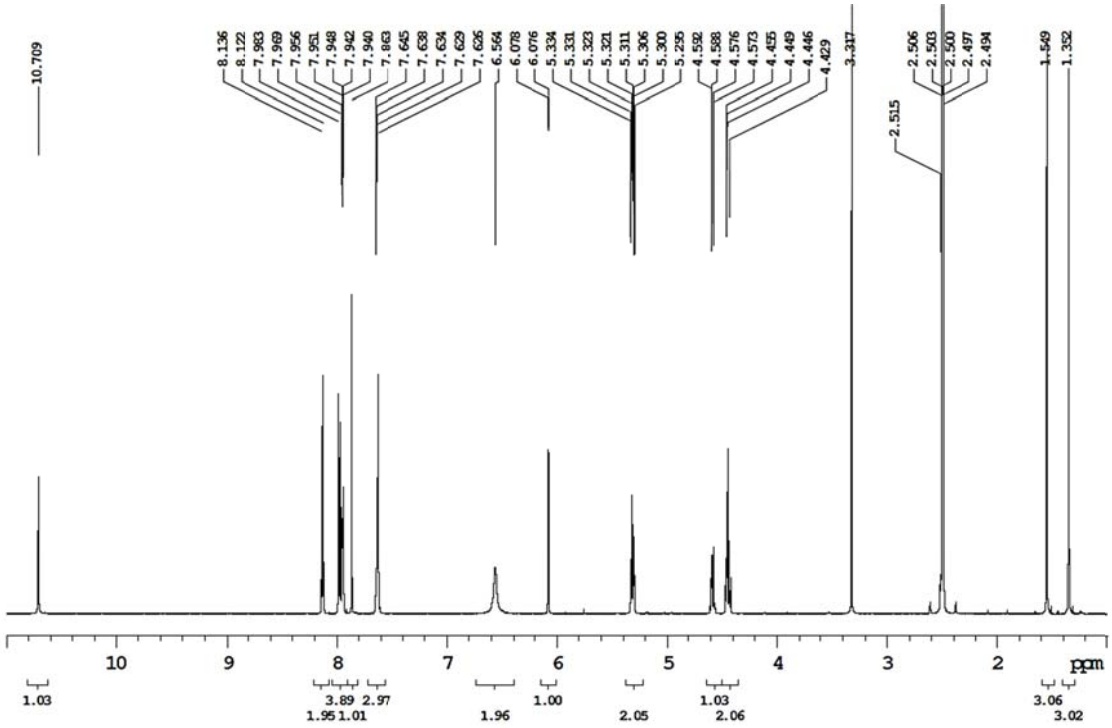

^{13}C-NMR Spectra (DMSO, 600 MHz):

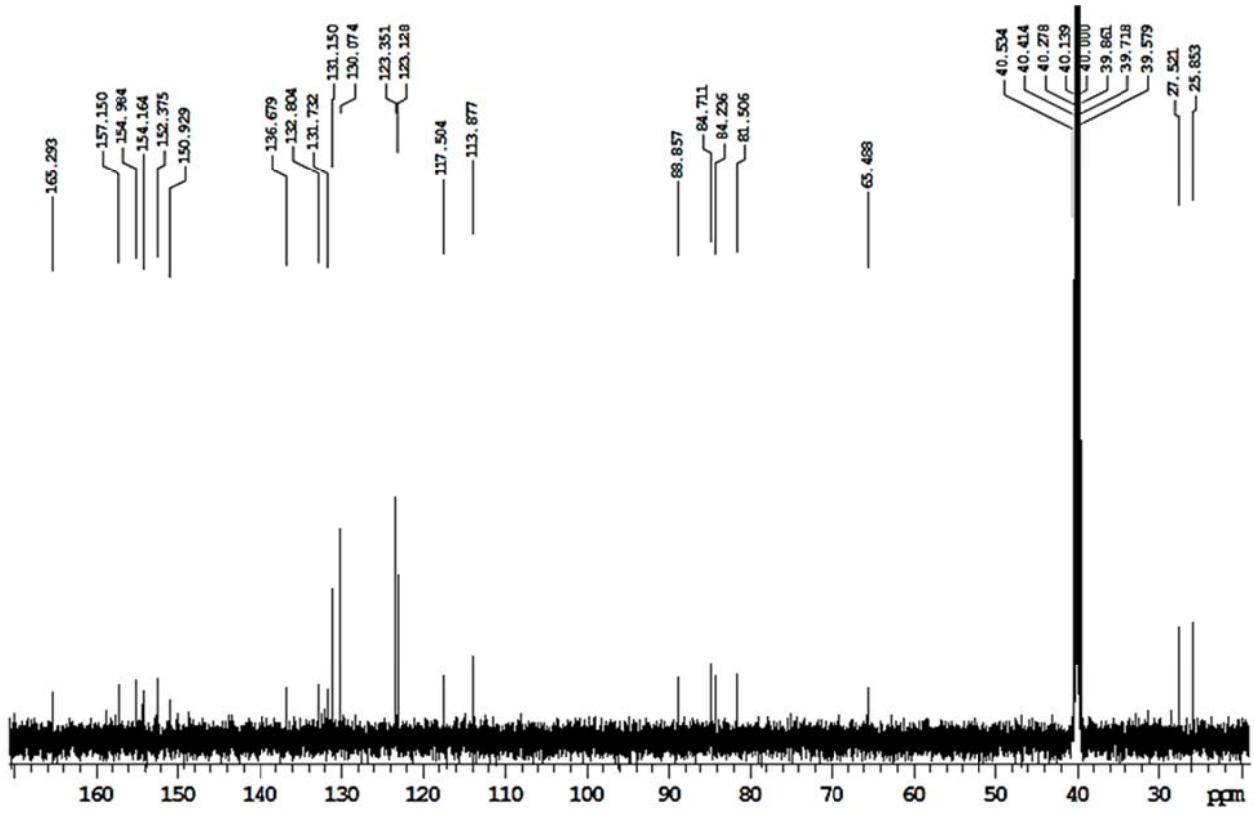

5'-O-(E)-4-(tert butoxycarbonyl)-carboxy-azobenzene-2'-3'-O-isopropylideneguanosine (30)

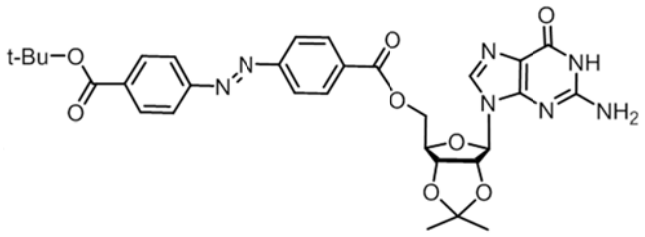

30

To a suspension of (E)-4-(tert-butoxycarbonyl)phenyl)diazenyl benzoic acid **3**, (1.2 eq, 0.503 g, 1.5 mmol) in dry DMF, 10 mL, under nitrogen, was added *N,N'*-Dicyclohexylcarbodiimide, (2.4 eq, 0.639 g, 3.1 mmol). After stirring the mixture for 30 minutes at room temperature, 2'-3'-O-Isopropylideneguanosine, (0.417 g, 1.3 mmol) and 1 eq of DMAP as catalyst (0.160 g, 1.3 mmol) were added. All reagents were previously vacuum dried over P_2O_5 at 50 °C for 4 hours. The reaction was carried out for 42 hours, and monitored by TLC (dichloromethane/methanol, 9:1). Then, after evaporating the solvent, the crude product was dissolved in CH_2Cl_2 and extracted with a saturated aqueous $NaHCO_3$ solution. The organic layer was dried over $MgSO_4$, filtered and concentrated; the crude product was purified through chromatography on silica gel (dichloromethane/methanol 9:1) to afford 0.349 g (0.55 mmol) of 5'-O-(E)-4-(tert butoxycarbonyl)-carboxy-azobenzene-2'-3'-O-Isopropylideneguanosine as an orange solid (yield = 42.8%).

Rf: 0.55 dichloromethane/methanol, 9:1.

ESI-MS: calculated m/z: 631.65 $[M+H]^+$; found 630 $[M-H]^-$; 632.1 $[M+H]^+$; 654 $[M+Na]^+$;

^{1}H-NMR Spectra (DMSO, 600 MHz):

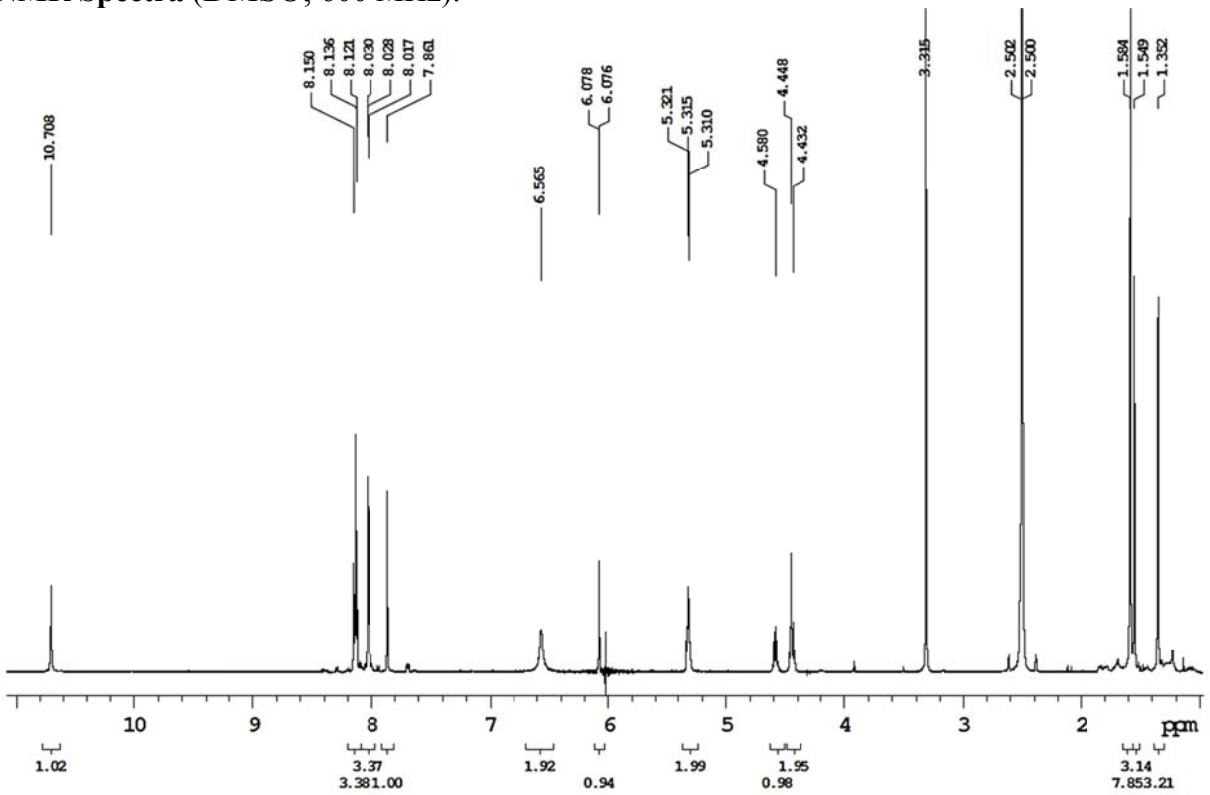

^{13}C-NMR Spectra (DMSO, 600 MHz)

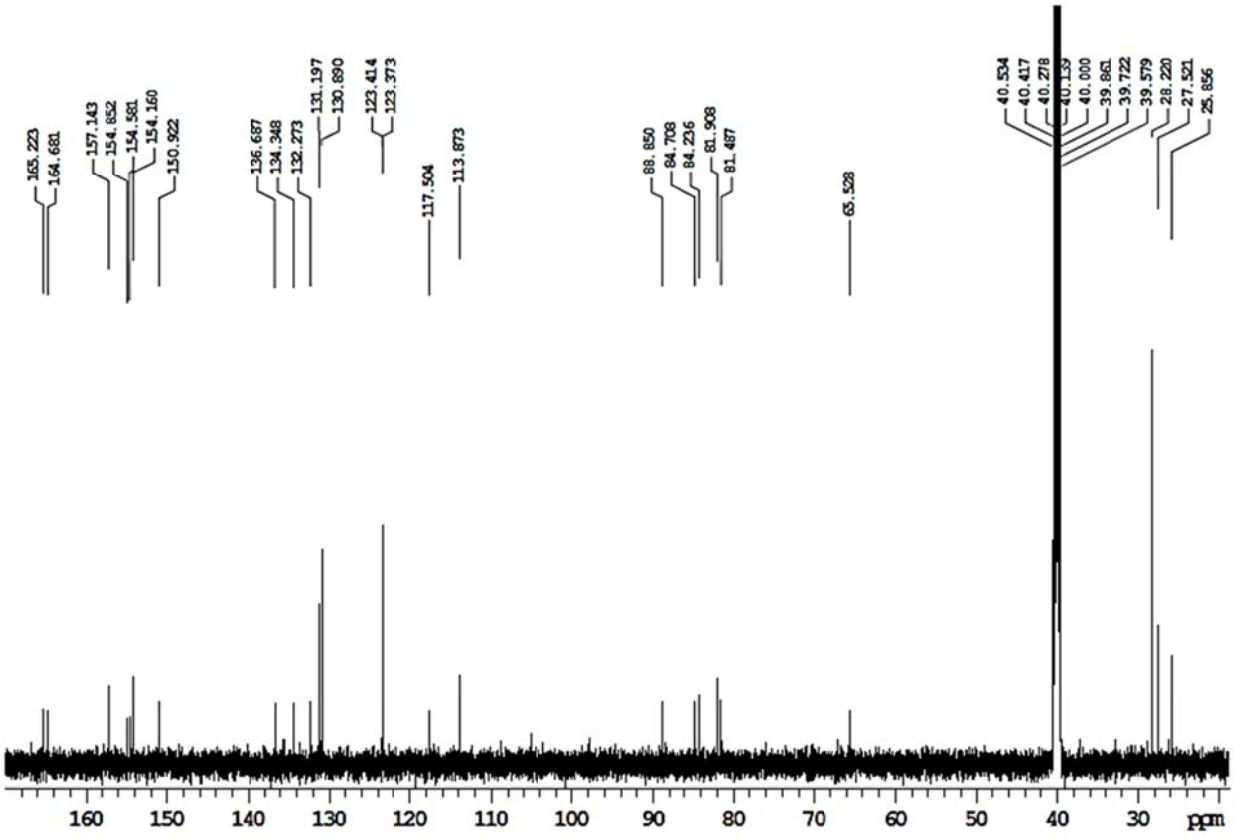

2'-3'- O-12-tricosildeneguanosine (31)

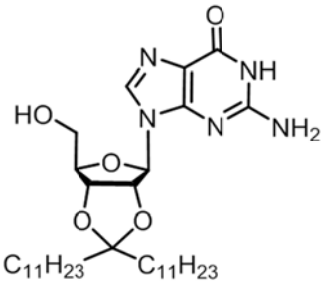

31

To a solution of guanosine (0.506 g, 1.79 mmol) in dry dioxane (15 mL) under nitrogen was added in this order tricosan-12-one (2.16 eq, 1.311 g, 3.87 mmol), trimethyl orthoformate (2.9 eq, 5.6 mg, 0.576 mL) and p-toulensulfonic acid (1.3 eq, 0.406 g, 2.36 mmol). All reagents were previously vacuum dried over P_2O_5 at 50 °C for 4 hours. The reaction was carried out at room temperature for 5 hours and in order to improve the solubility the suspension was sonicated every 15 minutes for 3 hours. The mixture was quenched by addition of a saturated aqueous $NaHCO_3$ solution and extracted with dichloromethane (5 x 20 mL). Finally, the solution was dried over anhydrous Na_2SO_4, filtered, and concentrated. The crude product was purified by chromatography on silica gel using dichloromethane/ methanol to afford 0.757 g (1.235 mmol) of 2'-3'-tricosildeneguanosine (yield = 70%).

Rf: 0.35 Dichloromethane/Methanol, 92:8

ESI-MS: calculated m/z: 604.8 $[M+H]^+$; found 602.2 $[M-H]^-$, 626.3 $[M+Na]^+$;

^{1}H-NMR Spectra (DMSO, 600 MHz):

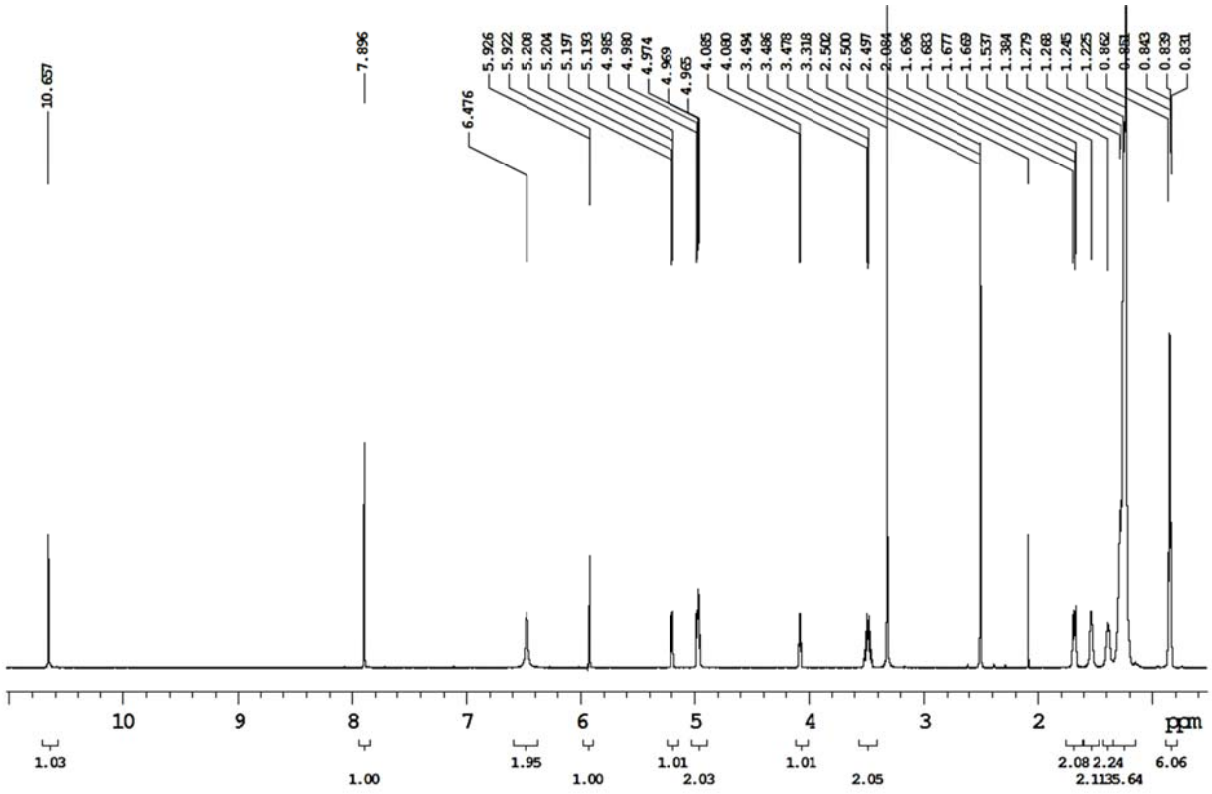

5'-O-(E)-4-(phenyldiazenyl)benzoate-2'-3'-O-12-tricosildeneguanosine (32)

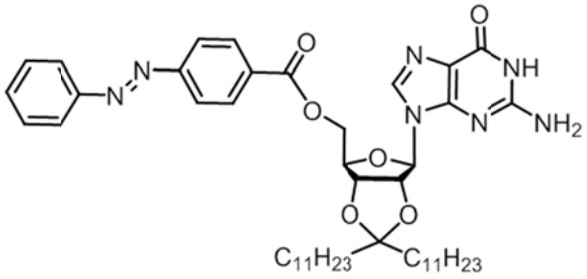

32

To a suspension of (E)-4-(phenyldiazenyl)benzoic acid **2**, (1.2 eq, 0.097 g, 0.43 mmol) in dry DMF, 10 mL, under nitrogen, *N,N'*-Dicyclohexylcarbodiimide, (2.4 eq, 0.172 g, 0.83 mmol) was added. After stirring the mixture for 30 minutes at room temperature, 2'-3'-O-12-tricosildeneguanosine, (0.200 g, 0.33 mmol), and 1 eq of DMAP as catalyst (0.049 g, 0.39 mmol) were added. All the reagents were previously vacuum dried over P_2O_5 at 50 °C for 4 hours. The reaction was carried out for 2 days, monitoring the disappearance of the acid by TLC (dichloromethane/ methanol 97:3). Then, after evaporating the solvent, the crude was solubilized in $CHCl_3$ and a gel was formed. The

gel was further diluted and washed with a diluted solution of aqueous HCl (pH around 5/6), to remove any remaining of DCC. The organic layer was dried over $MgSO_4$, filtered and concentrated; the crude product was purified through chromatography on silica gel (dichloromethane/methanol 9:1) to afford 0.082 g (0.1 mmol) of 5'-O-(E)-carboxy-azobenzene-2'-3'-O-12-tricosildeneguanosineas an orange solid (yield = 23.5%).

Rf: 0.53 dichloromethane/ Methanol, 9:1.

ESI-MS: calculated m/z: 811.50 $[M+H]^+$; found 812.5 $[M+H]^+$; 835.1 $[M+Na]^+$; 849.9 $[M+K]^+$;

^{1}H-NMR Spectra (DMSO, 600 MHz):

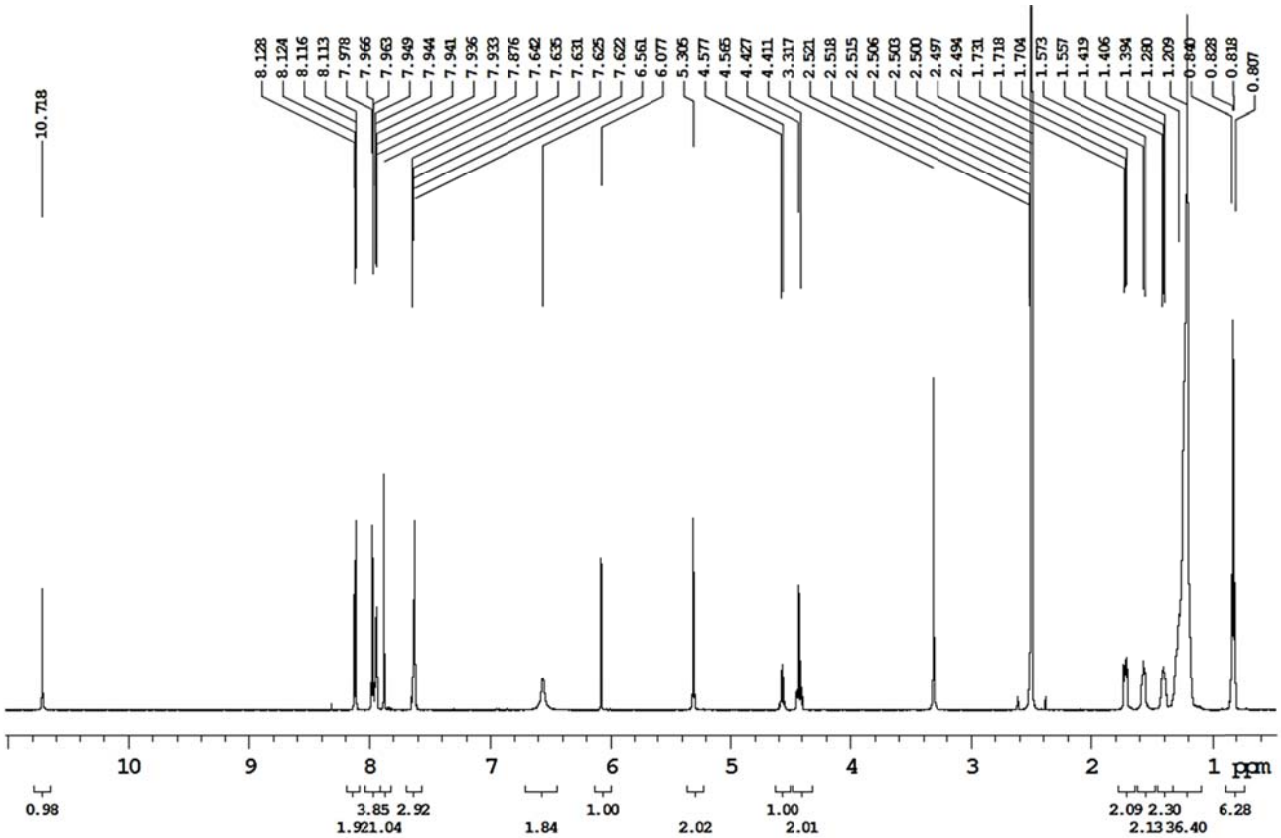

3'-5'-di-(E)- 4-(phenyldiazenyl)benzoate-2'-deoxyguanosine (33)

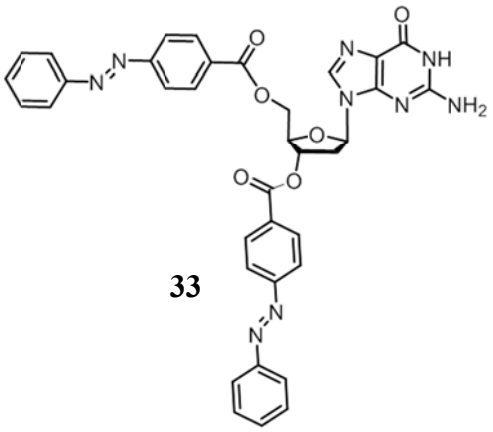

33

N,N'-Dicyclohexylcarbodiimide, (4 eq, 0.851 g, 3.9 mmol) was added to a solution (E)-4-(phenyldiazenyl)benzoic acid **2**, (2.4 eq, 0.571 g, 2.5 mmol) in dry DMF, 10 mL, under nitrogen. After stirring the mixture for 30 minutes at room temperature, deoxyguanosine, (0.303 g, 1.05 mmol) and 1 eq of DMAP as catalyst (0.123 g, 1.0 mmol) were added. All reagents were previously vacuum dried over P_2O_5 at 50 °C for 12 hours. After one day an orange precipitate was formed and the reaction was carried out for 2 days until disappearance of deoxyguanosine. Then, after distillation of the solvent, the crude was diluted with water and extracted with CH_2Cl_2. The organic layer was dried over $MgSO_4$, filtered and concentrated; the crude product was purified through chromatography on silica gel (dichloromethane/methanol, 96:4) to afford 0.323 g (0.61 mmol) of product as an orange solid (yield = 61%).

Rf: 0.48 dichloromethane/methanol, 96:4.

ESI-MS: calculated m/z: 683.68 $[M+H]^+$; found 706.7 $[M+Na]^+$.

^{1}H-NMR Spectra (DMSO, 600 MHz):

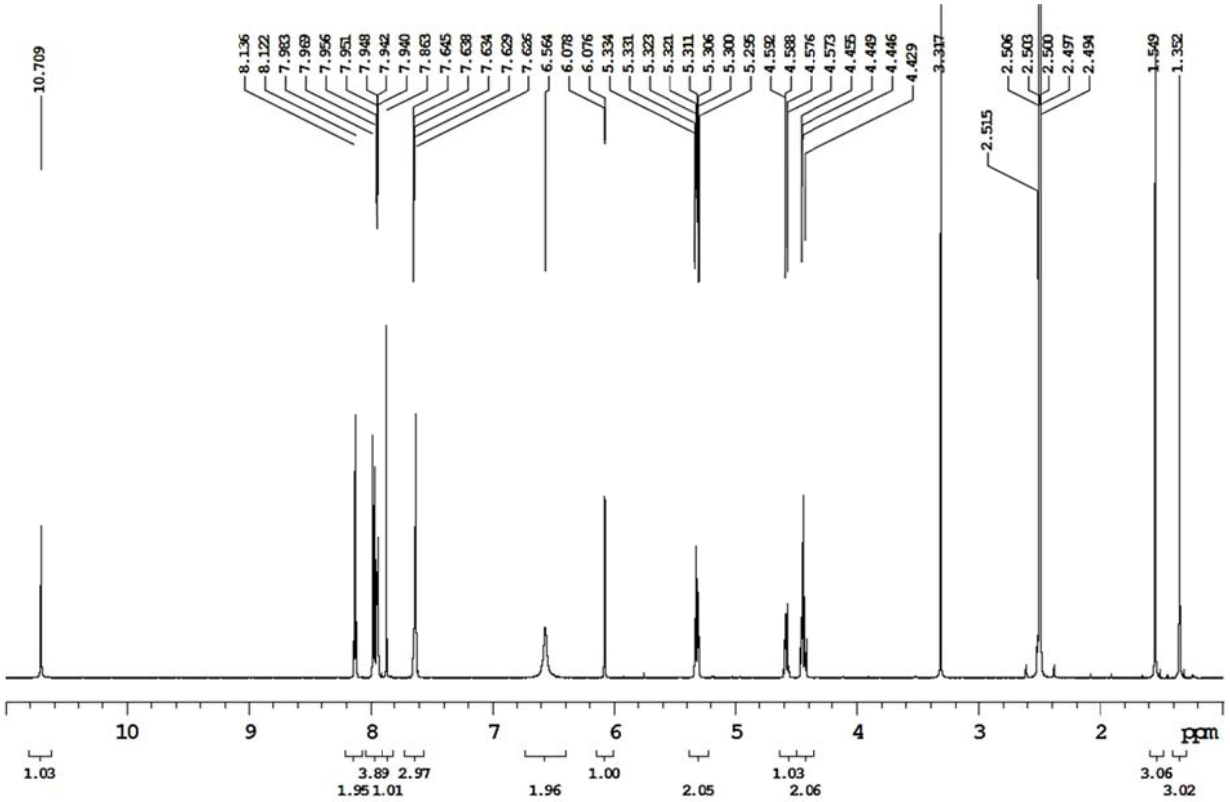

2'-3'-5'-O-tri-(E)-4-(tert butoxycarbonyl)-1-carboxy-azobenzeneguanosine (34)

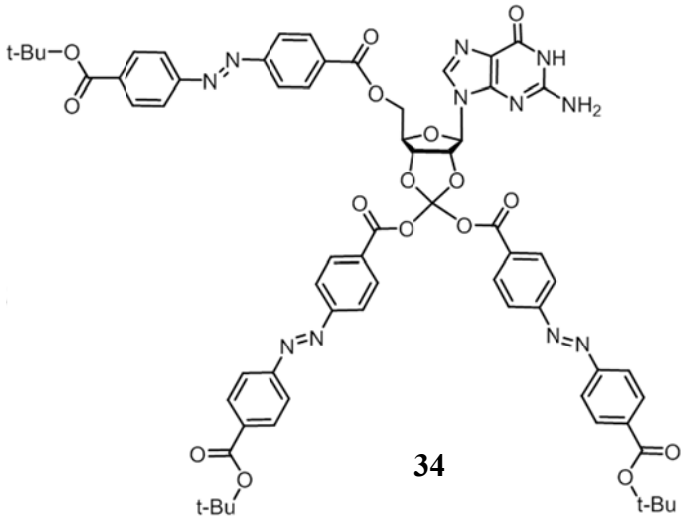

34

In ice bath, redistilled EtN_3, (7eq, 0.278 mL, 2 mmol) and $MeSO_2Cl$, (3.6 eq, 0.088 mL, 1.08 mmol) were added in this order to a solution of (E)-4-(phenyldiazenyl)benzoic acid **3**, (3.6 eq, 0.351

g, 1.08 mmol) in dry THF, 7 mL, under nitrogen. The solution becomes turbid and in order to increase the solubility it was necessary to sonicate for at least one hour. Then ice bath was removed and guanosine, (0.085 g, 0.3 mmol) and DMAP as catalyst were added. All reagents were previously vacuum dried over P_2O_5 at 50 °C for 4 hours. The reaction was carried out for 2 days and the disappearance of the acid was monitorated by TLC, (dichloromethane/methanol 96/4). The reaction was quenched adding a saturated aqueous $NaHCO_3$ solution and extracted with dichloromethane (5 x 20 mL). Finally, the solution was dried over anhydrous Na_2SO_4, filtered, and concentrated. The crude product was purified by chromatography on silica gel using dichloromethane/ methanol, 98/2, as eluent and crystallized from MeOH to afford 0.176 g (0.146 mmol) of 2'-3'-5'-O-tri-(E)-4-(tertbutoxycarbonyl)-1-carboxy-azobenzeneguanosine as an orange solid, (yield = 48.5%).

Rf: 0.33 dichloromethane/methanol, 97:3.

ESI-MS: calculated m/z: 1208 $[M+H]^+$; found 1207.6 $[M-H]^-$, 1230.5 $[M+Na]^+$; 1249.4 $[M+K]^+$;

^{1}H-NMR Spectra (DMSO, 600 MHz):

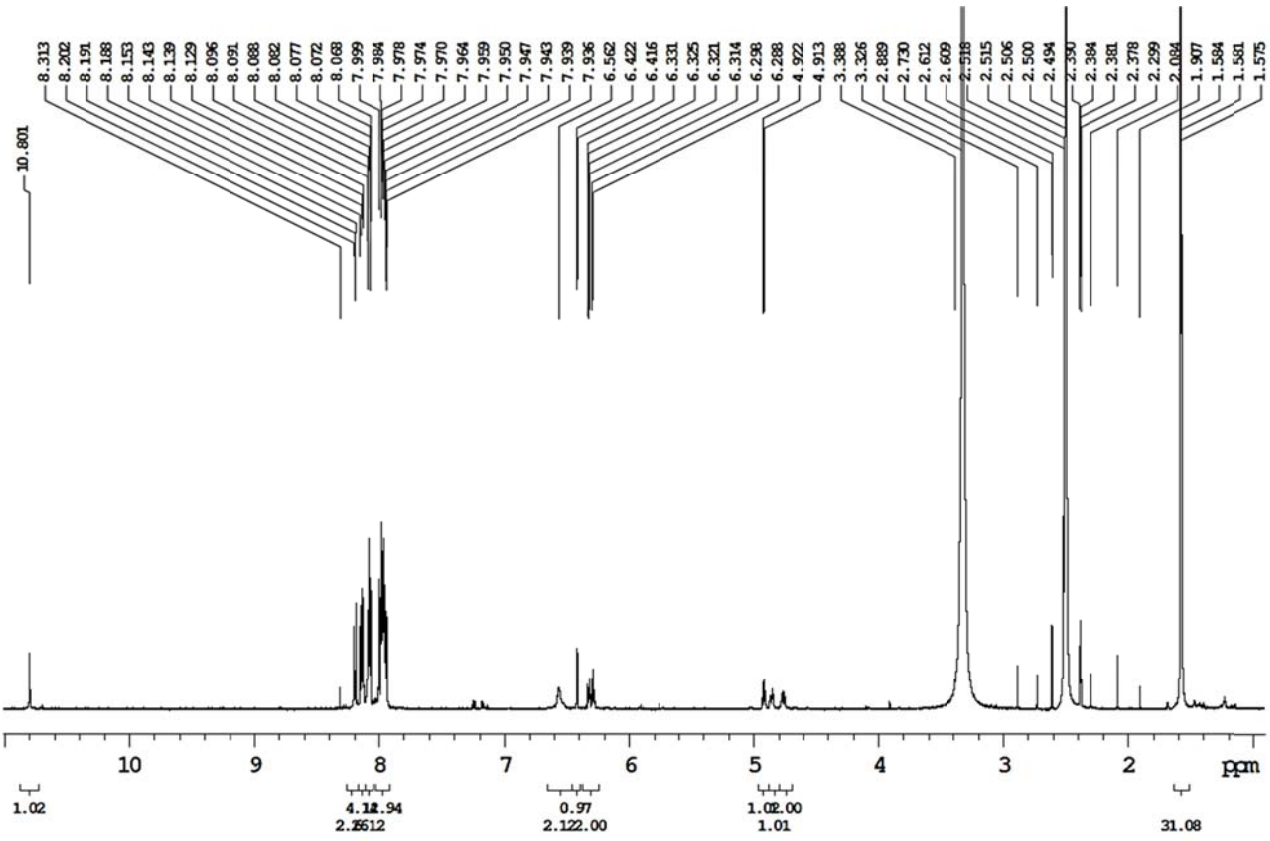

6 Oligo-azobenzene

tert-butyl-(4-aminophenyl)carbamate (35)

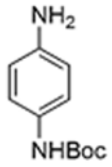

35

An aqueous solution of potassium carbonate (1.52 g, 11 mmol in 5 ml of water) was added to a solution of 1,4-diaminobenzene (3.24 g, 30 mmol) in THF (30 ml) and DMF (10 ml). To this mixture was added di-*tert*-butyl pyrocarbonate, Boc_2O (2.18 g, 10 mmol), dropwise over 0.5 h. The reaction mixture was stirred for an additional 4 h at room temperature.

The mixture was then poured into cold water (40 ml) and extracted with chloroform (3 x 50 ml). The combined organic phases were dried over $MgSO_4$ and concentrated to yield a brown residue which was subjected to flash chromatography (dichloromethane/acetone, 5:1) to afford **35** as a pale yellow solid (1.98 g, 9.5 mmol, y= 95%) (based on Boc_2O).

ESI-MS calculated m/z: 208.1; found 209.2 $[M+H]^+$; 231.1 $[M+Na]^+$.

^{1}H-NMR Spectra ($CDCl_3$, 600 MHz):

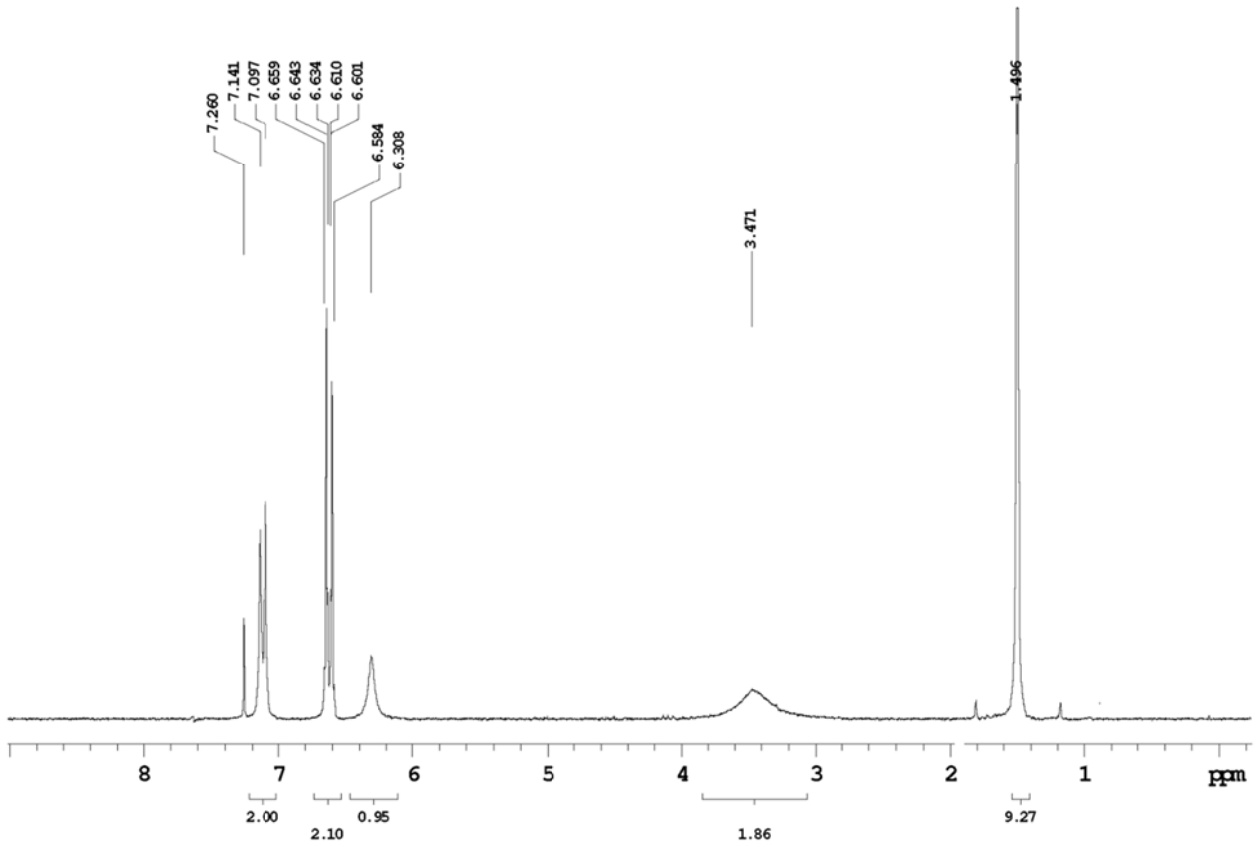

^{13}C-NMR Spectra ($CDCl_3$, 600 MHz):

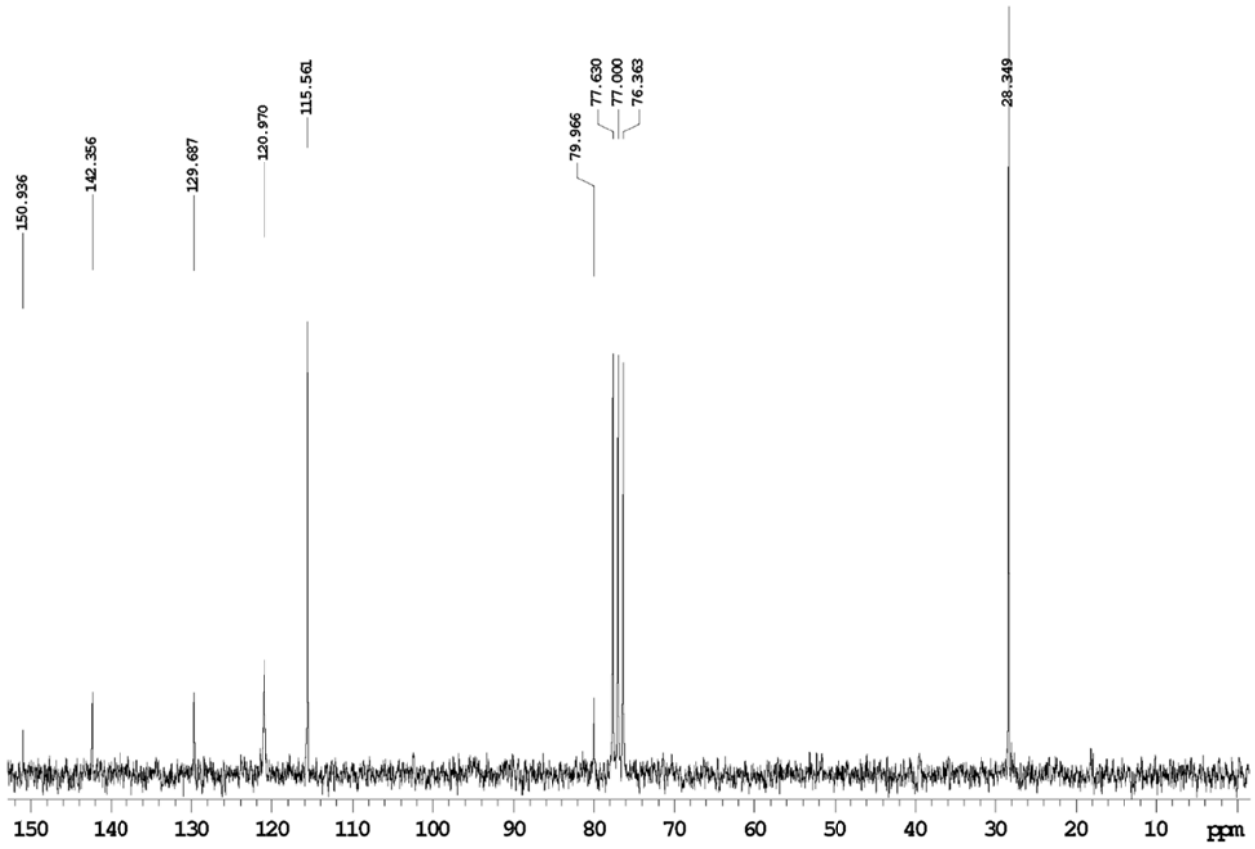

***tert*-butyl-(4-nitrosophenyl)carbamate (36)**

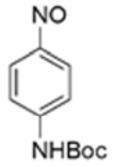

36

To a solution of **35** (1 g, 4.8 mmol) in ethyl acetate (50 mL) were added Oxone® (5.9 g, 9.6 mmol) and $NaHCO_3$ (890 mg, 10.6 mmol) dissolved in water (50 mL) and the solution was stirred under argon at room temperature. The reaction mixture was monitored by TLC and after 2 hours, no more starting material was present. After separation of the layers, the aqueous layer was extracted with ethyl acetate (2 x 25 mL) and the combined organic layers were washed with water (2x10 mL), brine (2x10 mL) and dried over $MgSO_4$. After filtration, and removal of the solvent from the filtrate in vacuo, the crude was purified by silica gel chromatography (petroleum ether/ethyl acetate 8:2),

affording **36** (770 mg, y= 72%) as a green solid.

ESI-MS calculated m/z: 222.1; found 223.2 $[M+H]^+$; 245.2 $[M+Na]^+$.

^{1}H-NMR Spectra ($CDCl_3$, 600 MHz):

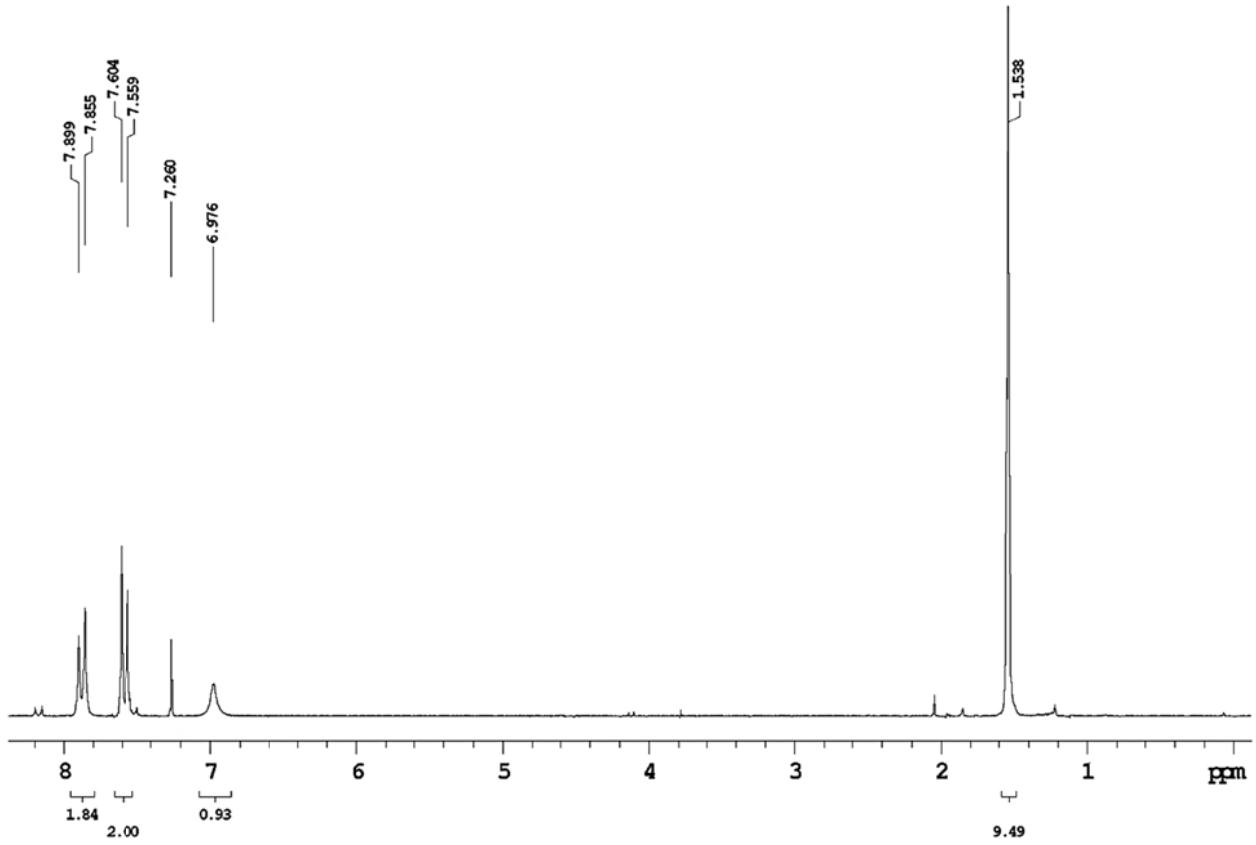

^{13}C-NMR Spectra ($CDCl_3$, 600 MHz):

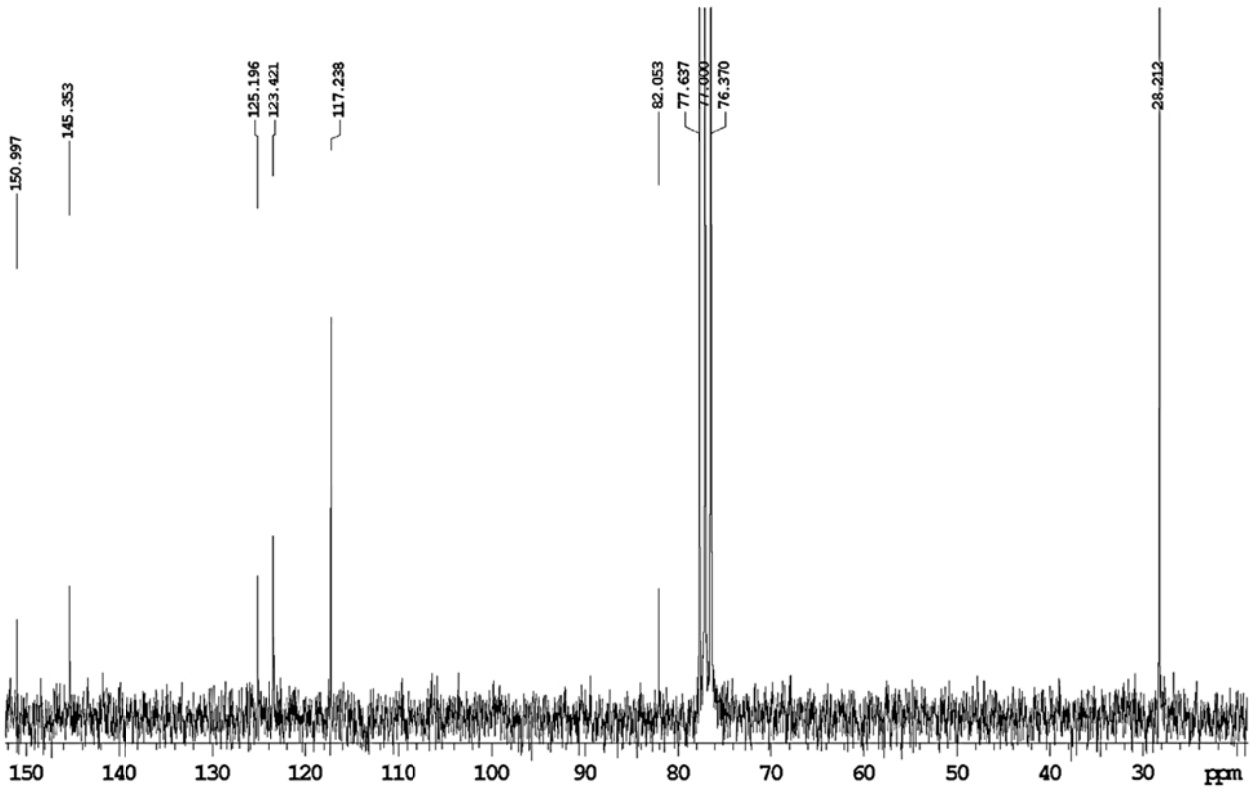

(*E*)-4-(*o*-tolyldiazenyl)aniline (37)

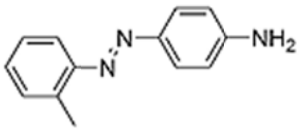

37

2-Nitrosotoluene (5 g, 41.3 mmol) and p-phenylenediamine (5.35 g, 49.6 mmol) were dissolved in ethanol (149 mL) then an aqueous buffer solution made of acetic acid (145 mmol, 8.29 mL) and sodium acetate (41.3 mmol, 3.39 g) in 16.5 mL of water was added. The stirred reaction mixture was heated to 70°C and monitored by TLC until total consumption of the nitroso reagent. A sat. $NaHCO_3$ solution (50 mL) was added and the product was extracted with ethyl acetate (3 x 50 mL). The combined organic layers were washed with water (2 x 25 mL), brine (2 x 25 mL) and dried over $MgSO_4$. After filtration and removal of the solvent from the filtrate in vacuo, the crude was purified by silica gel chromatography (petroleum ether/ethyl acetate 5:1), affording **37** (6.0 g, y= 69%) as a red oil.

ESI-MS calculated m/z: 211.1; found 212.2 $[M+H]^+$; 234.2 $[M+Na]^+$.

^{1}H-NMR Spectra ($CDCl_3$, 600 MHz):

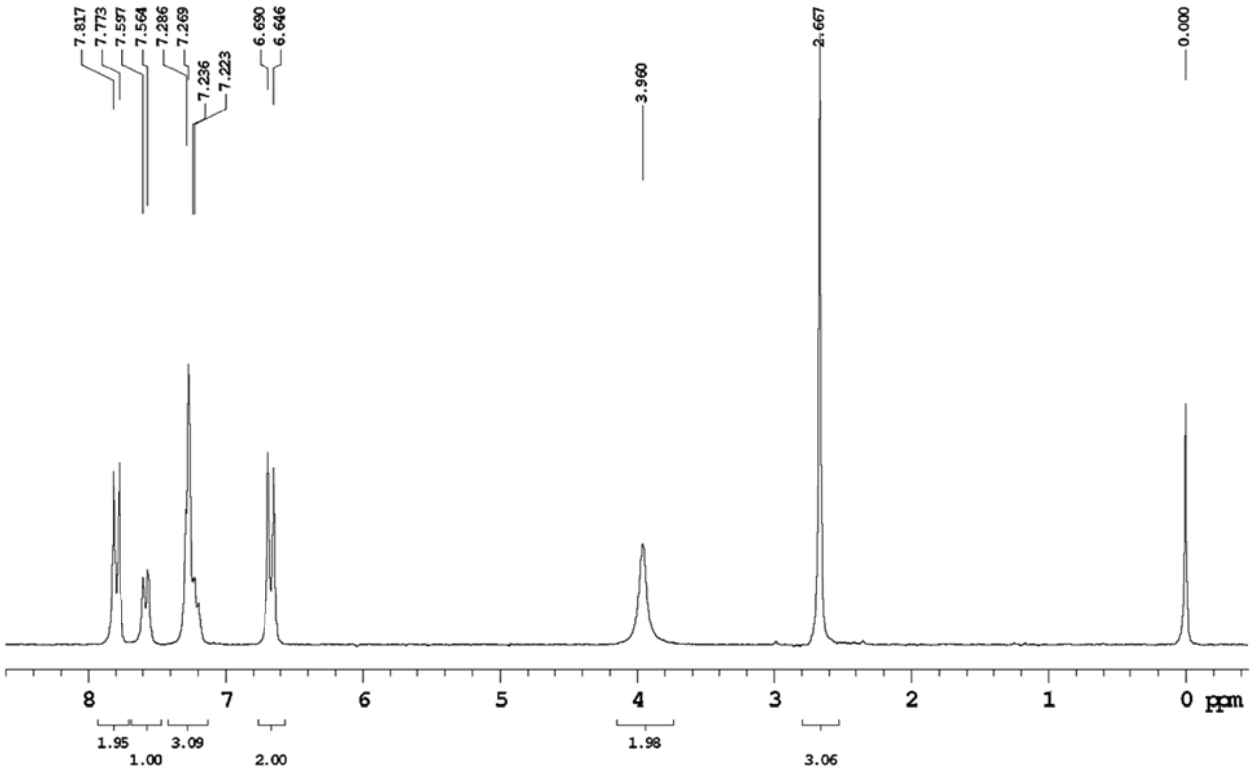

^{13}C-NMR Spectra ($CDCl_3$, 600 MHz):

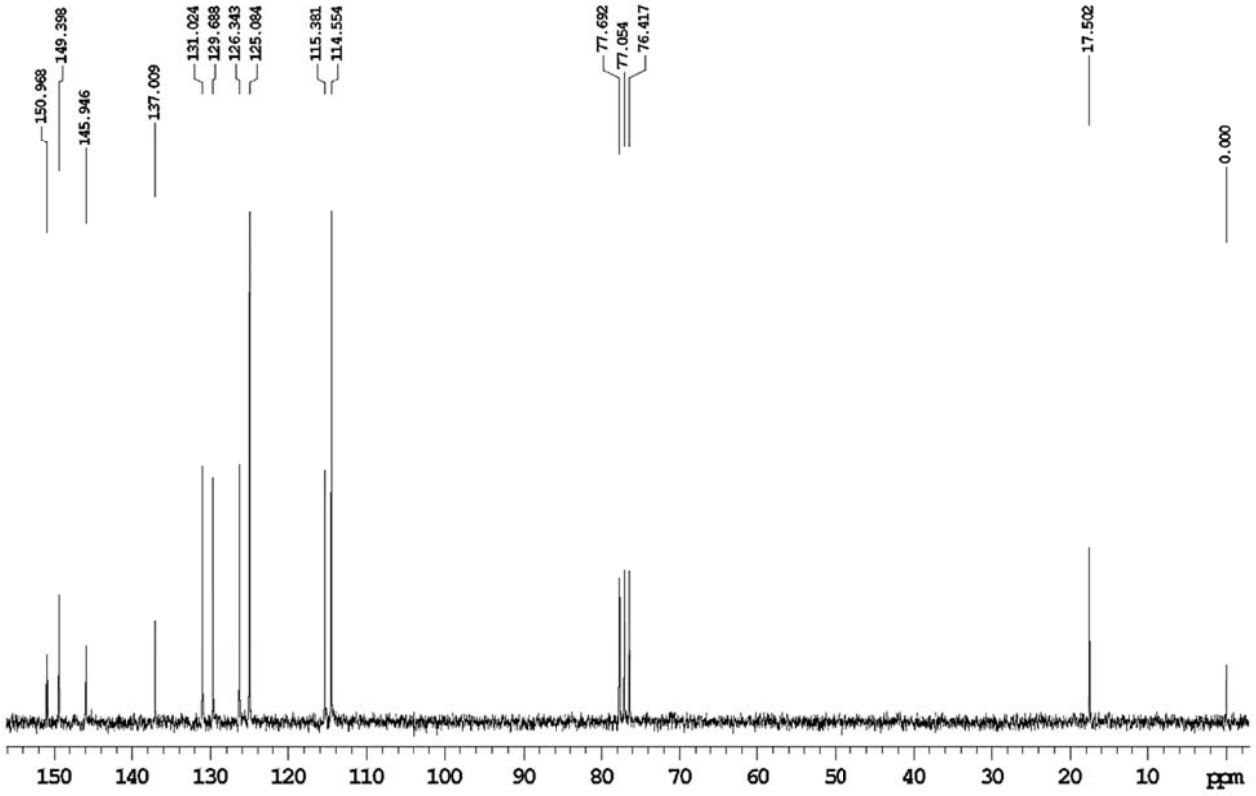

***tert*-butyl (E)-(4-((4-(*tert*-butyl)phenyl)diazenyl)phenyl)carbamate (38)**

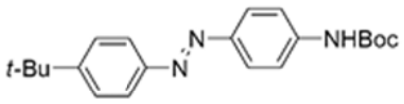

38

4- *tert*-butyl aniline (224 mg, 1.5 mmol) and **36** (333 mg, 1.5 mmol) were dissolved in ethanol (5.5 mL) and then an aqueous buffer solution made of acetic acid (5.3 mmol, 0.3 mL) and sodium acetate (1.5 mmol, 123 mg) in 0.5 mL of water was added. The stirred reaction mixture was heated to 70°C and monitored by TLC until total consumption of the nitroso starting material. A sat. $NaHCO_3$ solution (10 mL) was added and the product was extracted with ethyl acetate (3 x 10 mL). The combined organic layers were washed with water (2 x 5 mL), brine (2 x 10 mL) and dried over $MgSO_4$. After filtration and removal of the solvent from the filtrate in vacuo, the crude was purified by silica gel chromatography (petroleum ether/ethyl acetate 92:8), affording **38** (0.4 g, y= 75%) as an orange solid.

ESI-MS: calculated m/z: 353.2; found 354.2 $[M+H]^+$; 376.1 $[M+Na]^+$; 729.4 $[2M+Na]^+$.

^{1}H-NMR Spectra: ($CDCl_3$, 600 MHz)

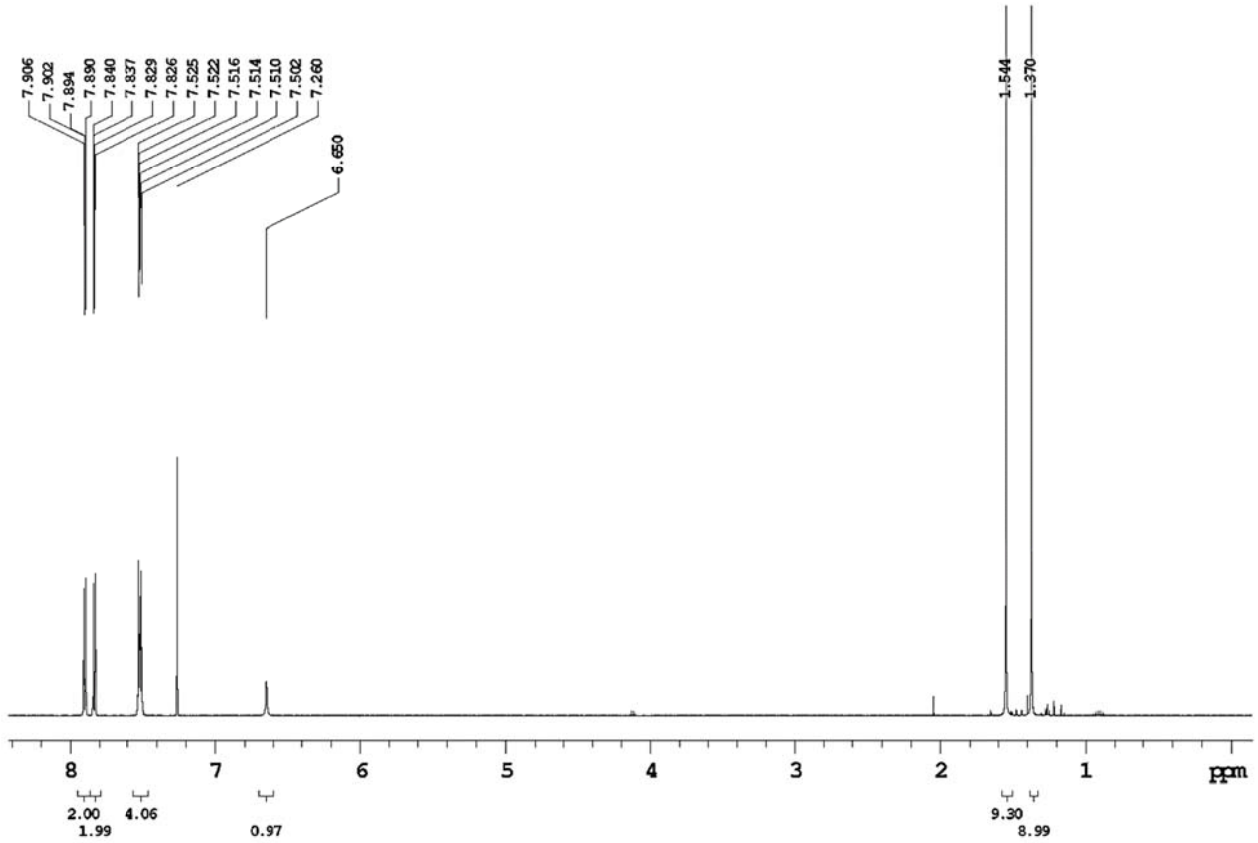

^{13}C-NMR Spectra: ($CDCl_3$, 600 MHz)

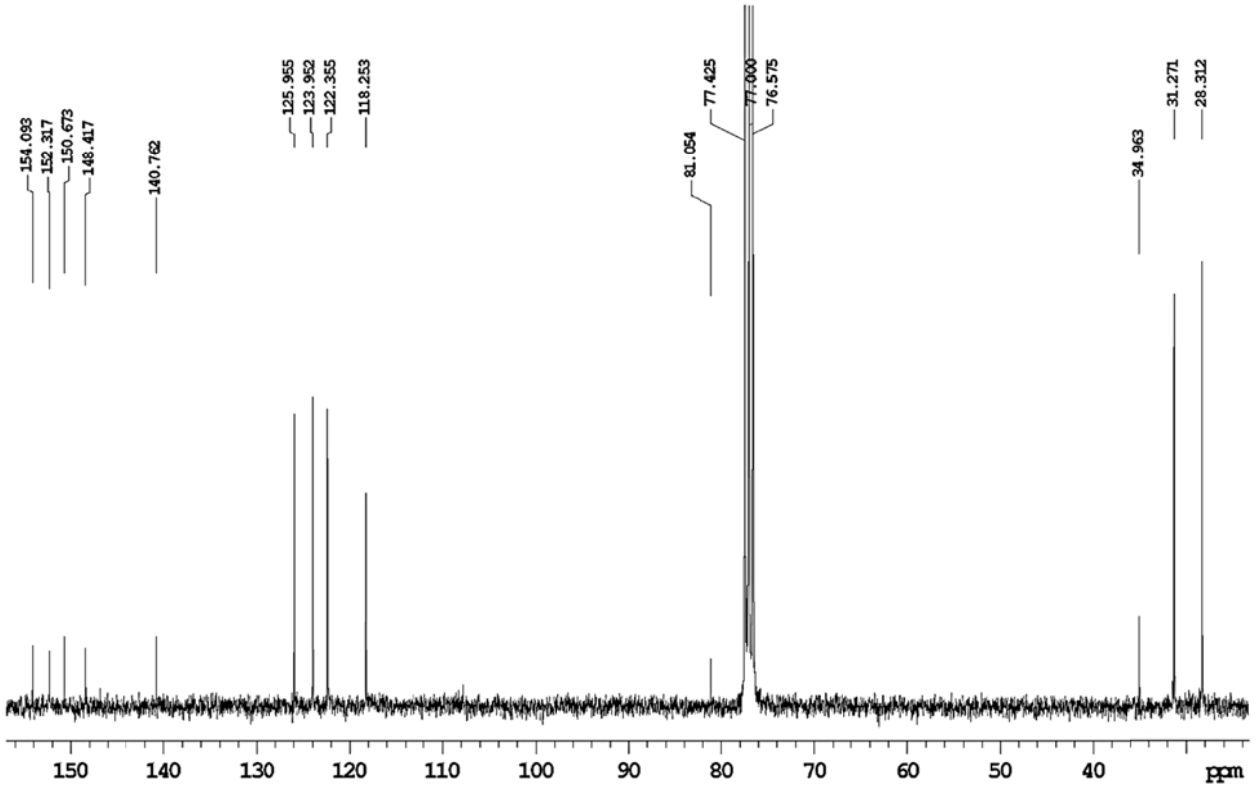

(E)-4-((4-(*tert*-butyl)phenyl)diazenyl)aniline (39)

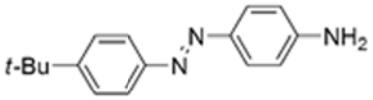

39

38 (353 mg, 1 mmol) was dissolved in a CH_2Cl_2/TFA (2:1 v/v, 6 mL) mixture and stirred at room temperature for 1 h. Diethyl ether (30 mL) was added and the organic layer was washed with water (2 x 20 mL), a sat. $NaHCO_3$ solution (2 x 20 mL), brine (2 x 20 mL) and dried over $MgSO_4$. Filtration and removal of the solvent from the filtrate in vacuo, yielded **39** as an orange solid (226 mg, y= 89%), which was used without further purification**.**

ESI-MS calculated m/z: 253.2; found 254.2 $[M+H]^+$; 276.2 $[M+Na]^+$.

^{1}H-NMR Spectra: ($CDCl_3$, 600 MHz)

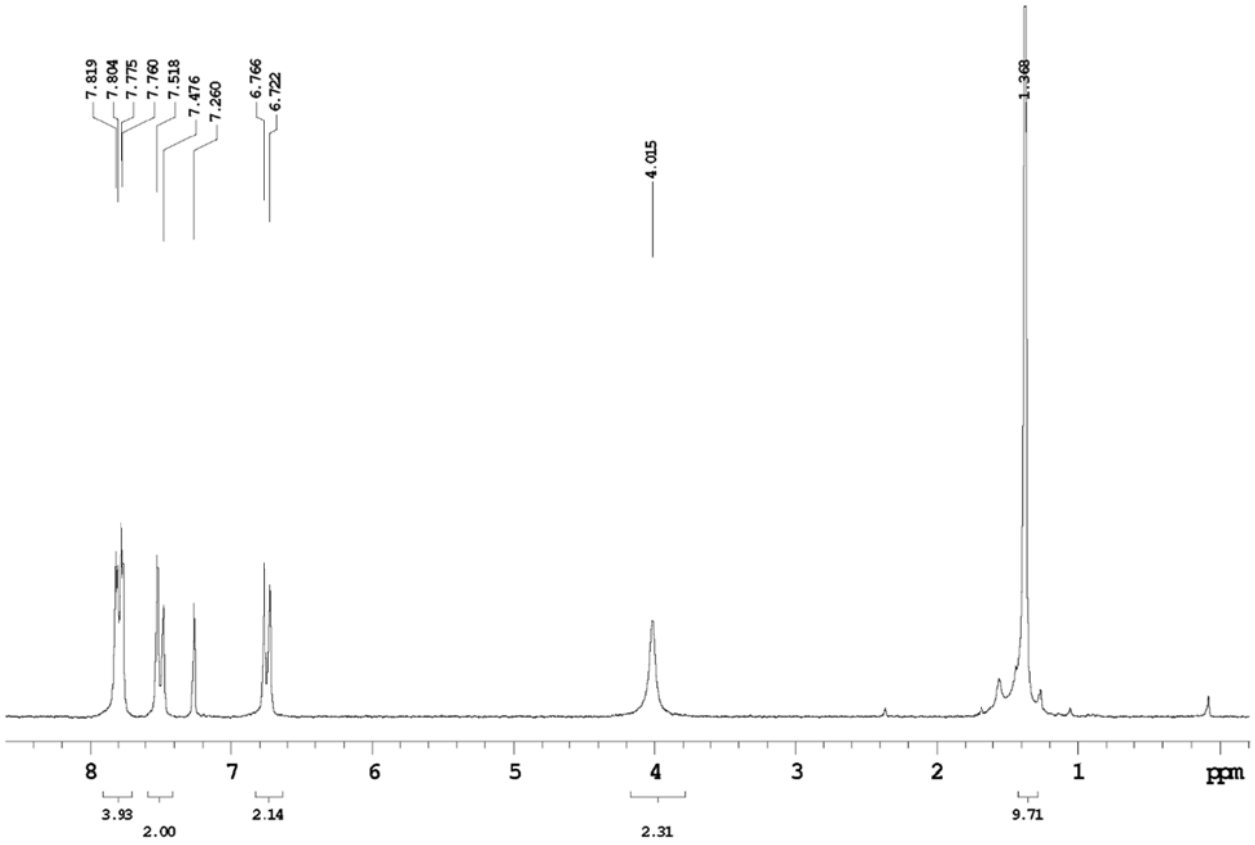

^{13}C-NMR Spectra: ($CDCl_3$, 600 MHz)

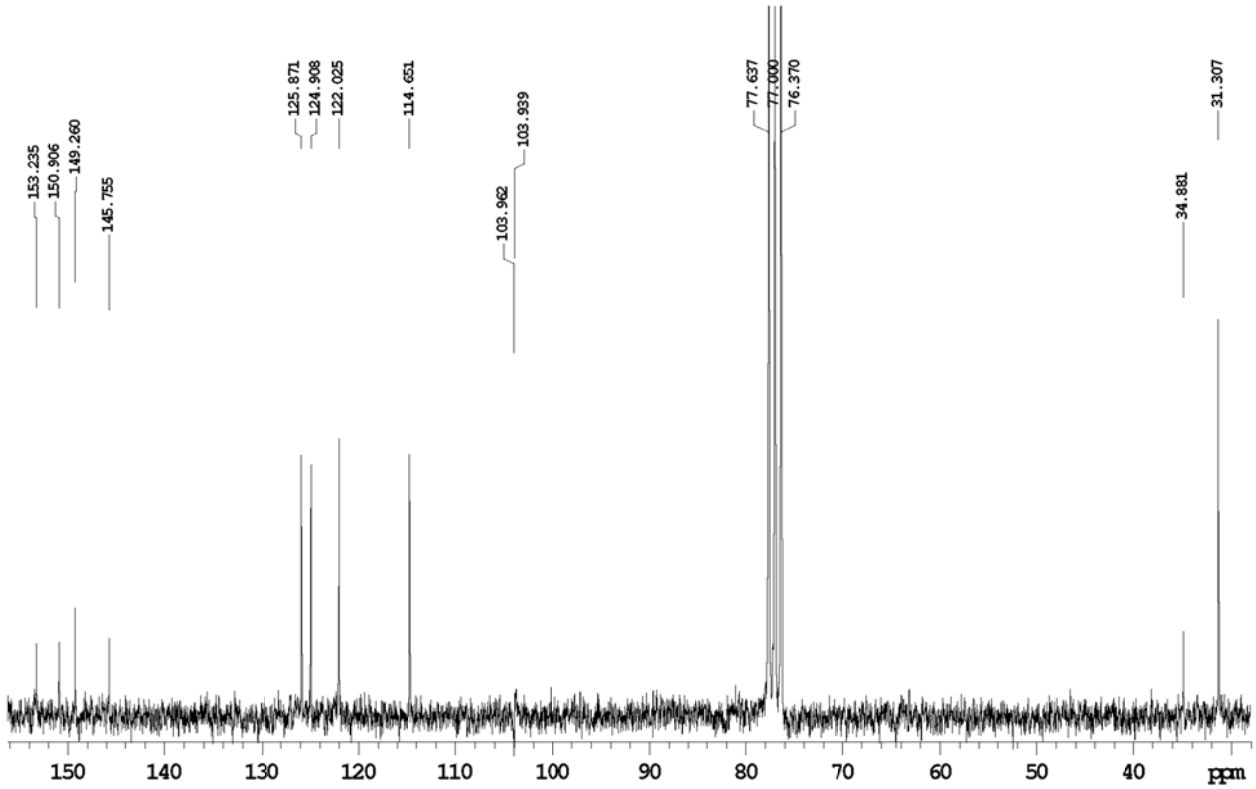

(E)-1,2-bis(4-((E)-o-tolyldiazenyl)phenyl)diazene (40)

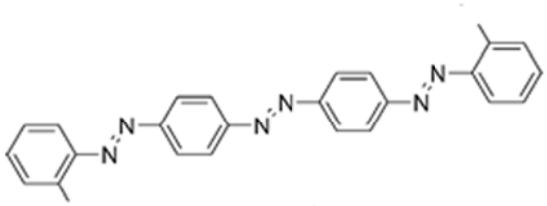

40

In an apparatus open to air, (*E*)-4-(*o*-tolyldiazenyl)aniline (**37**) (211 mg, 1 mmol), CuBr (4.3 mg, 0.03 mmol) and pyridine (7.11 mg, 0.09 mmol) were mixed in toluene (4 mL**)**. The reaction mixture was stirred vigorously at 60°C overnight. After cooling down to room temperature, the reddish precipitate was filtered in vacuo and washed with toluene. The residue was dissolved in CH_2Cl_2 and purified by flash chromatography on silica gel (eluent: petroleum ether/toluene 5:1) to afford 75 mg (36%) of **40** as an orange solid.

ESI-MS calculated m/z: 418.2; found 419.0 $[M+H]^+$; 441.4 $[M+Na]^+$.

^{1}HNMR Spectra: ($CDCl_3$, 600 MHz)

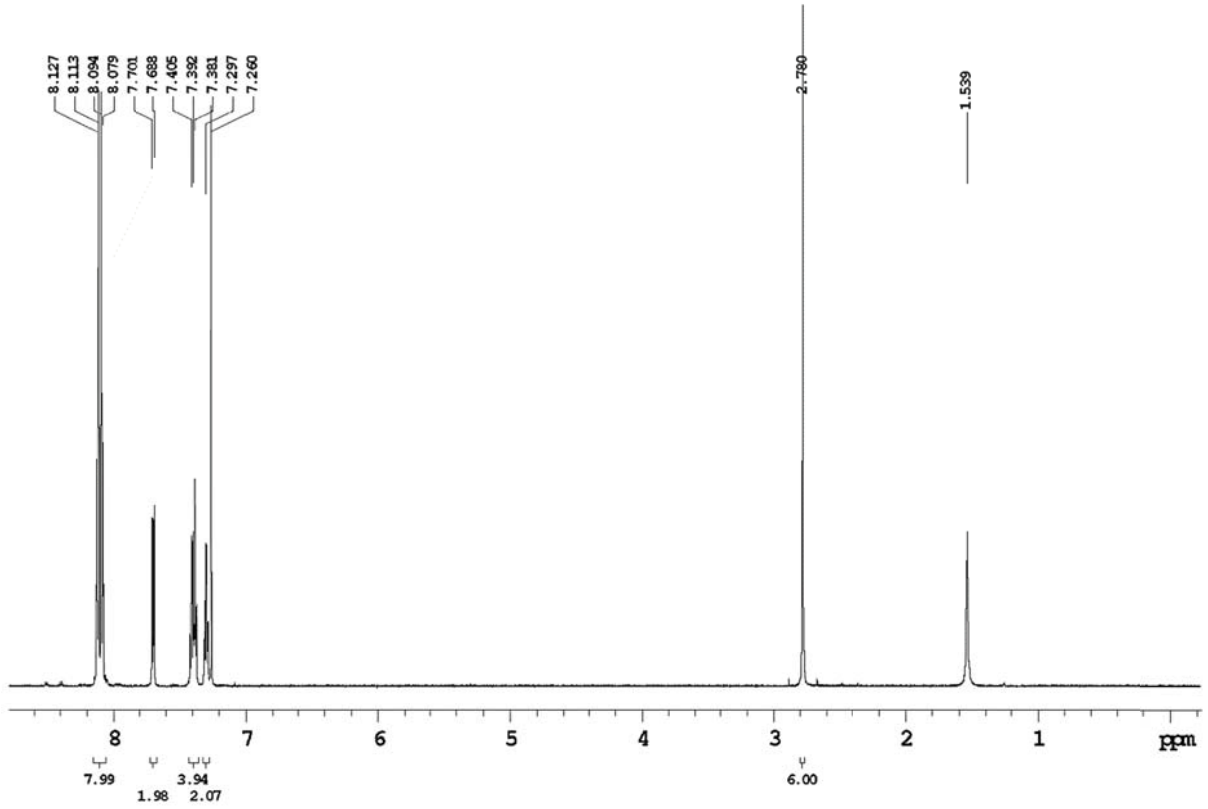

^{13}C-NMR Spectra: ($CDCl_3$, 600 MHz)

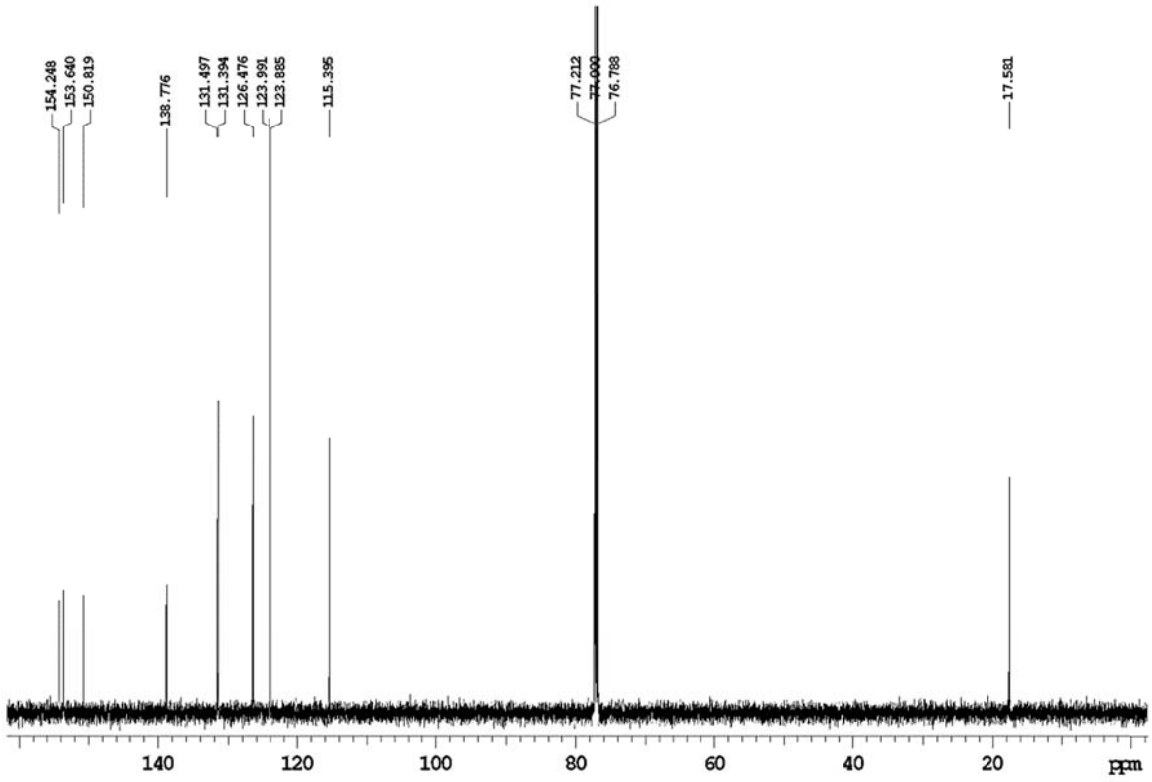

(E)-1,2-bis(4-((E)-(*tert*-butyl)phenyl)diazenyl)phenyl)diazene (41)

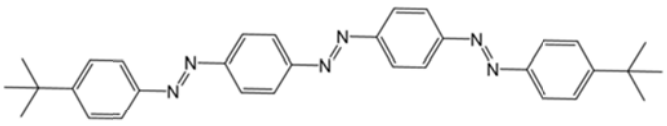

41

In an apparatus open to air, (E)-4-((4-(*tert*-butyl)phenyl)diazenyl)aniline (**39**) (253 mg, 1 mmol), CuBr (4 mg, 0.03 mmol) and pyridine (7 mg, 0.09 mmol) were mixed in toluene (4 mL). The reaction mixture was stirred vigorously at 60°C overnight. After cooling down to room temperature, the brownish precipitate was filtered under vacuum and washed with toluene. The residue was dissolved in CH_2Cl_2 and purified by flash chromatography on silica gel (eluent: cyclohexane: CH_2Cl_2 1:1) to afford 175 mg (35%) of **41** as an orange solid.

ESI-MS calculated m/z: 502.3; found 502.7 $[M+H]^+$; 525.7 $[M+Na]^+$.

[1]HNMR Spectra: ($CDCl_3$, 600 MHz):

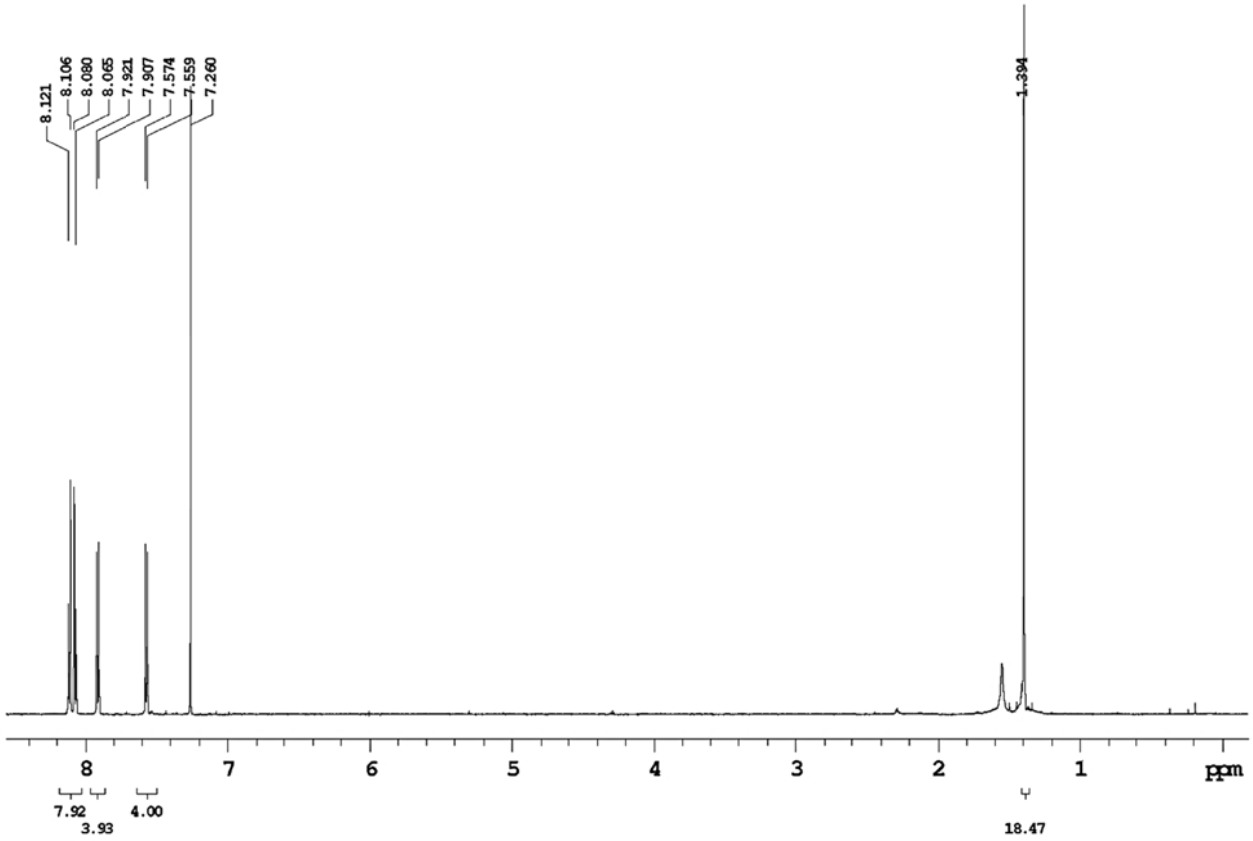

[13]CNMR Spectra: ($CDCl_3$, 600 MHz):

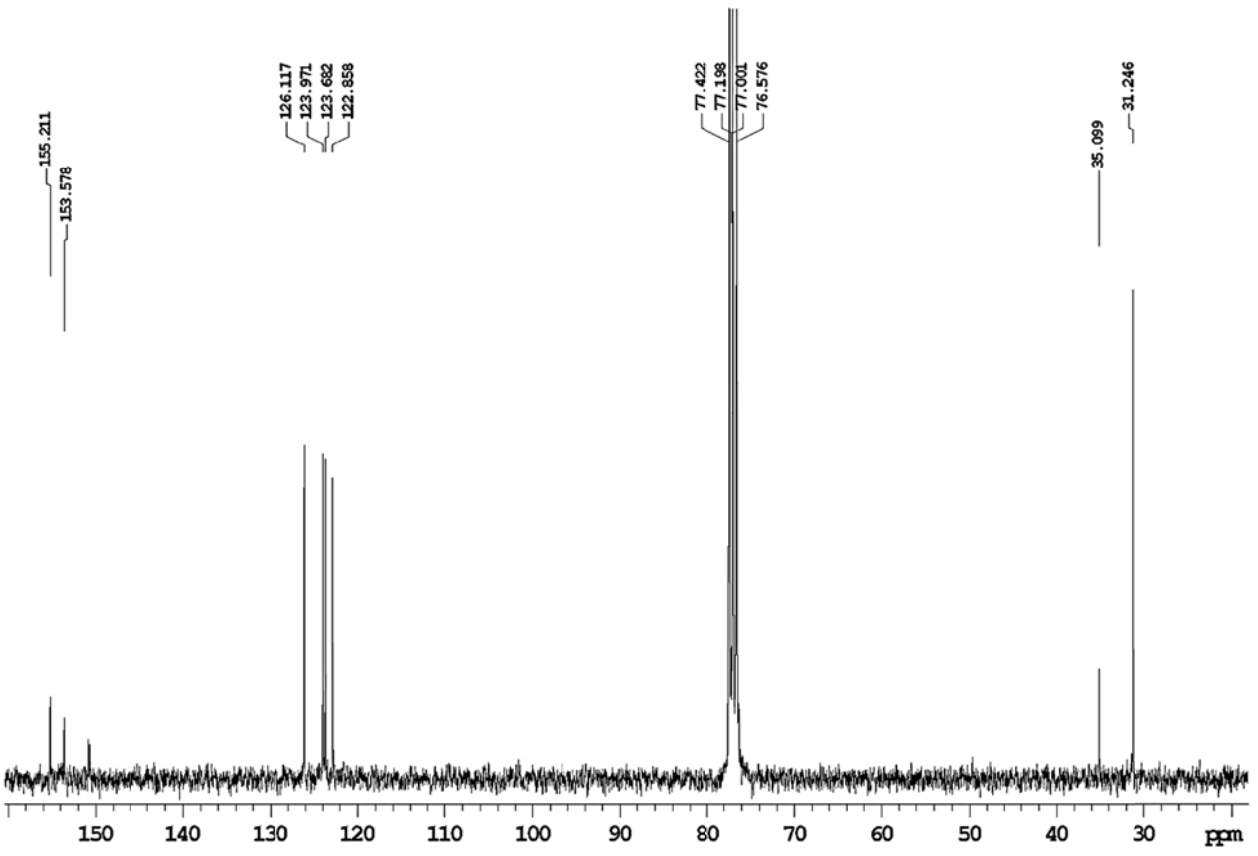

2,4,6-tris(phenyldiazenyl)benzene-1,3-diamine, (42)

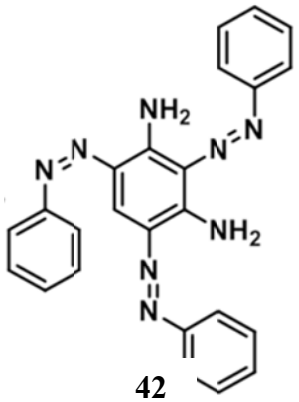

42

Aryl dazonium salt was prepared by treatment of aniline (0.5 g, 5.4 mmol) with $NaNO_2$ (1.1 eqv, 0.41 g, 5.9 mmol) and 3 eq. of HCl conc. (1,35 mL) in water (15 mL). The formation of the diazonium salt was monitored with KI/starch paper. An aqueous solution, (2 mL), of m-phenylenediamine, (0.33 eqv, 0.191 g, 1.8 mmol) was then added and the pH was adjusted at about 4. The reaction mixture was stirred overnight. The mixture was then filtered, washed with water, and extracted with chloroform (3 x 50 mL). The combined organic phases were dried over $MgSO_4$ and concentrated to yield a red residue which was subjected to flash chromatography (Cyclohexane/ethyl acetate, 8:2), to afford the product as a violet solid (0.98 g, 2.3 mmol, yield= 43.2%).

ESI-MS: calculated m/z: 420.18; found 421 [M+H]+; 443 [M+Na]+

^{1}H-NMR Spectra ($CDCl_3$, 600 MHz):

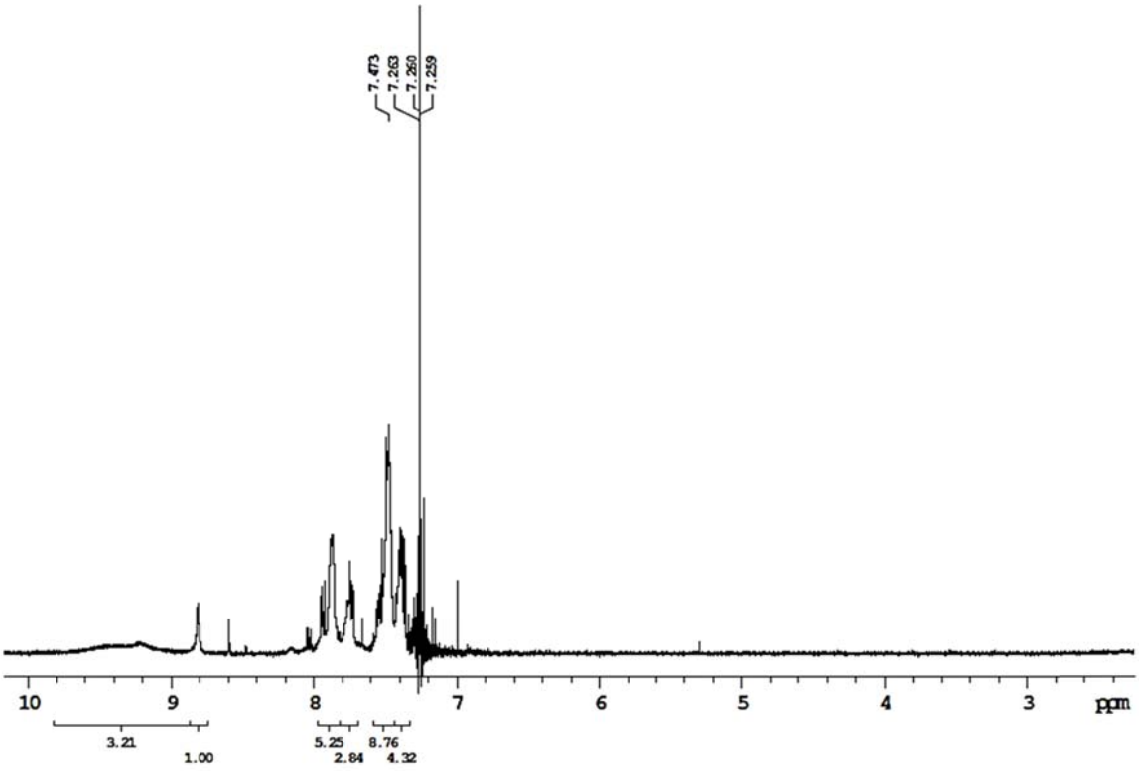

2,4-bis((E)-(4-((E)-o-tolyldiazenyl)phenyl)diazenyl)benzene-1,3-diamine (43)

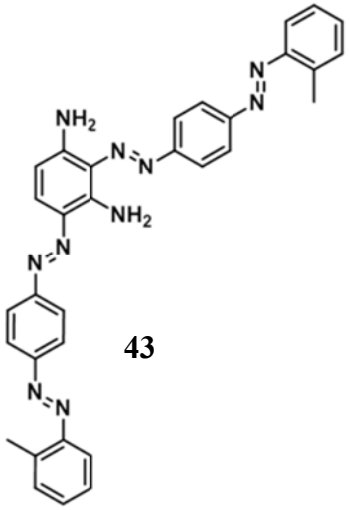

43

Aryl diazonium salt was prepared by treatment of (E)-4-(o-tolyldiazenyl)aniline (0.313 g, 1.5 mmol) with $NaNO_2$ (1.1 eqv, 0.114 g, 1.65 mmol) and 3 eq. of HCl conc. (0.370 mL) in a mixture water/acetone 1:1 ratio, (10 mL). After it was monitorated by potassium iodide map the disappearance of the nitrites, it was added a solution of *m*-phenylenediamine, (0.33 eqv, 0.055 g, 0.5 mmol) and fixed pH (about 4). The reaction mixture was stirred overnight. The mixture was then

filtered, washed with water, and extracted with chloroform (3 x 50 mL). The combined organic phases were dried over $MgSO_4$ and concentrated to yield a red residue which was subjected to flash chromatography (Cyclohexane/ethyl acetate, 8:2), (Rf = 0.45 Cyclohexane/ethyl acetate, 8:2), to afford the product as a red solid (0.32 g, 0.57 mmol, yield = 38.6%).

ESI-MS: calculated m/z: 552; found 553 $[M+H]^+$

^{1}H-NMR Spectra (DMSO, 600 MHz):